# Early clinical development of ACT-1004-1239, a first-in-class CXC chemokine receptor 7 (CXCR7) antagonist

**Inauguraldissertation**

Zur

Erlangung der Würde eines Doktors der Philosophie

Vorgelegt der

Philosophisch-Naturwissenschaftlichen Fakultät der Universität Basel

Von

**Christine Huynh**

2023

**Genehmigt von der Philosophisch-Naturwissenschaftlichen Fakultät auf Antrag von**

Dr. Patricia N. Sidharta

Prof. Dr. Henriette Meyer zu Schwabedissen

Prof. Dr. Alexander Jetter

**Basel, 21. Februar 2023**

Dekan

Prof. Dr. Marcel Mayor

# TABLE OF CONTENTS

## LIST OF FIGURES



## LIST OF TABLES

# LIST OF ABBREVIATIONS AND ACRONYMS

| | |
|---|---|
| ACKR | Atypical chemokine receptor |
| ADME | Absorption, distribution, metabolism, and excretion |
| ADMET | Absorption, distribution, metabolism, excretion, and toxicity |
| Akt | Protein kinase B |
| ALI | Acute lung injury |
| $AUC_{0-\infty}$ | Area under plasma concentration-time curve from zero to infinity |
| BAL | Bronchoalveolar lavage |
| BBB | Blood-brain barrier |
| $^{14}C$ | Carbon 14 (radiocarbon) |
| CI | Confidence interval |
| CK | Creatine kinase |
| $C_{max}$ | Maximum plasma concentration |
| CNS | Central nervous system |
| CSF | Cerebrospinal fluid |
| CXCR | CXC chemokine receptor |
| CXCL | CXC chemokine ligand |
| CYP | Cytochrome P450 |
| DDI | Drug-drug interaction |
| EAE | Experimental autoimmune encephalomyelitis |
| ERK | Extracellular signal-regulated kinase |
| GMP | Good Manufacturing Practice |
| GPCR | G protein coupled receptor |
| HIF-1α | Hypoxia-inducible factor 1α |
| HTS | High throughput screening |
| IFN | Interferon |
| ITAC | Interferon-inducible T cell α chemoattractant |
| KOR | Kappa-opioid receptor |
| LPS | Lipopolysaccharide |
| MAPK | Mitogen-activated protein kinase |
| MHC | Major histocompatibility complex |
| MOG | Myelin oligodendrocyte glycoprotein |
| MS | Multiple sclerosis |
| NK | Natural killer cell |

| | |
|---|---|
| NSC | Neural stem cell |
| o.d. | Once daily |
| OPC | Oligodendrocyte precursor cell |
| PD | Pharmacodynamic(s) |
| PK | Pharmacokinetic(s) |
| PLP | Proteolipid protein |
| QTc | QT interval corrected |
| SDF-1α | Stromal-derived factor |
| $t_{1/2}$ | Terminal half-life |
| $t_{max}$ | Time to reach maximum plasma concentration |
| VEGF | Vascular endothelial growth factor |

# ACKNOWLEDGEMENTS

The work accomplished and described in this thesis would not have been possible without the support, advice, and encouragement of several people.

First of all, I would like to thank Patricia Sidharta, who kindly “adopted” me into her team during a difficult period of my PhD. She not only supervised me but also guided me through my project and was willing to share her scientific knowledge with me. Furthermore, she exposed me to cross-functional discussions, thereby allowing me to deepen my knowledge of clinical development.

Furthermore, I would like to convey my huge gratitude to my professor Henriette Meyer zu Schwabedissen for her academic supervision during my PhD, her great scientific support, and her valuable personal/mental guidance. I really appreciated being part of her research group which enabled me to have fruitful interactions with fellow students and to gain insight into other interesting projects.

I would also like to thank Prof. Dr. Alexander Jetter who was willing to join my PhD committee as an external expert.

Moreover, I would like to express my sincere gratitude to Jasper Dingemanse for allowing me to enroll and complete my PhD in his department (Clinical Pharmacology) at Idorsia Pharmaceuticals Ltd. Without his support in promoting young professionals, I would not have been able to have such an exceptional PhD position that enabled me to gain practical work experience in pharmaceutical industry in parallel to my studies.

I am grateful to my colleagues in Clinical Pharmacology for being a bunch of fun but also of knowledge. I enjoyed spending time with them at work and also socializing outside work hours. Moreover, I would like to thank the study team members, who significantly contributed to the success of the studies which are described in my thesis.

Moreover, special thanks to Karolina, Katie, and Alexey for proofreading my thesis and providing constructive feedback.

I want to express my deepest appreciation to my friends who accompanied me along my PhD journey. In particular, I would like to thank my best friend Lena for her almost 20 years of friendship and her unique personality of seeing everything in a positive way. Furthermore, I am grateful to my friends, Sharavan and Tobias, who supported me in every work-related and/or personal matter. Special thanks go to my partner Christian, for always being there for me and with whom I can share all my emotions.

Finally, but most importantly, I would like to thank my parents, Linda and Alex, and my siblings, Nancy and Michael, for their unconditional love, unlimited support, and encouragement in my decisions. I cannot describe in words how grateful I am to be part of this family. Without them, I would not be who and where I am. Thanks a lot!

## SUMMARY

The human body is highly dependent on signaling proteins such as chemokines to maintain its physiology. The CXC chemokine receptor 7 (CXCR7) and its interacting chemokines, CXC chemokine ligand (CXCL) 11 and CXCL12, play a crucial role in several processes, for instance homeostasis, and therefore are vital components in human biology. CXCR7 functions as a decoy receptor for its chemokines, and hence modulates their extracellular concentrations. As CXCL11 and CXCL12 bind not only to CXCR7 but also to CXCR3 and CXCR4, respectively, the scavenging activity of CXCR7 can indirectly impact CXCR3- and CXCR4-mediated functions. Apart from physiological conditions, the CXCR3/CXCR4/CXCR7–CXCL11/CXCL12 axis is assumed to have a relevant role in various diseases and is widely discussed in the field of cancer and multiple sclerosis (MS). Under these pathophysiological conditions, there is evidence that these chemokine-receptor interactions can modulate several cell signaling pathways including but not limited to cell proliferation, differentiation, and maturation, and therefore, contribute to disease induction. Changes to the CXCR3/CXCR4/CXCR7–CXCL11/CXCL12 axis by modulators demonstrated an improved disease outcome in several preclinical studies. CXCR7 in particular provided promising data as a druggable target due to its close network to CXCR3 and CXCR4. However, to date, only a few CXCR7 modulators have been used for preclinical investigations, and none have been clinically investigated. Idorsia Pharmaceuticals Ltd developed a potent and selective first-in-class CXCR7 antagonist ACT-1004-1239, which showed favorable efficacy in animal models of MS. ACT-1004-1239 fulfilled all the preclinical prerequisites to enter the clinical development stage. Here, two clinical pharmacology studies including a single- and multiple-ascending dose study with ACT-1004-1239 are reported. In the single-ascending dose study, besides the investigation of safety/tolerability, pharmacokinetics (PK), and pharmacodynamics (PD) of single-dose ACT-1004-1239, several additional assessments were incorporated into the study design to evaluate food effect, absolute bioavailability, and absorption, distribution, metabolism and excretion (ADME) characteristics. An integrated approach was also applied for the multiple-ascending dose study. In addition to investigation of safety/tolerability, PK, and PD of multiple-dose ACT-1004-1239, the study incorporated the evaluation of the concentration-QTc relationship. The incorporation of various sub-investigations in both studies enabled a thorough characterization of ACT-1004-1239 in healthy adult human subjects. ACT-1004-1239 was safe and well tolerated up to and including a dose of 200 mg after single-and multiple-dose administration. The PK profile was characterized by a fast absorption, high volume of distribution, almost no accumulation, and an elimination that fits with a once-daily dosing regimen. No clinically relevant changes were observed for sex (males vs. females) or food state (fasted vs. fed). The evaluation of ADME revealed that ACT-

1004-1239 is extensively metabolized and predominantly eliminated through a pathway that is catalyzed by cytochrome P450 (CYP) 3A4. Consequently, this indicated the need of a follow-up clinical pharmacology study, i.e., drug-drug interaction (DDI) study with a strong CYP3A4 inhibitor. Such a study was conceptualized by taking several factors into consideration (e.g., study design, treatment duration, dose strength) and finally, a suitable DDI study design for ACT-1004-1239 was established. Besides PK, the PD profile of ACT-1004-1239 was also evaluated in both studies using CXCL12 plasma concentration as biomarker. Target engagement of ACT-1004-1239 was demonstrated in both studies, reflected in a dose-dependent increase of the CXCL12 plasma concentration. An increase in CXCL12 concentrations was preclinically associated with efficacy. However, this remains to be investigated in patients.

In conclusion, the two completed clinical pharmacology studies generated convincing data for ACT-1004-1239 in healthy subjects for further clinical investigations in patients.

# CHAPTER 1

## Introduction

Physiological role of CXCR7

CXCR3 and CXCR4: interacting receptors of CXCR7

Trio receptor interaction: Crosstalk of CXCR3, CXCR4, and CXCR7

Pathophysiological role of the CXCR3/CXCR4/CXCR7–CXCL11/12 axis

CXCR3/CXCR4/CXCR7/CXCL11/CXCL12 modulators

Aims of the thesis

# 1 INTRODUCTION

Cytokines are small proteins involved in several signaling processes within the immune system and therefore are known as immunomodulators [1]. Chemokines, also known as small chemotactic proteins, belong to the cytokine family and can bind to their respective receptors. More than 50 chemokines have been identified so far, and most of them contain four conserved cysteines which are responsible for the tertiary structure of the protein. The configuration of the two cysteines closest to the N-terminus of the chemokine amino acid sequence is used to divide the chemokines into four categories: CXC, CC, C, and $CX_3C$. Chemokines and chemokine receptors are classified using the chemokine nomenclature, which consists of the name of the subgroup followed by L (for chemokine, also known as ligand; e.g., CXCL or CCL) or R (for chemokine receptor; e.g., CXCR or CCR) and a number [2–6].

Chemokine-receptor interactions are critical in a variety of physiological and pathological processes that rely on the chemokines' homeostatic or inflammatory qualities. In detail, homeostatic chemokines are constitutively expressed and are responsible for cell trafficking, migration, and homing, whereas inflammatory chemokines are mainly expressed during inflammatory conditions and function as chemoattractant for immune cells. Most chemokine receptors, such as CXC chemokine receptor (CXCR) 3, interact with inflammatory chemokines, while some, like CXCR7, bind with both homeostatic and inflammatory chemokines, while yet others, like CXCR4, exclusively bind with homeostatic chemokines [6,7]. Due to the seven transmembrane helices and the ability to conduct G protein-mediated (canonical) signaling, chemokine receptors belong to G protein coupled receptors (GPCR). A few chemokine receptors that lack the ability to perform canonical signaling are considered as atypical chemokine receptors (ACKRs). One of these ACKRs is CXCR7 (other common names include ACKR3 and RDC1). CXCR7 acts as a scavenger receptor for its ligands, CXC chemokine ligand (CXCL) 11 (also known as interferon-inducible T cell α chemoattractant [ITAC]) and CXCL12 (also called stromal-derived factor [SDF-1α]) [7–9]. However, CXCL11 and CXCL12 do not solely bind to CXCR7, but also exhibit low affinity to CXCR3 and CXCR4, respectively [10–15]. Given the special "scavenging function", CXCR7 can have impact on both the CXCR3- and the CXCR4-mediated signaling function.

This chapter introduces CXCR7 and its physiological role as a stand-alone receptor as well as an interacting receptor of CXCR3 and CXCR4. In addition, it provides an overview of disease areas in which CXCR7 is assumed to be of relevance such as cancer and immunodeficient disorders. Finally, within this chapter, current known modulators affecting CXCR7, its interacting receptors, and its ligands CXCL11 and CXCL12 in the field of cancer and multiple sclerosis (MS) are discussed.

Information provided in this chapter is based on a previously published literature review, in which the relevance of the CXCR4/CXCR7–CXCL12 axis in (patho)physiological conditions was elaborated in detail [6].

## 1.1 Physiological role of CXCR7

CXCR7 was originally cloned from a dog thyroid cDNA library in 1989 and named RDC1 [11]. Thereafter, based on its structural similarity to CXC receptors, it was renamed to CXCR7 according to the nomenclature used for chemokine receptors [5,11,14].

CXCR7 was mainly detected on human endothelial cells in the vasculature of different organs, including but not limited to brain, colon, small intestine, and testis [16] where it serves as a scavenger and/or decoy receptor for its ligands. Indeed, after binding of either ligand, CXCL11 or CXCL12, the CXCR7-ligand complex is internalized, which results in the breakdown of the CXCR7-ligand complex and the return of the receptor to the cell membrane, i.e., receptor recycling (Figure 1) [8,9,14,17]. This scavenging activity of CXCR7 is a homeostatic mechanism and can facilitate the establishment and the maintenance of a concentration gradient for its respective ligands. For example, the migration of primordial germ cells towards the gonadal primordium in zebrafish was demonstrated to be facilitated by a CXCR7-controlled CXCL12 concentration gradient [18]. Moreover, by maintaining CXCL11 and CXCL12 gradients, CXCR7 eases the attraction of CXCR3+ and CXCR4+ cells in various physiological and pathological situations [19–21]. The ability of CXCR7 to establish the ligands gradients is likely independent of the extracellular ligand concentrations, as the CXCR7 scavenging activity appeared not to be saturable [9]. This was demonstrated in studies showing that CXCR7 scavenges CXCL12 linearly upon elevation of chemokine concentrations [22].

The ability to serve as a scavenger receptor is not a classical characteristic of chemokine receptors. Most of the chemokine receptors that are members of the GPCR superfamily induce G protein subunit (α, β, and γ) driven cell signaling upon binding of their chemokine ligands. Interestingly, despite being a chemokine receptor, CXCR7 is unable to perform such G protein subunit-coupled cell signaling due to a change in the sequence of the DRYLAIV motif which is thought to be responsible for canonical signaling [23]. Due to this absence of canonical signaling, CXCR7 belongs to the ACKR family and is also known as ACKR3. Despite this characteristic, CXCR7 is capable of inducing cell signaling via β-arrestin (Figure 1). Binding of either CXCL11 or CXCL12 on CXCR7-transfected cells initiated recruitment of β-arrestin, through G protein receptor kinase, to the plasma membrane or cytoplasmic vesicles, respectively [8]. Several studies share the observation that, following the recruitment of β-arrestin, CXCR7 is able to induce G protein subunit-independent signaling (i.e., β-arrestin-biased cell signaling) [24], such as downstream activation of extracellular signal-regulated kinase (ERK) and protein kinase B (also known as Akt) in diseased and healthy cells (Figure 1) [8,25–29]. CXCR7-induced cell signaling has also been found to be important in organogenesis and, as a result, also in embryogenesis. This was observed in CXCR7-deficient mice, who had heart abnormalities such as

cardiomyocyte hyperplasia and cardiac valve anomalies, which resulted in postnatal death despite normal hematopoiesis [30–33].

Taken together, CXCR7 is an atypical chemokine receptor which serves as a scavenger receptor for its ligands, CXCL11 and CXCL12, and thus regulates the extracellular ligand concentrations while inducing cell signaling through β-arrestin recruitment.

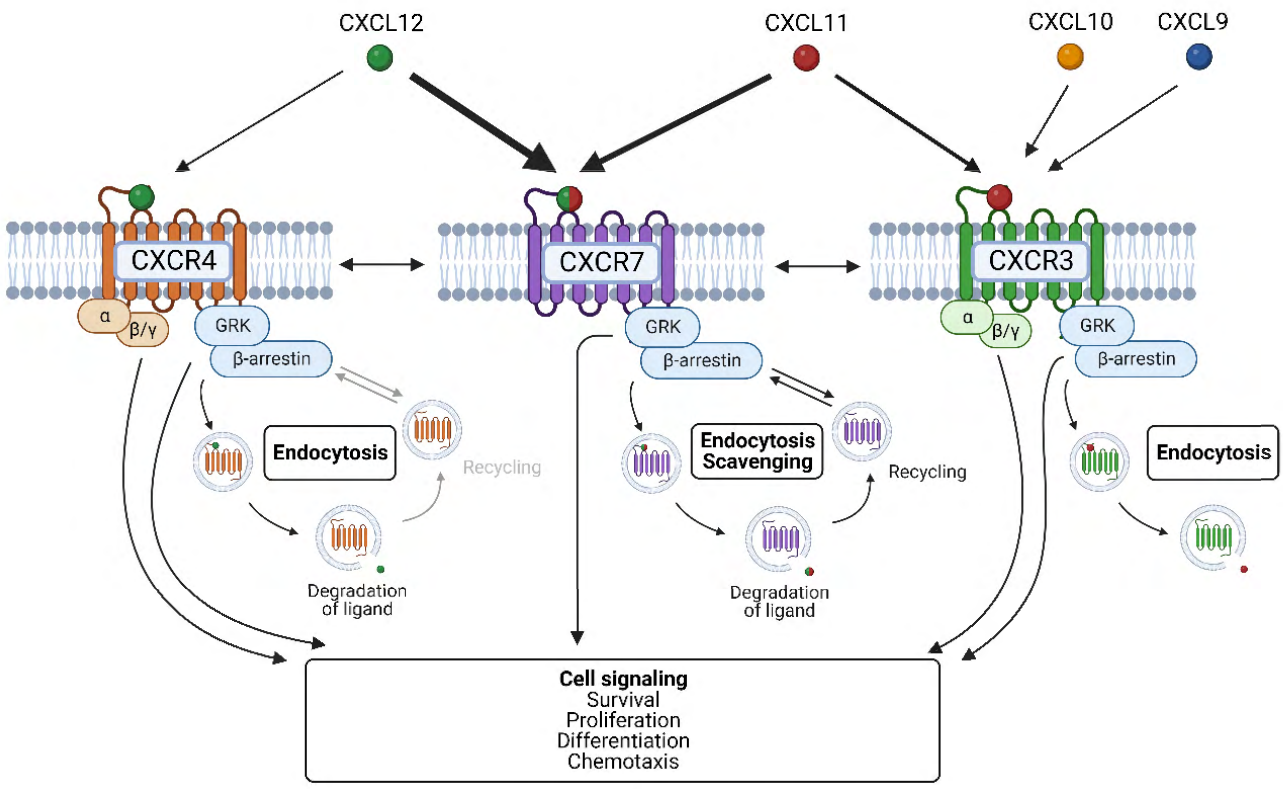


**Figure 1: Overview of CXCR3, CXCR4, and CXCR7 interactions with their respective ligands**

CXCR7 serves predominantly as a scavenger receptor for its ligands CXCL11 and CXCL12 with subsequent receptor recycling. Therefore, it can regulate the availability of its ligands in the extracellular matrix and indirectly impacts the functions of CXCR3 and CXCR4. Furthermore, CXCL11 and CXCL12 bind with a higher affinity to CXCR7 (indicated by thickness of the arrows: a thick arrow shows high affinity and thin arrow shows weak affinity) than to CXCR3 and CXCR4. In contrast to CXCR3 and CXCR4, CXCR7 lacks the ability to elicit G protein subunit-induced cell signaling due to a change in the sequence of the canonical DRYLAIV motif, which is typically required for G protein signaling. However, CXCR7 can elicit cell signaling through the recruitment of β-arrestin similar to CXCR3 and CXCR4. CXCR3 and CXCR4 mainly perform internalization of the receptor-ligand complex (i.e., endocytosis) following binding of the ligands. CXCR3 has three ligands (i.e., CXCL9, CXCL10, and CXCL11), while CXCR4 has one ligand only (CXCL12). Figure created with biorender.com. CXCL = CXC chemokine ligand; CXCR = CXC chemokine receptor; GRK = G protein-coupled receptor kinase.

## 1.2 CXCR3 and CXCR4: interacting receptors of CXCR7

The CXCR7 ligands, CXCL11 and CXCL12, are also ligands of CXCR3 and CXCR4, respectively. Due to the scavenging property of CXCR7 (i.e., internalization of CXCL11 and CXCL12), the receptor is indirectly linked to CXCR3 and CXCR4. Therefore, CXCR3 and CXCR4 can be considered as interacting receptors of CXCR7. Besides their function as interacting receptors, both CXCR3 and CXCR4 exhibit their own unique properties as stand-alone receptors (Figure 1).

CXCR3 (CD182) was discovered and characterized in 1996 due to its selectivity for CXCL9 (monokine induced by interferon [IFN] γ [MIG]) and CXCL10 (IFNγ-inducible protein 10 [IP-10]) [34,35]. Subsequently, CXCL11 (ITAC), another IFN-inducible chemokine with an even higher affinity to CXCR3 was identified [36]. CXCR3 is expressed by a variety of T cells, including CD4+ Type-1 T helper cells, T regulatory cells, and CD8+ (cytotoxic) T cells [34,37]. Moreover, T cells activated by dendritic cells are highly enriched with CXCR3 when compared to native T cells, suggesting a proinflammatory role of CXCR3 in the immune response [37–40]. Furthermore, CXCR3 expressed on activated lymphocytes is more responsive to its ligands in terms of cell signaling and chemotaxis compared to CXCR3 expressed on non-activated lymphocytes [34,40]. Apart from T cells, CXCR3 was also detected on other immune cells such as natural killer (NK) cells, B cells, granulocytes, monocytes, and endothelial cells [40–42]. Following an immune response, T- and NK cell-mediated IFN excretion induces the production of CXCL9, CXCL10, and CXCL11 in various cell types such as endothelial cells or fibroblasts [35,43]. Binding of these ligands triggers the activation of a G protein subunit, which was shown to be responsible for chemotactic CXCR3-mediated T cell migration towards higher concentrations of the chemokines, i.e., the site of inflammatory reaction [44,45]. The ability to induce chemotaxis or other cell signaling-related properties may also depend on the splice variant of CXCR3. To date, three different splice variants of CXCR3 are known: CXCR3-A, CXCR3-B, and CXCR3-alt. CXCR3-A is predominantly expressed by most cells including lymphocytes, whereas CXCR3-B is highly expressed on endothelial cells. This difference may be responsible for the opposing functions caused by CXCR3-A and CXCR3-B. While stimulation of CXCR3-A by its ligands induces chemotaxis and cell proliferation by G protein- or β-arrestin-induced downstream signaling, stimulation of CXCR3-B causes inhibition of cell migration, proliferation and induction of apoptosis without any sign of chemotaxis [34,36,40,46–48]. The function of CXCR3-alt remains largely unknown so far and requires further investigation.

Besides its role in inducing cell signaling, CXCR3 can be internalized upon binding of its ligands, with CXCL11 being the most potent chemokine in diminishing CXCR3 expression [49]. However, following internalization, there was no evidence of receptor recycling (Figure 1) [50]. In contrast to CXCR7

depletion, knockout of CXCR3 expression had no relevant impact on organogenesis. This was shown in CXCR3-deficient mice, which were viable, fertile, and did not experience any obvious developmental abnormalities compared to wild-type mice [51].

CXCR4 (initially called leukocyte-expressed seven-transmembrane-domain receptor [LESTR]), was first cloned from a human monocyte cDNA library in 1994 [52]. Next, CXCR4 was identified as a co-receptor for the human immunodeficiency virus 1 which enables the virus to enter CD4+ T cells [53] and as a receptor of CXCL12 [54]. Since then, the interaction of CXCR4 with CXCL12 and its function have been thoroughly investigated. Similar to CXCR7, binding of CXCL12 to CXCR4 results in internalization of the receptor-ligand complex. CXCL12 and CXCR4 are both predominantly ubiquitinated and degraded by lysosomes. Alternatively, CXCR4 can be recycled, although, to a lesser extent, when compared to CXCR7 [55,56]. Cell signaling can be initiated by the CXCR4–CXCL12 axis in two ways: through the G protein subunit cascade or independent of the G protein subunit (Figure 1) [57]. The G protein unit cascade can directly initiate multiple downstream signals such as phospholipase C [58] and mitogen-activated protein kinase/ERK (MAPK/ERK) leading to cell proliferation, differentiation, migration, and survival [57–62]. In contrast, the cascade independent of the G protein subunit requires the recruitment of β-arrestin in order to activate cell signaling that also leads to cell proliferation, differentiation, migration, and survival (Figure 1) [63,64]. Notably, in β-arrestin deficient mice the absence of β-arrestin-induced cell signaling was compensated by enhanced CXCR4-mediated G protein coupled signaling [65], suggesting that cell signaling via β-arrestin is of lower relevance compared to the one via the G protein subunit.

Similar to CXCR7 and in contrast to CXCR3, several studies highlighted the importance of CXCR4-induced signaling during embryogenesis. This was demonstrated in animal models missing CXCL12 and CXCR4 expression, which caused perinatal lethality attributed to defects in heart, brain, and large vessels development [66–71]. For example in context of brain development, studies in CXCR4 and CXCL12 knockout mice indicated a lack in directional migration of neuronal stem cell in embryos and in adults [68,71]. This vital function of CXCR4 may be explained by its expression site, which is mainly on hematopoietic stem and progenitor cells of various organs required for organogenesis [72].

In summary, based on their ability to initiate various cell signals following activation by their ligands, CXCR3 and CXCR4 play an important role in homeostasis and in immune response. Furthermore, they are highly dependent on the availability of their ligands, which can be modulated by CXCR7.

## 1.3 Trio receptor interaction: Crosstalk of CXCR3, CXCR4, and CXCR7

In view of the shared ligands, CXCL11 and CXCL12, it is likely that there is crosstalk between CXCR7 and its interacting receptors, CXCR3 and CXCR4.

First, CXCR4 and CXCR7 can impact each other on a cell signaling level depending on how they are expressed on cells. Indeed, CXCR4 can form heterodimers with CXCR7 [73], resulting in augmented CXCL12-induced signaling through the G protein [31,74,75]. For example, co-expression of CXCR4 and CXCR7 on transfected HEK293 cells showed a greater calcium flux through activation of the ERK downstream signaling compared to cells transfected only with CXCR4 [31]. The change in calcium release was explained by the conformational adaptation of the CXCR4/G protein complex due to heterodimerization with CXCR7. As a result, CXCR7 is proposed to modulate CXCR4/G protein subunit signaling [75]. Apart from the G protein subunit signaling, simultaneous expression of CXCR4 and CXCR7 on cell membrane increases β-arrestin recruitment after CXCL12 but not after CXCL11 activation. Further, enhanced β-arrestin recruitment was accompanied by an amplification in MAPK/ERK, and p38 signaling, which are known to be linked to cell proliferation and survival [74]. Besides these findings, *in vitro* studies demonstrated in addition an increase in cell migration when CXCR7 was co-expressed with CXCR4 [74,75].

In addition to the crosstalk at the cell signaling level, CXCR7 develops and maintains a homeostatic CXCL12 gradient through its scavenging activity and, consequently, can regulate CXCR4+ cell migration. Such cell migrations have been reported to play a crucial role in certain developmental processes in organogenesis and embryogenesis. For example, in the embryogenesis of zebrafish it was shown that CXCR7 provides directionality for CXCR4/CXCL12-mediated primordium cell migration [76]. Although CXCL12-mediated chemotactic cell migration is maintained in the absence of CXCR7, CXCR4+ migrating cells can end up in the wrong location due to the loss of the required CXCL12 gradient [77,78]. Furthermore, during mouse embryogenesis, it was shown that CXCR7 expressed on neurons regulates the availability of CXCL12 which guides CXCR4-expressing interneurons to develop the cortex [79].

Finally, due to the scavenging activity of CXCR7 it can modulate the CXCL12 level accessible to CXCR4 to perform cell signaling such as cell proliferation. High abundance of CXCR7 positively correlated with reduced CXCL12. Therefore, less CXCL12 is available to activate CXCR4+ neuronal cell differentiation [80,81]. However, this crosstalk has been mainly studied in the context of pathophysiological conditions. Further investigations are required to support such interaction in physiological states.

Likewise, the interaction between CXCR3 and CXCR7 in physiological conditions is sparsely studied. This may be explained by a prominent role of CXCR3 in inflammation and, consequently, its negligible expression levels under physiological conditions [37–40]. Nevertheless, given the fact that both, CXCR3 and CXCR7, share the same ligand (CXCL11), it is plausible that they can influence each other during inflammatory and/or pathophysiological conditions. In fact, an inflammatory disease model demonstrated that CXCR7 may also develop and maintain a CXCL11 gradient, and as a consequence regulate CXCR3+ cell migration [82].

In summary, CXCR7 can impact CXCR4 cell signaling through its expression site or indirectly through CXCL12. Furthermore, due to its scavenging activity it can develop and sustain CXCL11 and CXCL12 gradients, and therefore, regulate CXCR3+ and CXCR4+ cell migration.

## 1.4 Pathophysiological role of the CXCR3/CXCR4/CXCR7–CXCL11/12 axis

The interplay between CXCR3/CXCR4 and CXCR7 via their shared ligands CXCL11 and CXCL12 is considerably complex in non-pathological conditions. Importantly, it is assumed that dysregulation of expression of any of these receptors and/or the varying ligand concentration can promote the development and progression of pathophysiological conditions such as cancer, autoimmune, central nervous system (CNS), and cardiovascular disorders. In these conditions, the CXCR4/CXCR7–CXCL12 axis has been intensively investigated and is well characterized in both *in vitro* and *in vivo* models. In contrast to the CXCR4/CXCR7–CXCL12 axis, there is only limited *in vitro* and *in vivo* data concerning the role of CXCR3 and its splice variants in response to CXCL11 during pathophysiological conditions. This may be explained by the lack of CXCL11 expression in certain mouse strains often used for the *in vivo* models [31]. Nevertheless, since CXCR7 can internalize CXCL11 and thus, limits its availability to interact with CXCR3, it is likely that the CXCR3/CXCR7–CXCL11 axis has a relevant role in the aforementioned conditions in which the immune system is highly involved. In the past decades, high attention was given to the interplay of CXCR3/CXCR4/CXCR7 and their shared ligands in the field of cancer and MS, which is summarized in the following sections.

### 1.4.1 Cancer

CXCR3, CXCR4, and CXCR7 and their ligands are mainly linked to immunological processes due to their high expression on immune and endothelial cells. Besides their substantial impact on immune cell function, it was shown that these chemokine receptors are also expressed on tumor cells and are capable of modulating the properties of these cells and their microenvironment. This role of the CXCR3/CXCR4/CXCR7–CXCL11/CXCL12 axis in numerous cancer types in different organs has been investigated in multiple studies [83–103]. Briefly, cancerous tissues can be regulated by this axis by several mechanisms, which results in a change in cancer biology: expression of these chemokines and their receptors within the tumor microenvironment can i) activate tumor cell signaling, promoting cell migration and proliferation (i.e., tumor growth); ii) induce the release of certain growth factors, such as the vascular endothelial growth factor (VEGF) within the tumor microenvironment, and thus, support tumor progression via generation of new blood vessels (i.e., angiogenesis); and iii) support tumor survival and growth by initiation of tumor cell invasion into other organs (i.e., metastasis). These mechanisms are dependent on the abundance of these receptors and chemokines which, in turn, is dependent on the nature of the cancer type. Studies demonstrated that several cancer types with high expression of CXCR3-A, CXCR4, or CXCR7, or even simultaneous expression of these receptors are associated with increasing tumor grade [97]. Therefore, it is assumed that the regulation of any of the components of the CXCR3/CXCR4/CXCR7–CXCL11/CXCL12 axis with a receptor or ligand

modulator (e.g., antagonist) may influence the path of cancer development. Each mechanism is detailed in the following paragraphs.

First, the CXCR3/CXCR4/CXCR7–CXCL11/CXCL12 axis may affect tumor cell proliferation (Figure 2, upper panel). Tumor cells are known for a life span beyond that of normal cells and are characterized by an abnormal proliferation rate. Cell proliferation can be activated through various signaling cascades such as G protein-mediated activation of ERK and Akt pathways [84,95,104]. When stimulated by their ligands, CXCR3-A and CXCR4 can activate these downstream targets. Additionally, stimulation of CXCR7 has shown proliferative effect via induction of ERK and Akt through more complex pathways (i.e., β-arrestin-based cell signaling). The proliferative signaling can be further achieved following simultaneous expression of CXCR4 on CXCR7 on cancer cells, which allows the activation of G protein-mediated signaling [89]. Moreover, it is suggested that proliferation of cancer cells could be attributed to the CXCR7-mediated prevention of tumor cells' undergoing apoptosis, additionally to Akt induction [25]. Blockade of CXCR4 or CXCR7 with (functional) antagonists attenuated tumor growth [85,86,88,102]. With regard to CXCR3, as mentioned earlier, opposing effects on cell signaling were seen for the splice variants. While CXCR3-A induces cell proliferation, activation of CXCR3-B inhibits cell proliferation [46,47]. In cancer cells, an upregulated CXCR3-A abundance with low CXCR3-B abundance indicated a pro-tumorigenic effect. This effect was attributed to CXCR3-A, which can induce proliferative behavior of the tumor. In line with this are findings showing that silencing of CXCR3-A significantly inhibits cell proliferation, while down-regulation of CXCR3-B enhances tumor cell proliferation [99,100].

Tumor cell proliferation and growth are closely related to angiogenesis, i.e., the process of formation of new blood vessels within the tumor tissue. Angiogenesis is essential for tumor progression as it supplies the tumor with sufficient nutrients and oxygen. There are several factors that promote angiogenesis, with VEGF one of the most well-known [98]. Production of VEGF can be stimulated by cytokines or other growth factors, including but not limited to hypoxia-inducible factor 1α (HIF-1α). Hypoxic conditions within the cancerous tissue induce HIF-1α production and thereby promote production of VEGF [83]. In some cancer types, elevated production of HIF-1α was linked to increased expression of CXCR4, CXCR7, and CXCL12 [105–108], which correlates positively to VEGF release, and angiogenesis, and thus, to tumor progression [25,87,109,110] (Figure 2, middle panel). The latter was prevented upon inhibition of CXCR7 with a functional antagonist, namely CCX771 [86,111]. Besides CXCR7, CXCR3 was also considerably expressed in the endothelium. Previous studies observed that CXCR3 inhibits angiogenesis in response to CXCL11 stimulation [112]. However, there is also a controversy on the involvement of CXCR3 in angiogenesis due to the opposing effects of its splice

variants. The majority of data suggest that CXCR3-B, in contrast to CXCR7, exerts angiostatic activity following stimulation by CXCL10. Since opposing effects were reported for CXCR3-A and CXCR3-B, it is likely that CXCR3-A may cause angiogenic effects. However, to date, little is known about the involvement of CXCR3-A in angiogenesis and it remains to be further elucidated [113,114].

Another key factor involved in tumor growth and survival is the ability of tumor cells to invade to adjacent circulating and lymphatic systems. Tumor cells can travel via these systems and form new tumors in other parts of the body following their escape from the circulating and lymphatic systems. This process is known as metastasis. Due to their multifaceted functions, chemokine receptors have the ability to modulate this metastasis. It is suggested that the CXCR4/CXCR7–CXCL12 axis is highly involved in the formation of metastases in various tumor types including but not limited to prostate, breast, bladder, gastric, and colorectal cancer [25,90–92,101,103]. However, the current understanding of the underlying mechanisms varies across the different cancer types. It was postulated that the expression of CXCR7 facilitates adhesion and invasion of tumor cells, and therefore enables the formation of metastases [25]. On the other hand, the CXCR4–CXCL12 and CXCR7–CXCL11 axes are assumed to promote endothelial to mesenchymal transition [91,92]. This process describes the phenotypic switch of endothelia cells to mesenchymal-like cells. These modified cells are able to change the endothelial barrier and favor the intra- and extravasation of tumor cells, i.e., induction of metastasis [115]. Other studies suggested that stimulation of CXCR4/CXCR7 can form metastases through specific signaling pathways, such as toll-like receptor 4 / myeloid differential protein-2 [90] and MAPK [101] pathways (Figure 2, lower panel). Similar to CXCR4 and CXCR7, stimulation of CXCR3 by its ligands has been associated with the formation of metastases, however, the underlying mechanism remains unknown. Comparable to tumor cell proliferation, CXCR3-A was determined as the most effective CXCR3 splice variant of the formation of metastases [94,96]. Importantly, antagonism of these chemokine receptors (CXCR3, CXCR4, and CXCR7) was associated with a reduction of metastasis [111,116–118].

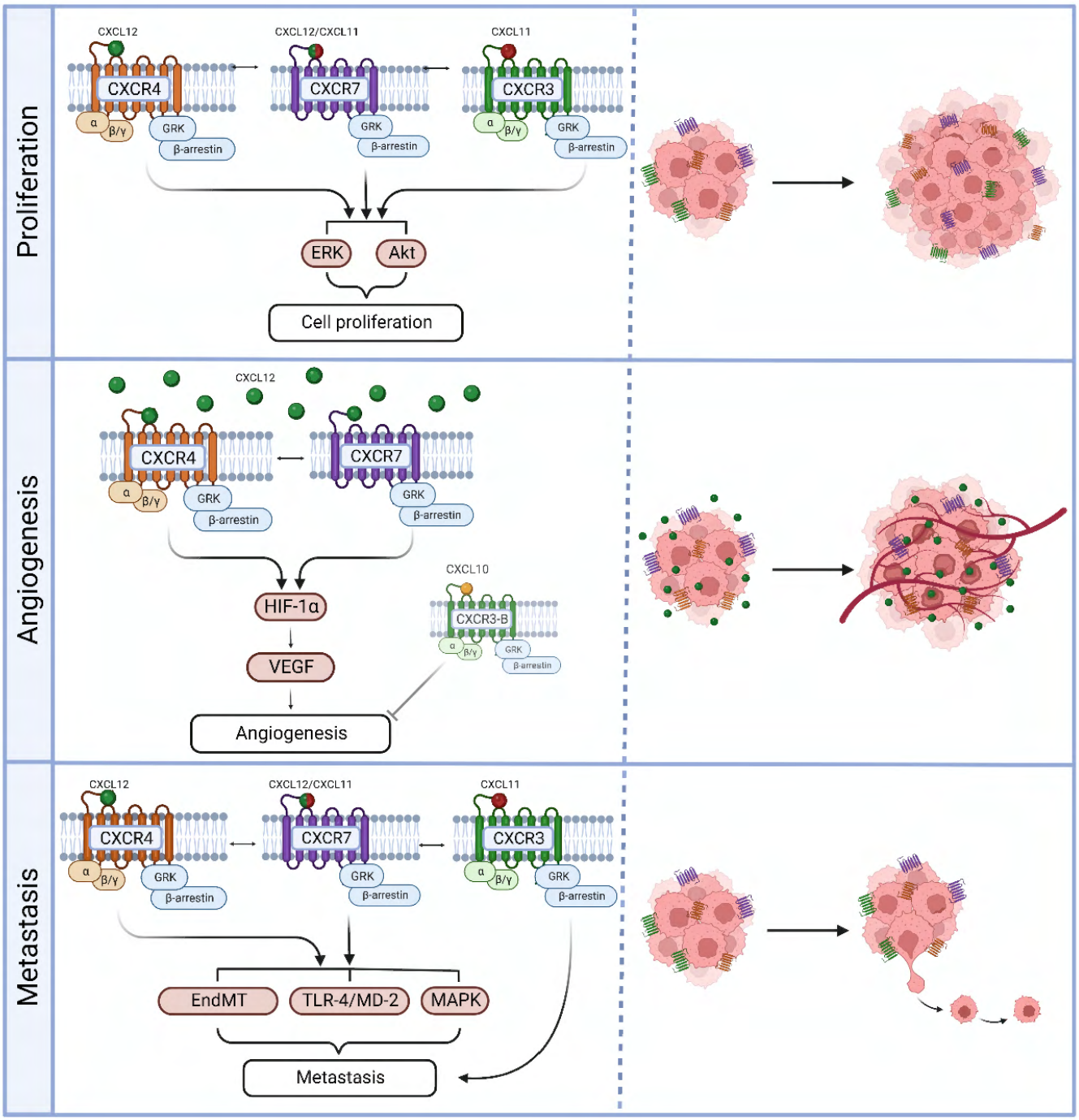


**Figure 2: Overview of the pathophysiological role of the CXCR3/CXCR4/CXCR7–CXCL11/CXCL12 axis in cancer**

The CXCR3/CXCR4/CXCR7–CXCL11/CXCL12 axis can regulate the biology of the cancerous tissue in several different ways including cell proliferation (upper panel), angiogenesis (middle panel), and metastasis (lower panel). First, tumor cell proliferation can occur upon activation of the ERK or Akt signaling cascades initiated by CXCR3, CXCR4, or CXCR7 and their ligands. Second, angiogenesis in cancer can be associated with increased expression of CXCR4, CXCR7, and CXCL12 resulting in enhanced production of the angiogenic factor HIF-1α followed by augmented VEGF release. Third, spread of tumor cells in the body (i.e., metastasis) can be achieved through CXCR4- and CXCR7-induced activation of several signaling cascades (i.e., EndMT, TLR-4/MD-2, and MAPK). Furthermore, formation of metastases is positively correlated with CXCR3 expression. Figure created with biorender.com. Akt = protein kinase B; CXCL = CXC chemokine ligand; CXCR = CXC chemokine receptor; EndMT = endothelial to mesenchymal transition; ERK = extracellular signal-regulated kinase; GRK = G protein-coupled receptor kinase; HIF-1α = hypoxia-inducible factor 1α; MAPK = mitogen-activated protein kinase; MD-2 = myeloid differential protein-2; TLR-4 = toll-like receptor 4; VEGF = vascular endothelial growth factor.

### 1.4.2 Multiple sclerosis

MS is an autoimmune disorder in which the myelin sheath that covers the nerves and enables quick and efficient transmission of electrical impulses between nerves, is destroyed by the immune system. CXCR4 and CXCR7 are widely expressed in various CNS cells such as astrocytes, oligodendrocytes, and microglia, and are assumed to contribute to the maintenance of certain brain function processes [81,119–123]. Therefore, in the context of MS, the role of the CXCR4/CXCR7–CXCL12 axis has been studied. In fact, it was predominantly studied for its ability to regulate immune cell migration and its function to induce cell proliferation and differentiation. Hence, the investigation of the CXCR4/CXCR7–CXCL12 axis in MS can be divided in two main mechanisms [124]: i) an immunomodulatory effect regulated, amongst others, through chemotactic activities; ii) a (pro-)myelinating effect induced through CNS cell proliferation and differentiation. Both mechanisms may occur at the same time as the sites of action are mostly different. While the immunomodulatory effects act mainly at the site of the blood-brain barrier (BBB), the (pro-)myelinating effect shows its action in the CNS (i.e., parenchyma).

With regard to the immunomodulatory effect, there is evidence showing that the CXCR4/CXCR7–CXCL12 axis can impact the extent of myelin damage by regulating immune cell infiltration into the CNS [125–127]. CXCR4 and CXCR7 and their ligand CXCL12 are expressed in adult humans and their expressions are increased during neuroinflammation [119,124,125,128]. In a healthy CNS, CXCL12 is constitutively expressed at the abluminal side of endothelial cells where it contributes to the homing of CXCR4+ leukocytes within the perivascular space and prevents parenchymal infiltration in the CNS; However, in MS patients, CXCL12 levels are increased at the BBB and CXCL12 shifts from the abluminal to the luminal region of the endothelium [125,129,130]. This change in CXCL12 location may be explained by an increase in CXCR7 expression on the abluminal site of endothelia. Here, CXCR7 enhances the internalization of CXCL12 resulting in low levels in the abluminal region, while there are high levels in the luminal region [131]. The change in the CXCL12 localization with enhanced levels at the luminal site is assumed to enable CXCR4+ leukocyte infiltration from the blood into the parenchymal CNS, and is thus, assumed to worsen the disease. This assumption is supported by immunohistochemical stainings of brain sections of MS patients. The analysis revealed that the redistribution of CXCL12 significantly correlates with disease severity reflected by enhanced demyelination and macrophage infiltration [130]. Moreover, it is assumed that the increase in luminal CXCL12 levels induces the expression of integrins. These integrins contribute to the arrest of recruited CXCR4+ leukocytes on the endothelium and therefore, may facilitate the migration of immune cells to the perivascular space [132,133]. It is proposed that perivascular infiltrates may be activated by antigen-

presenting cells such as reactive microglia expressing major histocompatibility complex (MHC) class II [127], and consequently, can migrate to parenchyma, where inflammatory cytokines can be released leading to neuroinflammation and demyelination [129]. Blockade of CXCR7 by CCX771 (a functional CXCR7 antagonist) results in improvement of disease recovery due to reduced parenchymal leukocytes infiltration [131]. An illustration showing the immunomodulatory effect caused by CXCL12 redistribution within the CXCR4/CXCR7–CXCL12 axis in MS is depicted in Figure 3.

Likewise, microglia that have diverse functions in modulating CNS cells are shown to be implicated in neuroinflammatory processes [124,134]. Previous studies have shown that the CXCR4/CXCR7–CXCL12 axis contributes to the transmigration of monocytes across the BBB and thus induces monocyte-endothelial cell interaction that facilitates lymphocytes infiltration [135,136]. Furthermore, expression of CXCR7 on microglia was positively correlated with the clinical severity score of experimental autoimmune encephalomyelitis (EAE). This may be explained by CXCR7/CXCL11/CXCL12–induced activation of the ERK downstream cascade, which, in response, stimulates chemotaxis on activated microglia that can also cause inflammation. Neutralization of CXCR7 stops the ERK downstream cascade and decreases the clinical severity of EAE in animals. This supports the relevance of the CXCR7–CXCL11/CXCL12 axis in modulating the outcome of CNS-related autoimmune diseases [137].

Apart from microglia, CXCR7 is expressed on astrocytes both under physiological and pathophysiological conditions (e.g., CNS insult) [124]. As astrocytes are arranged around the BBB, modulation of astrocytic functions during inflammation can favor the formation of lesions within the BBB and result in immune cell infiltration towards the parenchyma [138]. Augmented expression of CXCR7 was observed on astrocytes in response to pro-inflammatory conditions such as hypoxia and/or increased levels of IFNγ [139]. Moreover, IFNγ-induced CXCR7 expression on astrocytes was linked to the extent of inflammation in the spinal cord and the associated infiltration of immune cells into the CNS [140].

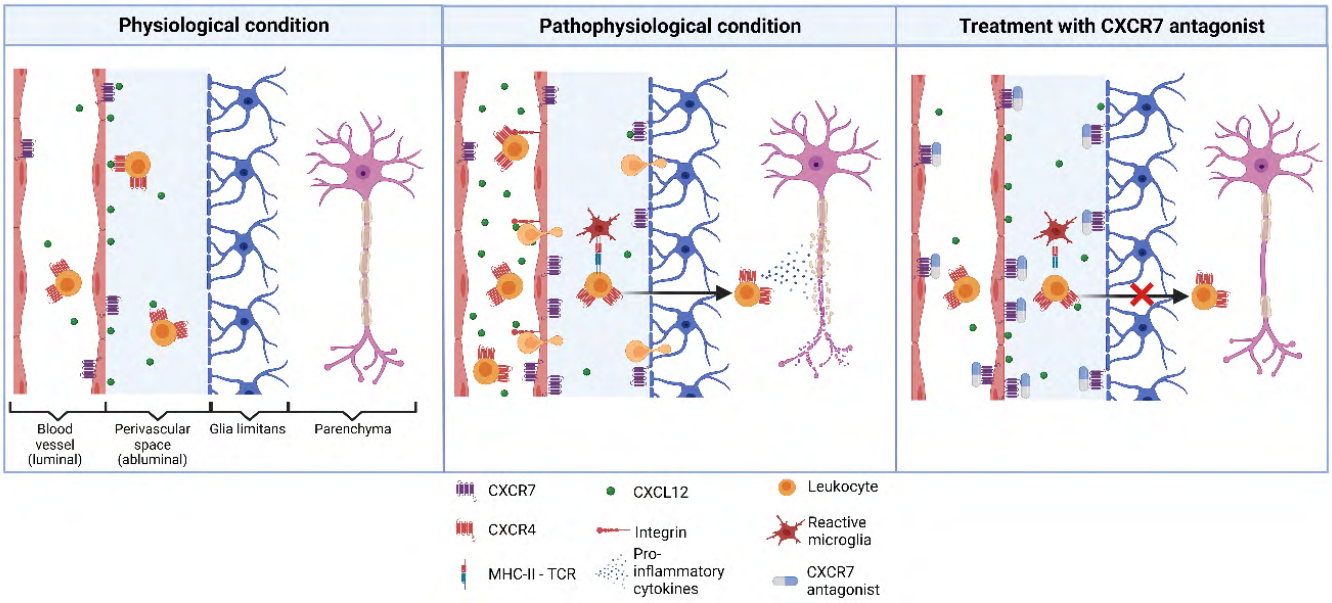


**Figure 3: Immunomodulatory effect of the CXCR4/CXCR7–CXCL12 axis in MS through CXCL12 redistribution at the BBB**
Under physiological conditions, CXCL12 is predominantly expressed on the abluminal site of the endothelium. There it may prevent CXCR4+ leukocyte infiltration towards the parenchyma (left panel). Under MS (pathophysiological) conditions, CXCR7 expression is augmented at the abluminal endothelium, and consequently this leads to a decrease in CXCL12 level at the abluminal site due to the scavenging activity, while there is an increase in CXCL12 at the luminal site. Increase in CXCL12 is associated with the production of integrins, which facilitate infiltration of leukocytes into the perivascular space where they are activated by reactive microglia expressing MHC class II. Due to the lack of CXCL12 in the perivascular space, immune cells can migrate further into the parenchyma and cause neuroinflammation resulting in demyelination (i.e., damage of myelin sheath that covers the axon) (middle panel). Inhibition of CXCR7 is proposed to restore the distribution of CXCL12, and thus, prevent CXCR4+ leukocytes infiltration into the CNS (right panel). Figure created with biorender.com. BBB = blood-brain barrier; CNS = central nervous system; CXCL = CXC chemokine ligand; CXCR = CXC chemokine receptor MHC = major histocompatibility complex; MS = multiple sclerosis; TCR = T cell receptor.

Besides the immunomodulatory effect and the associated immune cell infiltration into the CNS, the CXCR4/CXCR7–CXCL12 axis is assumed to directly impact MS disease severity through its effect on remyelination after axonal myelin damage by immune cells. Indeed, several *in vitro* and *in vivo* MS models show that the CXCR4–CXCL12 axis can initiate oligodendrocyte precursor cell (OPC) and neural stem cell (NSC) migrations, proliferation, and differentiation during disease and spontaneous recovery (observed in the course of EAE, i.e., spontaneous neuronal/myelin repair), implying its involvement in neuro-/oligodendrogenesis [122,141,142]. Moreover, CXCL12 is expressed and significantly increased in activated astrocytes and microglia at the site of MS lesions. This elevation is associated with an increase in the number of OPCs expressing CXCR4 [122,125]. Blocking either CXCR4 or CXCL12 in a murine viral-induced demyelinating model led to impaired migration and proliferation of NSCs [141]. Similar observations were made in a cuprizone-induced demyelination *in vivo* model. This study demonstrated that the reduction of CXCR4 expression by RNA silencing resulted in impaired OPC maturations and finally, a failure in remyelination [122]. These findings underpin the relevance of the CXCR4–CXCL12 axis as a mechanism for enhancing OPC differentiation into mature myelinating oligodendrocytes in the process of remyelination. Yet, the CXCR4–CXCL12 axis and the

associated remyelination can be impacted by the scavenger receptor CXCR7. Remarkably, CXCR7 expression is enhanced on various cells such as astrocytes and OPCs during demyelination in MS-like disease murine models. This is related to a reduction in CXCL12 levels, triggering a decrease in CXCR4-induced OPC differentiation and proliferation [80,81]. The functional CXCR7 antagonist, CCX771, reduces CXCL12 internalization, resulting in enhanced activation of CXCR4/CXCL12 signaling followed by remyelination [80]. These findings suggest that CXCR7 can influence CXCL12 concentrations and, as a response, CXCR4/CXCL12-induced signaling like cell proliferation and differentiation [79].

Besides CXCR4, induction of kappa-opioid receptor (KOR) expressed on OPCs was also found to enhance OPCs proliferation and differentiation leading to subsequent remyelination *in vivo* [143]. This KOR downstream pathway can be activated by opioid peptides including the subfamily of dynorphins, which binds preferably to KOR [144]. Interestingly, recent *in vitro* data indicated that CXCR7 can function as a scavenger receptor for opioid peptides including but not limited to the subfamily of dynorphins [145]. However, it remains unknown if increased expression of CXCR7 on KOR-expressing OPCs can modulate the availability of opioid peptides to such an extent that the KOR-induced remyelination is affected [124]. Further investigations are required to underpin the relevance of the interplay of CXCR7 and the KOR-opioid axis in the context of the remyelination process. An illustration showing the (pro-)myelinating effect of the CXCR4/CXCR7/KOR–CXCL12/opioid axis in MS is depicted in Figure 4.

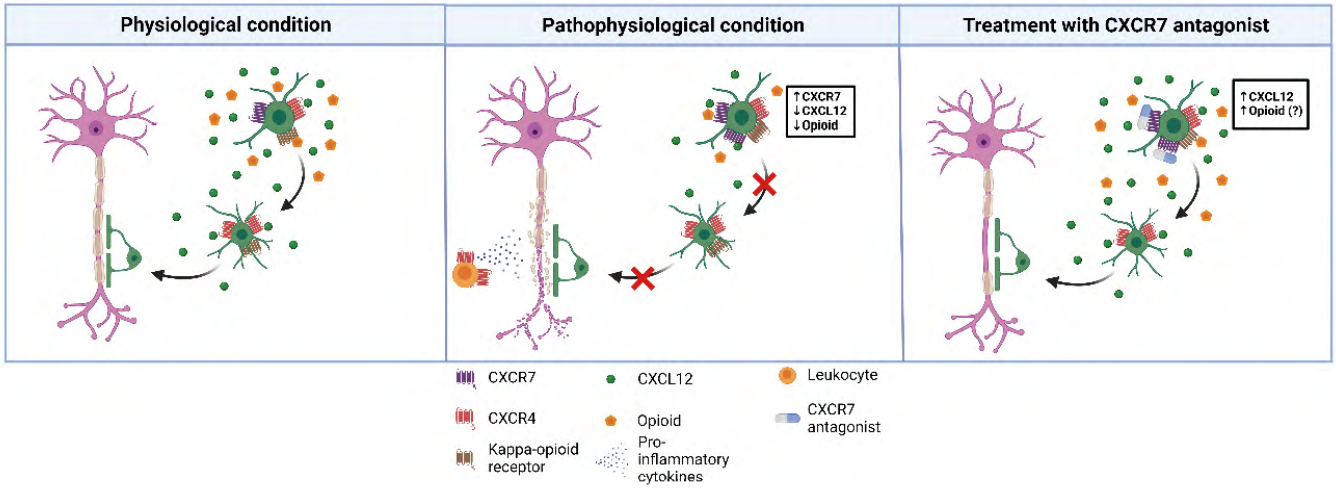


**Figure 4: (Pro-)myelinating effect of the CXCR4/CXCR7–CXCL12 axis in MS brain (parenchyma) through differentiation of OPCs**

Under physiological conditions, CXCR4 and KOR expressed on OPCs enable cell proliferation and differentiation to myelinating oligodendrocytes through CXCL12 and opioid peptides, respectively (left panel). Increased CXCR7 co-expression on OPCs under pathophysiological conditions can diminish CXCL12 and opioid peptide levels in the CNS (middle panel). Blockade of CXCR7 with a functional antagonist was associated with an increase in CXCL12 level in the CNS, resulting in an increase in OPCs differentiation to myelinating oligodendrocytes. Theoretically, this can be applied to the KOR/CXCR7-opioid axis however, this is not yet proven experimentally (right panel). Figure created with biorender.com. CNS = central nervous system; CXCL = CXC chemokine ligand; CXCR = CXC chemokine receptor; KOR = kappa-opioid receptor; OPC = oligodendrocyte progenitor cell.

In contrast to the CXCR4/CXCR7–CXCL12 axis, the role of the CXCR3/CXCR7–CXCL11 axis is not well known thus far. This may be explained by the lack in CXCL11 expression in mouse strains that are often used as *in vivo* models for MS [146]. Furthermore, there are contradicting data regarding the correlation of CXCL11 and MS. In detail, Szczuciński *et al.* did not observe any differences between CXCL11 serum or cerebrospinal fluid (CSF) concentrations of MS patients compared to controls, indicating no relevant implication of CXCL11 in MS [147]. However, Mellergård *et al*. reported that CXCL11 concentration was enhanced in CSF but not in plasma of MS patients in comparison to healthy subjects [148]. This contradiction and its underlying mechanism warrant further investigations of the CXCR3/CXCR7–CXCL11 axis in MS.

In conclusion, several investigations revealed that the CXCR4/CXCR7–CXCL12 axis has immunomodulatory as well as remyelinating potential in neuroinflammatory diseases such as MS. Further studies are required to assess the relevance of the CXCR3/CXCR7–CXCL11 axis in the progression and development of MS.

## 1.5 CXCR3/CXCR4/CXCR7/CXCL11/CXCL12 modulators

### 1.5.1 (Pre)clinical development of CXCR3/CXCR4/CXCR7/CXCL11/CXCL12 modulators in cancer and multiple sclerosis

Modulation of the CXCR3/CXCR4/CXCR7–CXCL11/CXCL12 axis has been shown to alter disease severity in different preclinical disease models, especially in models for various types of cancer and MS. Among the various modulators, few have reached the clinical development stage (Table 1).

To date, only one CXCR3 antagonist has reached clinical development, namely, AMG-487, which is a selective and potent small molecule. However, due to the lack of efficacy in patients with an autoimmune disease (i.e., psoriasis), further clinical development of AMG-487 was stopped. Subsequent preclinical investigations demonstrated that AMG-487 inhibits metastasis formation in various tumor models, indicating promising efficacy in the treatment of cancer [116,117,149–151].

Inhibition of CXCR3 in the context of MS was mainly studied using CXCR3 knockout animals. In addition, multiple patent applications for small-molecule CXCR3 antagonists were filed for the treatment of (auto)immune diseases emphasizing the potential of CXCR3 modulators in this field. Unfortunately, on these, only limited data are publicly available [152]. JT07, an antibody inhibiting CXCR3 and CXCR7, is being developed as a treatment against inflammatory bowel diseases and solid tumors by Jyant Technologies Inc [153]. JT06, which is an anti-CXCL11 antibody, is being preclinically developed by the same company as a treatment for MS [153]. Unfortunately, no published data detailing their physicochemical properties and/or preclinical *in vitro/vivo* profiles are available. Another CXCL11 modulator is BKT130, a peptibody that demonstrated inhibitory properties of multiple chemokines including but not limited to CXCL11. In an EAE model, BKT130 inhibited infiltration of immune cells into the CNS and reduced demyelination [154]. However, as BKT130 also binds to other chemokines it is assumed that the improvement in the disease outcome upon treatment cannot only be attributed to CXCL11.

The CXCR4 antagonist plerixafor (AMD3100) was evaluated in numerous animal models and was investigated in humans for the treatment of acute myeloid leukemia, among other diseases (Table 1) [155,156]. Plerixafor (Mozobil®) is authorized to mobilize hematopoietic stem cells in non-Hodgkin's lymphoma patients. Further testing in metastatic pancreatic cancer is planned. Other CXCR4 antagonists that have been investigated in clinical studies include ulocuplumab (BMS-936564), a monoclonal antibody for the treatment of acute myeloid leukemia [157,158], LY2510924, a small molecule against advanced cancer [159], motixafortide (BL-8040, BKT140), a short synthetic peptide for mobilization of hematopoietic stem cells for treatment of acute myeloid leukemia and solid tumors [160–162], balixafortide (POL6326), a cyclic peptide for the treatment of metastatic breast cancer [163],

USL311, a small molecule against solid tumors and relapsed/recurrent glioblastoma, and burixafor (TG-0054), which is a small molecule investigated as treatment in patients with multiple myeloma, non–Hodgkin's lymphoma, Hodgkin's lymphoma, or prostate cancer [164]. Noxxon Pharma developed the oligonucleotide olaptesed pegol (NOX-A12) to target CXCL12 in different types of cancer including glioblastoma, metastatic pancreatic, and colorectal cancer [165,166]. Recently, Song *et al.* discovered a selective and potent CXCR4 antagonist, namely, BPRCX807, which is in the preclinical stage being developed for the treatment of hepatocellular carcinoma [118].

CXCR4 and CXCL12 modulators have generally demonstrated favorable safety and tolerability profiles in adults with different types of cancer (Table 1). The incidence of adverse events in clinical trials was comparable across the CXCR4 and CXCL12 modulator groups [155,158,161,165,167–170]. The most commonly reported adverse events in clinical trials were injection site reaction, gastrointestinal disorders such as diarrhea and nausea, and hematological changes (e.g., neutropenia). Thus far, safety and tolerability data in children were reported for the approved CXCR4 modulator plerixafor only. In children, plerixafor provoked CNS-related adverse events including but not limited to visual hallucinations and nightmares. Therefore, treatment with plerixafor in children should be carefully assessed [171,172].

Based on the available study results from patient trials listed in Table 1, treatment with a CXCR4 or CXCL12 modulator showed, in general, beneficial efficacy results based on, e.g., overall survival or disease progression. However, some studies could not demonstrate efficacy. For example, although treatment with LY2510924 was safe and well tolerated, the effect in patients with RCC showed no improved efficacy compared to the anti-angiogenic treatment group [168]. Furthermore, recent preliminary data indicated no improvement in disease response in patients with HER2-negative breast cancer upon treatment with balixafortide. Despite the unfavorable results of the clinical trial in advanced breast cancer, additional oncology and non-oncology indications for balixafortide will be evaluated. Of note, none of the CXCR4 or CXCL12 modulators have been tested in patients with MS yet, even though promising preclinical efficacy data were presented [129].

CXCR7 modulators have not been clinically investigated to date. However, a number of CXCR7 antagonists (CCX771, CCX662, CCX733, CCX754, and CCX777) have been investigated in preclinical models [173,174]. While CCX771 demonstrated antagonism of CXCR7 in animals, it also showed agonistic properties due to its ability to recruit β-arrestin [175]. Pfizer discovered a selective CXCR7 antagonist (described as "compound 10"), which competes with CXCL12 to bind CXCR7 and can inhibit the β-arrestin pathway *in vitro*. According to the *in vitro* and *in vivo* PK profiles, compound 10

requires further optimization in terms of absorption, distribution, metabolism, and excretion (ADME) characteristics and potency, in order to test it in *in vivo* animal models [176].

In summary, currently very sparse published data are available from safety studies in animals with CXCR7 modulators, although several pharmacology studies with these modulators have been performed. Additional toxicological characterization in animals and further investigations in humans are needed to understand the impact of CXCR7 modulation in cancer and MS.

**Table 1: (Pre)clinical development of CXCR3/CXCR4/CXCR7–CXCL11/CXCL12 axis in cancer and MS**

| Compound | Indication | References | Development stage |
|---|---|---|---|
| **AMG487** | Breast cancer | [116,151] | Preclinical |
| | Colon carcinoma | [117] | Preclinical |
| | Osteosarcoma | [149,150] | Preclinical |
| | Psoriasis | n.a. | Clinical |
| **JT07** | Solid tumors (and inflammatory bowel diseases) | [153] | Preclinical |
| **JT06** | MS | [153] | Preclinical |
| **BKT130** | MS | [154] | Preclinical |
| **Plerixafor (AMD3100)** [b] | Multiple myeloma | [170]; NCT00103662 | Clinical |
| | Non-Hodgkin's lymphoma | [169]; NCT00733824 | Clinical |
| | Relapsed/refractory AML | [155]; NCT00512252 | Clinical |
| | Head and neck cancer | NCT04058145 | Clinical |
| | Chronic lymphocytic leukemia or small lymphocytic lymphoma | [167]; NCT00694590 | Clinical |
| | Metastatic pancreatic cancer | NCT04177810 | Clinical |
| | Glioblastoma | NCT03746080 | Clinical |
| | Ovaria cancer | [92] | Preclinical |
| | MS | [129] | Preclinical |
| **USL311** | Solid tumor and relapsed/recurrent glioblastoma | NCT02765165 | Clinical |
| **Burixafor (TG-0054)** | Multiple myeloma; non–Hodgkin's lymphoma; Hodgkin's lymphoma | [164]; NCT01458288; NCT02104427; NCT01018979 | Clinical |
| | Prostate cancer | NCT02478125 | Clinical |
| **Ulocuplumab (BMS-936564)** | Relapsed multiple myeloma | [158] | Clinical |
| **LY2510924** | Relapsed/refractory AML | NCT02652871 | Clinical |
| | Small cell lung carcinoma | NCT01439568 | Clinical |
| | RCC | [168] | Clinical |
| | Non–Hodgkin's lymphoma; RCC; lung, breast, and colon cancer cells | [177] | Preclinical |
| | Metastatic pancreatic cancer | NCT02826486, NCT03193190 | Clinical |

| Compound | Indication | References | Development stage |
|---|---|---|---|
| **Motixafortide BL-8040, BKT140)** | Locally advanced unresectable or metastatic gastric or gastroesophageal junction cancer or esophageal cancer | NCT03281369 | Clinical |
| | Relapsed/refractory AML | NCT02763384, NCT01838395, NCT03154827 | Clinical |
| | Multiple myeloma | [160,161], NCT03246529 | Clinical |
| | Non-small cell lung cancer | [178] | Preclinical |
| | Non-Hodgkin's lymphoma | [179] | Preclinical |
| | CML | [180] | Preclinical |
| **Balixafortide (POL6326)** | Metastatic breast cancer | [163], NCT01837095, NCT03786094 | Clinical |
| | Multiple myeloma | NCT01105403 | Clinical |
| | Hematologic malignancies | NCT01413568 | Clinical |
| **BPRCX807** | Hepatocellular carcinoma | [118] | Preclinical |
| **Olaptesed pegol (NOX-A12)** | Relapsed/refractory CLL | [165], NCT01486797 | Clinical |
| | Relapsed multiple myeloma | [181], NCT01521533 | Clinical |
| | Glioblastoma | NCT04121455 | Clinical |
| | Colorectal and pancreatic cancer | [166,182], NCT03168139 | Clinical |
| **CCX771** | Castration-resistant prostate cancer | [86] | Preclinical |
| | Breast cancer | [111] | Preclinical |
| | Glioblastoma | [183] | Preclinical |
| | Pulmonary inflammation | [184] | Preclinical |
| | MS | [80,131] | Preclinical |
| **CCX662** | Glioblastoma | [183] | Preclinical |
| **X7Ab** | Glioblastoma | [185] | Preclinical |

This table provides an overview of CXCR3, CXCR4, CXCR7, CXCL11, and CXCL12 modulators tested for cancer and MS in preclinical and clinical development. Adapted from [6].

[a] Several reports/publications claimed that AMG-487 failed to demonstrate efficacy leading to study termination however, data are not publicly available.

[b] A detailed summary of clinical trials which investigated plerixafor for the indications multiple myeloma and non-Hodgkin's lymphoma is provided in the Mobozil product monograph [186].

AML = acute myeloid leukemia; CCL = chronic lymphocytic leukemia; CML = chronic myeloid leukemia; MS = multiple sclerosis; n.a. = not available; RCC = renal cell carcinoma.

### 1.5.2 ACT-1004-1239, a first-in-class CXCR7 antagonist

To date, several CXCR7 modulators have been investigated however, thus far only for non-clinical purposes. It has been emphasized that CXCR7 is involved in several diseases including cancer and MS and its antagonism results in an improvement of disease outcome in preclinical animal models. Hence, there is an unmet need for a CXCR7 antagonist for clinical use. ACT-1004-1239 represents a first-in-class CXCR7 antagonist, which exhibits promising preclinical characteristics and supports further investigations in humans. This novel CXCR7 antagonist was selected out of 300'000 compounds of the high throughput screening (HTS) deck from Idorsia Pharmaceuticals Ltd. using an innovative HTS assay. The optimal candidate, ACT-1004-1239, was chosen based on the structure-activity and structure-property relationships of the functional groups of the molecule as described in detail by Richard-Bildstein *et al.* [187]. In a nutshell, the selection of the lead compound was driven by several considerations, including the potency, hERG channel inhibitory activity, ADME and toxicity (ADMET) characteristics, and physicochemical properties such as solubility and basicity. While the potency and the hERG channel inhibitory activity were mainly assessed using the $IC_{50}$ values for the respective targets, the early determination of the ADMET characteristics focused predominantly on the intrinsic clearance parameter. Finally, ACT-1004-1239 was defined as a potent and selective small molecule (Figure 5). It also shows an insurmountable behavior, which describes the ability of the compound to have constant potency in the presence of increasing concentrations of the natural ligands, i.e., CXCL11 and CXCL12 [187].

Based on preclinical pharmacokinetic (PK) studies, ACT-1004-1239 was considered a high-clearance drug in rats and a low-clearance drug in dogs. The absolute bioavailability was higher in dogs (61%) than in rats (35%). These data supported the selection of dose levels and dosing regimen in subsequent animal studies. Subsequent studies in healthy mice were conducted to evaluate *in vivo* target engagement of ACT-1004-1239 by measuring CXCL11 and CXCL12 plasma concentrations after single oral doses ranging from 1 to 100 mg/kg ACT-1004-1239. CXCL12 plasma concentration increased in a dose-dependent manner, and the duration of increase correlated positively with the dose. In contrast, there was no significant increase in CXCL11 plasma concentration observed as could be expected in healthy animals [187].

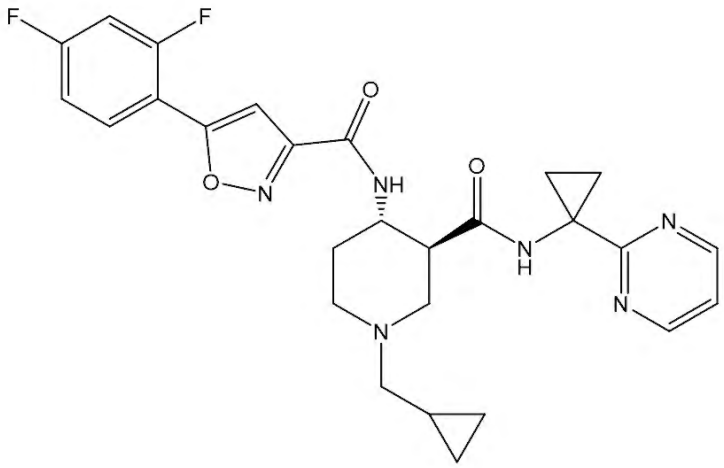


**Figure 5: Molecular structure of ACT-1004-1239**
Adapted from [188].

Following drug discovery and first investigations of ACT-1004-1239 in healthy animals, the effect of ACT-1004-1239 was further evaluated in various animal models of MS and acute lung injury (ALI). In myelin oligodendrocyte glycoprotein- (MOG) induced EAE mice representing a model of MS, treatment with ACT-1004-1239 led to a significant dose-dependent increase in CXCL12 plasma concentration along with almost complete inhibition of CXCR4+ leukocyte infiltration into the CNS. This finding confirmed the previous assumption that inhibition of the scavenging activity of CXCR7 in plasma would lead to disruption of the chemokine concentration gradient. In addition, the increase in CXCL12 plasma levels was positively correlated with an overall reduction in disease score in the murine model. Unfortunately, the impact of ACT-1004-1239 on CXCL11 levels could not be assessed due to the absence of CXCL11 expression in the mouse strain used for the study. Hence, the role of the CXCR3/CXCR7–CXCL11 axis could not be investigated in this MOG-induced EAE model [146]. Nevertheless, in a CXCL11-expressing EAE model (proteolipid protein- [PLP] induced), CXCL11 and CXCL12 plasma concentrations were elevated after treatment with ACT-1004-1239. Apart from plasma, ACT-1004-1239 was detected in the brain leading also to an increase in brain CXCL12 concentration [189]. In addition to the immunomodulatory effect, a pro-myelinating effect of ACT-1004-1239 was observed in a cuprizone-induced model. Treatment with ACT-1004-1239 resulted in a significant increase in myelination in the corpus callosum, which was shown to be linked to an OPC maturation. This promotion of OPC maturation into mature myelinating oligodendrocytes was suggested to be driven by the CXCR4–CXCL12 axis [146]. While the MS models indicated a dual mode of action of ACT-1004-1239 (i.e., immunomodulatory and pro-myelinating effects), the immunomodulatory effect was verified in an animal model of ALI. Results from the ALI model confirmed the immunomodulatory effect of ACT-1004-1239 observed in the MS model. In detail, mice that were treated with nebulized lipopolysaccharide (LPS) experienced a significant increase in CXCR3

and CXCR4 ligands, including CXCL11 and CXCL12, in the bronchoalveolar lavage (BAL), resulting in a significant local increase in CXCR3+ lymphoid and CXCR4+ myeloid cells. Treatment with ACT-1004-1239 led to a dose-dependent increase of CXCL11 and CXCL12 plasma levels accompanied by a significant decrease in CXCR3+ and CXCR4+ immune cell infiltration. These data suggest a treatment-related disruption of the chemokine gradients towards the inflamed lung tissue. Furthermore, CXCR7 antagonism by treatment with ACT-1004-1239 reduced vascular permeability and breathing dysfunction [82]. A summary of the main preclinical characteristics of ACT-1004-1239 is provide in Table 2.

**Table 2: Preclinical characteristics of ACT-1004-1239**

| ACT-1004-1239 characteristics | | |
|---|---|---|
| **Physicochemical properties** [187] | | |
| Basicity | Weak base | pKa = 7.7 |
| Lipophilicity | Log D | <2.7 |
| Solubility | Aqueous | 374 mg/mL (pH = 7) |
| | FaSSIF | 513 mg/mL |
| | FeSSIF | >880 mg/mL |
| Potency to CXCR7 ($IC_{50}$) | Human | 3.2 nM |
| | Dog | 2.3 nM |
| | Rat | 3.1 nM |
| | Mouse | 2.3 nM |
| **Animal pharmacokinetics** [187] | | |
| $t_{max}$ | Dog | 1.5 h |
| | Rat | 0.5 h |
| CL | Dog | 2.8 and 3.8 mL/min/kg (low-clearance drug) |
| | Rat | 70 mL/min/kg (high-clearance drug) |
| $V_{ss}$ | Dog | 1.6 L/kg |
| | Rat | 3.6 L/kg |
| Absolute bioavailability | Dog | 61% |
| | Rat | 35% |
| **Animal disease models** | | |
| Multiple sclerosis [124,146,189] | – Plasma CXCL11 ↑<br>– Plasma CXCL12 ↑<br>– Brain CXCL12 ↑<br>– Immune cell infiltration to the brain ↓<br>– OPC maturation and remyelination ↑ | |
| Acute lung injury[82] | – Plasma CXCL11 ↑<br>– Plasma CXCL12 ↑<br>– Immune cell infiltration to the BAL ↓<br>– Breathing pattern ↑<br>– Vascular barrier dysfunction ↓ | |

This table summarizes the main preclinical data of ACT-1004-1239.

BAL = bronchoalveolar lavage; CL = clearance; FaSSIF = fasted state simulated intestinal fluid; FeSSIF = fed state simulated intestinal fluid; $IC_{50}$ = half maximal inhibitory concentration; OPC = oligodendrocyte precursor cell; $t_{max}$ = time to reach maximum plasma concentration; $V_{ss}$ = volume of distribution at steady state.

Taken together, the potent, insurmountable, selective, and orally available small-molecule CXCR7 antagonist, ACT-1004-1239, exhibits physicochemical as well as biological properties that warrant continuation of drug development. The compound was efficacious in animal models of MS and ALI, as shown by an improvement in clinical score following treatment. The efficacy was predominantly attributed to inhibition of the scavenging activity of CXCR7 and the resulting increase in CXCL11 and CXCL12 plasma levels accompanied by a reduction in immune cell infiltration towards the inflamed tissue (i.e., immunomodulatory effect). In addition, the MS model provided evidence of a second mode of action describing an enhancement in myelination (i.e., pro-myelinating effect). Based on the overall preclinical data, ACT-1004-1239 showed favorable characteristics for further investigations in humans, and thus, represents a first-in-class CXCR7 antagonist.

# 2 AIMS OF THE THESIS

The overall aim of this dissertation is to investigate the clinical pharmacology profile of ACT-1004-1239, a first-in-class CXCR7 antagonist, in healthy subjects as part of the clinical development program. For this purpose, two clinical pharmacology studies were conducted, which were reported in three publications provided below. In addition, based on the results obtained from these two studies, the need for a drug-drug interaction (DDI) study was identified, and the study concept has been developed (described in Section 3.4).

1. **Single-ascending dose study with ACT-1004-1239**

   To investigate the safety/tolerability, PK (including food effect and absolute bioavailability), and PD of single-dose (1-200 mg) ACT-1004-1239 in healthy male subjects.

2. **Absorption, distribution, metabolism, and excretion profile of ACT-1004-1239**

   To investigate, supported by the use of preclinical data, the ADME characteristics of ACT-1004-1239 in healthy male subjects.

3. **Multiple-ascending dose study with ACT-1004-1239**

   To investigate the safety/tolerability, PK, PD, and concentration-QTc relationship of multiple-dose (30-200 mg) ACT-1004-1239 in healthy male and female subjects.

4. **Further clinical development of ACT-1004-1239: Drug-drug interaction study**

   To conceptualize a DDI study of ACT-1004-1239 with a strong CYP3A4 inhibitor.

# CHAPTER 2

# Clinical Pharmacology of ACT-1004-1239

Single-ascending dose study with ACT-1004-1239

Absorption, distribution, metabolism, and excretion profile of ACT-1004-1239

Multiple-ascending dose study with ACT-1004-1239

Further clinical development of ACT-1004-1239: Drug-drug interaction study

# 3 CLINICAL PHARMACOLOGY OF ACT-1004-1239

## 3.1 Single-ascending dose study with ACT-1004-1239

# A Multipurpose First-in-Human Study With the Novel CXCR7 Antagonist ACT-1004-1239 Using CXCL12 Plasma Concentrations as Target Engagement Biomarker

Christine Huynh[1,2], Andrea Henrich[1], Daniel S. Strasser[1], Marie- Laure Boof[1], Mohamed Al- Ibrahim[3], Henriette E. Meyer Zu Schwabedissen[2], Jasper Dingemanse[1] and Mike Ufer[1]

[1]Idorsia Pharmaceuticals Ltd, Department of Clinical Pharmacology, Allschwil, Switzerland
[2]University of Basel, Biopharmacy, Department of Pharmaceutical Sciences, Basel, Switzerland
[3]Pharmaron CPC Inc., Baltimore, MD, United States

Published in Clin Pharmacol Ther. 2021;109(6):1648-1659

ARTICLE

# A Multipurpose First-in-Human Study With the Novel CXCR7 Antagonist ACT-1004-1239 Using CXCL12 Plasma Concentrations as Target Engagement Biomarker

Christine Huynh[1,2], Andrea Henrich[1], Daniel S. Strasser[1], Marie-Laure Boof[1], Mohamed Al-Ibrahim[3], Henriette E. Meyer Zu Schwabedissen[2], Jasper Dingemanse[1] and Mike Ufer[1,*]

The C-X-C chemokine receptor 7 (CXCR7) has evolved as a promising, druggable target mainly in the immunology and oncology fields modulating plasma concentrations of its ligands CXCL11 and CXCL12 through receptor-mediated internalization. This "scavenging" activity creates concentration gradients of these ligands between blood vessels and tissues that drive directional cell migration. This randomized, double-blind, placebo-controlled first-in-human study assessed the safety, tolerability, pharmacokinetics, and pharmacodynamics of ACT-1004-1239, a first-in-class drug candidate small-molecule CXCR7 antagonist. Food effect and absolute bioavailability assessments were also integrated in this multipurpose study. Healthy male subjects received single ascending oral doses of ACT-1004-1239 ($n$ = 36) or placebo ($n$ = 12). At each of six dose levels (1–200 mg), repeated blood sampling was done over 144 hours for pharmacokinetic/pharmacodynamic assessments using CXCL11 and CXCL12 as biomarkers of target engagement. ACT-1004-1239 was safe and well tolerated up to the highest tested dose of 200 mg. CXCL12 plasma concentrations dose-dependently increased and more than doubled compared with baseline, indicating target engagement, whereas CXCL11 concentrations remained unchanged. An indirect-response pharmacokinetic/pharmacodynamic model well described the relationship between ACT-1004-1239 and CXCL12 concentrations across the full dose range, supporting once-daily dosing for future clinical studies. At doses ≥ 10 mg, time to reach maximum plasma concentration ranged from 1.3 to 3.0 hours and terminal elimination half-life from 17.8 to 23.6 hours. The exposure increase across the dose range was essentially dose-proportional and no relevant food effect on pharmacokinetics was determined. The absolute bioavailability was 53.0% based on radioactivity data after oral vs. intravenous $^{14}$C-radiolabeled microtracer administration of ACT-1004-1239. Overall, these comprehensive data support further clinical development of ACT-1004-1239.

## Study Highlights

**WHAT IS THE CURRENT KNOWLEDGE ON THE TOPIC?**

☑ The chemokine receptor CXCR7 modulates immune and cancer cell migration by scavenging CXCL11 and CXCL12. Preclinically, blockade of CXCR7 not only inhibits directional cell migration towards inflammatory sites or tumor tissue, but also has promyelinating effects, suggesting a dual mode of action for CXCR7 antagonists in the treatment of multiple sclerosis and other demyelinating diseases.

**WHAT QUESTION DID THIS STUDY ADDRESS?**

☑ This first-in-human study provides comprehensive pharmacokinetic (PK), pharmacodynamic (PD), and safety data for escalating single oral doses of the first-in-class candidate CXCR7 antagonist ACT-1004-1239.

**WHAT DOES THIS STUDY ADD TO OUR KNOWLEDGE?**

☑ ACT-1004-1239 was safe and well tolerated across a wide dose range in healthy subjects. It dose-dependently increased plasma concentrations of its ligand CXCL12, thereby confirming target engagement. Its PK and PD profiles allow for once-daily dosing in future clinical studies as confirmed by PK/PD modeling.

**HOW MIGHT THIS CHANGE CLINICAL PHARMACOLOGY OR TRANSLATIONAL SCIENCE?**

☑ These study data allow for further exploring the clinical efficacy of ACT-1004-1239 in patients and thereby of CXCR7 antagonism as new treatment modality in immunology and oncology.

[1]Idorsia Pharmaceuticals Ltd, Allschwil, Switzerland; [2]University of Basel, Basel, Switzerland; [3]Pharmaron CPC Inc, Baltimore, Maryland, USA.
*Correspondence: Mike Ufer (mike.ufer@idorsia.com)

Received September 21, 2020; accepted December 4, 2020. doi:10.1002/cpt.2154

Chemokine receptors are of major relevance for the development and progression of various pathological conditions, including different types of autoimmune disorders and cancer.[1–3] They can be classified into four subtypes, namely CXC, CC, C, or CX3C, based on the amino acid sequence of their chemokine ligands.[4] Upon activation they are involved in various inflammatory or homeostatic processes, including cell trafficking, to guide different cell types to specific locations in the body.[5]

The C-X-C chemokine receptor 7 (CXCR7) is mainly expressed in endothelial cells and known as atypical chemokine receptor (ACKR) 3, since it triggers cell signaling not via G proteins but through recruitment of ß-arrestin.[6] CXCR7 is primarily activated by two chemokine ligands, namely CXCL11 and CXCL12.[7,8] CXCL11 is an inflammatory chemokine that is induced in particular by interferon-ß /interferon-γ under certain inflammatory conditions.[9] By contrast, CXCL12 is a homeostatic chemokine with constitutive expression in several organs under physiological conditions and with increased expression under pathological conditions, including inflammation, hypoxia, or cancer.[10,11]

The binding affinity to CXCR7 is approximately 10-fold to 20-fold higher for CXCL12 than for CXCL11.[8,12] CXCL12 is also a ligand of CXCR4, but with an approximately 10-fold lower binding affinity than to CXCR7.[13,14] CXCL11 is not only a ligand of CXCR7, but also of CXCR3, whereas it does not bind to CXCR4.[8,15]

Mechanistically, binding of either CXCL11 or CXCL12 to CXCR7 leads to recruitment of ß-arrestin followed by internalization of the CXCR7-ligand complex, and subsequent degradation of the ligand.[6,16] This "scavenging" activity is a well-established function of CXCR7 that contributes to the establishment and maintenance of CXCL11 and CXCL12 concentration gradients, e.g., between blood vessels and tissues.[17] These gradients enable directional migration of CXCR4-positive cells to sites of inflammation.[18,19] Blocking this "scavenging" activity of CXCR7 can lead to increased systemic CXCL11 and CXCL12 concentrations, thereby disrupting the chemokine gradients and inhibiting the migration of those proinflammatory cells.[20]

In addition to effects on cell migration, blockade of CXCR7 and elevation of CXCL12 concentrations promote maturation of oligodendrocyte precursor cells (OPCs) via CXCR4 activation leading to myelin repair after a central nervous system injury.[21] Accordingly, the expression of CXCR7 on OPCs is enhanced during demyelination in different murine demyelination models[22] but returns to baseline during remyelination.[21] Therefore, CXCR7 and its ligands have been proposed as druggable targets for treatment of autoimmune diseases such as multiple sclerosis, an inflammatory demyelinating disease.[23] In addition, the CXCL12-CXCR4/CXCR7 pathway may also have therapeutic potential in the oncology field, as different agents targeting this pathway have been shown to reduce migration of myeloid cells to the tumor and enhance antitumor effects of both radiotherapy and antiangiogenic therapy.[3,24–27]

The immunomodulatory effects via inhibition of cell migration and the promyelinating effects via promotion of OPC maturation suggest a dual mode of action for CXCR7 antagonists in inflammatory demyelinating diseases (**Figure 1**).

Clinical data with a CXCR7 antagonist has not been reported until now and as such the potent and selective CXCR7 antagonist ACT-1004-1239 represents a first-in-class drug candidate. In preclinical studies, target engagement was determined in animal models indicated by a dose-dependent increase of CXCL12 plasma concentrations following single-dose administration of ACT-1004-1239.[28] Accordingly, plasma concentrations of CXCL11 and CXCL12 were also used as biomarkers of target engagement in this first-in-human (FIH) study, i.e., CXCR7 antagonism.

Here, we report on results from an FIH study that primarily determined the safety, tolerability, pharmacokinetics (PK), and pharmacodynamics (PD) of escalating doses of ACT-1004-1239 in healthy subjects. A multipurpose design has been applied to accelerate the clinical development of ACT-1004-1239 by assessing the effect of food intake on the PK of ACT-1004-1239 as well as its absolute bioavailability after oral administration of ACT-1004-1239 and intravenous administration of $^{14}$C-radiolabeled ACT-1004-1239 as microtracer followed by quantification using ultrasensitive accelerator mass spectrometry technology.

## METHODS

### Study design

This was a randomized, double-blind, placebo-controlled FIH study to investigate the safety, tolerability, PK, and PD of single ascending oral doses of ACT-1004-1239 in healthy male subjects (ClinicalTrials.gov: NCT03869320). In addition, the impact of food intake on the PK of ACT-1004-1239 and its absolute bioavailability were determined.

The study protocol was approved by the local Institutional Review Board (Austin, TX). The study was performed at a single center by Pharmaron CPC (Baltimore, MD) in accordance with Good Clinical Practice and the Declaration of Helsinki.

In total, six dose levels of ACT-1004-1239 were investigated, namely, 1, 3, 10, 30, 100, and 200 mg. At each dose level, six subjects received hard gelatin capsules of ACT-1004-1239 and two subjects matching placebo capsules. The capsules containing ACT-1004-1239 were formulated at dose strengths of 1, 10, and 100 mg. Following single oral dosing under fasted conditions in the morning, each study subject was kept domiciled at the study center for seven days. The end-of-study assessments were performed 14 days after study drug intake.

At each dose level, sentinel dosing was applied, i.e., two subjects were initially exposed to ACT-1004-1239 or placebo followed by a 24-hour safety observation period after which the other six subjects were exposed. After completion of each dose level, a thorough review of all available safety, tolerability, and PK data was done to decide on further dose escalation.

### Food effect and absolute bioavailability assessment

The effect of a US Food and Drug Administration (FDA)–standard high-fat breakfast on the PK of ACT-1004-1239 was investigated, applying a fixed-sequence, two-period design. Each subject received a single oral dose of 30 mg ACT-1004-1239 or placebo under fasted and fed conditions in the first and second period, respectively, separated by a washout period of at least 2 weeks.

The absolute bioavailability of ACT-1004-1239 was determined at the 200-mg dose level. For this purpose, each of the six subjects randomized to active treatment received an oral dose of nonradioactive ACT-1004-1239 followed by intravenous administration of 1 μCi (9.2 μg) $^{14}$C-radiolabeled ACT-1004-1239 as 15-minute infusion starting 3 hours after oral drug intake, i.e., approximately at the time of maximum plasma concentration ($t_{max}$) of ACT-1004-1239. Both subjects randomized to placebo received

ARTICLE

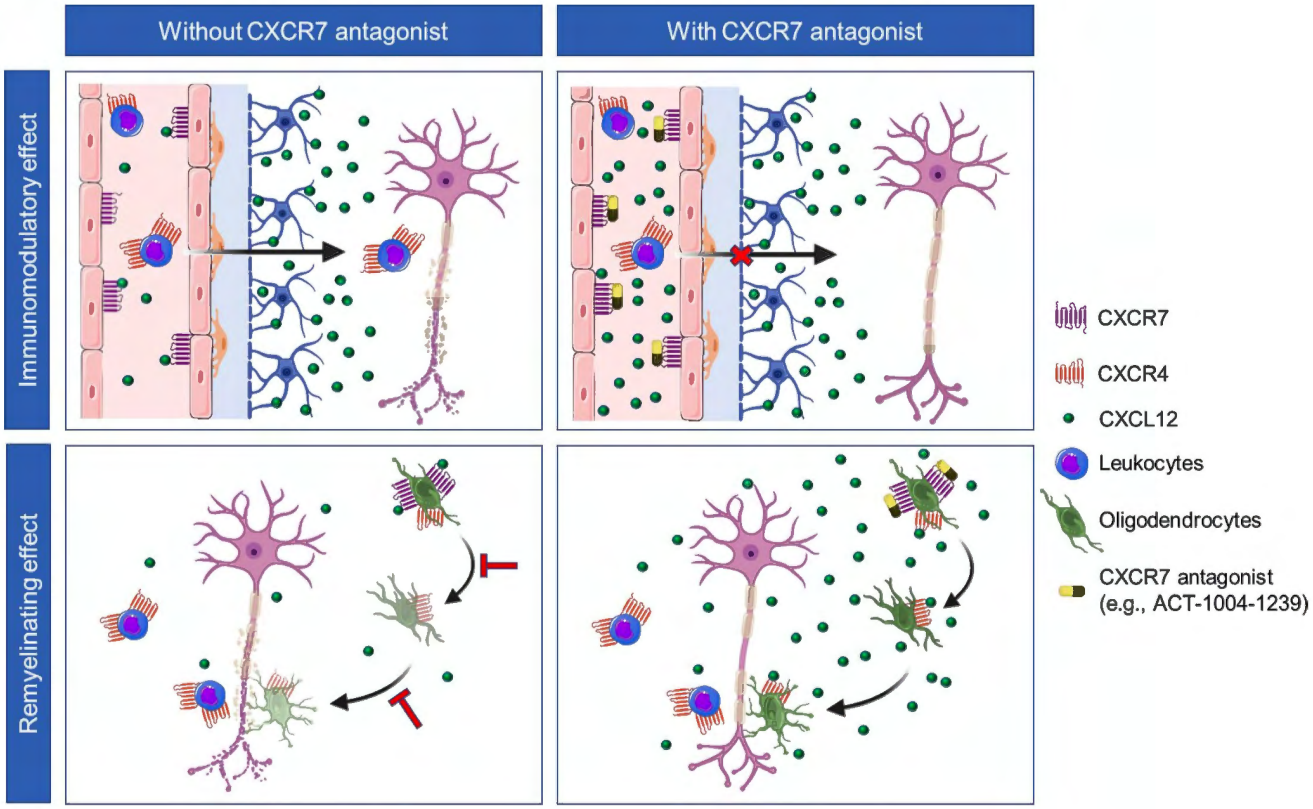


**Figure 1** Dual mode of action of CXCR7 antagonists in inflammatory demyelinating diseases. This figure illustrates the hypothesized dual mode of action (i.e., immunomodulatory and remyelinating effects) of a CXCR7 antagonist, like ACT-1004-1239, in the context of inflammatory demyelinating diseases such as multiple sclerosis. *Immunomodulatory effect:* In the absence of a CXCR7 antagonist (upper left), CXCL12 concentrations are higher in the parenchyma than in blood vessels due to augmented endothelial expression of CXCR7 and hence stronger scavenging/internalization of CXCL12. This concentration gradient triggers migration of CXCR4-positive inflammatory leukocytes. In the presence of a CXCR7 antagonist (upper right), the scavenging activity of CXCR7 is blocked, thereby disrupting the concentration gradient and hence inhibiting cell migration. *Remyelinating effect:* In the absence of a CXCR7 antagonist (lower left), increased CXCR7 expression on oligodendrocyte precursor cells (OPCs) with enhanced scavenging/internalization of CXCL12 leads to reduced CXCL12 concentrations and CXCL12-mediated activation of CXCR4, which in turn impairs cell maturation/differentiation. In the presence of a CXCR7 antagonist (lower right), increased CXCL12 concentrations result in greater CXCR4 activation expected to normalize cell maturation/differentiation and remyelination. CXCR7, C-X-C chemokine receptor 7.

placebo capsules followed by a 15-minute infusion of 0.9% sodium chloride.

Mass balance determination and metabolite profiling/identification were also integrated in the present study and will be reported separately. For this purpose, each of the six subjects randomized to active treatment orally received 1 μCi (9.2 μg) $^{14}$C-radiolabeled ACT-1004-1239 together with 100 mg of nonradioactive ACT-1004-1239.

### Study population

The study population comprised healthy male subjects aged between 18 and 55 years with a body mass index of 18.0 to 30.0 kg/m$^2$. Informed consent was obtained from each subject prior to any procedure, and eligibility was determined based on physical examination, medical history, vital sign, electrocardiogram (ECG), and clinical laboratory data.

### Safety and tolerability

Safety and tolerability were assessed based on adverse event (AE), vital sign (blood pressure, heart rate, and body temperature), 12-lead ECG, and clinical laboratory data. The intensity of each AE was classified according to the Common Terminology Criteria For Adverse Events (CTCAE) grading system (version 5) with AEs of mild, moderate, or severe intensity corresponding to CTCAE grades 1, 2, or 3, respectively.[29]

### Pharmacodynamic biomarker analysis and evaluation

In each subject, PD blood sampling was done before dosing and at 1, 2, 4, 6, 8, 10, 12, 24, 48, 72, 96, 120, and 144 hours after dosing. At each timepoint, ~ 4 mL blood was collected in EDTA-containing tubes. After centrifugation (1800 g; 10 minutes), aliquoted plasma samples were stored at −70°C until analysis.

CXCL11 plasma concentrations were determined by using an U-Plex Immunoassay kit (Meso Scale Diagnostics, Rockville, MD). The mean coefficient of variation of quality control samples was 14.5% and the lower limit of quantification was 7.6 pg/mL.

CXCL12 plasma concentrations were determined by an Ella immunoassay (Bio-Techne, Minneapolis, MN, US). The mean coefficient of variation of quality control samples was 6.8% and the lower limit of quantification was 604 pg/mL.

The maximum individual change from baseline of CXCL11 and CXCL12 plasma concentrations at any timepoint during the 144-hour collection interval was defined as maximum effect ($Eff_{max}$). In addition, the time to reach the $Eff_{max}$ and the area under the effect-time curve (AUEC) from 0 to 144 hours post dose were determined using the trapezoidal rule.

### Pharmacokinetic bioanalysis and evaluation

In each subject, PK blood sampling was done before dosing and at 0.5, 1, 1.5, 2, 3, 4, 6, 8, 10, 12, 14, 16, 24, 36, 48, 60, 72, 96, 120,

and 144 hours after dosing. At each timepoint, ~ 4 mL blood was collected in EDTA-containing tubes. For the absolute bioavailability assessment, 15 additional samples were collected at selected timepoints. After centrifugation, aliquoted plasma samples were stored at −70°C until analysis. Further details regarding the bioanalytical method and determination of PK parameters are provided as **supplementary material**.

### Pharmacokinetic/pharmacodynamic modeling

A population PK/PD model was developed. The PK model described plasma concentrations of ACT-1004-1239 and $^{14}$C-radiolabeled ACT-1004-1239. Linear one-compartment, two-compartment, and three-compartment models were investigated. In addition, nonlinear clearance, bioavailability, and distribution were tested. The effect of food was evaluated as covariate on absorption lag time. The PD model described CXCL12 concentrations by an indirect response with drug effect on the elimination rate constant of CXCL12, since ACT-1004-1239 blocks CXCR7-mediated scavenging of CXCL12. A positive feedback mechanism was investigated which reduced the elimination rate of CXCL12 with increasing plasma concentrations of CXCL12. CXCL12 baseline was described by using the observed baseline allowing for an exponential error similar to the previously published "baseline method B3."[30]

PK/PD modeling was performed sequentially using the estimated individual PK parameters as input for the PK/PD model. Interindividual variability was assumed to be exponentially distributed for all parameters except for absolute bioavailability with a logit distribution to restrict the absolute bioavailability range from 0 to 1. Proportional residual errors were assumed for PK and PD.

Model selection was based on objective function value (OFV) and diagnostic plots such as visual predictive checks (VPC). Simulations ($n$ = 1,000 subjects) were performed assuming absence of time-dependent PK and PD changes to predict multiple-dose PK and PD profiles at once-daily dosing for 7 days and continued up to 50 days to determine the accumulation ratio. In addition, the exposure–response relationship under multiple dosing was predicted.

The model was developed with Monolix 2019R2 (Lixoft, Antony, France). Parameters were estimated with the stochastic approximation expectation maximization algorithm. OFVs were derived by stochastic approximation and standard errors by linearization. Simulations were performed in R 3.6.1 (R Development Core Team, Vienna, Austria) using Simulx 2019R2 (Lixoft, Antony, France).

## RESULTS

### Study population

In total, 48 healthy male subjects received either active study treatment or placebo with a ratio of 6:2 at each of the six dose levels. The mean (range) age and body mass index were 37.7 (20–55) years and 26.4 (20.2–29.9) kg/m$^2$, respectively. The study subjects were predominantly Black or African American ($n$ = 31) and White ($n$ = 14) with only 3 subjects of another ethnicity.

### Safety and tolerability

In total, 21 subjects developed at least one AE, and the overall AE incidence was similar on active treatment and placebo (44.4% vs. 41.7%) without indication of dose-dependency or notable imbalance for any of the reported AEs. Most AEs were mild and transient, and no serious AE was reported (**Table 1**).

The most common AE of orthostatic tachycardia was reported both in subjects exposed to ACT-1004-1239 ($n$ = 4, i.e., 11.1%) or placebo ($n$ = 2, i.e., 16.7%). Each of these AEs was of mild intensity and concerned heart rate differences between supine and standing position in the context of repeated vital sign assessments. Each subject concerned was asymptomatic, and none of these AEs were accompanied by clinically relevant changes of blood pressure or other vital signs.

Elevated creatine phosphokinase (CPK) concentrations were reported as the second most common AE in four subjects at the same incidence on active treatment ($n$ = 3; 8.3%) and placebo ($n$ = 1; 8.3%). These CPK elevations on active treatment were reported as severe AEs although each subject concerned was asymptomatic and had CPK concentrations above the upper limit of normal (i.e., > 170 units/L) already at baseline. The onset time was 24 hours (placebo), 144 hours (200 mg ACT-1004-1239), 2 weeks (30 mg ACT-1004-1239), and 4 weeks (100 mg ACT-1004-1239), with the latter two subjects reporting strong physical exercise, which is a well-known trigger of CPK elevations,[31] during the week prior to the assessment. Overall, there was no indication of dose-dependent changes or postdose elevations of CPK concentrations or any other clinical laboratory parameters regarding clinical chemistry, hematology, coagulation, or urinalysis.

In three subjects, ECG morphology changes were reported as AEs (i.e., ST segment and T-wave abnormalities) of moderate intensity after active treatment ($n$ = 2; 5.5%) at a dose of 200 mg ACT-1004-1239 and of mild intensity after placebo ($n$ = 1; 8.3%). These AEs were asymptomatic and transient. Otherwise, there were no clinically relevant ECG findings or changes of ECG intervals (i.e., PR, QRS, QTcF, and RR). None of the subjects had a QTcF value > 500 milliseconds or a change from baseline of > 60 milliseconds at any timepoint.

### Pharmacodynamics

CXCL11 and CXCL12 plasma concentration-time profiles by dose are depicted in **Figure 2a** and the relationship between dose and CXCL12 plasma concentrations is depicted in **Figure 2c**.

The CXCL12 plasma concentration-time profile indicates maximum concentrations ~ 24 hours after dosing at most dose levels that essentially returned to baseline at 144 hours post dosing (**Figure 2a**).

CXCL12 plasma concentrations increased dose-dependently up to a dose of 100 mg ACT-1004-1239 as compared with mean (SD) baseline concentrations of 2,181 (436) pg/mL (range: 1355–3475). At the highest tested dose of 200 mg ACT-1004-1239, peak CXCL12 plasma concentrations were similar to those at the next lower dose level of 100 mg and more than doubled compared with baseline (**Figure 2c**).

Linear regression analyses of $AUEC_{0\text{-}144h}$ vs. $AUC_{0\text{-}144h}$ and $Eff_{max}$ vs. maximum plasma concentration ($C_{max}$) indicated an association between PD response and drug exposure in line with the dose-dependent increase of CXCL12 plasma concentrations (**Figure 3**).

In contrast to CXCL12, postdose concentrations of CXCL11 remained essentially unchanged from mean (SD) baseline concentrations of 41.3 (28.5) pg/mL (**Figure 2a**).

**Table 1 Incidence and number of adverse events by treatment**

| Adverse event | 1 mg (*N* = 6) | 3 mg (*N* = 6) | 10 mg (*N* = 6) | 30 mg (*N* = 6) | 100 mg (*N* = 6) | 200 mg (*N* = 6) | Active* (*N* = 36) | Placebo (*N* = 12) |
|---|---|---|---|---|---|---|---|---|
| Any adverse event | 3 (50.0) | — | 2 (33.3) | 5 (83.3) | 3 (50.0) | 3 (50.0) | 16 (44.4) | 5 (41.7) |
| Orthostatic tachycardia | — | — | — | 1 (16.7)<br>*1* | 2 (33.3)<br>*2* | 1 (16.7)<br>*1* | 4 (11.1)<br>*4* | 2 (16.7)<br>*3* |
| Elevated CPK concentration | — | — | — | 1 (16.7)[#]<br>*1* | 1 (16.7)[#]<br>*1* | 1 (16.7)[#]<br>*1* | 3 (8.3)[#]<br>*3* | 1 (8.3)<br>*1* |
| Dizziness | — | — | — | 2 (33.3)<br>*2* | — | — | 2 (5.6)<br>*2* | — |
| ECG ST segment abnormality | — | — | — | — | — | 2 (33.3)[§]<br>*3* | 2 (5.6)[§]<br>*3* | — |
| Headache | 2 (33.3)<br>*2* | — | — | — | — | — | 2 (5.6)<br>*2* | — |
| Rash | 1 (16.7)<br>*1* | — | — | 1 (16.7)<br>*1* | — | — | 2 (5.6)<br>*2* | — |
| Anemia | 1 (16.7)<br>*1* | — | — | — | — | — | 1 (2.8)<br>*1* | — |
| Constipation | — | — | — | — | 1 (16.7)<br>*1* | — | 1 (2.8)<br>*1* | — |
| Contact dermatitis | — | — | — | — | — | — | — | 1 (8.3)<br>*1* |
| ECG T-wave abnormality | — | — | — | — | — | — | — | 1 (8.3)<br>*1* |
| Elevated ALAT concentration | — | — | 1 (16.7)<br>*1* | — | — | — | 1 (2.8)<br>*1* | — |
| Elevated ASAT concentration | — | — | — | — | — | 1 (16.7)<br>*1* | 1 (2.8)<br>*1* | — |
| Memory impairment | — | — | 1 (16.7)<br>*1* | — | — | — | 1 (2.8)<br>*1* | — |
| Pain in extremity | — | — | — | — | — | — | — | 1 (8.3)<br>*1* |
| Presyncope | — | — | — | — | — | — | — | 1 (8.3)[§]<br>*1* |
| Proteinuria | — | — | — | 1 (16.7)<br>*1* | — | — | 1 (2.8)<br>*1* | — |
| Rhinorrhea | 1 (16.7)<br>*1* | — | — | — | — | — | 1 (2.8)<br>*1* | — |
| Sinus congestion | — | — | — | 1 (16.7)<br>*1* | — | — | 1 (2.8)<br>*1* | — |
| Throat irritation | — | — | — | 1 (16.7)<br>*1* | — | — | 1 (2.8)<br>*1* | — |

Data are displayed in descending order of frequency. Each row contains the number of subjects with at least one AE (i.e, AE incidence in %) and below the number of AEs in italic (i.e., AE frequency).
AE, adverse event; ALAT, alanine aminotransferase; ASAT, aspartate aminotransferase; CPK, creatine phosphokinase; ECG, electrocardiogram; —, no adverse event.
Moderate ([§]) and severe ([#]) AEs are tagged (i.e., Common Terminology Criteria For Adverse Events (CTCAE) grade 2 and 3, respectively). All other AEs were of mild intensity (i.e., CTCAE grade 1).
*refers to the overall AE incidence and number of AEs reported after any dose of ACT-1004-1239

### Pharmacokinetics

Mean plasma concentration-time profiles of ACT-1004-1239 and its PK parameters by dose are depicted in **Figure 2b** and **Table 2**, respectively. ACT-1004-1239 was quickly absorbed as indicated by $t_{max}$ ranging from 1.3 to 3.0 hours and eliminated with a terminal elimination half-life ($t_{1/2}$) from 17.8 to 23.6 hours at doses ≥ 10 mg.

Across the tested dose range, $C_{max}$ and $AUC_{0-\infty}$ essentially increased in a dose-proportional manner though not statistically confirmed by the Gough method, i.e., the 90% confidence interval (CI) of the slope estimate ($C_{max}$: 1.17–1.32; $AUC_{0-\infty}$: 0.98–1.14) was not fully contained within the critical interval, ranging from 0.87 to 1.13.[32]

### Food effect

After administration of 30 mg ACT-1004-1239, PK parameters were similar under fasted or fed condition, indicated by geometric

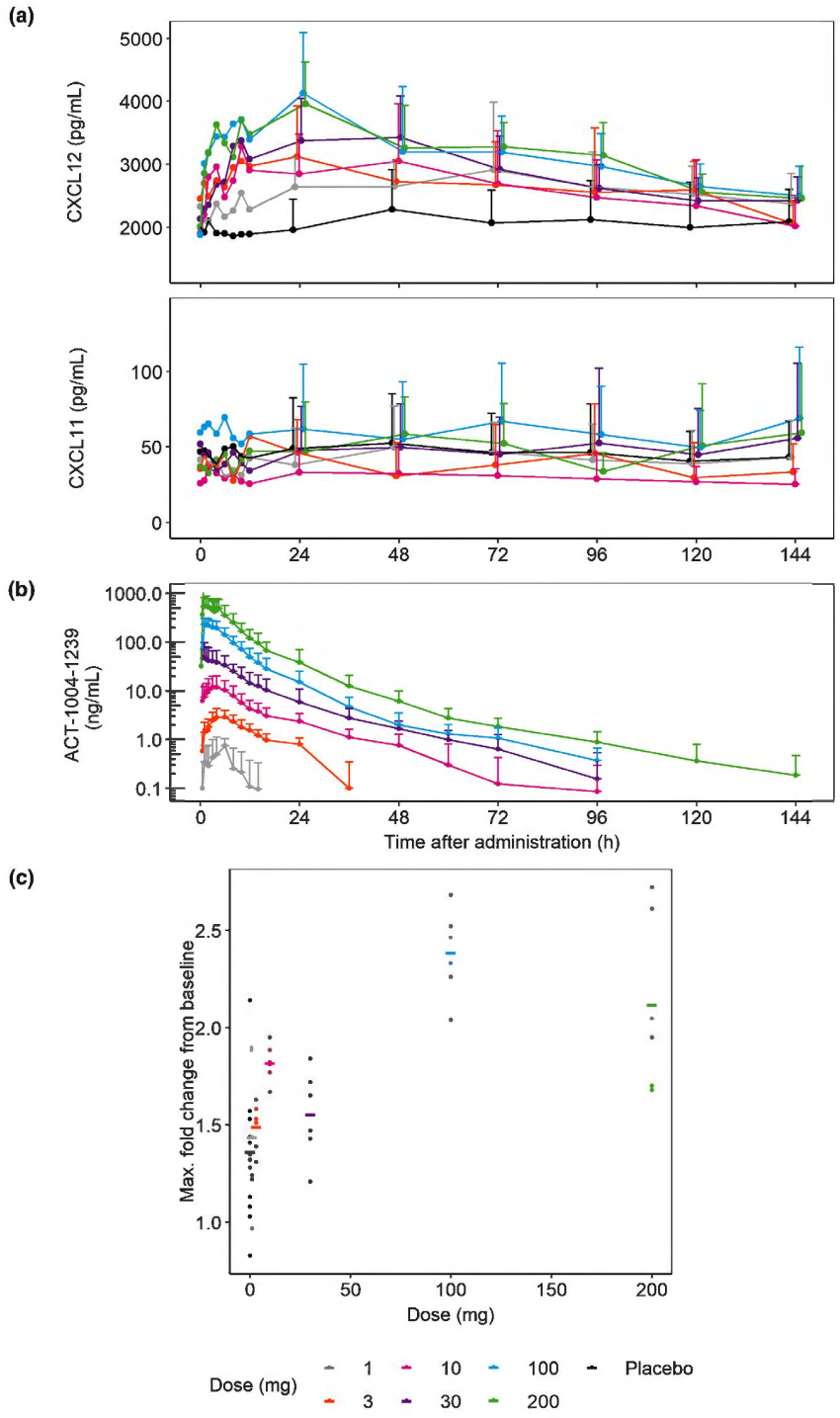


**Figure 2** PD and PK over time profiles and dose–response relationship of peak CXCL12 plasma concentrations. **(a,b)** PD and PK data are displayed as mean plasma concentrations of CXCL11/CXCL12 and ACT-1004-1239 by treatment with error bars representing standard deviations. **(c)** Peak CXCL12 plasma concentration data are expressed as relative change from baseline and displayed as mean (horizontal lines) and individual data (dots). *N* = 6 on each dose of ACT-1004-1239; *N* = 12 on placebo. CXCL11/CXCL12, C-X-C chemokine ligands 11 and 12; PD, pharmacodynamic; PK, pharmacokinetic.

mean $C_{max}$, $AUC_{0-\infty}$, and $t_{½}$ ratios (90% CI) of 0.93 (0.54–1.58), 1.16 (0.99–1.36), and 0.86 (0.72–1.03), respectively. The median $t_{max}$ was longer under fed than under fasted conditions (6.0 vs. 1.3 hours).

### Absolute bioavailability

Geometric mean absolute bioavailability was 53.0% (95% CI: 45.2–60.8) as determined from the dose-adjusted AUC ratio after oral vs. intravenous $^{14}$C-radiolabeled microtracer administration

ARTICLE

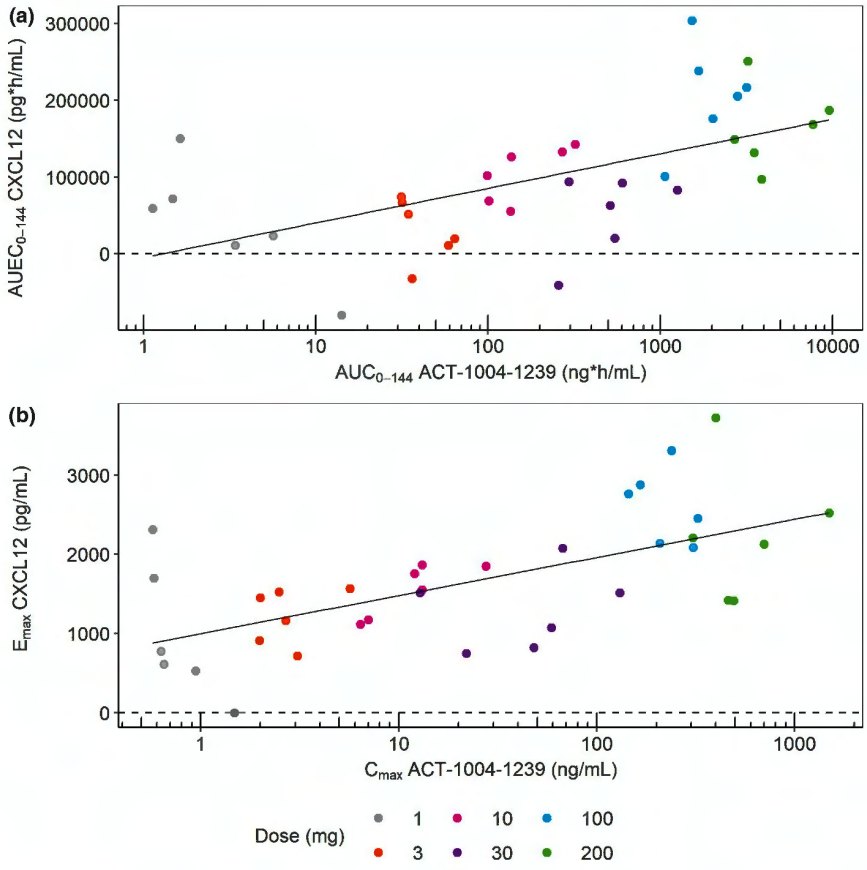


**Figure 3** Exposure–response relationship of $Eff_{max}$ vs. $C_{max}$ and AUEC vs. AUC based on plasma concentrations of CXCL12 and ACT-1004-1239. Dots represent individual data pairs. Linear regression analysis has been applied. $Eff_{max}$ vs. $C_{max}$: $r^2 = 0.384$ for ($y = 481$ $x + 998$). AUEC vs. AUC: $r^2 = 0.343$ for ($y = 45{,}070$ $x - 4{,}912$). $AUC_{0–144}$, area under the concentration-time curve from time 0 to 144 hours; $AUEC_{0-144h}$, area under the effect-time curve from time 0 to 144 hours; $C_{max}$, maximum plasma concentration; $Eff_{max}$, maximum effect; CXCL12, C-X-C chemokine ligand 12.

of ACT-1004-1239 (**Figure 4**). Based on the $^{14}$C-radioactivity data, the geometric mean clearance was estimated to be 23.2 L/hour (95% CI: 16.0–30.5) and the volume of distribution at steady state was 183 L (95% CI: 136-231).

### Pharmacokinetic/pharmacodynamic modeling

PK were best described by a three-compartment model with nonlinear distribution to the first peripheral compartment (**Figure 5a**). Key model development steps are provided (**Table S1**), and parameters were estimated with high precision, i.e., relative standard error ≤ 20% for all fixed-effects and random-effects parameters except for the half maximal inhibitory concentration, with 41.2% (**Table S2**). Observed vs. predicted plasma concentrations of ACT-1004-1239 were equally distributed around the line of identity (**Figure S2a,b**). VPCs did not show a systematic model misspecification across doses (**Figure S1a**).

**Table 2 Pharmacokinetic parameters of ACT-1004-1239**

| Parameter (unit) | 1 mg (*n* = 6) | 3 mg (*n* = 6) | 10 mg (*n* = 6) | 30 mg[a] (*n* = 6) | 100 mg (*n* = 6) | 200 mg (*n* = 6) |
|---|---|---|---|---|---|---|
| $C_{max}$ (ng/mL) | 0.76 (0.51–1.12) | 2.78 (1.85–4.18) | 11.7 (6.73–20.3) | 43.8 (18.2–105) | 222 (158–311) | 554 (309–993) |
| $t_{max}$ (hour) | 5.00 (1.00–6.00) | 6.01 (4.00–8.00) | 3.00 (1.0–6.0) | 1.28 (0.50–8.00) | 1.31 (1.00–4.00) | 1.75 (0.80–3.00) |
| $AUC_{0–144h}$ (ng*hour/mL) | 2.16 (0.61–7.69) | 36.7 (25.6–52.7) | 155 (90.7–263) | 495 (271–905) | 1,904 (1246–2,910) | 4,534 (2,645–7,772) |
| $AUC_{0–\infty}$ (ng*hour/mL) | 14.6 (0.10–2052) | 53.0 (38.9–72.3) | 171 (103–283) | 516 (286–930) | 1,921 (1,259–2,931) | 4,558 (2,665–7,795) |
| $t_{1/2}$ (hour) | 7.92 (0.68–92.2) | 15.1 (9.9–23.3) | 17.8 (12.9–24.4) | 19.0 (14.1–25.7) | 17.8 (10.5–30.1) | 23.6 (17.1–32.5) |

Data is displayed as geometric means (95% CI) except for $t_{max}$ that is provided as median (range).
AUC, area under the plasma concentration-time curve; $AUC_{0-144}$, area under the plasma concentration-time curve from 0 to 144 hours; AUC0–∞, area under the plasma concentration-time curve from 0 to infinity; CI, confidence interval; $C_{max}$, maximum plasma concentration; $t_{max}$, time to reach maximum plasma concentration; $t_{1/2}$, terminal elimination half-life.
[a]Data are provided for fasted conditions.

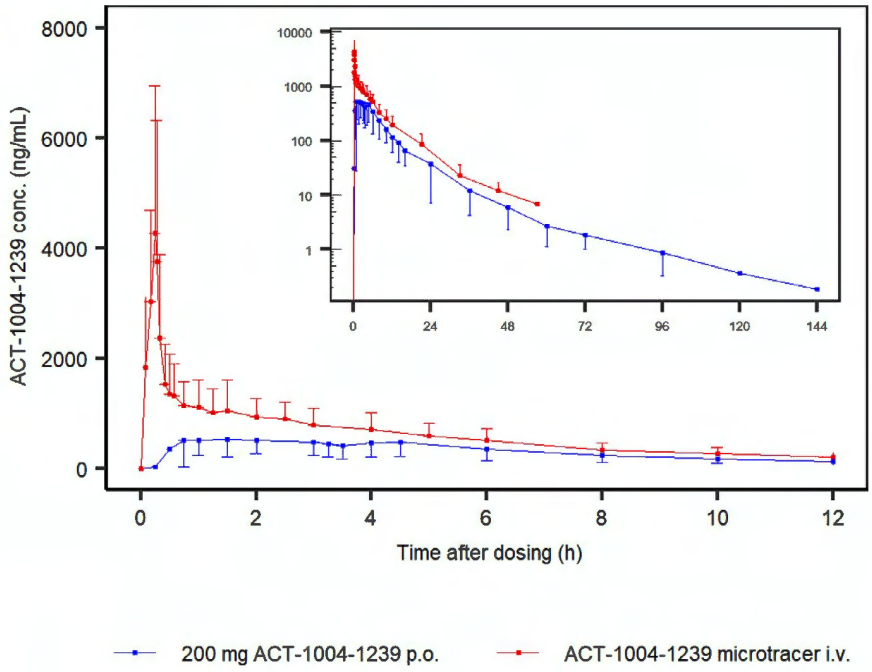


**Figure 4** Plasma concentration-time profile of ACT-1004-1239 (200 mg) after oral administration and of dose-adjusted $^{14}$C-radiolabeled ACT-1004-1239 after intravenous administration. Data from *N* = 6 subjects is displayed as mean concentrations by treatment. Error bars represent standard deviations. The linear data display is restricted to the 0–12 hours timeframe to ease visibility. Semilogarithmic data are displayed as inset and refer to the entire 144-hour sampling period. conc., concentration; h, hours; i.v., intravenous; p.o., per oral.

The nonlinear distribution to the first of two peripheral compartments was implemented to better describe the earlier $t_{max}$ at higher plasma concentrations of ACT-1004-1239. At plasma concentrations < 75 ng/mL, distribution to the first peripheral compartment was not yet saturated and hence faster than to the second peripheral compartment. However, at plasma concentrations ≥ 75 ng/mL, distribution to the first peripheral compartment was nonlinear, suggesting saturation and hence distribution to the second peripheral compartment becoming predominant.

The indirect-response model for PD was extended by a positive feedback mechanism which strongly improved the model fit with a single additional parameter (OFV decrease of 1013.02 points, with 3.84 being the threshold for significance). In line with this positive feedback mechanism, an increase of CXCL12 concentrations from baseline by a factor of 1.5 was predicted to result in a reduction of the elimination rate constant ($k_{out}$) by 9.5%, whereas $k_{out}$ reduction by 15.7% was predicted in the case of a doubling of CXCL12 concentrations as obtained at the top dose of 200 mg.

$E_{max}$ was assessed empirically and fixed to 0.8 to stabilize the estimation (theoretical range between 0 and 1, with 1 corresponding to full inhibition of the receptor, i.e., no elimination of CXCL12). Interindividual variability was implemented for the half maximal inhibitory concentration, $E_{max}$, and $k_{out}$. PD parameters were estimated with sufficient precision (relative standard error ≤ 41.2 for all fixed-effects and random-effects parameters). Observed plasma concentrations of CXCL12 were within the predicted percentiles for most doses and timepoints, although high CXCL12 concentrations were slightly underpredicted (**Figure S2c,d**). VPCs did not show a systematic model misspecification across doses (**Figure S1b**).

Simulations of PK and PD profiles at a once-daily dose of 100 mg showed that PK steady state was reached within 3 days (median AUC on day 3 > 99.9% of median AUC after 50 days) with an accumulation ratio of 110.9% (i.e., AUC ratio between day 50 vs. day 1) (**Figure 5b**). In terms of PD, steady-state conditions were also quickly reached and CXCL12 plasma concentrations were predicted to remain above baseline at least until 96 hours post last dosing, i.e., beyond elimination of ACT-1004-1239 (**Figure 5c**). The once-daily dose of 100 mg for 7 days was estimated to result in ~ 90% of the anticipated $E_{max}$ at the highest tested dose of 200 mg (median: 90.2% with 80% of subjects expected between 86.8% and 92.1%) (**Figure 5d**).

## DISCUSSION

This randomized, double-blind, placebo-controlled dose escalation study provides the first human safety, tolerability, PK, and PD data for ACT-1004-1239, which is a first-in-class drug candidate antagonist of CXCR7 that is considered a promising, novel target mainly in the immunology and oncology fields.

Overall, ACT-1004-1239 was safe and well tolerated across the tested dose range up to a single oral dose of 200 mg. This is primarily based on the balanced incidence of AEs on active treatment and placebo without indication of dose-dependency and on the absence of serious AEs or other relevant safety findings. Target engagement has been determined based on a dose-dependent increase in the plasma concentrations of CXCL12 representing a ligand of CXCR7 that has been utilized as the primary target engagement biomarker in this study.

At baseline, plasma concentrations of both CXCL11 and CXCL12 were in accordance with previously published data from

ARTICLE

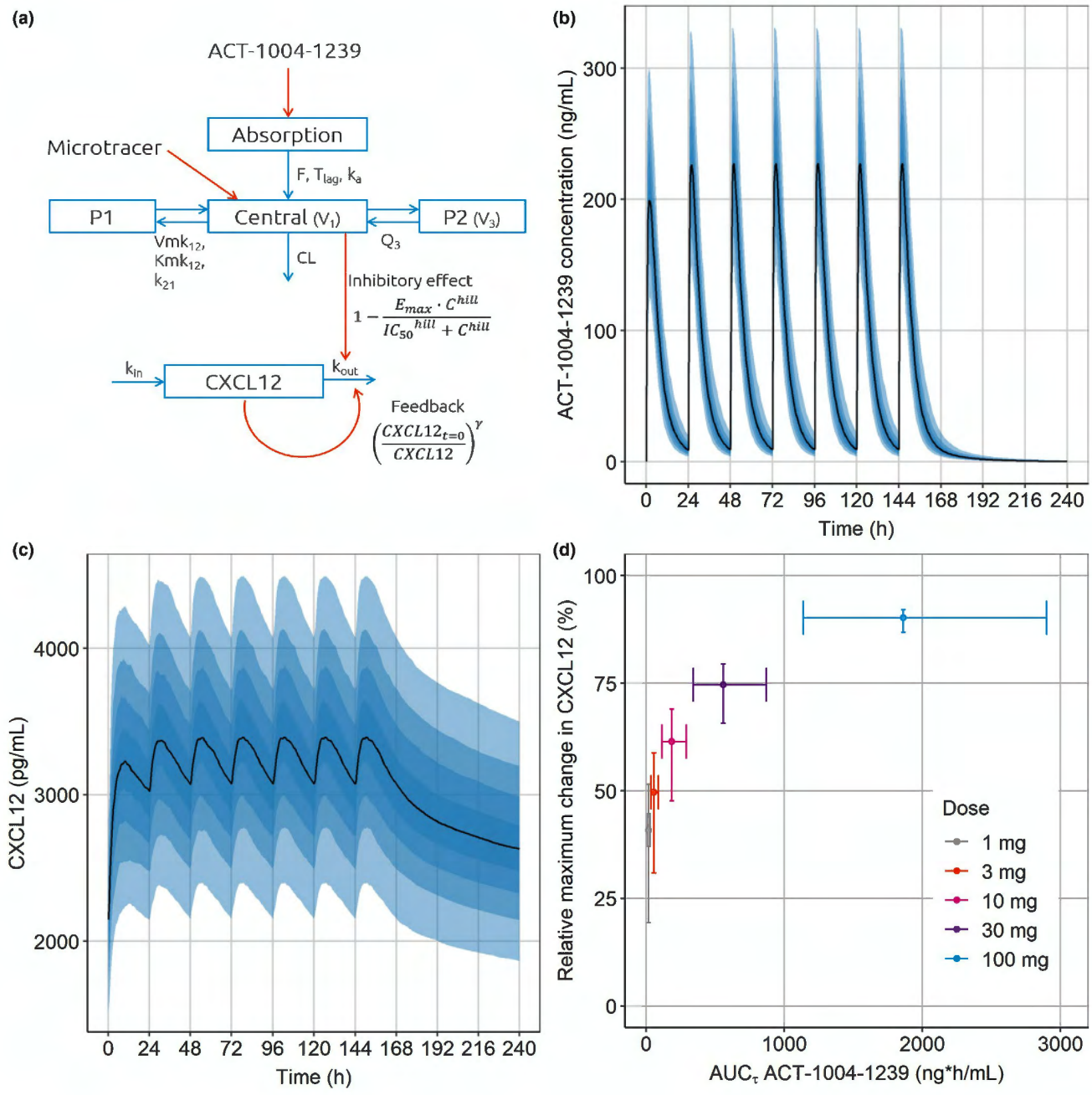


**Figure 5** Scheme of the population PK/PD model and simulation results. (**a**) Structure of the population PK/PD model. (**b,c**) Predicted plasma concentration/time profiles of (**b**) ACT-1004-1239 and (**c**) CXCL12 at a once-daily dose of 100 mg ACT-1004-1239 for 7 days ($n$ = 1,000 simulations). Black line: median; shaded areas with increasing intensity: 20%, 40%, 60%, and 80% prediction interval. (**d**) Predicted exposure–response relationship at steady state and stratified by dose. Median data are shown (points) with error bars representing the 80% prediction interval. Relative maximum change from baseline in CXCL12 plasma concentrations has been calculated with reference to an assumed maximum effect at a once-daily dose of 200 mg ACT-1004-1239 for 7 days ($n$ = 1,000 simulations). AUC, area under the plasma concentration-time curve; $C$, ACT-1004-1239 plasma concentration; CL, clearance; CXCL12, C-X-C chemokine ligand 12; $E_{max}$, maximum effect; F, absolute bioavailabilty; h, hours; hill, hill coefficient; $IC_{50}$, half maximal inhibitory concentration; ka, absorption rate constant; $k_{in}$, production rate constant; $Kmk_{12}$, half maximal distribution rate concentration; $k_{out}$, elimination rate constant; $k_{21}$, distribution rate from first peripheral compartment into central compartment; PK/PD, pharmacokinetic/pharmacodynamic; P1, first peripheral compartment; P2, second peripheral compartment; $T_{lag}$, absorption lag time; $Vmk_{12}$, maximum distribution rate; V1, distribution volume of central compartment; V3, distribution volume of second peripheral compartment; γ: exponent of feedback function.

healthy subjects.[33,34] Peak CXCL12 concentrations increased dose-dependently and more than doubled compared with baseline at 100 mg and 200 mg (**Figure 2c**). The relevance of this magnitude of effect for clinical efficacy is difficult to judge at this early stage of clinical development of ACT-1004-1239, owing to its first-in-class drug candidate status, i.e., in absence of clinical data

from patients obtained with other CXCR7 antagonists. However, the similarity in CXCL12 concentrations obtained at the top doses of 100 mg and 200 mg suggests that sufficiently high drug exposure has been achieved in this study to explore the full range of the dose–response relationship with saturation of PD effects.

Peak CXCL12 concentrations were reached ~ 24 hours post dosing (i.e., later than $t_{max}$ of ~ 1–3 hours) and essentially returned to baseline at 144 hours post dosing (i.e., later than 5× terminal $t_{1/2}$ of ~ 20 hours). Accordingly, persistent PD effects beyond elimination of ACT-1004-1239 were also predicted when simulating a multiple-dose scenario by PK/PD modeling. This aspect was further evaluated by PK/PD modeling. As CXCL12 is not only degraded via CXCR7, but also via CXCR4, a fixed $E_{max}$ of 0.8 was assumed for numerical stability in line with the observed data.[35] A positive feedback component significantly improved the model fit and semimechanistically contributed to the observed extent and delay of the PD effect, i.e., with increasing plasma concentrations of CXCL12 the elimination of this chemokine was predicted to decrease. Conceptually, this is in line with the previously published reduced total expression of CXCR7 at the membrane of breast cancer cells secondary to increased concentrations of its ligand CXCL12, although this was accompanied by an only minimally altered receptor internalization.[3,36]

In terms of CXCL11, baseline concentrations were approximately 20-fold lower than those of CXCL12, which is in line with previously published human data.[33,34] This is presumably due to the lower constitutive expression of the *CXCL11* gene as compared with *CXCL12*.[37-39] After administration of ACT-1004-1239, CXCL11 concentrations remained unchanged in this healthy subject population. This lacking modulation of CXCL11 concentrations after single-dose administration of ACT-1004-1239 has also been observed in naive mice.[28] Yet, these data do not preclude a relevant modulation of CXCL11 by ACT-1004-1239 after multiple doses or in patients with presumably elevated CXCL11 concentrations.

As ACT-1004-1239 is a noncytotoxic compound, it was feasible to conduct this FIH study in healthy subjects and hence avoid any confounding factors due to concomitant drug treatment or underlying disease. As this more standardized approach allows for a "cleaner" understanding of the safety, tolerability, and PK/PD properties of a novel compound, it is increasingly applied also in drug development of immuno-oncology products.[40,41] Conceptually, the determined exposure–response relationship in healthy subjects in combination with relevant efficacy data from animal models enables a more rational, model-based selection of expectedly efficacious doses for proof-of-concept studies. This approach hence also allows for minimizing the number of patients to be exposed and for increasing the probability of success.

Another recent evolution in early drug development concerns the integrated assessment of multiple PK and PD aspects in FIH dose escalation studies to obtain as much information as possible at the earliest possible stage, thereby accelerating the development of a novel compound.[42] This may allow for obtaining waivers for dedicated studies such as thorough QT; human absorption, distribution, metabolism, and elimination; absolute bioavailability; and other clinical pharmacology studies.[43,44] In this spirit, an innovative approach has been employed in this multipurpose FIH study by integrating the assessment of food effect on the PK of ACT-1004-1239 and absolute bioavailability by means of a microtracer approach with quantification of $^{14}C$ radioactivity by ultrasensitive accelerator mass spectrometry technology.[45,46]

The PK characteristics of ACT-1004-1239 could be well determined with this integrated approach. After oral administration, ACT-1004-1239 was rapidly absorbed at doses ≥ 10 mg and had an absolute bioavailability of 53.0%. Across the full dose range, exposure increased in an essentially dose-proportional manner. Absence of any relevant food effect was determined except for a later $t_{max}$ under fed conditions, which has also been observed in dogs. This may be due to delayed gastric emptying following a high-fat meal as also indicated by the PK/PD model.

The determined clearance of 23.2 L/hour and the volume of distribution of 183 L suggest ACT-1004-1239 to be a low-clearance drug with significant distribution to extravascular compartments. The terminal $t_{1/2}$ of ~ 20 hours alongside the predicted persistent CXCL12 elevation at the time of almost complete elimination of ACT-1004-1239 (i.e., 5× $t_{1/2}$) allows for once-daily administration in future clinical studies.

The three-compartment PK model best described the data with a nonlinear distribution to the first peripheral compartment that was applicable at plasma concentrations > 75 ng/mL and not anticipated based on the known physicochemical properties of ACT-1004-1239. In line with a low degree of plasma protein binding (i.e., ~ 25%), saturation of plasma protein binding was observed *in vitro* only at plasma concentrations of >100 μg/mL that are far in excess of those reached at the top dose in the present study (i.e., geometric mean $C_{max}$ of 0.55 μg/mL at 200 mg ACT-1004-1239) (Idorsia Pharmaceuticals, data on file) and hence may essentially be excluded as a potential cause of nonlinear distribution. Target-mediated drug disposition has also been reported as a potential cause of nonlinear distribution for both small and large molecules.[47] However, it is unlikely in the case of ACT-1004-1239 as its target (i.e., CXCR7) is mainly expressed on the endothelium of blood vessels and hence one would have expected saturation of the central rather than of the first peripheral compartment in case of nonlinear distribution due to target-mediated disposition.

ACT-1004-1239 is the first CXCR7 antagonist that has been administered to humans. Some functional CXCR7 antagonists have reached the preclinical stage of development including CCX662 and CCX771.[3] Alternatively, compounds solely targeting the CXCL12-CXCR4 pathway have already entered the clinical development stage or even approval in case of the small-molecule CXCR4 antagonist plerixafor (i.e., AMD3100; Mozobil), which has been approved for mobilization of hematopoietic stem cells from the bone marrow of patients with non-Hodgkin's lymphoma or multiple myeloma for subsequent autologous transplantation.[48,49] Other CXCR4 antagonists under clinical development include small molecules such as motixafortide (i.e., BL-8040)[50] or mavorixafor[51] as well as antibodies such as ulocuplumab (i.e., BMS-936564).[24] These CXCR4 antagonists do not increase the plasma concentrations of CXCL11 and CXCL12 and are therefore not expected to have a dual mode of action as applicable to CXCR7 antagonists. Another mode of action that is being explored targets the CXCR4/CXCR7 ligand CXCL12. Here, olaptesed pegol

(NOX-A12) is currently in clinical development as combination therapy in patients with different types of cancer such as glioblastoma, metastatic pancreatic, and colorectal cancer.[52]

In conclusion, this FIH study with the first-in-class candidate CXCR7 antagonist ACT-1004-1239 provided a comprehensive set of safety, tolerability, PK, and PD data delivering the opportunity to seek clinical pharmacology study waivers and thereby accelerate its development. Overall, these data demonstrate compound properties in favor of further clinical development in immunological disorders and oncology.

### SUPPORTING INFORMATION

Supplementary information accompanies this paper on the *Clinical Pharmacology & Therapeutics* website (www.cpt-journal.com).

### ACKNOWLEDGMENTS

The authors would like to thank Stephen English from Pharmaron CPC Inc for coordinating the AMS analyses as well as team members from Idorsia Pharmaceuticals Ltd for their dedicated support in terms of data generation and/or discussion, including Geoffroy Bourquin, Susanne Globig, Anne-Sophie Guern, Julie Hoerner, Martin Holdener, Marcel Keller, Marianne Martinic, Alexandre Mathis, Laetitia Pouzol, Racheal Rowles, and Giancarlo Sabattini.

### FUNDING

This study was sponsored by Idorsia Pharmaceuticals Ltd, Allschwil, Switzerland.

### CONFLICT OF INTEREST

C.H., A.H., D.S.S., M.-L.B., J.D., and M.U. are full-time employees of Idorsia Pharmaceuticals Ltd. M.A.-I. is the principal investigator, who is employed by Pharmaron CPC Inc. H.E.M.Z.S. declared no competing interests for this work.

### AUTHOR CONTRIBUTIONS

C.H. and M.U. wrote the manuscript. C.H., M.-L.B., J.D., and M.U. designed the research. A.H. and M.A.-I. performed the research. C.H., A.H., D.S.S., M.-L.B., H.E.M.Z.S., J.D., and M.U. analyzed the data.



1. Franciszkiewicz, K., Boissonnas, A., Boutet, M., Combadière, C. & Mami-Chouaib, F. Role of chemokines and chemokine receptors in shaping the effector phase of the antitumor immune response. *Cancer Res.* **72**, 6325–6332 (2012).
2. Proudfoot, A.E. Chemokine receptors: multifaceted therapeutic targets. *Nat. Rev. Immunol.* **2**, 106–115 (2002).
3. Huynh, C., Dingemanse, J., Meyer zu Schwabedissen, H.E. & Sidharta, P.N. Relevance of the CXCR4/CXCR7-CXCL12 axis and its effect in pathophysiological conditions. *Pharmacol. Res.* **161**, 105092 (2020).
4. Murphy, P.M. *et al*. International union of pharmacology. XXII. Nomenclature for chemokine receptors. *Pharmacol. Rev.* **52**, 145–176 (2000).
5. Raman, D., Sobolik-Delmaire, T. & Richmond, A. Chemokines in health and disease. *Exp. Cell Res.* **317**, 575–589 (2011).
6. Rajagopal, S. *et al*. Beta-arrestin- but not G protein-mediated signaling by the "decoy" receptor CXCR7. *Proc. Natl. Acad. Sci. USA*. **107**, 628–632 (2010).
7. Wang, C., Chen, W. & Shen, J. CXCR7 targeting and its major disease relevance. *Front. Pharmacol.* **9**, 641 (2018).
8. Burns, J.M. *et al*. A novel chemokine receptor for SDF-1 and I-TAC involved in cell survival, cell adhesion, and tumor development. *J. Exp. Med.* **203**, 2201–2213 (2006).
9. Yang, C.H. *et al*. Identification of CXCL11 as a STAT3-dependent gene induced by IFN. *J. Immunol.* **178**, 986–992 (2007).
10. Li, M. & Ransohoff, R.M. The roles of chemokine CXCL12 in embryonic and brain tumor angiogenesis. *Semin. Cancer Biol.* **19**, 111–115 (2009).
11. Karin, N. The multiple faces of CXCL12 (SDF-1alpha) in the regulation of immunity during health and disease. *J. Leukoc. Biol.* **88**, 463–473 (2010).
12. Sánchez-Martin, L., Sánchez-Mateos, P. & Cabañas, C. CXCR7 impact on CXCL12 biology and disease. *Trends. Mol. Med.* **19**, 12–22 (2013).
13. Balabanian, K. *et al*. The chemokine SDF-1/CXCL12 binds to and signals through the orphan receptor RDC1 in T lymphocytes. *J. Biol. Chem.* **280**, 35760–35766 (2005).
14. Crump, M.P. *et al*. Solution structure and basis for functional activity of stromal cell-derived factor-1; dissociation of CXCR4 activation from binding and inhibition of HIV-1. *Embo J.* **16**, 6996–7007 (1997).
15. Puchert, M., Obst, J., Koch, C., Zieger, K. & Engele, J. CXCL11 promotes tumor progression by the biased use of the chemokine receptors CXCR3 and CXCR7. *Cytokine* **125**, 154809 (2020).
16. Hoffmann, F. *et al*. Rapid uptake and degradation of CXCL12 depend on CXCR7 carboxyl-terminal serine/threonine residues. *J. Biol. Chem.* **287**, 28362–28377 (2012).
17. Naumann, U. *et al*. CXCR7 functions as a scavenger for CXCL12 and CXCL11. *PLoS One* **5**, e9175 (2010).
18. Lewellis, S.W. *et al*. Precise SDF1-mediated cell guidance is achieved through ligand clearance and microRNA-mediated decay. *J. Cell. Biol.* **200**, 337–355 (2013).
19. Tiveron, M.-C. & Cremer, H. CXCL12/CXCR4 signalling in neuronal cell migration. *Curr. Opin. Neurobiol.* **18**, 237–244 (2008).
20. Lewellis, S.W. & Knaut, H. Attractive guidance: how the chemokine SDF1/CXCL12 guides different cells to different locations. *Semin. Cell Dev. Biol.* **23**, 333–340 (2012).
21. Williams, J.L., Patel, J.R., Daniels, B.P. & Klein, R.S. Targeting CXCR7/ACKR3 as a therapeutic strategy to promote remyelination in the adult central nervous system. *J. Exp. Med.* **211**, 791–799 (2014).
22. Banisadr, G., Podojil, J.R., Miller, S.D. & Miller, R.J. Pattern of CXCR7 gene expression in mouse brain under normal and inflammatory conditions. *J. Neuroimmune. Pharmacol.* **11**, 26–35 (2016).
23. Chu, T., Shields, L.B.E., Zhang, Y.P., Feng, S.-Q., Shields, C.B. & Cai, J. CXCL12/CXCR4/CXCR7 chemokine axis in the central nervous system: therapeutic targets for remyelination in demyelinating diseases. *Neuroscientist* **23**, 627–648 (2017).
24. Ghobrial, I.M. *et al*. A Phase Ib/II trial of the first-in-class anti-CXCR4 antibody ulocuplumab in combination with lenalidomide or bortezomib plus dexamethasone in relapsed multiple myeloma. *Clin. Cancer Res.* **26**, 344–353 (2020).
25. Gravina, G.L. *et al*. The brain-penetrating CXCR4 antagonist, PRX177561, increases the antitumor effects of bevacizumab and sunitinib in preclinical models of human glioblastoma. *J. Hematol. Oncol.* **10**, 5 (2017).
26. Jung, K. *et al*. Targeting CXCR4-dependent immunosuppressive Ly6C$^{low}$ monocytes improves antiangiogenic therapy in colorectal cancer. *Proc. Natl. Acad. Sci. USA* **114**, 10455–10460 (2017).
27. Walters, M.J. *et al*. Inhibition of CXCR7 extends survival following irradiation of brain tumours in mice and rats. *Br. J. Cancer* **110**, 1179–1188 (2014).
28. Richard-Bildstein, S. *et al*. Discovery of the potent, selective, orally available CXCR7 antagonist ACT-1004-1239. *J. Med. Chem.* **63**, 15864–15882 (2020).
29. National Cancer Institute, US Department of Health and Human Services. Common terminology criteria for adverse events (CTCAE) Version 5.0 <https://ctep.cancer.gov/protocoldevelopment/electronic_applications/ctc.htm> (2017).
30. Dansirikul, C., Silber, H.E. & Karlsson, M.O. Approaches to handling pharmacodynamic baseline responses. *J. Pharmacokinet. Pharmacodyn.* **35**, 269–283 (2008).
31. Baird, M.F., Graham, S.M., Baker, J.S. & Bickerstaff, G.F. Creatine-kinase- and exercise-related muscle damage implications for

muscle performance and recovery. *J. Nutr. Metab.* (2012). https://doi.org/10.1155/2012/960363.
32. Gough, K. *et al*. Assessment of dose proportionality: report from the statisticians in the pharmaceutical industry/pharmacokinetics UK Joint Working Party. *Ther. Innov. Regul. Sci.* **29**, 1039–1048 (1995).
33. Butera, D. *et al*. Plasma chemokine levels correlate with the outcome of antiviral therapy in patients with hepatitis C. *Blood* **106**, 1175–1182 (2005).
34. Kirkpatrick, B., Nguyen, L., Kondrikova, G., Herberg, S. & Hill, W.D. Stability of human stromal-derived factor-1alpha (CXCL12alpha) after blood sampling. *Ann. Clin. Lab Sci.* **40**, 257–260 (2010).
35. Tarasova, N.I., Stauber, R.H. & Michejda, C.J. Spontaneous and ligand-induced trafficking of CXC-chemokine receptor 4. *J. Biol. Chem.* **273**, 15883–15886 (1998).
36. Luker, K.E., Steele, J.M., Mihalko, L.A., Ray, P. & Luker, G.D. Constitutive and chemokine-dependent internalization and recycling of CXCR7 in breast cancer cells to degrade chemokine ligands. *Oncogene* **29**, 4599–4610 (2010).
37. Cole, K.E. *et al*. Interferon-inducible T cell alpha chemoattractant (I-TAC): a novel non-ELR CXC chemokine with potent activity on activated T cells through selective high affinity binding to CXCR3. *J. Exp. Med.* **187**, 2009–2021 (1998).
38. Janssens, R., Struyf, S. & Proost, P. The unique structural and functional features of CXCL12. *Cell. Mol. Immunol.* **15**, 299–311 (2018).
39. Tokunaga, R. *et al*. CXCL9, CXCL10, CXCL11/CXCR3 axis for immune activation — a target for novel cancer therapy. *Cancer Treat. Rev.* **63**, 40–47 (2018).
40. Gupta, P., Gupta, V. & Gupta, Y.K. Phase I clinical trials of anticancer drugs in healthy volunteers: need for critical consideration. *Indian J. Pharmacol.* **44**, 540–542 (2012).
41. Iwamoto, M., Iannone, R. & Wagner, J.A. Use of healthy volunteers drives clinical oncology drug development decision making. *Clin. Pharmacol. Ther.* **92**, 571–574 (2012).
42. Muehlan, C., Heuberger, J., Juif, P.-E., Croft, M., van Gerven, J. & Dingemanse, J. Accelerated development of the dual orexin receptor antagonist ACT-541468: integration of a microtracer in a first-in-human study. *Clin. Pharmacol. Ther.* **104**, 1022–1029 (2018).
43. Darpo, B., Garnett, C., Keirns, J. & Stockbridge, N. Implications of the IQ-CSRC prospective study: time to revise ICH E14. *Drug. Saf.* **38**, 773–780 (2015).
44. Ufer, M., Juif, P.-E., Boof, M.-L., Muehlan, C. & Dingemanse, J. Metabolite profiling in early clinical drug development: current status and future prospects. *Expert. Opin. Drug Metab. Toxicol.* **13**, 803–806 (2017).
45. Lappin, G. Approaches to intravenous clinical pharmacokinetics: Recent developments with isotopic microtracers. *J. Clin. Pharmacol.* **56**, 11–23 (2016).
46. Lappin, G., Noveck, R. & Burt, T. Microdosing and drug development: past, present and future. *Expert. Opin. Drug Metab. Toxicol.* **9**, 817–834 (2013).
47. An, G. Concept of pharmacologic target-mediated drug disposition in large-molecule and small-molecule compounds. *J. Clin. Pharmacol.* **60**, 149–163 (2020).
48. Steinberg, M. & Silva, M. Plerixafor: A chemokine receptor-4 antagonist for mobilization of hematopoietic stem cells for transplantation after high-dose chemotherapy for non-Hodgkin's lymphoma or multiple myeloma. *Clin. Ther.* **32**, 821–843 (2010).
49. Keating, G.M. Plerixafor: a review of its use in stem-cell mobilization in patients with lymphoma or multiple myeloma. *Drugs* **71**, 1623–1647 (2011).
50. Abraham, M. *et al*. Single dose of the CXCR4 antagonist BL-8040 induces rapid mobilization for the collection of human $CD34^+$ cells in healthy volunteers. *Clin. Cancer Res.* **23**, 6790–6801 (2017).
51. Dale, D.C. *et al*. Results of a Phase 2 Trial of an Oral CXCR4 antagonist Mavorixafor for treatment of WHIM syndrome. *Blood* **136**, 2994–3003 (2020).
52. Steurer, M. *et al*. Olaptesed pegol (NOX-A12) with bendamustine and rituximab: a phase IIa study in patients with relapsed/refractory chronic lymphocytic leukemia. *Haematologica* **104**, 2053–2060 (2019).

## 3.2 Absorption, distribution, metabolism, and excretion profile of ACT-1004-1239

# Absorption, Metabolism, and Excretion of ACT-1004-1239, a First-In-Class CXCR7 Antagonist: In Vitro, Preclinical, and Clinical Data

Christine Huynh[1,2], Swen Seeland[3], Jerome Segrestaa[3], Carmela Gnerre[3], Jens Hogeback[4], Henriette E. Meyer zu Schwabedissen[2], Jasper Dingemanse[1], Patricia N. Sidharta[1]

[1]Idorsia Pharmaceuticals Ltd, Department of Clinical Pharmacology, Allschwil, Switzerland

[2]University of Basel, Biopharmacy, Department of Pharmaceutical Sciences, Basel, Switzerland

[3]Idorsia Pharmaceuticals Ltd, Department of Preclinical Drug Metabolism and Pharmacokinetics, Allschwil, Switzerland

[4]A&M Labor für Analytik und Metabolismusforschung Service GmbH, Bergheim, Germany

Published in Front Pharmacol. 2022;13(March):1-15

frontiers in Pharmacology

ORIGINAL RESEARCH
published: 30 March 2022
doi: 10.3389/fphar.2022.812065

# Absorption, Metabolism, and Excretion of ACT-1004-1239, a First-In-Class CXCR7 Antagonist: *In Vitro*, Preclinical, and Clinical Data

*Christine Huynh[1,2]*, Swen Seeland[3], Jerome Segrestaa[3], Carmela Gnerre[3], Jens Hogeback[4], Henriette E. Meyer zu Schwabedissen[2], Jasper Dingemanse[1] and Patricia N. Sidharta[1]*

[1]Department of Clinical Pharmacology, Idorsia Pharmaceuticals Ltd., Allschwil, Switzerland, [2]Department of Pharmaceutical Sciences, Biopharmacy, University of Basel, Basel, Switzerland, [3]Department of Preclinical Drug Metabolism and Pharmacokinetics, Idorsia Pharmaceuticals Ltd., Allschwil, Switzerland, [4]A&M Labor für Analytik und Metabolismusforschung Service GmbH, Bergheim, Germany

ACT-1004-1239 is a potent, selective, first-in-class CXCR7 antagonist, which shows a favorable preclinical and clinical profile. Here we report the metabolites and the metabolic pathways of ACT-1004-1239 identified using results from *in vitro* and *in vivo* studies. Two complementary *in vitro* studies (incubation with human liver microsomes in the absence/presence of cytochrome P450- [CYP] specific chemical inhibitors and incubation with recombinant CYPs) were conducted to identify CYPs involved in ACT-1004-1239 metabolism. For the *in vivo* investigations, a microtracer approach was integrated in the first-in-human study to assess mass balance and absorption, distribution, metabolism, and excretion (ADME) characteristics of ACT-1004-1239. Six healthy male subjects received orally 100 mg non-radioactive ACT-1004-1239 together with 1 µCi $^{14}$C-ACT-1004-1239. Plasma, urine, and feces samples were collected up to 240 h post-dose and $^{14}$C-drug-related material was measured with accelerator mass spectrometry. This technique was also used to construct radiochromatograms of pooled human samples. Metabolite structure elucidation of human-relevant metabolites was performed using high performance liquid chromatography coupled with high resolution mass spectrometry and facilitated by the use of rat samples. CYP3A4 was identified as the major CYP catalyzing the formation of M1 *in vitro*. In humans, the cumulative recovery from urine and feces was 84.1% of the dose with the majority being eliminated via the feces (69.6%) and the rest via the urine (14.5%). In human plasma, two major circulating metabolites were identified, i.e., M1 and M23. Elimination *via* M1 was the only elimination pathway that contributed to ≥25% of ACT-1004-1239 elimination. M1 was identified as a secondary amine metabolite following oxidative N-dealkylation of the parent. M23 was identified as a difluorophenyl isoxazole carboxylic acid metabolite following central amide bond hydrolysis of the parent. Other metabolites observed in humans were A1, A2, and A3. Metabolite A1 was identified as an analog of M1 after oxidative defluorination, whereas both, A2 and A3, were identified as a reduced analog of M1 and parent, respectively, after addition of two hydrogen atoms at the isoxazole ring. In conclusion, CYP3A4 contributes to a relevant extent to ACT-1004-1239 disposition and two major circulating metabolites were observed in humans.

OPEN ACCESS

**Edited by:**
*Yurong Lai,*
*Gilead, United States*

**Reviewed by:**
*Xingxing Diao,*
*Shanghai Institute of Materia Medica (CAS), China*
*Alfin Vaz,*
*Vaz Consultancy LLC, United States*

***Correspondence:**
*Christine Huynh*
*christine.huynh@idorsia.com*

**Specialty section:**
*This article was submitted to Drug Metabolism and Transport, a section of the journal Frontiers in Pharmacology*

**Received:** *09 November 2021*
**Accepted:** *21 January 2022*
**Published:** *30 March 2022*

**Citation:**
*Huynh C, Seeland S, Segrestaa J, Gnerre C, Hogeback J, Meyer zu Schwabedissen HE, Dingemanse J and Sidharta PN (2022) Absorption, Metabolism, and Excretion of ACT-1004-1239, a First-In-Class CXCR7 Antagonist: In Vitro, Preclinical, and Clinical Data. Front. Pharmacol. 13:812065. doi: 10.3389/fphar.2022.812065*

**Clinical Trial Registration:** (https://clinicaltrials.gov/ct2/show/NCT03869320) ClinicalTrials.gov Identifier NCT03869320.

**Keywords: CXCR7, ADME, accelerator mass spectrometry, microtracer, CYP3A4, $^{14}$C-ACT-1004-1239, first-in-human**

## INTRODUCTION

ACT-1004-1239 is an orally available, potent, selective, insurmountable, small-molecule CXCR7 antagonist (Richard-Bildstein et al., 2020). Preclinically, ACT-1004-1239 showed dose-dependent efficacy in various animal models such as of multiple sclerosis (Pouzol et al., 2021a) and acute lung injury (Pouzol et al., 2021b) using its ligands CXCL11 and CXCL12 as biomarker of target engagement. Dose-dependent increases in CXCL11 and CXCL12 plasma concentration were associated with a reduction in immune cell infiltrates into the central nervous system (Pouzol et al., 2021c) or the bronchoalveolar space (Pouzol et al., 2021b). ACT-1004-1239 is rapidly absorbed in rats. It displays a high clearance and a volume of distribution in excess of total body water (Richard-Bildstein et al., 2020). So far, two clinical studies with ACT-1004-1239 were conducted and showed favorable safety and tolerability profiles over the investigated dose range of 1–200 mg, following single- (Huynh et al., 2021b) and multiple-dose (Huynh et al., 2021a) administration in healthy humans. Pharmacokinetic (PK) and pharmacodynamic (PD) profiles suggested a once-daily dosing regimen in further clinical studies. In male and female subjects, ACT-1004-1239 was rapidly absorbed (time to reach maximum plasma concentration [$t_{max}$] 1-3 h) and its exposure increased dose-dependently between 1 and 200 mg (Huynh et al., 2021a; Huynh et al., 2021b). At doses ≥10 mg, ACT-1004-1239 distributed to multiple compartments and was eliminated with a terminal half-life [$t_{1/2}$] ranging from 18 to 24 h. Systemic exposure to ACT-1004-1239 reached steady-state conditions by Day 3 with almost no accumulation (Huynh et al., 2021a). Food had no relevant effect on the PK and the absolute bioavailability of ACT-1004-1239 was 53%. Furthermore, ACT-1004-1239 showed a large volume of distribution (183 L) and is considered a low-clearance drug in humans (Huynh et al., 2021b). Compared to male subjects, female subjects had overall higher ACT-1004-1239 exposure (Huynh et al., 2021a).

In the context of drug development, characterization of absorption, distribution, metabolism, and excretion (ADME) properties including but not limited to the identification of major metabolites is required to ascertain whether these may cause pharmacological or toxicological effects. Additionally, it provides key information on relevant drug interactions or dosing of special patient populations such as renally or hepatically impaired patients. Given the importance of understanding those characteristics, human ADME studies should be conducted during early clinical development (Spracklin et al., 2020). This can be achieved, for example, with a human microtracer component incorporated into a first-in human (FIH) study. The conduct of such integrated studies requires a highly sensitive analytical method for the determination of very low amounts of administered radioactivity by using accelerator mass spectrometry (AMS). AMS allows for detection of drug in the femtogram range, or below, by measuring the isotopic ratio of carbons (i.e., $^{12}$C/$^{14}$C) (Graham and Garner, 2003; Lappin et al., 2006). Due to its high analytical sensitivity, AMS has a wide range of applications (Arjomand, 2010). In the context of early clinical drug development, AMS has been applied to assess various drug characteristics including but not limited to PK, mass balance, absolute bioavailability, and metabolite profiling using a microdose/microtracer approach (Boddy et al., 2007; Arjomand, 2010; Muehlan et al., 2018; Huynh et al., 2021b).

Here we report the metabolites and the metabolic pathways of ACT-1004-1239 in humans using results from *in vitro* and *in vivo* studies: 1) metabolite profiling in human liver microsomes (HLM) and identification of CYPs involved in the formation of the main metabolites, and 2) the ADME characteristics in humans investigated in the FIH study applying a microtracer approach (Huynh et al., 2021b). Metabolite structure elucidation of major human metabolites was supported by the use of rat samples. Data on the distribution of ACT-1004-1239 have been previously reported (Huynh et al., 2021b), and are therefore not covered herein.

## MATERIALS AND METHODS

### Chemicals and Reagents

$^{14}$C-ACT-1004-1239 was synthesized at Pharmaron (Cardiff, United Kingdom) in a stock solution containing 3% (v/v) 2 M hydrochloric acid in ethanol with a radioactive concentration of 1 mCi/ml and a specific activity of 58 mCi/mmol. The $^{14}$C-ACT-1004-1239 working solution used for *in vitro* studies was prepared by diluting an aliquot of the stock solution in a 1:1 (v/v) mixture of acetonitrile and water to reach a final concentration of 1 mM. This working solution was stored at –20°C. Prior to the experiments, the compound purity of the working solution was monitored. $^{14}$C-ACT-1004-1239 microtracer solution for oral administration in humans was prepared at the clinical site (Pharmaron, Baltimore, MD, United States). The $^{14}$C-ACT-1004-1239 stock solution was diluted to a final target microtracer concentration of 0.067 μCi/ml in a 5% (w/v) solution of mannitol and sterile water. The matching placebo oral solution consisted of 5% (w/v) mannitol and sterile water. ACT-1004-1239 capsules for clinical use were manufactured at Idorsia Pharmaceuticals Ltd. (Allschwil, Switzerland).

ACT-1004-1239 and synthetic reference standards of metabolites (M1, M23, and M38) were synthesized at Idorsia Pharmaceuticals Ltd. (Allschwil, Switzerland). For the NADPH-regenerating system, glucose-6-phosphate (disodium salt) and

$NADP^+$ were purchased from Sigma-Aldrich (Buchs, Switzerland) and glucose-6-phosphate dehydrogenase was supplied by Roche Diagnostics (Mannheim, Germany). Pooled HLMs were obtained from Becton Dickinson (Basel, Switzerland), while cDNA-expressed human CYPs (CYP1A1, CYP1A2, CYP2B6, CYP2C8, CYP2C9, CYP2C19, CYP2D6, CYP3A4, and control bactosomes) and co-expressing CYP reductase derived from *Escherichia coli* were purchased from Cypex Ltd. (Dundee, United Kingdom). The CYP-specific inhibitors furafylline, ketoconazole, quinidine, sulfaphenazole, and ticlopidine were purchased from Sigma-Aldrich (Buchs, Switzerland). Montelukast and N-benzylnirvanol were obtained from LKT Laboratories (St. Paul, MN, United States) and Becton Dickinson (Basel, Switzerland), respectively. All other chemicals and solvents used for analytical measurements were obtained from commercial sources.

## *In Vitro* Studies

Identification of the human CYPs metabolizing ACT-1004-1239 was performed using two complementary approaches: 1) incubation with HLMs in the absence and presence of CYP chemical inhibitors, and 2) experiments with recombinant CYPs.

### Incubation With HLMs and CYP-Specific Inhibitors

$^{14}$C-ACT-1004-1239 was incubated with HLMs at a final concentration of 10 µM. For this purpose, an aliquot of the $^{14}$C-ACT-1004-1239 stock solution was added to 100 mM phosphate buffer (pH 7.4) containing 1 mg/ml of microsomal protein. The reaction was initiated by addition of the pre-warmed NADPH-regenerating system and the incubation continued for 30 min at 37°C. The NADPH-regenerating system was prepared as a 10-fold concentrated stock solution. It consisted of 11 mM $NADP^+$, 100 mM glucose-6-phosphate, 50 mM magnesium chloride in 0.1 M phosphate buffer (pH 7.4), and glucose-6-phosphate dehydrogenase (20 IU/ml). The latter was added shortly before the use of the NADPH-regenerating system. In the experiments with the competitive inhibitors sulfaphenazole (3 µM, CYP2C9 inhibitor), quinidine (1 µM, CYP2D6 inhibitor), montelukast (3 µM, CYP2C8 inhibitor), N-benzylnirvanol (5 µM, CYP2C19 inhibitor), and ketoconazole (1 µM, CYP3A4 inhibitor), a 5 µl-aliquot of the inhibitor stock solution was added to the reaction mixture prior to the initiation of the reaction. In incubations with the mechanism-based inhibitors, furafylline (20 µM, CYP1A2 inhibitor) and ticlopidine (0.5 µM, CYP2B6 inhibitor), the HLMs were pre-incubated for 10 min at 37°C in the presence of these inhibitors and the NADPH-regenerating system. The reaction was initiated by the addition of $^{14}$C-ACT-1004-1239. The organic solvent concentration in all incubations was kept at 1% (v/v). The reactions were terminated by the addition of one volume equivalent acetonitrile. The samples were centrifuged (for 10 min at 20,800 g and 10°C), and high performance liquid chromatography (HPLC) analysis (as described in *Analytical Method for Metabolite Profiling*) was applied to the resulting supernatants.

### Incubations With Recombinant Human CYPs

$^{14}$C-ACT-1004-1239 was incubated for 60 min with 100 pmol/ml of the respective recombinant CYP (CYP1A1, CYP1A2, CYP2B6, CYP2C8, CYP2C9, CYP2C19, CYP2D6, or CYP3A4) in 100 mM phosphate buffer (pH 7.4) at a final $^{14}$C-ACT-1004-1239 concentration of 10 µM. The incubation was initiated by addition of the pre-warmed NADPH-regenerating system and terminated by the addition of one volume equivalent acetonitrile. The NADPH-regenerating system was prepared as described in *Incubation With HLMs and CYP-Specific Inhibitors*. The organic solvent concentration in all incubations was kept at 0.5% (v/v). Control incubations in the absence of the NADPH-regenerating system or CYP, as well as incubations with control bactosomes, were performed in parallel under otherwise identical conditions. The samples were centrifuged for 10 min at 20,800 g and 10°C to obtain the supernatant which was used for HPLC analysis (as described in *Analytical Method for Metabolite Profiling*). The resulting data were further used to determine their contribution to the metabolic clearance *in vitro* by applying the intersystem extrapolation scaling approach as described by Chen et al. (2011).

### Analytical Method for Metabolite Profiling

The HPLC-system for the recording of $^{14}$C metabolic profiles consisted of two Shimadzu pumps LC30AD (Shimadzu, Reinach, Switzerland) equipped with a Shimadzu column oven CTO-20A and a Shimadzu autosampler model SIL30AC. $^{14}$C-radiochemical detection was performed by a Berthold radioflow detector LB513 with a 200 µl-liquid cell Z-200-6M and an LB5036 pump for supplementing liquid scintillation cocktail at 3 ml/min (Berthold AG, Regensdorf, Switzerland). Data acquisition for metabolic profiling was done using the RadioStar software package (version 5.0.12.5; Berthold AG, Regensdorf, Switzerland).

Chromatographic separation of $^{14}$C-ACT-1004-1239 and its metabolites, derived from *in vitro* samples, was achieved on a Phenomenex Luna Phenyl-Hexyl column (250 × 4.6 mm ID, 3 µm, Torrance, CA, United States) at 40°C with a flow of 1 ml/min. Mobile phases consisted of 20 mM ammonium bicarbonate, adjusted to pH 8.6 with ammonium hydroxide (phase A), and acetonitrile (phase B). Parent drug and metabolites were eluted with the following linear gradient program: equilibration at 3 min, 10% B; 3-45 min, 10-30% B; 45-65 min, 30-40% B; 65-85 min, 40-50% B; 85-95 min, 50-85% B; 95-100 min, 85% B; 100-101 min, 85-10% B; 101-110 min, 10% B. Using these chromatographic conditions, $^{14}$C-ACT-1004-1239 had an average retention time of 67 min. The variability in retention time did not exceed 0.3 min.

## Human Study

### Study Design

Before study initiation, the study was approved by IntegReview Institutional Review Board (Austin, TX, United States) and performed in accordance with Good Clinical Practice and the Declaration of Helsinki.

The investigation of mass balance and ADME characteristics reported here was incorporated in the single-center, randomized, double-blind, placebo-controlled FIH study (ClinicalTrials.gov: NCT03869320) assessing safety, tolerability, PK, and PD of single-ascending, oral doses of ACT-1004-1239 (1, 3, 10, 30, 100, and 200 mg) as previously reported (Huynh et al., 2021b).

Mass balance and the ADME characteristics were investigated at the 100 mg dose level. At this dose level, six subjects assigned to ACT-1004-1239 received in addition to the non-radioactive treatment concomitantly 9.2 μg (i.e., 1 μCi) $^{14}$C-ACT-1004-1239 as an oral solution. Two placebo subjects received a matching placebo solution.

Following dosing, all subjects stayed at the study site for at least 7 days. Each subject was requested to remain at the clinical site for an extension period until all subjects receiving active treatment met at least one of the following discharge criteria: individual cumulative radioactivity recovery in urine and feces >85% or total combined daily radioactive excretion in urine and feces in two consecutive 24 h collection intervals <1% of the administered dose. The end-of-study visit was on Day 14.

### Study Population

For the assessment of mass balance and ADME characteristics, six healthy male subjects aged between 18 and 55 years with a body mass index of 18.0–30.0 kg/m$^2$ were enrolled. Informed consent was obtained from each subject prior to any procedure and eligibility was determined based on various safety parameters including but not limited to vital signs, electrocardiogram (ECG), clinical laboratory data, physical examination, medical history, and previous exposure to radiation.

### Sample Management: Collection, Processing, and Storage

Blood samples for the determination of total $^{14}$C-radioactivity PK in plasma and for metabolic profiling were drawn at pre-dose, 0.5, 1, 1.5, 2, 3, 4, 6, 8, 10, 12, 14, 16, 24, 36, 48, 60, 72, 96, 120, and 144 h post-dose. Following centrifugation for 10 min at 1800 g, plasma was collected and aliquoted. Urine samples were collected during the following intervals: pre-dose (within 24 h prior to dosing), 0-8, 8-16, and 16-24 h post-dose, and thereafter over 24 h intervals until Day 7. Feces samples were collected at pre-dose (within 72 h prior to dosing), and thereafter at 24 h intervals until Day 7. In subjects, who had to stay for the extension period, blood, urine, and feces samples were collected over additional 24 h intervals up to 240 h post-dose. Urine and feces samples obtained within a collection interval were pooled and aliquoted. Prior to aliquoting, the pooled feces sample was homogenized with water (1:1 to 1:2, w/w). All samples were stored at −70°C prior analysis at Pharmaron ABS (Germantown, MD, United States).

### Pharmacokinetic Evaluation

PK parameters of total $^{14}$C-radioactivity in plasma were obtained by non-compartmental analysis using Phoenix WinNonlin (version 8.0, Certara, Princeton, NJ, United States). Individual measured plasma concentrations were directly used to determine $t_{max}$ and maximum plasma concentration ($C_{max}$), whereas area under the plasma concentration-time curve from 0 to infinity ($AUC_{0-\infty}$) was calculated according to the linear trapezoidal rule. The terminal $t_{1/2}$ of total $^{14}$C-radioactivity was calculated with the following formula: $t_{1/2} = \ln(2)/\lambda_z$, where $\lambda_z$ represents the terminal elimination rate constant.

### Mass Balance

The amount of $^{14}$C-drug-related material in plasma, urine, and homogenized feces samples was analyzed using AMS (NEC SSAMS-250, National Electrostatics Corp., Middleton, WI, United States). Just prior to analysis, frozen samples were thawed and mixed in a multi-tube vortex for 5 min at 2000 rpm. Pre-dose samples were also analyzed for subtraction of inherent $^{14}$C background levels. Before drying all samples under vacuum, sodium benzoate (Alfa Aesar, Tewksbury, MA, United States) used as carbon carrier was added to plasma and urine samples in order to reach approximately 1.7 mg carbon (i.e., minimum amount of carbon required for AMS analysis) in the final samples. Dried samples were added to a sample oxidizer (Model 307, Perkin Elmer, Waltham, MA, United States) and processed to graphite prior loading those samples into cathodes of the AMS. The AMS determined isotope ratios (i.e., $^{12}$C$^{14}$C) of each sample. For this purpose, negative carbon ions were produced through a caesium ion beam that was directed to the graphite-containing cathode. The resulting ions were extracted and forwarded to an accelerator, which caused electron stripping resulting in positively charged carbon ions. These ions were thereafter mass and charge separated by a magnet and an electrostatic analyzer, respectively. The total numbers of $^{12}$C+, $^{13}$C+, and $^{14}$C+ ions were finally counted. Raw data were expressed as percent modern carbon (pMC) and converted into radioactivity data with 100 pMC corresponding to 13.56 disintegrations per minute (dpm)/g carbon. These radioactivity data were further transformed into ng equivalents (ng-eq) per ml (plasma, urine) or per g (feces) based on the specific activity of the tracer and the dose administered.

### Sample Preparation for Metabolite Profiling

For each subject, plasma samples were pooled based on the Hamilton pooling scheme (Hamilton et al., 1981) with samples collected within 72 h. Thereafter, a single cross-subject plasma pool was prepared by using a constant proportion of each individual Hamilton pool. Proportional pooling was applied for urine and homogenized feces samples. Individual pools were prepared using 0.05 and 0.75% of each urinary and homogenized fecal void collected over 72 and 144 h, respectively. A single cross-subject pool for both excreta was prepared by taking a sample representing 10% of each individual pool to obtain a representative pool of at least 95% of the total excreted $^{14}$C across all subjects.

Pooled plasma and feces samples were further purified by liquid-liquid extraction prior to HPLC analysis. The pooled plasma sample (4,000 μl) was extracted with 1200 μl acetonitrile:methanol (80:20, v/v) (Thermo Fisher Scientific, Waltham, MA, United States). After mixing for 1 min, the sample was centrifuged for 10 min at 3,750 rpm and 10°C followed by a drying process at room temperature under a stream of nitrogen. Thereafter, the supernatant was collected, dried, and aliquoted for analysis. These extraction steps were repeated two additional times with the remaining pellet to obtain a high extraction recovery. The homogenized feces sample (200 mg) was extracted by addition of 800 μl acetonitrile,

followed by centrifugation for 5 min at 3,750 rpm and 4°C. The supernatant was collected and dried with nitrogen at 40°C. The remaining pellet was extracted by addition of 800 µl acetonitrile: water (1:1, v/v) followed by a drying process with nitrogen. The dried extract was reconstituted with acetonitrile:mobile phase A (see *Analytical Method for Metabolite Profiling*) (1:9, v/v) and vortexed for 5 min. The extraction recoveries were 93.6 and 86.9% for plasma and feces, respectively. Urine samples were directly used for analysis.

### Metabolite Profiling

Metabolite profiles were generated by using HPLC together with an AMS detector. The plasma extract (120 µl), the feces extract (10 µl), and urine (100 µl) were injected onto the HPLC (Agilent 1290, Agilent Technologies, Santa Clara, CA, United States) equipped with a binary pump G4220A (Agilent Technologies), an autosampler G4226A (Agilent Technologies), a column compartment G1316C (Agilent Technologies), and a fraction collector G1364C (Agilent Technologies). Chromatographic separation of $^{14}$C-ACT-1004-1239 and its metabolites was achieved at 40°C with a flow rate of 1 ml/min. Mobile phases consisted of 20 mM ammonium formate adjusted to pH 9.5 with ammonium hydroxide (phase A) and a 7:2:1 (v/v/v) mixture of acetonitrile, methanol, and mobile phase A (phase B). Parent drug and metabolites were eluted with the following linear gradient program: equilibration at 3 min, 10% B; 3-10 min, 10-25% B; 10-20 min, 25% B; 20-30 min, 25-30% B; 30-60 min, 30% B; 60-70 min, 30-35% B; 70-90 min, 35% B; 90-100 min, 35-40% B; 100-110 min, 40-70% B; 110-120 min, 70-95% B; 120-125 min, 95% B; 125-126 min, 95-10% B; and 126-135 min, 10% B. Using these chromatographic conditions, $^{14}$C-ACT-1004-1239 had an average retention time of 107 min. The variability in retention time did not exceed 0.8 min The reference standards were used to assess the reproducibility of the method and to confirm the retention times. Column recovery, which met the acceptance criteria (i.e., 80-120%), was investigated with AMS by measuring $^{14}$C concentration of each sample prior and after analysis by HPLC. Following HPLC analysis, pools of HPLC fractions were prepared by taking equivalent portions of consecutive individual fractions for analysis with AMS (SSAMS-250, National Electrostatics Corp., Middleton, WI, United States). The amounts of $^{14}$C in each fraction and fraction pool were summed and compared to the solution injected onto the HPLC for the determination of profile recovery.

## Metabolite Identification and Structure Elucidation *In Vivo*

### Rat

Following the human ADME study, metabolite profiling data from rats were retrospectively compared to the ones of humans. Rat metabolite profiling data were obtained from bile-duct cannulated animals ($n$ = 2) after intravenous administration of 1.7 mg/kg (200 µCi/kg) $^{14}$C-ACT-1004-1239. Rat urine samples were selected for metabolite identification as this matrix contained the major metabolites observed in humans (i.e., M1 and M23). Moreover, urine samples were preferred over plasma, bile, or feces samples due to their relatively large volumes and metabolite concentrations, that could be directly analyzed without extensive sample preparation.

Rat urine samples collected up to 72 h post dosing were centrifuged for 10 min at 20,800 g and aliquots of 25 µl were directly injected onto the liquid chromatography combined with high resolution mass spectrometry (LC-HRMS) system.

Chromatographic separation of $^{14}$C-ACT-1004-1239 and its metabolites derived from rat urine samples was achieved on a Phenomenex Gemini NX-C18 column (250 × 4.6 mm ID, 3 µm, Torrance, CA, United States) using otherwise the same analytical method as described in *Metabolite Profiling*. Using these chromatographic conditions, $^{14}$C-ACT-1004-1239 had an average retention time of 109 min. The variability in retention time did not exceed 0.5 min.

LC-HRMS analysis was performed on an LTQ Orbitrap Velos Pro (Thermo Scientific, San Jose, CA, United States) in positive and negative heated electrospray ionization mode with source voltage at 3.0 and 2.5 kV, respectively. A capillary temperature at 300°C and nitrogen sheath gas flow rate at 40 arbitrary units were used. The orbitrap resolution was set at 60,000 for full scan mode and 15,000 for $MS^n$. Fragmentation experiments were performed with a collision energy set at 35% for $MS^n$ using collision induced dissociation (CID) and high energy collision induced dissociation (HCD). Full scan LC-HRMS chromatograms were generated to identify metabolites using the Xcalibur 3.0 and Compound Discoverer 1.0 software packages (Thermo Electron, San Jose, CA, United States). Selected ion chromatograms of standard metabolic transformations were generated and checked for the presence of signals in the respective chromatograms. The presence of metabolites was confirmed by accurate mass measurement and structure elucidation was performed using $MS^n$. Finally, metabolite identity was confirmed by comparing the retention time, calculated/exact mass, and MS fragment pattern with the corresponding data of reference compounds.

### Human

Structures of metabolites that were not observed in rats were identified at A&M Labor für Analytik und Metabolismusforschung Service GmbH (Bergheim, Germany) with LC-HRMS. The LC-HRMS system consisted of an analytical column (Gemini NX-C18, 250 × 4.6 mm, 3 µm, Phenomenex Inc., Torrance, CA, United States), a guard column (C18, 4 × 3 mm, Phenomenex Inc.), a binary HPLC-pump Series 1290 (Agilent Technologies, Waldbronn, Germany), an HTC-PAL autosampler (CTC Analytics AG, Zwingen, Switzerland), column oven Series 1260 (Agilent Technologies), and a QExactive mass spectrometer (Thermo Scientific, Bremen, Germany). The samples were fractionated with HPLC using identical conditions as described in *Metabolite Profiling*. Due to the low amount of drug-related material excreted via the urinary tract and the low abundance of unknown metabolites within this matrix (see results *Cumulative Recovery of $^{14}$C-Radioactivity (Mass Balance) in Urine and Feces*; *Metabolite Profiling in Human Plasma, Urine, and Feces*), only metabolites in pooled plasma and feces samples were identified. In order to compare LC-HRMS and AMS results, sample

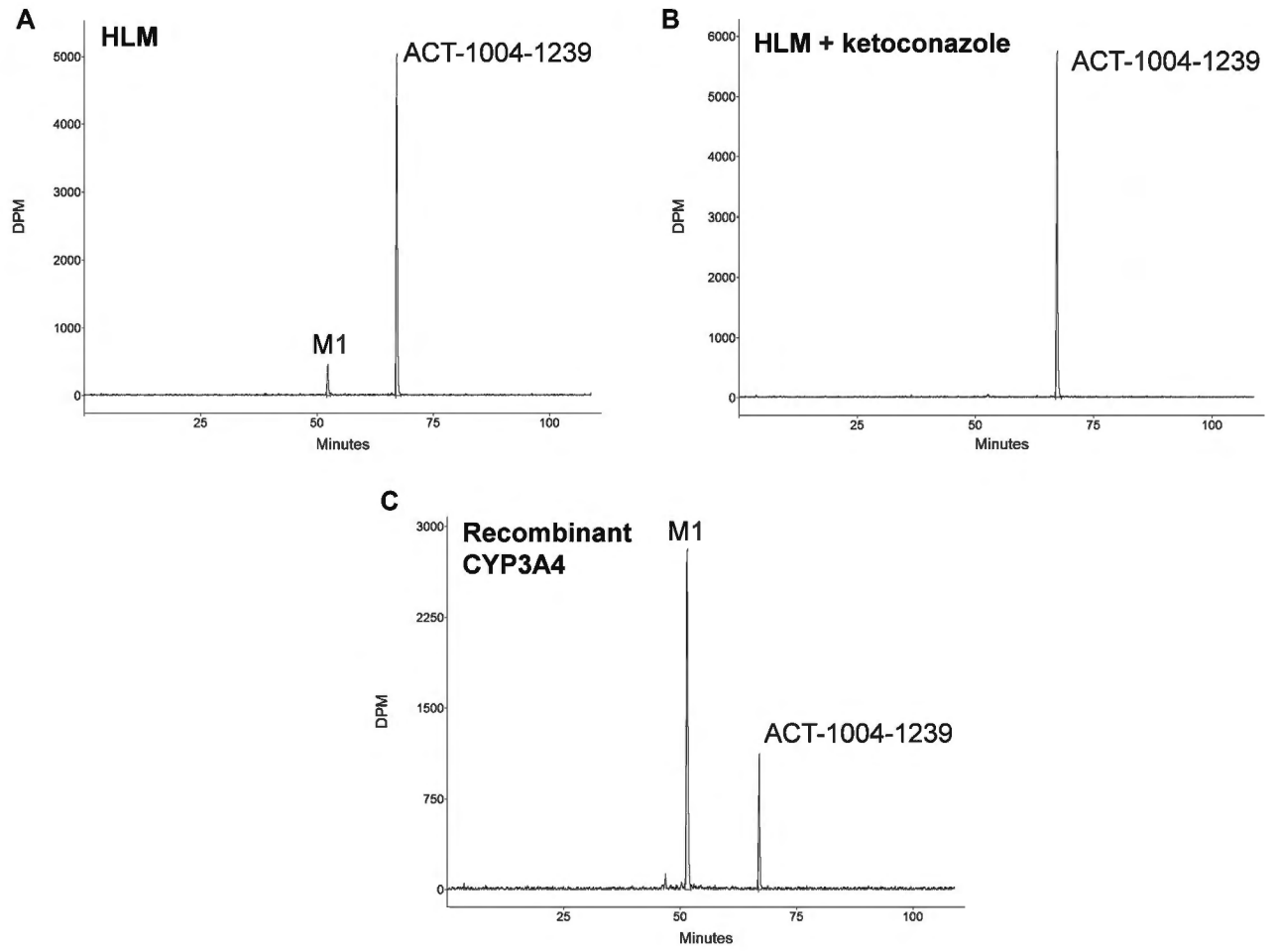


**FIGURE 1 |** *In vitro* studies: metabolic profiles of ACT-1004-1239 following incubation with **(A)** human liver microsomes (HLM), **(B)** HLM and 1 μM ketoconazole, or **(C)** recombinant CYP3A4.

preparation and the chromatographic method at A&M were identical to those at Pharmaron ABS. For the mass spectrometric analysis, heated electrospray ionization was performed in both positive and negative ionization mode with a source voltage at 3.5 kV and −3.5 kV, respectively. A capillary temperature at 300°C and nitrogen sheath gas flow rate at 65 arbitrary units were used. The orbitrap mass resolution was set at 140,000 for full scan mode and 17,500 for $MS^2$. Fragmentation experiments were performed with a collision energy set at 20, 35, 50, and 65% for $MS^n$ using HCD. Mass chromatograms were acquired with the Xcalibur 3.0 and 4.2 and data evaluation was supported by Compound Discoverer 3.1 software package (Thermo Scientific).

In total, four synthetic references (ACT-1004-1239, M1, M23, and M38) were available to support metabolite identification of non-radioactive material. The most abundant metabolites seen in the AMS chromatograms and M38 were identified by comparing the retention time, calculated/exact mass, and the $MS^2$ fragment pattern with the corresponding data of reference compounds. Structures of unknown metabolites (i.e., no synthetic reference available) were further elucidated by the interpretation of correlating fragment masses and fragment structures of non-radioactive material. Metabolites previously identified in preclinical studies were denoted with the letter "M," whereas the ones not observed in rats and only identified during this clinical study were denoted with the letter "A". The numbers following the letters were consecutively assigned based on the appearance of the metabolites within different stages of drug development.

## RESULTS

### *In Vitro* Studies

#### Incubation With HLMs and CYP-Specific Inhibitors

Incubations of $^{14}$C-ACT-1004-1239 with HLMs exclusively produced the metabolite M1 (**Figure 1A**). M1 was formed in the range of 7.5–12.0% of total chromatogram radioactivity. No metabolites were observed in the absence of the NADPH-regenerating system or HLMs. Testing the impact of validated inhibitors revealed ketoconazole as a potent inhibitor, where

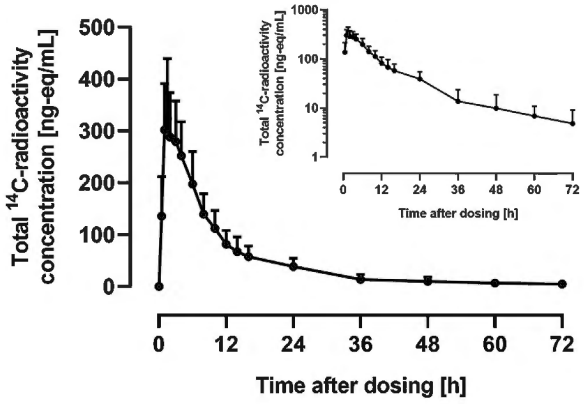


**FIGURE 2 |** Arithmetic mean (+SD) concentration vs. time profile of total $^{14}$C-radioactivity in plasma on linear and semilog (inset) scale following a single oral administration of 9.2 μg $^{14}$C-ACT-1004-1239 on top of 100 mg non-radioactive ACT-1004-1239 ($N$ = 6).

formation of M1 was completely abolished suggesting that CYP3A4 predominantly catalyzed this reaction (**Figure 1B**). In contrast, the presence of inhibitors of CYP1A2, CYP2B6, CYP2C8, CYP2C9, CYP2C19, and CYP2D6 had no effect on M1 formation (data not shown).

### Incubation With Recombinant Human CYPs

Incubation of $^{14}$C-ACT-1004-1239 with recombinant CYPs (CYP1A1, CYP1A2, CYP2B6, CYP2C8, CYP2C9, CYP2C19, CYP2D6, and CYP3A4) showed that ACT-1004-1239 was metabolized by CYP1A1, CYP2C8, CYP2C19, and CYP3A4. M1 was, as in the experiments with HLMs, the only metabolite formed. A representative chromatogram of ACT-1004-1239 metabolism by recombinant CYPs is provided in **Figure 1C**. Based on the intersystem extrapolation scaling approach, CYP3A4 was the main CYP catalyzing the formation of M1 accounting for 94% of total M1 formation, and thus, total turnover *in vitro*. CYP2C19 and CYP2C8 contributed 5.2 and 1.2% to M1 formation, respectively. The contribution of CYP1A1 to M1 formation was not further investigated due the low liver abundance of CYP1A1 in human (Stiborová et al., 2005).

## Human Study.

### Study Population

For the assessment of mass balance and ADME characteristics, six healthy male subjects received $^{14}$C-ACT-1004-1239 concomitantly with non-radioactive ACT-1004-1239. The mean (range) age and body mass index of these subjects were 31.2 (26.0-43.0) years and 25.4 (21.0-29.6) kg/m$^2$, respectively. Most subjects were Black or African American ($n$ = 5) and one subject was White. All subjects continued the extension period for additional collection of plasma, urine, and feces.

### Pharmacokinetics of Total $^{14}$C-Radioactivity

The arithmetic mean +SD plasma concentration of total $^{14}$C-radioactivity after administration of 9.2 μg $^{14}$C-ACT-1004-1239 and 100 mg ACT-1004-1239 is shown in **Figure 2**.

Following administration of $^{14}$C-ACT-1004-1239, drug-related material was rapidly absorbed. Disposition of $^{14}$C-drug-related material was covered by at least two compartments. After 72 h post-dose, the concentration of $^{14}$C-drug-related material was not measurable any longer (i.e., below the limit of quantification). PK parameters of total $^{14}$C-radioactivity in plasma are provided in **Table 1**.

### Cumulative Recovery of $^{14}$C-Radioactivity (Mass Balance) in Urine and Feces

The mass balance using the cumulative recovery of $^{14}$C-drug-related material collected in urine and feces is shown in **Figure 3**.

The geometric mean (95% confidence interval) cumulative recovery of total radioactivity was 84.1% (76.8-92.2) of dose administered. $^{14}$C-drug-related material was mainly eliminated in feces with a mean cumulative recovery in feces and urine of 69.6% (63.8-75.9) and 14.5% (12.5-16.9), respectively.

### Metabolite Profiling in Human Plasma, Urine, and Feces

Radiochromatograms of the human plasma and feces extracts, and urine sample were generated to identify ACT-1004-1239 and its radioactive metabolites. The radiochromatogram of each matrix is shown in **Figure 4**. The identities of ACT-1004-1239 and its metabolites, M1 and M23, were confirmed using reference compounds. **Table 2** summarizes the relative abundancies of ACT-1004-1239 and its metabolites in plasma, urine, and feces samples as well as the percentages of $^{14}$C-radioactive dose administered in urine and feces.

In the plasma sample, unchanged ACT-1004-1239 was the most abundant entity identified with a relative abundance of 53.9% of total radioactivity. In addition, there were two major circulating metabolites (defined as >10% of total drug exposure [AUC]), i.e., M1 and M23 accounting for 10.3 and 21.1% of total radioactivity in plasma, respectively. All other metabolites accounted for <5% of total radioactivity and were therefore not identified.

In urine, the most dominant entity detected was unchanged ACT-1004-1239 with a relative abundance of 69.6% of total radioactivity of the urine sample. Besides this, M1 was observed with much lower abundance (9.7% of total radioactivity of the urine sample). All other metabolites were significantly lower in abundance (i.e., <5% of total radioactivity in the urine sample) and were therefore not identified.

In feces, there were two dominant entities observed, i.e., M1 and A2, which accounted for 34.1 and 22.0% of total radioactivity of the feces sample, respectively. Unchanged ACT-1004-1239 and the metabolites A1 and A3 were seen with a relative abundance of 7.5, 5.8, and 3.9% of total radioactivity of the feces sample, respectively. All other metabolites were not identified due to their low signal abundance (i.e., <5% of total radioactivity in the feces sample).

Based on the cumulative recovery of $^{14}$C-drug-related material, 25.1% of the administered $^{14}$C-radioactive dose was excreted as M1 (1.4% in urine, 23.7% in feces) and 15.3% each as unchanged ACT-1004-1239 (10.1% in urine, 5.2% in feces) as

**TABLE 1 |** Pharmacokinetic parameters of total $^{14}$C-radioactivity in human plasma.

| | $t_{max}$ (h) | $C_{max}$ (ng-eq/ml) | $AUC_{0-\infty}$ (ng-eq*h/ml) | $t_{1/2}$ (h) |
|---|---|---|---|---|
| Geometric mean (95% CI) | 1.5 (1.0-3.0)[a] | 325 (240-439) | 3,759 (2,738-5,162) | 34.6 (16.8-71.4) |
| $CV_{ln}$ (%) | - | 29 | 31 | 78 |

[a]*Data is displayed as median (range).*

*$AUC_{0-\infty}$, area under the plasma concentration-time curve from 0 to infinity; CI, confidence interval; $C_{max}$, maximum plasma concentration; $CV_{ln}$, geometric coefficient of variation; $t_{1/2}$, terminal half-life; $t_{max}$, time to reach maximum plasma concentration.*

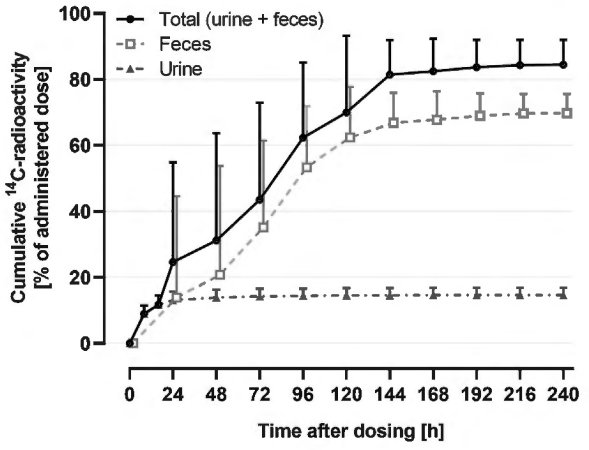


**FIGURE 3 |** Arithmetic mean (+SD) cumulative recovery vs. time profile of total $^{14}$C-radioactivity in urine and feces (shown as % of administered dose) following a single oral administration of 9.2 µg $^{14}$C-ACT-1004-1239 on top of 100 mg non-radioactive ACT-1004-1239 (*N* = 6).

well as A2 (in feces only). All other metabolites were excreted with <5% of $^{14}$C-radioactive dose (**Table 2**).

## Metabolite Identification and Structure Elucidation *In Vivo*

### Rat

A representative radiochromatogram of rat urine containing the major human metabolites (i.e., M1 and M23) is shown in **Figure 5**. Besides $^{14}$C-ACT-1004-1239, M1, and M23, also metabolites M9, M11, and M24 were detected. However, M9, M11, and M24 were not observed in humans with an abundance >5% per matrix (**Figure 4**), and therefore, their structure will not be further discussed. Based on the structural elucidation of M23, it was suggested that a counterpart metabolite M38 may exist which does not carry the radiolabel. This may explain the absence of M38 in the radiochromatogram of rat urine. To confirm presence of M1, M23, and M38 in urine, synthetic references were used for unequivocal structural identification. The mass spectrometric outputs (including, amongst others, accurate and calculated/exact masses, and *m/z* values of diagnostic fragment ions) of $^{14}$C-ACT-1004-1239, M1, M23, and M38 from rat urine are provided in **Table 3**. The accurate mass of each fragment provided in the MS spectra was compared to the calculated/exact mass. The MS key fragmentation pattern of $^{14}$C-ACT-1004-1239 (m/z 525) is shown in **Figure 6**. Structures of $^{14}$C-ACT-1004-1239, M1, M23, and M38 are shown in **Figure 7**, and were elucidated and identified in rat urine as described below.

- $^{14}$C-AC T-1004-1239

The fragmentation patterns of $^{14}$C-ACT-1004-1239 ($[M + H]^+$ *m/z* 525.2292) did not differ significantly between the ion trap CID or HCD fragmentation techniques. Therefore, all fragment ions reported herein refer to either of the two techniques. Additional insight into structural elucidation was achieved using $MS^3$ fragmentation of the most abundant $MS^2$ fragment ions. In positive ionization mode, the most intense fragment ion was with *m/z* 390. Less abundant fragment ions were fragments with *m/z* 336, 299, 216, and 136.

- M1

With a $[M + H]^+$ *m/z* 471.1823 M1 was identified as a secondary amine metabolite resulting from the loss of the methyl cyclopropyl moiety (i.e., oxidative N-dealkylation) of the parent. This was consistent with the absence of fragment ions with *m/z* 390 and 299, and the presence of the fragment with *m/z* 336 with two other fragments with *m/z* 216 and 136. The structure was confirmed using its chemical reference as shown in the supplemental material (**Supplementary Figure S1**).

- M23

M23 was identified as the difluorophenyl isoxazole carboxylic acid metabolite resulting from the central amide bond hydrolysis of the parent. This metabolite was not detected in positive ionization mode but in negative ionization mode. In negative ionization mode, the theoretical exact mass of $[M-H]^-$ *m/z* 226 was not detected. However, an ion with $[M-H]^-$ *m/z* 182.0302 was seen instead, most likely following loss of $CO_2$ in the source. $MS^2$ fragmentation of this ion yielded two fragments, i.e., with *m/z* 162 following loss of hydrogen fluoride and with *m/z* 138 corresponding to the loss of $^{14}CCH_2O$. The structure was confirmed using its chemical reference as shown in the supplemental material (**Supplementary Figure S2**).

- M38

M38, with a $[M + H]^+$ *m/z* 316.2132 was identified as the counterpart of M23 resulting from the central amide bond hydrolysis of the parent. This was consistent with the presence of fragment ions with *m/z* 299 and 216. The structure was confirmed using its chemical reference as shown in the supplemental material (**Supplementary Figure S3**).

### Human

Metabolites that were not identified in rat urine but were observed with considerable abundance in human feces

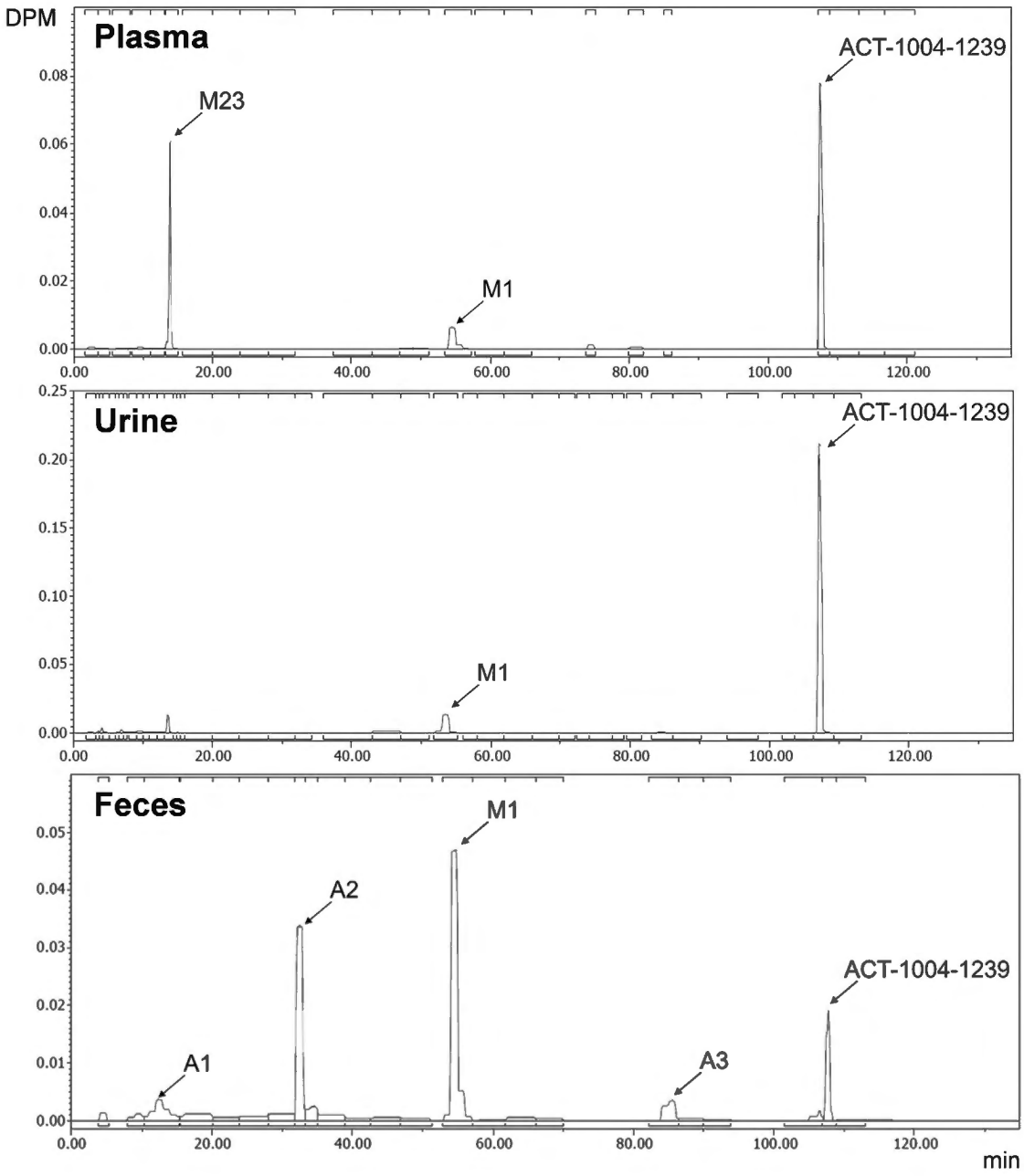


**FIGURE 4 |** Metabolic profiles of ACT-1004-1239 in human plasma (top), urine (middle), and feces (bottom) pools. Squared brackets placed above and below each radiochromatogram indicate metabolites with a relative abundance of <5%.

(**Figure 4**) were A1, A2, and A3. In order to elucidate the structures of these unknown metabolites, their calculated/exact mass and $MS^2$ fragment patterns were compared with the ones of ACT-1004-1239 and M1. The mass spectrometric outputs (including amongst others accurate and calculated/exact masses and *m/z* values of diagnostic fragment ions) of ACT-1004-1239, M1, A1, A2, and A3 from human feces are provided in **Table 4**. The MS key fragmentation pattern of $^{14}$C-ACT-1004-1239 (m/z 525) is shown in **Figure 6**. The structures of these unknown metabolites were elucidated and identified in human feces as described below.

- A1

A1 was identified as an analog of M1 after oxidative defluorination at the difluorophenyl moiety (fragment ion with *m/z* 141). This was consistent with the $MS^2$ fragmentation spectra, which showed a fragment ion with *m/z* 139 representing a hydroxyfluorobenzoic acid fragment instead of *m/z* 141 and a fragment ion with *m/z* 332 instead of *m/z* 334. Other fragment ions (with *m/z* 136 and 216) were available in both spectra. However, it remains unknown which of the two fluorine atoms was substituted with a hydroxy function. The MS2

**TABLE 2 |** Summary of relative abundance of ACT-1004-1239 and its metabolites.

| Compound ID | Plasma | Urine | | Feces | | Urine + feces |
|---|---|---|---|---|---|---|
| | % in sample | % in sample | % of dose[a] | % in sample | % of dose[a] | % of dose |
| ACT-1004-1239 | 53.9 | 69.6 | 10.1 | 7.5 | 5.2 | 15.3 |
| M1 | 10.3 | 9.7 | 1.4 | 34.1 | 23.7 | 25.1 |
| M23 | 21.1 | - | - | - | - | - |
| A1 | - | - | - | 5.8 | 4.0 | 4.0 |
| A2 | - | - | - | 22.0 | 15.3 | 15.3 |
| A3 | - | - | - | 3.9 | 2.7 | 2.7 |
| Other[b] | 14.7 | 20.7 | 3.0 | 26.7 | 18.6 | 21.6 |
| Total | - | - | 14.5 | - | 69.6 | 84.1 |

[a]*Calculations were based on geometric mean of total cumulative excretion in urine/feces.*
[b]*Refers to the sum of metabolites with a relative abundance of <5%.*

spectra of A1 and M1 $[M + H]^+$ ions are provided in the supplemental material (**Supplementary Figure S4**).

- A2

A2 was identified as a reduced analog of M1 after addition of two hydrogen atoms. The fragment ions with *m/z* 136, 141, and 216 were present in the spectra of A2 and M1, whereas the fragment ions with *m/z* 210 and 336 were only detectable in the $MS^2$ spectrum of A2. This indicated that the addition of two hydrogen atoms had taken place at the isoxazole moiety of the molecule which may have led to ring opening resulting in an imine and hydroxy group. The MS2 spectra of A2 and M1 $[M + H]^+$ ions are provided in the supplemental material (**Supplementary Figure S5**).

- A3

A3 was identified as a reduced analog of the parent compound after addition of two hydrogen atoms. Upon comparison of $MS^2$

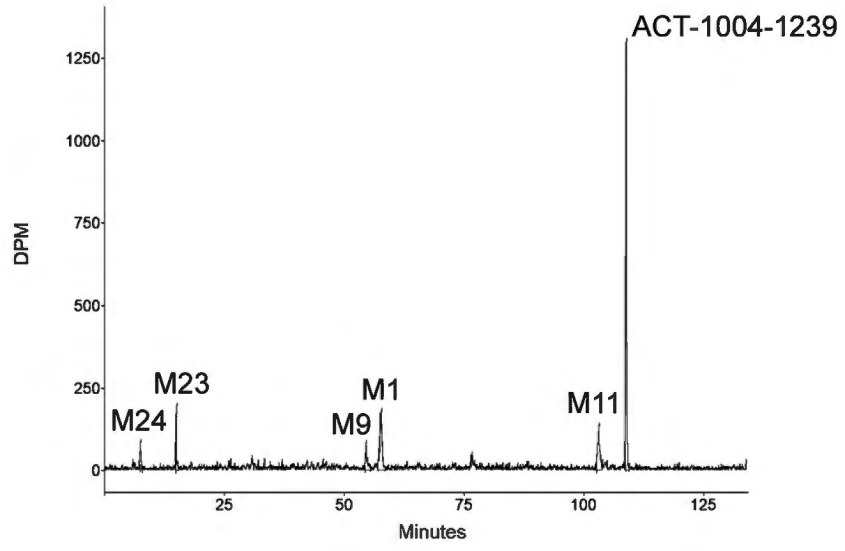


**FIGURE 5 |** Representative metabolic profile of ACT-1004-1239 in rat urine after intravenous dosing of $^{14}$C-ACT-1004-1239.

**TABLE 3 |** Mass spectrometric identification of $^{14}$C-ACT-1004-1239 and its metabolites in rat urine.

**Positive ionization mode**

| Compound | Retention time (min) | Accurate mass $[M + H]^+$ | Calculated/exact mass $[M + H]^+$ | Diagnostic fragment ions ($MS^n$) | Identity |
|---|---|---|---|---|---|
| ACT-1004-1239 | 106.5 | 525.2292 | 525.2296 | 390, 336, 299, 216, 136 | - |
| M1 | 54.4 | 471.1823 | 471.1827 | 336, 216, 136 | - $C_4H_6$ (oxidative N-dealkylation) |
| M38 | 19.9 | 316.2132 | 316.2132 | 299, 216 | - $C_{10}H_3F_2NO_2$ (hydrolysis) |

**Negative ionization mode**

| Compound | Retention time (min) | Accurate mass $[M-H]^-$ | Calculated/exact mass $[M-H]^-$ | Diagnostic fragment ions ($MS^n$) | Identity |
|---|---|---|---|---|---|
| M23[a] | 13.4 | 182.0302 | 182.0299 | 182, 162, 138 | - $C_{17}H_{23}N_5O$+ O (hydrolysis) |

*For all compounds, except M38, the presented data refer to radiolabeled material (e.g., $^{14}$C-ACT-1004-1239).*
[a]*Source fragmentation, the [M-H]- ion was not directly observed, [M-$CO_2$-H]- was detected instead.*

spectra of ACT-1004-1239 and A3, the fragment ions with *m/z* 136, 141, and 216 were present in both spectra, whereas the fragment ions with *m/z* 210 and 390 were only detectable in the spectrum of A3. All other diagnostic fragment ions were similar to the fragments of ACT-1004-1239. This indicated that the addition of two hydrogen atoms had taken place at the isoxazole moiety of the molecule which may have led to ring opening resulting in an imine and hydroxy group. The MS2 spectra of A3 and parent drug $[M + H]^+$ ions are provided in the supplemental material (**Supplementary Figure S6**).

Taken together, based on the results from metabolite profiling, identification, and elucidation, the metabolic pathways in humans are proposed as depicted in **Figure 7**. The elimination of ACT-1004-1239 via M1 was the only metabolic pathway that contributed to ≥25% of elimination:

- Oxidative N-dealkylation of ACT-1004-1239 to M1 (representing 25.1% of $^{14}$C-radioactive dose). M1 thereafter undergoes two notable reactions: a) oxidative defluorination to A1 (representing 4.0% of $^{14}$C-radioactive dose) and b) reduction to A2 (representing 15.3% of $^{14}$C-radioactive dose).

Apart from this, a minor elimination pathway was via A3 (i.e., 2.7% of $^{14}$C-radioactive dose).

## DISCUSSION

ACT-1004-1239 is an orally available, potent, and selective first-in-class CXCR7 antagonist that showed efficacy in preclinical animal models of multiple sclerosis (Pouzol et al., 2021a) and acute lung injury (Pouzol et al., 2021b), and had a favorable clinical profile following single- (Huynh et al., 2021b) and multiple-dose (Huynh et al., 2021a) administration. In context of drug development, identification of metabolites and metabolic pathways of a drug is of utmost relevance. Therefore, *in vitro* and *in vivo* studies were conducted to 1) identify human enzymes involved in the metabolism of ACT-1004-1239 and 2) characterize ADME in humans with the use of rat samples for metabolite structure elucidation of major human metabolites.

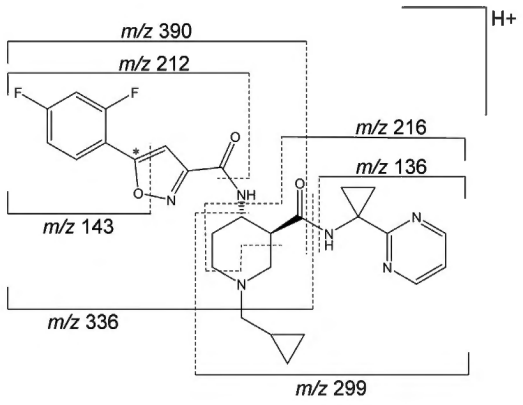


**FIGURE 6 |** Mass spectrometric fragmentation pattern of $^{14}$C-ACT-1004-1239. The asterisk (*) indicates the position of the $^{14}$C label, which was taken into consideration for the applicable accurate fragment masses (*m/z*). The fragment ion with m/z 212 includes in addition to the depicted pattern two hydrogen atoms.

*In vitro*, two complementary approaches (incubation with HLMs in the absence/presence of CYP-specific chemical inhibitors and experiments with recombinant CYPs) were chosen to identify the CYPs involved in the metabolism of ACT-1004-1239. It was shown that ACT-1004-1239 was particularly metabolized to M1 via phase I biotransformation enzymes including CYP1A1, CYP2C8, CYP2C19, and CYP3A4. Additional analyses using the intersystem extrapolation scaling approach (Chen et al., 2011) revealed that CYP3A4 was the main contributor to ACT-1004-1239 metabolic clearance, accounting for 94% of total turnover *in vitro*.

The ADME characteristics in humans were investigated in the context of an FIH study applying a microtracer approach (Huynh et al., 2021b). Such integrative studies have previously been successfully conducted (Muehlan et al., 2018, Muehlan et al., 2019). The integration of a human ADME study in early clinical studies (e.g., FIH study) is an innovative approach to accelerate clinical development (Muehlan et al., 2018). It enables characterization of metabolites during the early stage of clinical development, which is encouraged by United States Food and Drug Administration (FDA) (United States Department of Health and Human Services Food and Drug Administration Center for Drug Evaluation and Research, 2020b) and it allows to enhance resource efficiency. Indeed, for the integrated approach only very low amounts of radiolabeled compound are needed, so that no determination of radiation burden is required, and hence, no quantitative whole-body autoradiography in rodents is to be conducted. In addition, the very low amounts used do not require to be produced according to Good Manufacturing Practice (Ufer et al., 2017; Spracklin et al., 2020). However, for such an integrative approach a highly sensitive technique is needed, which is realized by the application of AMS (Graham and Garner, 2003; Lappin et al., 2006). In contrast to most conventional ADME studies, the conduct of such integrative studies typically uses different formulations for non-radioactive and radioactive drug. This could possibly result in non-homogenous absorption resulting in unequal quantitative data between non-radioactive and radioactive material. Retrospective quantitative analysis of non-radioactive parent drug and metabolites using the standard addition approach confirmed their relative abundance in plasma as observed for radioactive equivalents provided in **Table 1**. These data support the homogeneity in absorption in this study.

Based on the results obtained in the human ADME study, it was shown that the concentration-time profile of total $^{14}$C-radioactivity was similar to the one of non-radioactive ACT-1004-1239 (Huynh et al., 2021b) with comparable $t_{max}$ and $C_{max}$. However, the geometric means of $AUC_{0-\infty}$ and terminal $t_{1/2}$ of total $^{14}$C-radioactivity were approximately 2-fold higher than the ones of 100 mg non-radioactive

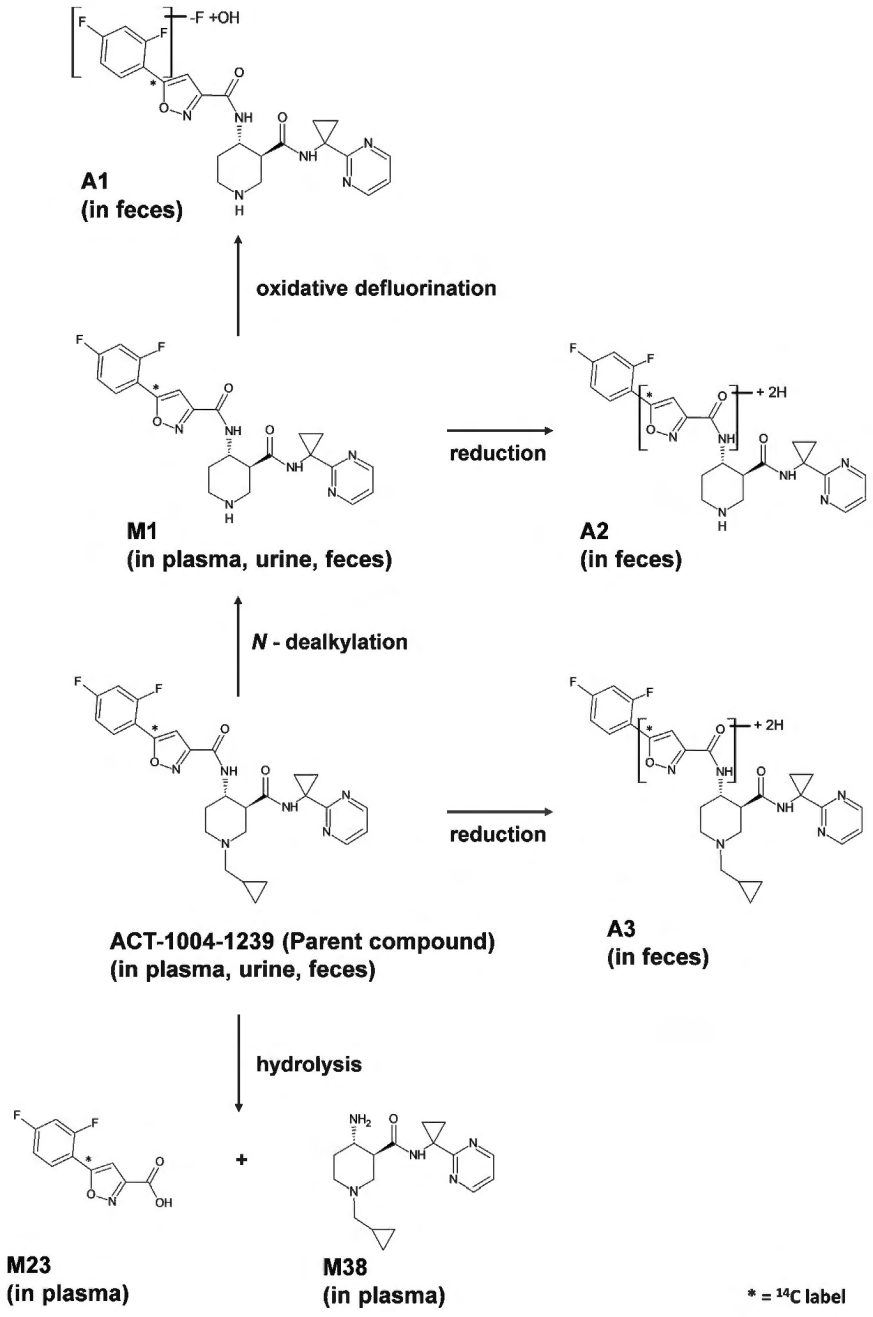


**FIGURE 7 |** Proposed metabolic pathways of ACT-1004-1239 in humans.

ACT-1004-1239. This suggests that the metabolism of ACT-1004-1239 in humans results in metabolites, which have a lower elimination rate, and thus, cause the increase in $AUC_{0-\infty}$ and $t_{1/2}$ as previously observed (Roffel et al., 2017; Muehlan et al., 2019). Following oral administration of 9.2 μg $^{14}$C-ACT-1004-1239, the mean cumulative recovery of radioactivity in urine and feces was approximately 84%, which is above the generally acceptable threshold for human ADME studies (>80%) (Roffey et al., 2007). These data are in line with previous observations showing that compounds with a radioactivity $t_{1/2}$ < 50 h achieve at least 80% of cumulative recovery (Roffey et al., 2007). Investigation of mass balance revealed that ACT-1004-1239 was predominantly eliminated *via* feces and to a lesser extent in urine. Based on the totality of radioactivity recovered in feces and urine, it is unlikely that ACT-1004-1239 is eliminated *via* other elimination routes. This is supported by the physicochemical properties of ACT-1004-1239 (Richard-Bildstein et al., 2020).

Profiling the human plasma samples for metabolites revealed two major circulating metabolites (i.e., M1 and M23) besides the

**TABLE 4 |** Mass spectrometric identification of ACT-1004-1239 and its metabolites in human feces.

| Compound | Retention time (min) | Accurate mass $[M + H]^+$ | Calculated/exact mass $[M + H]^+$ | Diagnostic fragment ions ($MS^n$) | Identity |
|---|---|---|---|---|---|
| ACT-1004-1239 | 107.6 | 523.2265 | 523.2264 | 388, 334, 216, 141, 136 | - |
| M1 | 55.7 | 469.1795 | 469.1794 | 334, 216, 141, 136 | - $C_4H_6$ (oxidative N-dealkylation) |
| A1 | 12.0 | 467.1851 | 467.1838 | 332, 216, 139, 136 | M1 - F + OH (oxidative defluorination) |
| A2 | 33.0 | 471.1949 | 471.1951 | 336, 216, 210, 141,136 | M1 + $H_2$ (reduction) |
| A3 | 85.6 | 525.2425 | 525.2420 | 390, 216, 210, 141, 136 | + $H_2$ (reduction) |

*Data are displayed in positive ionization mode.*
*For all compounds, the presented data refer to non-radiolabeled material (e.g., ACT-1004-1239).*

parent compound. As these metabolites were also present in rats (i.e., not human-specific), their structures were elucidated using highly concentrated rat urine samples. M1 is the product of oxidative N-dealkylation with loss of the cyclopropylmethyl moiety from the parent. On the other hand, M23 results most likely from hydrolysis of the central amide bond of the parent. Exploratory *in vitro* studies investigating enzymes that could catalyze the formation of M23 excluded the involvement of carboxylesterases (i.e., CES1b, CES1c, and CES2) which are known to hydrolyze amide bonds (Idorsia Pharmaceuticals Ltd., data on file). Additional investigations with other hydrolases such as amidases or epoxide hydrolases are to be considered in order to understand formation of M23 (Magdalou et al., 2003). Formation and structural elucidation of M23 suggested the theoretical presence of its metabolite counterpart. This metabolite was detected and identified as M38. As it was devoid of the radiolabel, M38 was not detectable in the rat radiochromatogram. However, the analysis using MS confirmed the presence of M38 in rat urine. Similar to rats, M38 was not detectable in the human radiochromatograms. Nevertheless, quantification of M38 in the pooled human plasma using a synthesized reference indicated that its presence was negligible, and hence, it is not considered a major circulating metabolite. In contrast to M1 and M38, M23 was not detectable in the positive ionization mode, but only in negative ionization mode, most likely as the weakly basic isoxazole ring did not allow for an efficient protonation (Palmer, 2003).

Major circulating metabolites constituted >10% of total drug exposure (AUC) like M1 and M23 have to be cautiously investigated for any relevant human safety concern (e.g., disproportionality). For this purpose, it is required to examine according to the guidance for *Safety Testing of Drug Metabolites* (United States Department of Health and Human Services Food and Drug Administration Center for Drug Evaluation and Research, 2020b) whether the human plasma exposure to such metabolites is distinctly greater than the maximum exposure in animals used for toxicological evaluation of ACT-1004-1239. This additional investigation is to be performed before the initiation of any large-scale clinical trials. Besides the identification of major circulating metabolites, another objective of a human ADME study is the identification of main metabolic pathways. For this purpose, the metabolites A1, A2, and A3 were elucidated in human feces. A1 was identified as a secondary product following oxidative defluorination of M1. This type of biotransformation reaction can be catalyzed by CYPs (e.g., CYP3A4 and CYP1A1/2) and/or oxygenases such as flavin-containing monooxygenases and was previously observed in the metabolism of other drugs (Xie et al., 2013; Amaya et al., 2018). The reductive metabolites, A2 and A3, were formed following reductive cleavage of the isoxazole ring (i.e., N-O bond) to an imine intermediate which was thereafter hydrolyzed. This ring opening may be explained by the chemical properties of the isoxazole ring containing, adjacent to the nitrogen, an oxygen atom with greater electronegativity which may increase the susceptibility to reduction (Dalvie et al., 2002). The reductive cleavage of the isoxazole ring was also observed with other xenobiotics and was catalyzed by the gut microflora, CYPs, and aldehyde oxidase (Mannens et al., 1993; Sugihara et al., 1996; Kalgutkar et al., 2003; Zhang et al., 2008). Additional exploratory investigations with, for example, gut microflora could aid in elaboration of the formation of A2 and A3. Except for A1, A2, and A3, no metabolites were structurally elucidated in human excreta, due to their significantly lower abundance (i.e., <5% of total radioactivity per excreta sample). M1 was the only known metabolite that was confirmed in human urine and feces. Taking the retention time and its appearance in rat urine into consideration, it is likely that M23 is also present in human urine. However, the identity of M23 in human urine sample was not further investigated and was therefore not confirmed.

Based on metabolite profiling results, only one metabolic pathway contributed to ≥25% of ACT-1004-1239 elimination:

- Oxidative N-dealkylation of ACT-1004-1239 to M1. M1 undergoes thereafter two reactions: a) oxidative defluorination to A1 and b) reduction to A2.

Since the reaction from ACT-1004-1239 to M1 is predominantly catalyzed by CYP3A4, it is recommended to clinically investigate possible drug-drug interactions of ACT-1004-1239 using strong index inhibitors and/or inducers of this enzyme (United States Department of Health and Human Services Food and Drug Administration Center for Drug Evaluation and Research, 2020a). In addition, according to health authorities guidelines (United States Department of Health and Human Services Food and Drug Administration Center for Drug Evaluation and Research, 2003; European

Medicines Agency Evaluation of Medicines for Human Use, 2018), it is recommended to conduct PK studies in subjects with hepatic impairment when the hepatic metabolism and/or excretion accounts for a substantial portion (>20%) of the elimination of parent compound. Thus, such aforementioned PK studies should be conducted in the clinical development program of ACT-1004-1239.

## CONCLUSION

Taken together, integration of an ADME study using the microtracer approach in conjunction with the AMS methodology in an FIH study facilitated the elucidation of the metabolism of ACT-1004-1239, a first-in-class CXCR7 antagonist, in early clinical development. Results from *in vitro* and *in vivo* studies underpin the relevance of preclinical investigations to support the identification of metabolites in humans. In this human study, the disposition and metabolic pathways of ACT-1004-1239 were sufficiently characterized, allowing to determine potential successive clinical studies. It was shown that elimination of ACT-1004-1239 mainly occurred through feces following major metabolism via CYP3A4. Besides ACT-1004-1239, two major circulating metabolites were identified in human plasma.

## DATA AVAILABILITY STATEMENT

The original contributions presented in the study are included in the article/**Supplementary Material**, further inquiries can be directed to the corresponding author.

## ETHICS STATEMENT

The studies involving human participants were reviewed and approved by IntegReview Institutional Review Board. The patients/participants provided their written informed consent to participate in this study. The animal study was reviewed and approved by Basel Cantonal Veterinary Office.

## AUTHOR CONTRIBUTIONS

CH, SS, and JS wrote the manuscript. CG, JH, HM, JD, and PS reviewed and edited the manuscript. SS, JS, and CG designed and analyzed the preclinical data. CH, JH, JD, and PS designed and analyzed the clinical data. All authors reviewed and approved the final manuscript.

## FUNDING

The authors declare that this study was sponsored by Idorsia Pharmaceuticals Ltd. The sponsor was involved in the study design, collection, analysis, interpretation of data, the writing of this article/the decision to submit it for publication.

## ACKNOWLEDGMENTS

The authors would like to thank Stephen English from Pharmaron ABS (Germantown, MD, United States) for coordinating the AMS analyses as well as the principal investigator of the study Mohammed Al-Ibrahim (Pharmaron CPC Inc., Baltimore, MD, United States). In addition, the authors would like to thank colleagues from Idorsia Pharmaceuticals Ltd. for their dedicated support in terms of data generation or discussion including Hamed Aissoui, Marie-Laure Boof, Florian Franz, Jérôme Gabillet, Susanne Globig, Anne-Sophie Guern, Martin Holdener, Anna Luciuk, Racheal Rowles, Giancarlo Sabattini, and Mike Ufer.

## SUPPLEMENTARY MATERIAL

The Supplementary Material for this article can be found online at: https://www.frontiersin.org/articles/10.3389/fphar.2022.812065/full#supplementary-material

## REFERENCES

Amaya, G. M., Durandis, R., Bourgeois, D. S., Perkins, J. A., Abouda, A. A., Wines, K. J., et al. (2018). Cytochromes P450 1A2 and 3A4 Catalyze the Metabolic Activation of Sunitinib. *Chem. Res. Toxicol.* 31, 570–584. doi:10.1021/acs.chemrestox.8b00005

Arjomand, A. (2010). Accelerator Mass Spectrometry-Enabled Studies: Current Status and Future Prospects. *Bioanalysis* 2, 519–541. doi:10.4155/bio.09.188

Boddy, A. V., Sludden, J., Griffin, M. J., Garner, C., Kendrick, J., Mistry, P., et al. (2007). Pharmacokinetic Investigation of Imatinib Using Accelerator Mass Spectrometry in Patients with Chronic Myeloid Leukemia. *Clin. Cancer Res.* 13, 4164–4169. doi:10.1158/1078-0432.CCR-06-2179

Chen, Y., Liu, L., Nguyen, K., and Fretland, A. J. (2011). Utility of Intersystem Extrapolation Factors in Early Reaction Phenotyping and the Quantitative Extrapolation of Human Liver Microsomal Intrinsic Clearance Using Recombinant Cytochromes P450. *Drug Metab. Dispos.* 39, 373–382. doi:10.1124/dmd.110.035147

Dalvie, D. K., Kalgutkar, A. S., Khojasteh-Bakht, S. C., Obach, R. S., and O'Donnell, J. P. (2002). Biotransformation Reactions of Five-Membered Aromatic Heterocyclic Rings. *Chem. Res. Toxicol.* 15, 269–299. doi:10.1021/tx015574b

European Medicines Agency Evaluation of Medicines for Human Use (2018). Guideline on Strategies to Identify and Mitigate Risks for First-In-Human and Early Clinical Trials with Investigational Medicinal Products. Available at: https://www.ema.europa.eu/en/documents/scientific-guideline/guideline-strategies-identify-mitigate-risks-first-human-early-clinical-trials-investigational_en.pdf (Accessed September 29, 2021).

Graham, L., and Garner, R. C. (2003). Big Physics, Small Doses: The Use of AMS and PET in Human Microdosing of Development Drugs. *Nat. Rev. Drug Discov.* 2, 233–240. doi:10.1038/nrd1037

Hamilton, R. A., Garnett, W. R., and Kline, B. J. (1981). Determination of Mean Valproic Acid Serum Level by Assay of a Single Pooled Sample. *Clin. Pharmacol. Ther.* 29, 408–413. doi:10.1038/clpt.1981.56

Huynh, C., Brussee, J. M., Pouzol, L., Fonseca, M., Meyer zu Schwabedissen, H. E., Dingemanse, J., et al. (2021a). Target Engagement of the First-In-Class CXCR7 Antagonist ACT-1004-1239 Following Multiple-Dose Administration in Mice

and Humans. *Biomed. Pharmacother.* 144, 112363. doi:10.1016/j.biopha.2021.112363

Huynh, C., Henrich, A., Strasser, D. S., Boof, M. L., Al-Ibrahim, M., Meyer zu Schwabedissen, H. E., et al. (2021b). A Multipurpose First-In-Human Study with the Novel CXCR7 Antagonist ACT-1004-1239 Using CXCL12 Plasma Concentrations as Target Engagement Biomarker. *Clin. Pharmacol. Ther.* 109, 1648–1659. doi:10.1002/cpt.2154

Kalgutkar, A. S., Nguyen, H. T., Vaz, A. D. N., Doan, A., Dalvie, D. K., McLeod, D. G., et al. (2003). *In Vitro* METABOLISM STUDIES ON THE ISOXAZOLE RING SCISSION IN THE ANTI-INFLAMMATORY AGENT LEFLUNOMIDE TO ITS ACTIVE α-CYANOENOL METABOLITE A771726: MECHANISTIC SIMILARITIES WITH THE CYTOCHROME P450-CATALYZED DEHYDRATION OF ALDOXIMES. *Drug Metab. Dispos.* 31, 1240–1250. doi:10.1124/dmd.31.10.1240

Lappin, G., Kuhnz, W., Jochemsen, R., Kneer, J., Chaudhary, A., Oosterhuis, B., et al. (2006). Use of Microdosing to Predict Pharmacokinetics at the Therapeutic Dose: Experience with 5 Drugs. *Clin. Pharmacol. Ther.* 80, 203–215. doi:10.1016/j.clpt.2006.05.008

Magdalou, J., Fournel-Gigleux, S., Testa, B., and Ouzzine, M. (2003). "Biotransformation Reactions," in *The Practice of Medicinal Chemistry* (London: Elsevier), 517–543. doi:10.1016/B978-012744481-9/50035-0

Mannens, G., Huang, M. L., Meuldermans, W., Hendrickx, J., Woestenborghs, R., and Heykants, J. (1993). Absorption, Metabolism, and Excretion of Risperidone in Humans. *Drug Metab. Dispos* 21, 1134–1141. Available at: http://dmd.aspetjournals.org/content/21/6/1134.abstract.

Muehlan, C., Fischer, H., Zimmer, D., Aissaoui, H., Grimont, J., Boss, C., et al. (2019). Metabolism of the Dual Orexin Receptor Antagonist ACT-541468, Based on Microtracer/Accelerator Mass Spectrometry. *Curr. Drug Metab.* 20, 254–265. doi:10.2174/1389200220666190206141814

Muehlan, C., Heuberger, J., Juif, P. E., Croft, M., van Gerven, J., and Dingemanse, J. (2018). Accelerated Development of the Dual Orexin Receptor Antagonist ACT-541468: Integration of a Microtracer in a First-In-Human Study. *Clin. Pharmacol. Ther.* 104, 1022–1029. doi:10.1002/cpt.1046

Palmer, D. C. (2003). *Oxazoles: Synthesis, Reactions, and Spectroscopy, Part A*, Vol. 60. Raritan, NJ: John Wiley & Sons.

Pouzol, L., Baumlin, N., Sassi, A., Tunis, M., Marrie, J., Vezzali, E., et al. (2021a). ACT-1004-1239, a First-in-class CXCR7 Antagonist with Both Immunomodulatory and Promyelinating Effects for the Treatment of Inflammatory Demyelinating Diseases. *FASEB j.* 35, 1–17. doi:10.1096/fj.202002465R

Pouzol, L., Sassi, A., Baumlin, N., Tunis, M., Strasser, D. S., Lehembre, F., et al. (2021b). CXCR7 Antagonism Reduces Acute Lung Injury Pathogenesis. *Front. Pharmacol.* 12, 748740. doi:10.3389/fphar.2021.748740

Pouzol, L., Tunis, M., Baumlin, N., Sassi, A., Marrie, J., Vezzali, E., et al. (2021c). CXCR7 Antagonism with ACT-1004-1239 Reduces Neuroinflammation and Accelerates Remyelination in Murine Demyelinating Models (2236). *Neurology* 96, 2236. Available at: http://n.neurology.org/content/96/15_Supplement/2236.abstract.

Richard-Bildstein, S., Aissaoui, H., Pothier, J., Schäfer, G., Gnerre, C., Lindenberg, E., et al. (2020). Discovery of the Potent, Selective, Orally Available CXCR7 Antagonist ACT-1004-1239. *J. Med. Chem.* 63, 15864–15882. doi:10.1021/acs.jmedchem.0c01588

Roffel, A., Marle, S. v., Choi, S., Lee, H., Dueker, S., and Tiessen, R. (2017). Metabolism and Excretion of GCC-4401C, a Factor Xa Inhibitor, in Humans. *Int. J. Pharmacokinet.* 2, 93–104. doi:10.4155/ipk-2016-0015

Roffey, S. J., Obach, R. S., Gedge, J. I., and Smith, D. A. (2007). What Is the Objective of the Mass Balance Study? A Retrospective Analysis of Data in Animal and Human Excretion Studies Employing Radiolabeled Drugs. *Drug Metab. Rev.* 39, 17–43. doi:10.1080/03602530600952172

Spracklin, D. K., Chen, D., Bergman, A. J., Callegari, E., and Obach, R. S. (2020). Mini-Review: Comprehensive Drug Disposition Knowledge Generated in the Modern Human Radiolabeled ADME Study. *CPT Pharmacometrics Syst. Pharmacol.* 9, 428–434. doi:10.1002/psp4.12540

Stiborová, M., Martínek, V., Rýdlová, H., Koblas, T., and Hodek, P. (2005). Expression of Cytochrome P450 1A1 and its Contribution to Oxidation of a Potential Human Carcinogen 1-Phenylazo-2-Naphthol (Sudan I) in Human Livers. *Cancer Lett.* 220, 145–154. doi:10.1016/j.canlet.2004.07.036

Sugihara, K., Kitamura, S., and Tatsumi, K. (1996). Involvement of Mammalian Liver Cytosols and Aldehyde Oxidase in Reductive Metabolism of Zonisamide. *Drug Metab. Dispos.* 24, 199–202. Available at: http://dmd.aspetjournals.org/content/24/2/199.abstract.

Ufer, M., Juif, P. E., Boof, M. L., Muehlan, C., and Dingemanse, J. (2017). Metabolite Profiling in Early Clinical Drug Development: Current Status and Future Prospects. *Expert Opin. Drug Metab. Toxicol.* 13, 803–806. doi:10.1080/17425255.2017.1351944

United States Department of Health and Human Services Food and Drug Administration Center for Drug Evaluation and Research (2020a). *In Vitro* Drug Interaction Studies - Cytochrome P450 Enzyme and Transporter Mediated Drug Interactions, Guidance for Industry. Available at: https://www.fda.gov/media/134582/download (Accessed September 1, 2021).

United States Department of Health and Human Services Food and Drug Administration Center for Drug Evaluation and Research (2003). Pharmacokinetics in Patients with Impaired Hepatic Function: Study Design, Data Analysis, and Impact on Dosing and Labeling, Guidance for Industry. Available at: https://www.fda.gov/media/71311/download (Accessed August 25, 2021).

United States Department of Health and Human Services Food and Drug Administration Center for Drug Evaluation and Research (2020b). Safety Testing of Drug Metabolites, Guidance for Industry. Revision 2. Available at: https://www.fda.gov/media/72279/download (Accessed August 16, 2021).

Xie, C., Zhou, J., Guo, Z., Diao, X., Gao, Z., Zhong, D., et al. (2013). Metabolism and Bioactivation of Famitinib, a Novel Inhibitor of Receptor Tyrosine Kinase, in Cancer Patients. *Br. J. Pharmacol.* 168, 1687–1706. doi:10.1111/bph.12047

Zhang, D., Raghavan, N., Chen, S. Y., Zhang, H., Quan, M., Lecureux, L., et al. (2008). Reductive Isoxazole Ring Opening of the Anticoagulant Razaxaban Is the Major Metabolic Clearance Pathway in Rats and Dogs. *Drug Metab. Dispos.* 36, 303–315. doi:10.1124/dmd.107.018416

**Conflict of Interest:** The authors declare that this study was sponsored by Idorsia Pharmaceuticals Ltd. The sponsor was involved in the study design, collection, analysis, interpretation of data, the writing of this article/the decision to submit it for publication.

## 3.3 Multiple-ascending dose study with ACT-1004-1239

# Target engagement of the first-in-class CXCR7 antagonist ACT-1004-1239 following multiple-dose administration in mice and humans

Christine Huynh[1,2], Janneke M. Brussee[1], Laetitia Pouzol[3], Marlene Fonseca[4], Henriette E. Meyer zu Schwabedissen[2], Jasper Dingemanse[1], Patricia N. Sidharta[1]

[1]Idorsia Pharmaceuticals Ltd, Department of Clinical Pharmacology, Allschwil, Switzerland

[2]University of Basel, Biopharmacy, Department of Pharmaceutical Sciences, Basel, Switzerland

[3]Idorsia Pharmaceuticals Ltd, Department of Pharmacology Immunology, Allschwil, Switzerland

[4]BlueClinical Phase 1, Hospital de Prelada, Porto, Portugal

Published in Biomed Pharmacother. 2021;144(September):112363

Biomedicine & Pharmacotherapy 144 (2021) 112363

Contents lists available at ScienceDirect

Biomedicine & Pharmacotherapy

journal homepage: www.elsevier.com/locate/biopha

# Target engagement of the first-in-class CXCR7 antagonist ACT-1004-1239 following multiple-dose administration in mice and humans

Christine Huynh [a,b,*], Janneke M. Brussee [a], Laetitia Pouzol [c], Marlene Fonseca [d], Henriette E. Meyer zu Schwabedissen [b], Jasper Dingemanse [a], Patricia N. Sidharta [a]

[a] Idorsia Pharmaceuticals Ltd, Department of Clinical Pharmacology, 4123 Allschwil, Switzerland
[b] Biopharmacy, Department of Pharmaceutical Sciences, University of Basel, 4056 Basel, Switzerland
[c] Idorsia Pharmaceuticals Ltd, Department of Pharmacology Immunology, 4123 Allschwil, Switzerland
[d] BlueClinical Phase 1, Hospital de Prelada, 4250-449 Porto, Portugal

ARTICLE INFO

*Keywords:*
CXCR7
CXCL12
ACT-1004-1239
Target engagement
Multiple-ascending dose study
Mice
Humans

ABSTRACT

Antagonism of the chemokine receptor CXCR7 has shown promising effects in diverse disease areas through modulation of its ligands, CXCL11 and CXCL12. Preclinical data of the first-in-class CXCR7 antagonist, ACT-1004-1239, showed efficacy in animal models of multiple sclerosis and acute lung injury. In healthy humans, single-dose administration of ACT-1004-1239 revealed a favorable clinical profile. Here, we report the target engagement of ACT-1004-1239 in healthy mice and humans after multiple doses using CXCL11 and CXCL12 as biomarkers. In addition, safety/tolerability, concentration-QTc relationship, and pharmacokinetics (PK) were assessed in a randomized, double-blind, placebo-controlled Phase 1 clinical study. Multiple-dose ACT-1004-1239 dose-dependently increased CXCL12 plasma concentration across the investigated dose range in mice and humans (mice: 1–100 mg/kg b.i.d.; humans: 30–200 mg o.d.) when compared to vehicle/placebo demonstrating target engagement. Mouse and human PK/PD models predicted that CXCL12 concentration approached a plateau within these dose ranges. In humans, ACT-1004-1239 was rapidly absorbed ($t_{max}$: 1.75–3.01 h) and the terminal $t_{1/2}$ was approximately 19 h. Steady-state conditions were reached by Day 3 with an accumulation index of 1.2. Female subjects had overall higher exposure compared to males. Multiple-dose ACT-1004-1239 was well tolerated up to 200 mg once daily in humans. There was no evidence of ACT-1004-1239-mediated QTc interval prolongation. Overall, multiple oral doses of ACT-1004-1239 showed target engagement with CXCR7 in healthy mice and humans, therefore, assessment of CXCL12 as translational tool for further investigations in patients is warranted. Favorable safety/tolerability and PK profiles allow for further clinical development.

## 1. Introduction

Chemokines and their receptors are known to contribute in (patho) physiological processes through their homeostatic and/or inflammatory properties [1]. They are involved in the development of various diseases such as different types of cancer, autoimmune diseases including multiple sclerosis (MS), and acute as well as chronic inflammation [2]. Therefore, chemokine receptors have evolved as a target of interest for drug development [3,4].

CXCR7, also known as atypical chemokine receptor (ACKR) 3, is mainly expressed on endothelial cells in the vasculature of different organs [5]. Although CXCR7 belongs to the G protein family, upon activation by its chemokine ligands (CXCL) 11 and CXCL12, its signaling is mainly triggered through the recruitment of β-arrestin and not via G

*Abbreviations:* ACKR, atypical chemokine receptor; AE, adverse event; AI, accumulation index; $AUC_{\tau}$, area under the plasma concentration-time curve within one dosing interval; $AUEC_{\tau}$, area under the effect-time curve within one dosing interval; b.i.d., twice daily; BMI, body mass index; $Cb_{max}$, maximum biomarker plasma concentration; CI, confidence interval; $C_{max}$, maximum plasma concentration; CNS, central nervous system; CXCL, C-X-C ligand; CXCR, C-X-C receptor; ΔΔQTcF, placebo-corrected change from baseline QT interval corrected for heart rate with Fridericia's formula; $E_{max}$, maximal effect; EOS, end-of-study; FIH, first-in-human; $IC_{50}$, concentration at half maximal effect; LC-MS/MS, liquid chromatography coupled to tandem mass spectrometry; MS, multiple sclerosis; o.d., once daily; PD, pharmacodynamics; PK, pharmacokinetics; SAEM, stochastic approximation of expectation-maximization; $t_{1/2}$, half-life; $t_{max}$, time to reach maximum plasma concentration; VPC, visual predictive check.

* Correspondence to: Department of Clinical Pharmacology, Idorsia Pharmaceuticals Ltd, Hegenheimermattweg 91, 4123 Allschwil, Switzerland.
*E-mail address:* christine.huynh@idorsia.com (C. Huynh).

https://doi.org/10.1016/j.biopha.2021.112363
Received 1 September 2021; Received in revised form 6 October 2021; Accepted 19 October 2021
Available online 28 October 2021

protein subunits [6]. Following binding of CXCL11 or CXCL12, CXCR7 has the ability to internalize and leading to degradation of the ligands [7]. This "scavenging-activity" regulates the extracellular concentrations of the ligands, and thus, the establishment and maintenance of the CXCL11 and CXCL12 concentration gradients. Of note, CXCL11 and CXCL12 are also ligands of CXCR3 and CXCR4, respectively [8,9]. Consequently, the CXCR3- and CXCR4-mediated signaling functions are modulated by, amongst others, CXCL11 and CXCL12, and thus, are influenced by the scavenging activity of CXCR7 [10].

Several preclinical studies suggested that blockade of CXCR7 was followed by disruption of the CXCL11 and CXCL12 concentration gradients and thereby, indirectly influenced the migration of CXCR3- and CXCR4-positive cells from blood vessels to inflamed tissues [11,12]. Therefore, targeting specifically CXCR7 in immune disorders gained attention within the last decades. For example, inhibition of CXCR7 using a functional antagonist (CCX771) was investigated preclinically in indications such as MS [13,14], acute pulmonary inflammation [15], and some cancer types including but not limited to breast [16] cancer and glioblastoma [4,17].

ACT-1004-1239 is an orally available, potent, selective, insurmountable, small-molecule CXCR7 antagonist [18], which showed target engagement in healthy animals [18] and humans [19] after single-dose administration.

Besides ACT-1004-1239, no clinical studies with CXCR7 antagonists have been published. The multipurpose first-in-human (FIH) study was designed for the investigations of several aspects of ACT-1004-1239 including safety, tolerability, pharmacokinetics (PK), pharmacodynamics (PD) using CXCL11 and CXCL12 as target engagement biomarkers, effect of food on PK, and absolute bioavailability. Single-ascending dose administration of ACT-1004-1239 was safe and well tolerated across the investigated dose range (1–200 mg) with similar incidence of adverse events (AEs) between active treatment and placebo. ACT-1004-1239 was quickly absorbed indicated by a median $t_{max}$ ranging from 1.3 to 3.0 h, had an absolute bioavailability of 53%, and was identified as a low-clearance drug in humans [19]. Disposition of ACT-1004-1239 was covered by three compartments and the elimination was characterized with a terminal elimination half-life ($t_{1/2}$) ranging from 17.8 to 23.6 h at doses $\geq$ 10 mg. Additional PK assessments indicated that the exposure to ACT-1004-1239 was not influenced by food intake. CXCL12 plasma concentration increased dose-dependently, demonstrating target engagement in humans. In contrast, plasma concentrations of the inflammatory chemokine CXCL11 did not change following single-dose administration in healthy subjects. Simulations based on the established PK/PD model suggested a once-daily (o.d.) dosing regimen for further clinical studies [19]. Unlike in humans, ACT-1004-1239 is a high-clearance drug with low bioavailability (35%) in rodents [18] necessitating a twice-daily (b.i.d.) dosing regimen in rodent studies. In addition, ACT-1004-1239 has been tested in several animal disease models, which showed dose-dependent efficacy in models of MS [20,21] and acute lung injury (ALI) [41] following multiple-dose administration. Specifically, treatment with ACT-1004-1239 induced a dose-dependent increase of CXCL11 and CXCL12 plasma levels, which correlated with a dose-dependent reduction in disease severity and immune infiltrates in the inflamed tissue [20,21].

Here, we report on the target engagement of ACT-1004-1239 using CXCL11 and CXCL12 as PD biomarkers, which were assessed in multiple-dose studies in healthy mice and humans. Mouse and human PK/PD models were utilized to support the use of CXCL12 as biomarker of target engagement in successive clinical studies. In addition, the safety and tolerability including the effect on the QTc interval using 24-h Holter monitoring, and PK of ACT-1004-1239 after repeated doses in healthy humans are reported.

## 2. Material and methods

### 2.1. Study in mice

#### 2.1.1. Study design

Male DBA/1 mice (60 mice with a mean body weight at study start of 23 g) were purchased from Janvier Laboratories (Le Genest-Saint-Isle, France) and allowed to acclimatize for at least 7 days before use. All mice were group-housed in a 12 h light/dark cycle and climate-controlled environment. Food and drinking water were available ad libitum. All animal experiments were carried out in accordance with the Swiss animal protection law, under protocols approved by the Basel Cantonal Veterinary Office.

ACT-1004-1239 was formulated in 0.5% methylcellulose and 0.5% Tween 80 (Sigma-Aldrich, Schnelldorf, Germany) in water. Repeated doses of ACT-1004-1239 (1, 10, 30, or 100 mg/kg) or vehicle (0.5% methylcellulose, 0.5% Tween 80, water) were administered by oral gavage b.i.d. in a volume of 5 mL/kg for 3 days, resulting in a total of 6 doses of treatment per mouse. The b.i.d. dosing regimen was selected based on previous observations, which showed that ACT-1004-1239 is a high-clearance drug in rodents [18]. The time between 2 subsequent gavages did not exceed 14 h.

#### 2.1.2. Pharmacokinetic and pharmacodynamic analyses

Blood samples for the assessment of PK were collected in EDTA-coated tubes (BD Microtainer, BD Biosciences, Franklin Lakes, NJ, USA) 0.5, 3, 6, and 24 h after the last oral dose of ACT-1004-1239 (n = 3 per time point and per dose). Blood was centrifuged (approximately 20,000 g for 5 min at 4 °C) to prepare plasma samples. ACT-1004-1239 plasma concentrations were measured using liquid chromatography coupled to tandem mass spectrometry (LC-MS/MS) with a lower limit of quantification of 1.52 ng/mL as previously described [18]. CXCL12 blood samples were collected at the same time points as for PK. CXCL12 concentrations were measured in plasma samples using a commercial mouse CXCL12/SDF1α Quantikine enzyme-linked immunosorbent assay kit (R&D Systems, Minneapolis, MN, USA) with an inter-assay precision of (coefficient of variation [%CV]) 7.2–7.6 according to manufacturer's instructions. The method was monitored using quality control samples provided in the assay kit.

Mouse CXCL11 was quantified in plasma samples collected at 24 h after the last dose of ACT-1004-1239, using an ultrasensitive immunoassay built on the Single Molecule Counting (SMC™) technology (Erenna® immunoassay system, Merck Millipore, Billerica, MA, USA). Briefly, paramagnetic microparticles (beads) coated with anti-mouse CXCL11 monoclonal antibody (R&D Systems, Minneapolis, MN, USA) were used as capturing antibody. Recombinant murine CXCL11 (Peprotech, Cranbury, NJ, USA) and fluor-labeled anti-mouse CXCL11 polyclonal antibody (R&D Systems, Minneapolis, MN, USA) were used as standard and detection antibody, respectively. The number of fluorescently labeled detection antibodies counted with the Erenna® System was directly proportional to the amount of murine CXCL11 present in plasma.

#### 2.1.3. PK/PD modeling and simulation

A PK/PD model was developed using non-linear mixed effects modeling (MonolixSuite 2020R1, Lixoft-Incuballiance, Antony, France) in a stepwise approach. To describe ACT-1004-1239 PK in mice, first-order absorption with and without lag time, one-, two-, and three-compartment models for distribution, and linear and non-linear elimination were considered.

An indirect response model with partial inhibition of CXCL12 degradation with/without sigmoidicity was evaluated with sequential PK/PD estimation [22]. Graphical and numerical methods were utilized for model evaluation. Graphical methods included observed vs model-predicted values, residual diagnostics, and visual predictive checks (VPCs). The objective function (−2 × log-likelihood) was chosen

as the measure for the goodness of fit of the model to the data. The stochastic approximation of expectation-maximization (SAEM) algorithm was used for parameter estimation using MonolixSuite 2020R1 (Lixoft-Incuballiance, Antony, France), and data were visualized in R version 4.0.4 (R Development Core Team, Vienna, Austria). Simulations were performed with Simulx (MonolixSuite 2020R1) for n = 1000 mice per dose level with samples taken 0.5, 3, 6, and 24 h post-dose following the last dose.

### 2.2. Study in humans

#### 2.2.1. Study design

This study was conducted at a single center, namely BlueClinical Phase 1 at the Hospital da Prelada (Porto, Portugal), following a, randomized, double-blind, multiple-ascending dose Phase 1 study design (ClinicalTrials.gov: NCT04286750). The study was approved by both the National Health Authority of Portugal (*Infarmed*) and the National Ethics Committee (*Comissão de Ética para a Investigação Clínica*) before any study initiation and performed in accordance with Good Clinical Practice and the Declaration of Helsinki.

This study investigated three sequential doses of ACT-1004-1239 namely 30, 100, and 200 mg. In each dose group 10 healthy subjects (n = 8 on ACT-1004-1239, n = 2 on placebo) were enrolled with a 1:1 ratio for males and females. Following an eligibility check during a screening period, the subjects were in the clinical site from Day −1 (one day before start of dosing) to Day 9 and received study treatment for 7 days o.d. (Day 1 to Day 7) in the morning under fasted conditions. Ambulatory visits were performed on Day 10 and Day 11 for blood collection and on Day 15 for the end-of-study (EOS) assessments. Safety follow-up was performed within 40 days after EOS visit or premature study discontinuation. The starting dose of 30 mg and the dosing regimen were selected based on data obtained in the single-ascending dose study [19] and were supported by the safety margins related to toxicology findings. Escalation to the subsequent planned doses was performed based on the overall assessment of safety, tolerability, PK, and PD data. The highest dose of 200 mg was selected as it has been the top dose investigated in the FIH study [19].

#### 2.2.2. Study population

In total, 30 healthy male and female subjects (1:1 ratio for sex) between 18 and 55 years were enrolled in this study. Each subject provided informed consent before they were tested for study eligibility during the screening period. The subjects had to be in a good health condition to investigate the study endpoints without any interference of underlying pathologic condition, concomitant treatment use, or other potentially confounding factors such as drug or alcohol consumption and smoking. Moreover, the subjects had to have a body mass index (BMI) between 18.0 and 29.9 kg/m$^2$, systolic and diastolic blood pressure of 100–140 mmHg and 50–90 mmHg, respectively, and a pulse rate of 45–90 bpm. Physical examination, 12-lead ECG, and clinical laboratory (hematology, clinical chemistry, and urinalysis) tests were also assessed to determine subjects' health conditions. Female subjects of childbearing potential had to have a negative serum pregnancy test and to agree to use a highly effective method of contraception from screening up to three months after last study treatment administration. Male subjects were requested to use condom during heterosexual intercourses from first up to three months after last study treatment administration unless they were vasectomized.

#### 2.2.3. Pharmacokinetic analysis

For the assessment of PK, blood was collected at predose, 0.5, 1, 1.5, 2, 3, 4, 6, 8, 10, 12, 14, and 16 h after dosing on Day 1 and Day 7. Additional blood samples were collected at trough (predose) from Day 2 to Day 6 and at 24, 36, 48, 72, 96, and 192 h after last dosing on Day 7. At each collection time point, approximately 3 mL of blood was collected in EDTA-containing tubes. The blood samples were centrifuged (approximately 1800 g for 10 min at 4 °C) within 30 min after collection. Subsequently, plasma was aliquoted and stored at − 80 °C for further analysis.

ACT-1004-1239 plasma concentrations were determined using a validated LC-MS/MS assay as previously described [19]. The method was monitored using quality control samples, which revealed an inter-batch precision %CV of ≤ 7.2%, whereas the inter-batch accuracy using the relative deviation from the nominal value (% RD) ranged from 2.6% to 6.2%. Concentrations below the limit of quantification (0.5 ng/mL) were set to "0".

PK parameters after the first and last dose were obtained by non-compartmental analysis using Phoenix WinNonlin version 8.0 (Certara, Princeton, NJ, USA). Measured ACT-1004-1239 plasma concentrations were directly used to determine $t_{max}$ and $C_{max}$, whereas the area under the plasma concentration-time curve within one dosing interval ($AUC_\tau$) was calculated according to the linear trapezoidal rule. Dose proportionality was assessed following the last dose of ACT-1004-1239 (i.e., Day 7) based on log-transformed $C_{max}$ and $AUC_\tau$ values across the tested dose range using a statistical power model described by Gough et al. [23]. The accumulation index (AI) was calculated using the following formula:

$$AI = AUC_\tau \text{ on Day 7 / } AUC_\tau \text{ on Day 1}$$

The attainment of steady-state conditions was determined by visual inspection of the trough plasma concentration-time profiles.

The differences in PK between male and female subjects were explored by a mixed-effects model using log-transformed PK parameters as dependent variable, sex and dose level as fixed effects, and subject as random effect.

#### 2.2.4. Pharmacodynamic analysis

For the assessment of CXCL11 and CXCL12, blood sampling was performed for each subject on Day −1, at predose, and 1, 2, 4, 8, 12, and 16 h after dosing on Day 1 and Day 7, and at trough on Day 2 to Day 6. Further PD blood samples were taken at 24, 36, 48, 72, 96, and 192 h after last dosing on Day 7. At each collection time point, approximately 5 mL of blood was drawn into EDTA-containing tubes and cooled in ice. The samples were centrifuged (1800 g for 10 min at 4 °C) within 30 min and aliquoted plasma samples were stored at − 80 °C until analysis.

Similar as in the single-ascending dose study [19], CXCL11 and CXCL12 plasma concentrations were determined using an U-Plex Immunoassay kit (Meso Scale Diagnostics, Rockville, MD, USA) and an Ella immunoassay (Bio-Techne, Minneapolis, MN, USA), respectively. Quality control samples were included in both assays and revealed an overall inter-batch precision %CV of ≤ 6% and ≤ 10% for the determination of CXCL11 and CXCL12, respectively.

Measured plasma concentrations of CXCL11 and CXCL12 were directly used to obtain maximum biomarker plasma concentration ($Cb_{max}$) determined based on all time points regardless of study day. The area under the effect-time curve within one dosing interval ($AUEC_\tau$) was calculated according to the linear trapezoidal rule using baseline-corrected CXCL11 and CXCL12 concentrations for the last dosing interval (Day 7, i.e., steady state) only. Individual baseline was defined as the mean of biomarker plasma concentrations measured on Day −1 and Day 1 at predose.

#### 2.2.5. PK/PD modeling and simulation

A PK/PD model was developed using non-linear mixed effects modeling (MonolixSuite 2020R1, Lixoft-Incuballiance, Antony, France) in a stepwise approach. Selection of a structural PK and PK/PD model was based on data from all subjects on active treatment in the single-ascending dose study [19], with sequential PK/PD estimation [22]. Next, the PK model structure was re-evaluated based on data from all subjects in both studies, and a covariate analysis with body weight, age, height, sex, race, and food status (fed/fasted) as candidate covariates

was performed. Lastly, the structural PD model was re-evaluated with sequential PK/PD estimation. Graphical and numerical methods were utilized for model evaluation. Graphical methods included observed vs model-predicted values, residual diagnostics, and VPCs. The objective function (−2 × log-likelihood) was chosen as the measure for the goodness of fit of the model to the data. The SAEM algorithm was used for parameter estimation, and data were visualized in R version 4.0.4 (R Development Core Team, Vienna, Austria). Simulations were performed with Simulx (MonolixSuite 2020R1) for n = 1000 subjects per dose level following the same sampling scheme as this study.

#### 2.2.6. Safety and tolerability evaluation

Safety and tolerability were assessed throughout the study based on the nature, frequency, and intensity of AEs. Post-dose results of vital signs including blood pressure and pulse rate, 12-lead ECG, clinical laboratory (including those monitoring liver and kidney function) variables, body weight, and physical examination were compared to baseline and placebo.

#### 2.2.7. 12-lead Holter ECG: concentration-QTc assessment

12-lead Holter ECGs (Mortara H12 + System, Hill-Rom Holdings, Inc., Chicago, IL, US) were recorded in each subject on Day 1 predose for the assessment of baseline and a 24-h continuous recording was performed on Day 7. Holter ECGs were read in triplicate at each PK time point by Biotrial (Rennes, France).

The relationship between ACT-1004-1239 plasma concentrations and the QTc interval was investigated by concentration-QTcF modeling [24] using a linear mixed-effect model [25]. The model was used to predict the two-sided 90% confidence interval (CI) of placebo-corrected ΔQTcF (ΔΔQTcF) to exclude an effect > 10 ms (i.e., of regulatory concern) on QTcF at clinically relevant plasma concentrations. The model was employed using intercept, slope, treatment (ACT-1004-1239/placebo), centered baseline QTcF, and scheduled time point as fixed effects. The model-derived two-sided 90% CI was predicted using the degrees of freedom from the Kenward-Roger method [26].

## 3. Results

### 3.1. Study in mice

#### 3.1.1. Pharmacokinetics and pharmacodynamics

The mean (+SD) plasma concentration-time profiles after repeated oral administration of ACT-1004-1239 at a range of 1–100 mg/kg, b.i.d.,

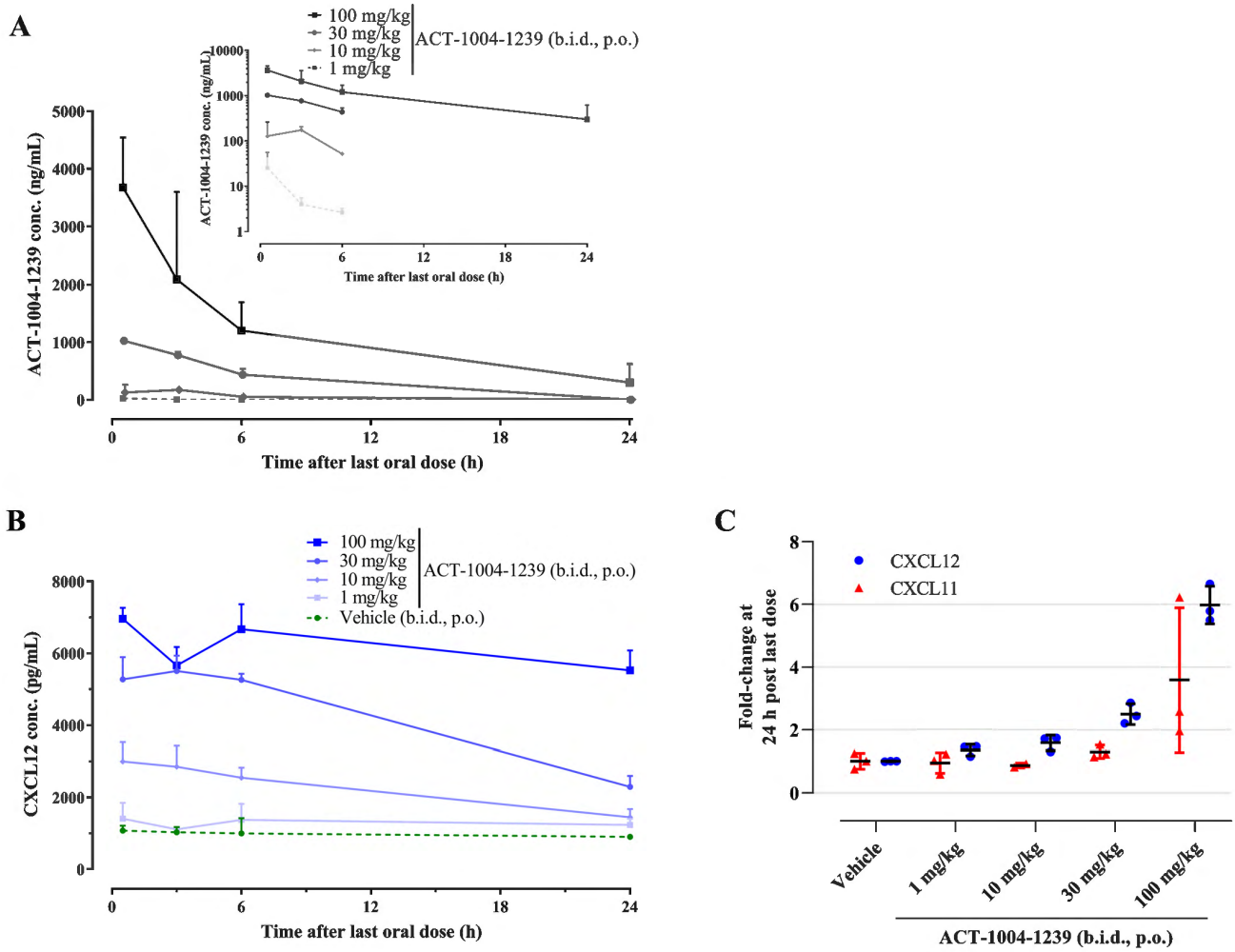


**Fig. 1.** ACT-1004-1239 and CXCL12 plasma concentration-time profiles and dose-response relationship in mice. Data are displayed as mean plasma concentration of ACT-1004-1239 in linear (A) and semi-log (A inset) scales and CXCL12 (B) by treatment with standard deviation. (C) Dose-response relationship of fold-change in CXCL11 and CXCL12 compared to vehicle-treated mice at 24 h post last dose. Data are presented as mean with individual data compared to the mean of vehicle-treated mice. N = 2–3 on each dose and on each time point. Vehicle N = 11. CXCL11/CXCL12, C-X-C chemokine ligands 11 and 12; b.i.d., twice daily; p.o.: oral gavage.

in healthy DBA/1 mice, are shown in Fig. 1A. ACT-1004-1239 was quickly absorbed and reached mean $C_{max}$ at 0.5 h post-dose, which ranged from 26 ± 17 ng/mL to 3675 ± 615 ng/mL across the investigated dose range. Plasma concentration of ACT-1004-1239 increased in a dose-dependent manner (Fig. 1A). Only at the highest dose tested (100 mg/kg, b.i.d.), ACT-1004-1239 could be measured (i.e., above the limit of quantification) at 24 h after the last dose.

Repeated oral doses of ACT-1004-1239 at a range of 1–100 mg/kg resulted in a dose- and time-dependent increase in CXCL12 plasma concentration in comparison to vehicle-treated mice (Fig. 1B). Only at the highest dose tested (100 mg/kg), repeated administration of ACT-1004-1239 maintained CXCL12 plasma elevation for 24 h after the last dose (Fig. 1B) and up to 6.0-fold relative to vehicle-treated mice (Fig. 1C).

In contrast, no changes in CXCL11 plasma concentration at doses < 100 mg/kg were observed. Only the highest dose of 100 mg/kg b.i.d. increased CXCL11 plasma concentration at 24 h up to approximately 4-fold compared to vehicle-treated mice, but with higher variability than for CXCL12 (Fig. 1C).

#### 3.1.2. PK/PD modeling and simulation

A one-compartment model with first-order absorption and linear elimination described ACT-1004-1239 PK in mice best. Due to the limited sampling, a peripheral compartment or non-linear elimination could not be determined. However, clearance was found to decrease with increasing dose, and therefore, dose was included as covariate on clearance.

An indirect response model of ACT-1004-1239 inhibiting the elimination rate of CXCL12 with a maximum effect of 0.83, and an estimated Hill coefficient of 3.1 described the CXCL12 concentration in mice best. Baseline CXCL12 concentration was estimated at 1.07 ng/mL and the $IC_{50}$, defining the ACT-1004-1239 concentration at half maximal effect ($E_{max}$), was estimated at 11.2 ng/mL (supplemental material, Table S1). ACT-1004-1239 concentrations were slightly underpredicted around the highly variable $C_{max}$, while CXCL12 concentrations were generally well described by the PK/PD model (supplemental material, Fig. S1, S2). The median predicted response of 1000 simulations in mice receiving six doses of 0, 1, 10, 30, and 100 mg b.i.d. is shown in Fig. 2A. Simulations showed that CXCL12 plasma concentration increased dose-dependently across the dose range and approached a plateau at doses ≥ 100 mg/kg b.i.d.

### 3.2. Study in humans

#### 3.2.1. Subjects

All subjects completed this study according to the study protocol, except for one female subject who prematurely discontinued the study due to an AE. This subject was excluded from the analysis of PK and PD. The mean (range) age of the subjects was 33.3 (20–30) years and they had a BMI of 24.8 (20.0–29.9) kg/m$^2$. Most subjects were White (n = 23, 76.7%) and the others were Black/African American (n = 3, 10.0%) or belonged to another ethnicity (n = 4, 13.3%).

#### 3.2.2. Pharmacokinetics

The mean (+SD) plasma concentration-time profiles after first and last dose administration of 30, 100, and 200 mg ACT-1004-1239 are shown in Figs. 3A and 3B, respectively. The PK parameters are provided in Table 1.

The PK profiles after multiple doses were comparable to the ones after the first dose (Fig. 3A/B). On both study days (Day 1 and Day 7), ACT-1004-1239 was rapidly absorbed as indicated by a median $t_{max}$ ranging from 1.75 to 3.01 h. After the last dose, ACT-1004-1239 underwent multiple phases of disposition that were comprised of at least two compartments (Fig. 3B inset). The last disposition phase was used to obtain the geometric mean terminal $t_{½}$, which ranged from 17.9 to 20.6 h across the tested dose range. No ACT-1004-1239 was detectable (i.e., below limit of quantification) at 192 h post last dose. Formal statistical analysis of dose-proportionality across the investigated dose range revealed that the 90% CI of the slopes for $C_{max}$ (0.84–1.26) and $AUC_{\tau}$ (0.94–1.26) of ACT-1004-1239 at steady state were fully contained within the critical interval of 0.63–1.37, therefore indicating a dose-proportional increase of ACT-1004-1239 exposure. Systemic exposure to ACT-1004-1239 reached steady-state conditions by Day 3 (Fig. 3C) with limited accumulation (accumulation index of approximately 1.2). Overall, female subjects had higher ACT-1004-1239 plasma concentrations compared to male subjects, resulting in $C_{max}$ and $AUC_{\tau}$ geometric means ratios (females/males) of 1.4 (90% CI: 1.1–1.9 for $C_{max}$ and 1.1–1.8 for $AUC_{\tau}$) on Day 1 and 1.3 (90% CI: 1.0–1.9 for $C_{max}$ and 1.1–1.7 for $AUC_{\tau}$) on Day 7.

#### 3.2.3. Pharmacodynamics

The baseline-corrected CXCL11 and CXCL12 plasma concentration-time profiles by dose are shown in Fig. 4A/B. Overall, mean (+SD) CXCL11 and CXCL12 baseline concentrations across the dose groups were 71.9 (30.0) pg/mL and 1774 (256) pg/mL, respectively.

Baseline-corrected CXCL12 plasma concentration increased dose-

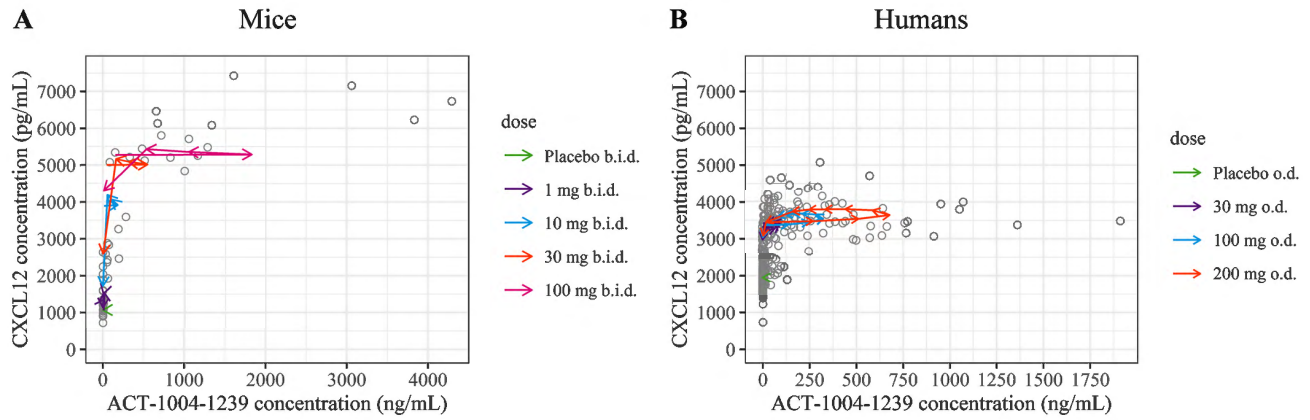


**Fig. 2.** PK/PD modeling and simulation results in mice and humans. (A) Observed (symbols) and simulated (lines) PK/PD concentration pairs in mice following 6 doses of vehicle (placebo), 1, 10, 30, or 100 mg b.i.d. are shown. The colored lines indicate the median of n = 1000 mice per dose level, with the arrows indicating the delay described in the indirect response model. (B) Observed (symbols) and simulated (lines) PK/PD concentration pairs on Day 7 in all subjects receiving placebo, 30, 100, or 200 mg o.d. are shown. The colored lines indicate the median of n = 1000 subjects per dose level, with the arrows indicating the delay described in the indirect response model. b.i.d., twice daily; o.d., once daily; PD, pharmacodynamics; PK; pharmacokinetics.

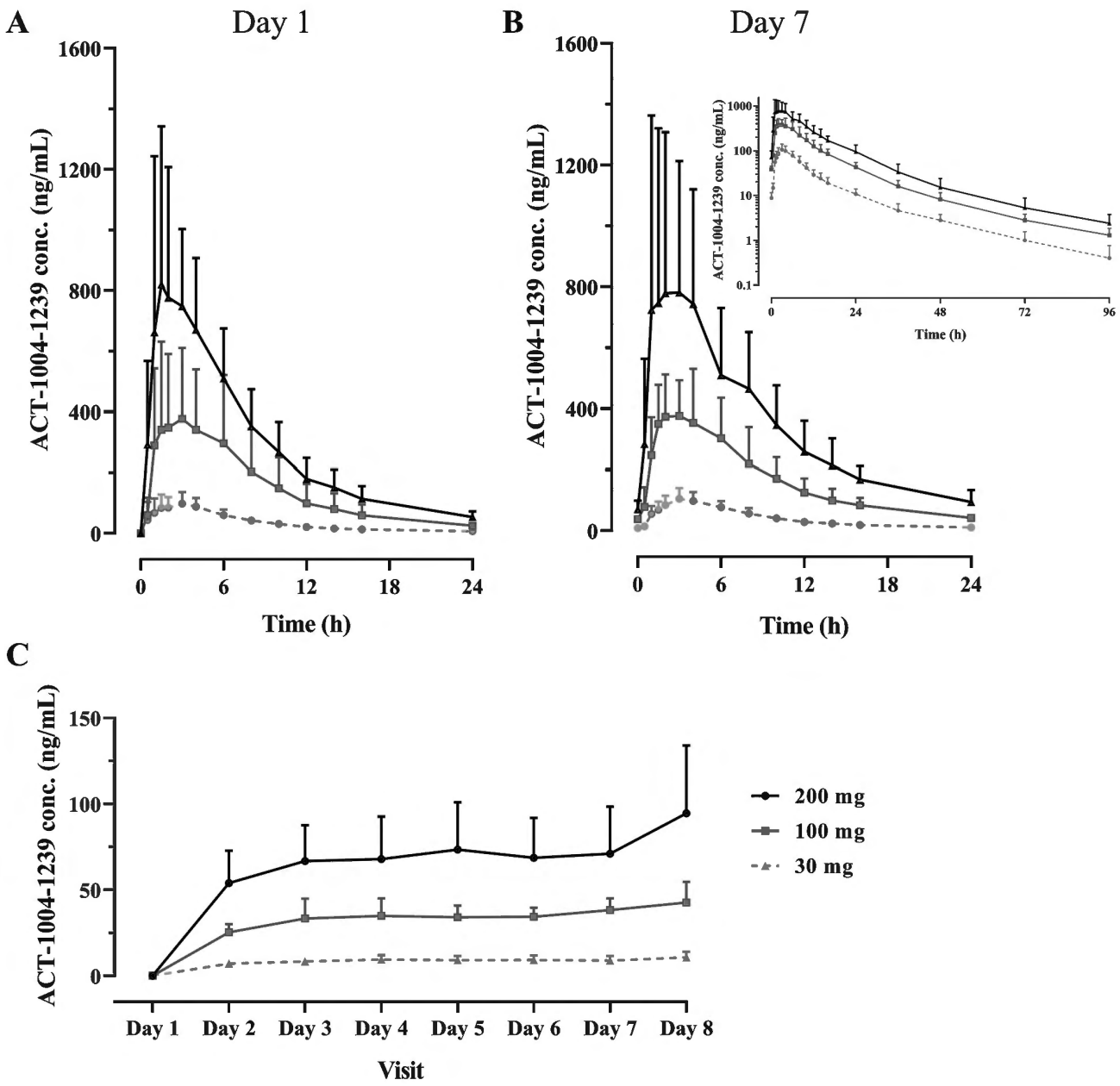


**Fig. 3.** ACT-1004-1239 plasma concentration-time profiles in humans. (A, B) Data are displayed as mean plasma concentrations of ACT-1004-1239 by dose with standard deviations after first (A) and last (B) oral dose administration in linear and semi-log (B inset) scales. (C) Mean trough plasma concentrations of ACT-1004-1239 by dose with standard deviations. N = 8 for 30 and 100 mg and N = 7 for 200 mg.

dependently up to 100 mg ACT-1004-1239 while it remained unchanged after treatment with placebo. Elevation of CXCL12 in the 200 mg dose group at steady-state conditions was comparable to that at 100 mg and almost 2-fold higher compared to baseline and/or placebo (Fig. 4A and C). In each dose group, the baseline-corrected CXCL12 plasma concentration started to increase already after the first dose, was sustained above baseline up to 48 h after the last dose, and did not fully return to baseline on Day 15 (i.e., EOS). The plasma exposure parameters for CXCL12 (i.e., $Cb_{max}$ and $AUEC_{\tau}$) increased in a dose-dependent fashion (Table 2).

In contrast, at the 30 and 100 mg dose levels, post-dose baseline-corrected CXCL11 plasma concentrations remained unchanged throughout the study, and were comparable to those observed after placebo treatment. Similar to CXCL12, a transient increase in CXCL11 plasma concentration was observed at the highest dose level of 200 mg at 48 h post first dose (i.e., predose of Day 3) only, which returned to baseline within the following dosing interval (Fig. 4B).

### *3.2.4. PK/PD modeling and simulation*

The structural model describing ACT-1004-1239 PK in humans best, was a three-compartment model, with first-order absorption with a lag time, saturable distribution to one of the peripheral compartments, and linear elimination. Body weight was included as covariate on all volume and clearance parameters using allometric scaling. No other covariates were identified. VPCs confirmed the data were described adequately (supplemental material, Fig. S3). An indirect response model with estimated elimination rate constant described CXCL12 concentration over time, with an inhibitory $E_{max}$ model and with estimated Hill coefficient

**Table 1**
Pharmacokinetic parameters in humans.

| Parameter [unit] | 30 mg N = 8 | 100 mg N = 8 | 200 mg N = 7 |
|---|---|---|---|
| Day 1 | | | |
| $t_{max}$ [h] | **3.00** (0.5–4.0) | **1.75** (1.0–4.0) | **2.00** (1.0–4.0) |
| $C_{max}$ [ng/mL] | **99.2** (70.5–140) | **371** (257–535) | **845** (573–1246) |
| $AUC_{\tau}$ [ng × h/mL] | **791** (603–1038) | **3160** (2178–4584) | **6479** (4522–9284) |
| Day 7 | | | |
| $t_{max}$ [h] | **3.00** (1.5–4.0) | **3.01** (1.5–4.0) | **3.00** (1.0–16.0) |
| $C_{max}$ [ng/mL] | **107** (84.7–136) | **421** (325–546) | **759** (395–1461) |
| $AUC_{\tau}$ [ng × h/mL] | **949** (742–1215) | **3778** (2929–4874) | **7525** (4979–11374) |
| $t_{½}$ [h] | **17.9** (14.3–22.6) | **18.6** (16.5–21.0) | **20.6** (15.0–28.2) |
| AI | **1.20** (1.06–1.36) | **1.20** (1.01–1.42) | **1.16** (1.02–1.32) |

Data are displayed as geometric means (95% CI) except for $t_{max}$ that is provided as median (range).
AI, accumulation index, AUCτ, area under the plasma concentration-time curve over a dosing interval; CI, confidence interval; $C_{max}$, maximum plasma concentration; N, number of subjects in the population; $t_{½}$, terminal half-life; $t_{max}$, time to reach maximum plasma concentration.

of 0.28 describing the effect of ACT-1004-1239 on the elimination rate of CXCL12. In contrast to the model based on FIH data only [19], a feedback mechanism of CXCL12 concentration affecting its elimination rate was not included, as the addition of either positive or negative feedback did not improve the model fit. The $E_{max}$ was fixed to 0.6 to stabilize the estimation (theoretical range between 0 and 1, with 1 corresponding to full inhibition of CXCL12 elimination). The $IC_{50}$, defining the ACT-1004-1239 concentration at half $E_{max}$, was estimated at 1.12 ng/mL. Also, VPCs confirmed that the model described the data well, except for discrepancies around samples taken 48 h after the first dose, but otherwise indicated good predictive model performance as empirical percentiles were largely within the respective CIs of the predictions (supplemental material, Fig. S4). All model parameter estimates are listed in the supplemental material (Table S2). The model was subsequently utilized to simulate plasma ACT-1004-1239 and CXCL12 concentrations over time in 1000 subjects receiving 0, 30, 100, and 200 mg o.d. for 7 days. Simulations showed that despite differences in ACT-1004-1239 concentration ranges following 100 and 200 mg o.d., only minor changes in CXCL12 concentration would be observed, indicating no additional increase in CXCL12 for doses > 100 mg (Fig. 2B).

### 3.2.5. *Safety and tolerability*

In total 24 subjects reported at least one AE across the tested dose range from 30 to 200 mg (Table 3). Most AEs were of mild intensity and only 2 AEs were considered as moderate. No severe or serious AE was reported in this study. One female subject, who enrolled in the 200 mg dose group, prematurely discontinued the study on Day 4, due to an AE of diarrhea of moderate intensity starting on Day 2. After treatment with loperamide and study treatment stop, the AE resolved within the same day.

The most commonly reported AE was headache, which was overall seen in 7 subjects. Out of these, 1 (12.5%), 2 (25.0%), 2 (25.0%), and 2 (33.3%) subjects were treated with 30, 100, 200 mg ACT-1004-1239, and placebo, respectively. AEs related to ECG morphology changes were abnormal T wave and incomplete right bundle branch block

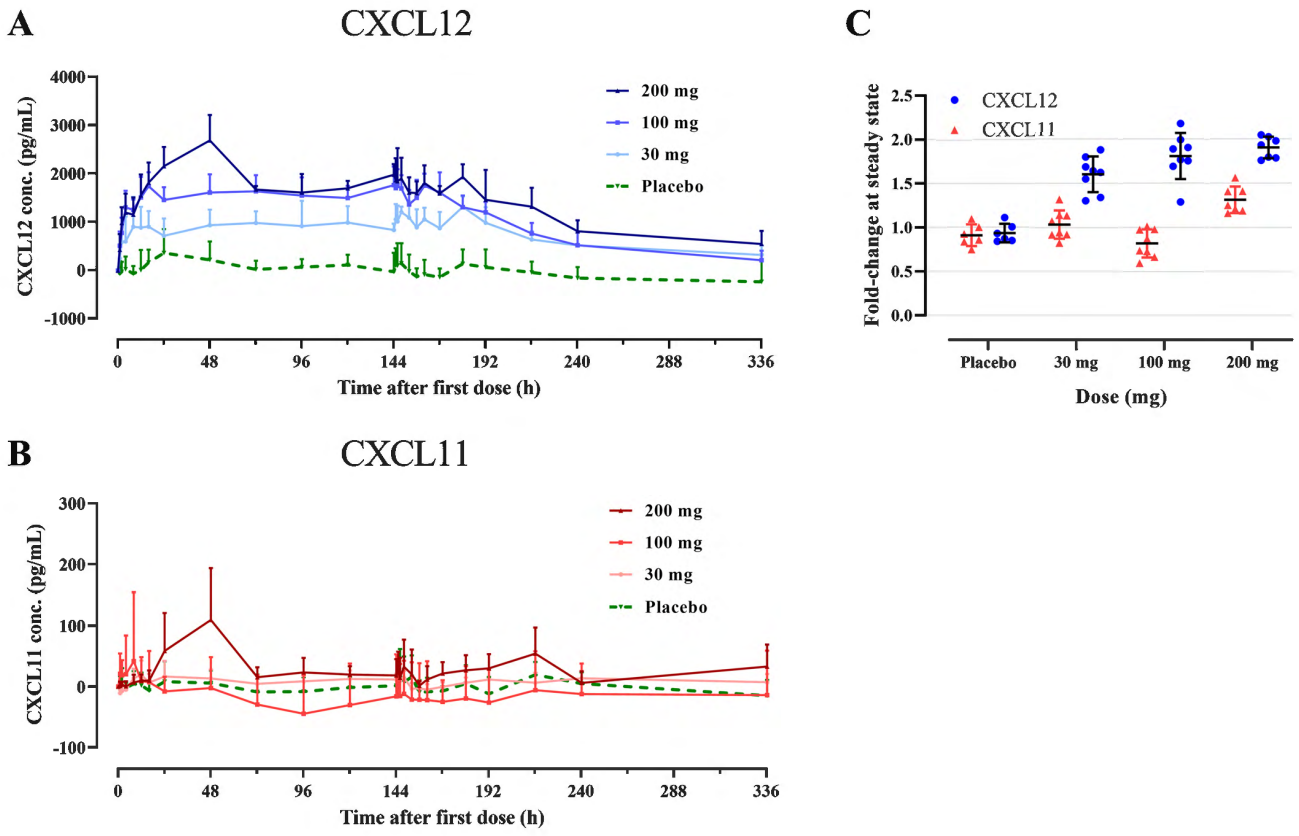


**Fig. 4.** CXCL11/CXCL12-time profiles and dose-response relationship in humans. (A, B) PD data are displayed as baseline-corrected mean plasma concentration of CXCL11/CXCL12 by treatment with standard deviations. (C) Fold-changes in CXCL11 and CXCL12 compared to baseline at steady state (24 h post last dose) are displayed as means with standard deviations and individual data. N = 8 for 30 and 100 mg and N = 7 for 200 mg; N = 6 for placebo. CXCL11/CXCL12, C-X-C chemokine ligands 11 and 12; PD, pharmacodynamics.

**Table 2**
Pharmacodynamic parameters in humans.

| | Parameter [unit] | Placebo N = 6 | 30 mg N = 8 | 100 mg N = 8 | 200 mg N = 7 |
|---|---|---|---|---|---|
| CXCL12 | $Cb_{max}$ (pg/mL) | **2417** (83.9–166.0) | **3014** (2755–3297) | **4242** (3969–4535) | **4566** (4014–5194) |
| | $AUEC_{\tau}$ D7 [pg*h/mL] | **-838** (−7644 to 5968) | **24349** (20002–28697) | **38636** (36241–41031) | **41286** (36529–46042) |
| CXCL11 | $Cb_{max}$ [pg/mL] | **118** (83.9–166.0) | **79.7** (51.6–123.0) | **124** (61.4–252.1) | **182** (118.0–281.6) |
| | $AUEC_{\tau}$ D7 [pg*h/mL] | **3.8** (−558.8 to 566.5) | **31.9** (−59.9 to 123.7) | **-478** (−1582.3 to 625.5) | **398** (−62.9 to 859.7) |

Data are displayed as geometric means (95% CI).
$AUEC_{\tau}$, area under the effect-time curve within one dosing interval; $Cb_{max}$, maximum biomarker plasma concentration; D7, Day 7.

**Table 3**
Incidence and number of adverse events by treatment.

| Adverse events (Preferred term) | 30 mg (N = 8) | | 100 mg (N = 8) | | 200 mg (N = 8) | | Active[a] (N = 24) | | Placebo (N = 6) | |
|---|---|---|---|---|---|---|---|---|---|---|
| | n (%) | nAEs | n (%) | nAEs | n (%) | nAEs | n (%) | nAEs | n (%) | nAEs |
| Any adverse event | 6 (75.0) | 13 | 6 (75.0) | 14 | 7 (87.5) | 15 | 19 (79.2) | 42 | 5 (83.3) | 14 |
| Headache | 1 (12.5) | 1 | 2 (25.0) | 2 | 2 (25.0) | 3 | 5 (20.8) | 6 | 2 (33.3) | 2 |
| ECG T wave abnormal | – | – | – | – | 3 (37.5) | 3 | 3 (12.5) | 3 | 1 (16.7) | 1 |
| Bundle branch block right[b] | – | – | 1 (12.5) | 1 | 1 (12.5) | 1 | 2 (8.3) | 2 | 1 (16.7) | 1 |
| Feces soft | – | – | 1 (12.5) | 1 | 1 (12.5) | 1 | 2 (8.3) | 2 | 1 (16.7) | 1 |
| Anemia | 2 (25.0) | 2 | – | – | – | – | 2 (8.3) | 2 | – | – |
| Dysmenorrhea | – | – | 2 (25.0) | 2 | – | – | 2 (8.3) | 2 | – | – |
| Asthenia | 1 (12.5) | 1 | – | | – | | 1 (4.2) | 1 | 1 (16.7) | 1 |
| Back pain | – | – | 1 (12.5) | 1 | – | – | 1 (4.2) | 1 | 1 (16.7) | 1 |
| Nightmare | – | – | 1 (12.5) | 1 | – | – | 1 (4.2) | 1 | 1 (16.7) | 1 |
| Pain in extremity | – | | – | | 1 (12.5) | 1 | 1 (4.2) | 1 | 1 (16.7) | 1 |

Only AEs reported by two or more subjects in the study are reported in the table.
AE, adverse event; ECG, electrocardiogram; N, number of subjects in the population, n, number of subjects; nAEs, number of adverse events.
[a] refers to all subjects receiving any dose of ACT-1004-1239.
[b] AE was described as incomplete right bundle branch block.

(IRBBB, coded to bundle branch block right). Abnormal T wave was mainly observed in the 200 mg dose group in 3 subjects (37.5%) and in 1 subject (16.7%) in the placebo group. IRBBB was reported in 3 subjects including 1 subject (12.5%) treated with 100 mg ACT-1004-1239, 1 subject (12.5%) treated with 200 mg ACT-1004-1239, and 1 subject (16.7%) under placebo. These AEs started on Day 6 and Day 7 and resolved without sequelae within a few days. All subjects who reported AEs related to ECG morphology changes were asymptomatic. Soft feces was reported with identical distribution of incidences of AEs across the dose range as the AE of IRBBB. Other AEs reported in 2 subjects included

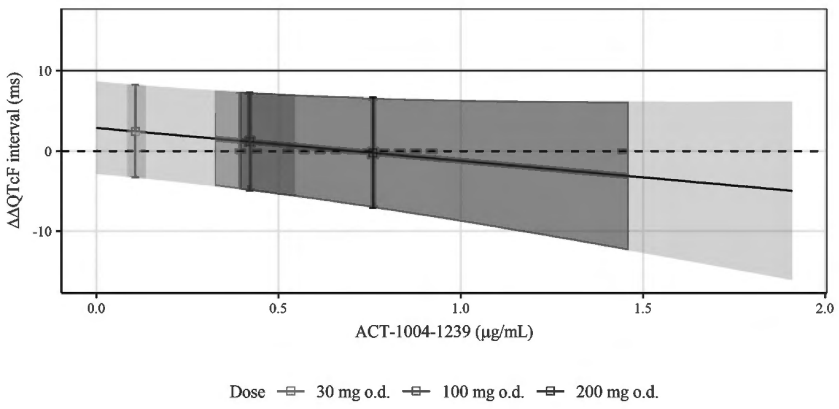


**Fig. 5.** Concentration-QT analysis: Model-predicted ΔΔQTcF vs concentration. Grey horizontal line, 10 ms threshold of regulatory concern; black line and height of shaded area, mean model-predicted ΔΔQTcF with two-sided 90% CI; width of highlighted shaded areas, two-sided 90% CI of geometric mean maximum concentration per treatment; points and error bars, predicted ΔΔQTcF with two-sided 90% CI at the geometric mean concentration per treatment. CI, confidence interval; ΔΔQTcF, placebo-corrected change from baseline QT interval corrected for heart rate with Fridericia's formula; o.d., once daily.

anemia, asthenia, back pain, dysmenorrhea, nightmare, and pain in extremity (Table 3).

There were no clinically significant changes in vital signs (including blood pressure and pulse rate), ECG, clinical laboratory variables (including liver and kidney variables), and body weight data.

*3.2.6. Concentration-QTc analysis*

The relationship between ACT-1004-1239 concentration and model-predicted ΔΔQTcF is presented in Fig. 5. The estimated slope of the concentration-QTc relationship was − 0.00413 ms per ng/mL (90% CI: –0.00917–0.000918) and not statistically different from 0 (p = 0.160). Mean ΔΔQTcF was predicted to be 2.5 ms (90% CI: −3.3 to 8.3), 1.2 ms (90% CI: –4.9–7.3), and − 0.2 ms (90% CI: –7.1–6.7) at a geometric mean $C_{max}$ of 107 ng/mL (30 mg), 421 ng/mL (100 mg), and 759 ng/mL (200 mg). Across the investigated dose range, no 90% CI exceeded the critical threshold of 10 ms suggesting no effect (i.e., prolongation) of ACT-1004-1239 on the QTc interval.

## 4. Discussion

ACT-1004-1239, an orally available, potent, and selective first-in-class CXCR7 antagonist showed favorable safety, PK, and PD profiles in healthy males after single-dose administration allowing for further clinical development using a o.d. dosing regimen [19]. In the here reported randomized, double-blind, placebo-controlled, multiple-ascending dose Phase 1 study, the safety/tolerability, including the concentration-QT relationship, and PK of ACT-1004-1239 after 7 days (o.d.) of treatment in healthy male and female subjects are presented. Furthermore, target engagement of ACT-1004-1239 using the PD biomarkers CXCL11 and CXCL12 was explored in healthy mice and humans following repeated-dose administration, allowing to obtain an insight in the mechanism of ACT-1004-1239.

In mice, the PK profiles were in line with previous observations after single-dose administration of ACT-1004-1239 [18]. CXCL12 plasma concentration increased dose-dependently after multiple doses of ACT-1004-1239 in healthy mice and approached a plateau over 24 h following repeated administration of 100 mg/kg. Due to the high clearance of ACT-1004-1239 in rodents [18], only the 100 mg/kg b.i.d. dosing regimen provided sufficient ACT-1004-1239 plasma exposure to maintain CXCL12 elevation over 24 h (Fig. 1B).

Pouzol et al. showed in preclinical disease models of MS that an increase in CXCL12 plasma levels was correlated with a reduction in clinical disease scores [20]. At the highest investigated dose of 100 mg/kg b.i.d. ACT-1004-1239, CXCL12 plasma concentrations observed in the healthy mice in the present study were similar to those observed in the disease models (approximately 7.0 ng/mL) [20], suggesting that inflammation did not affect the CXCL12 concentrations after treatment. In diseased mice, it was shown that these plasma concentrations were associated with a reduction in immune cell infiltrates into the central nervous system (CNS), especially of $CXCR4^+$ cells [20]. These studies in healthy and diseased mice suggest that sustained CXCL12 levels through treatment with ACT-1004-1239 can disrupt the CXCL12 concentration gradient and $CXCR4^+$ cells migration towards the site of inflammation. Similar findings were observed in a preclinical disease model of ALI [41]. In line with observed data, predictions using the mice PK/PD model showed that a plateau in CXCL12 concentration can be approached following b.i.d. dosing of $\geq$ 100 mg/kg ACT-1004-1239.

In healthy humans, CXCL12 plasma concentrations increased dose-dependently up to 2-fold compared to baseline and did not significantly increase further at doses > 100 mg ACT-1004-1239 o.d. In contrast to mice, a o.d. dosing regimen in healthy humans was appropriate to maintain increased CXCL12 plasma concentrations compared to baseline. Simulations showed that despite the differences in ACT-1004-1239 plasma concentrations between 100 and 200 mg, the CXCL12 concentrations were similar during a dose interval at steady state (Fig. 2B). In line with mouse simulations, these predictions suggest that a plateau had been reached. Compared to the previously described model [19], the model fit for the pooled data analysis set improved when no feedback mechanism was included and when fixing $E_{max}$ to 0.6. Although CXCR7 was reported as one of the main elimination routes for CXCL12 [7], the $E_{max}$ being lower than 1 underpins the involvement of other CXCL12 elimination pathways such as through CXCR4 [27,28], posttranslational modifications [29,30], or another to date unknown physiological mechanism. While ACT-1004-1239 was not detectable at the last collection time points in mice and humans, CXCL12 concentration was still significantly increased which was in accordance with the described indirect response model for both species (Fig. S5).

Taken together, there were dose-dependent increases of CXCL12 concentrations at a similar level in healthy and diseased mice, which were associated with dose-dependent efficacy in disease models. Since also a dose-dependency in CXCL12 concentration was observed in healthy humans, it is recommended to assess CXCL12 as target engagement biomarker in future clinical studies in patients with immunological disorders. However, whether an increase in CXCL12 plasma concentration in patients can be associated with efficacy remains unknown and necessitates further clinical investigations.

CXCL11 plasma concentration remained unchanged in healthy humans following 30 and 100 mg o.d. dosing of ACT-1004-1239, which can be explained by CXCL11′s characteristic of being an inflammatory chemokine that is mainly induced by interferon-β / interferon-γ under inflammatory conditions [31]. In line with this, in healthy humans lower *CXCL11* gene expression was found compared to *CXCL12* [32,33]. Nevertheless, in this study a transient increase was observed in healthy humans with peak CXCL11 plasma concentration upon attaining steady-state conditions (Day 3, i.e., 48 h post first dose) of high dose (200 mg, o.d.) ACT-1004-1239. A similar trend was seen in healthy mice at steady state following the highest investigated dose of 100 mg/kg ACT-1004-1239 b.i.d. with augmented CXCL11 plasma level, suggesting that in non-diseased species investigation of CXCL11 is less useful as CXCL11 modulation is difficult to investigate over a wide dose range.

Although no dose-dependent CXCL11 modulation in healthy mice and humans was seen, it does not preclude relevant changes in patients as statistically significant and dose-dependent increases in plasma CXCL11 levels were reported in preclinical disease models of MS and ALI. These increases were associated with a dose-dependent reduction in immune cell infiltrates into the CNS [21] or the bronchoalveolar space [41]. Confirmation of the translatability and relevance of this preclinical observation requires further clinical studies in patients.

The PK profiles of ACT-1004-1239 following single- (first) and multiple-dose administration of 30, 100, and 200 mg were comparable and characterized by a fast absorption and a terminal $t_{1/2}$ that confirms a o.d. dosing regimen [19]. The PK parameters $t_{max}$ and $t_{½}$ after the first dose (i.e., single dose) were similar to those observed in the FIH single-ascending dose study. However, in the here reported study, single-dose ACT-1004-1239 exposure was on average up to 1.8-fold higher than in the FIH study [19]. This may be due to the inclusion of female subjects who had higher plasma concentrations, and thus higher ACT-1004-1239 exposure compared to male subjects, which was accounted for in the PK/PD model by inclusion of body weight as covariate. A further explanation may be the difference in subjects' ethnicity with 65% Black/African Americans in the FIH study [19] and 77% White in this study. ACT-1004-1239 is mainly metabolized by CYP3A. Therefore, a higher expression of a specific *CYP3A5* allele in Black/African Americans [34–36] could lead to a more rapid metabolism resulting in lower ACT-1004-1239 exposures compared to White subjects. This was investigated by including race as a covariate in the PK/PD model. Due to lack of improvement of the model fit, it is unlikely that inter-racial polymorphism expression caused the difference in ACT-1004-1239 concentrations. In line with the PK predictions [19], ACT-1004-1239 quickly reached steady-state conditions (i.e., within 3 days) with almost no systemic accumulation.

In terms of safety and tolerability, multiple doses of ACT-1004-1239 for 7 days o.d. were well tolerated up to 200 mg with similar incidence of AEs between active treatment and placebo. Headache, considered as the most commonly reported AE in Phase 1 studies [37], was also the most frequently reported AE in this study. Abnormal T waves were mainly observed in subjects receiving 200 mg ACT-1004-1239. These findings were not accompanied by clinically significant changes in other ECG intervals such as QRS and all subjects reporting these AEs were asymptomatic. In addition, *de novo* T wave abnormalities have been reported as one of the most common ECG abnormalities in healthy subjects [38]. Of note, abnormal T wave changes were not seen in 24-h Holter monitoring assessments. Results of the 24-h Holter monitoring showed that ACT-1004-1239 did not cause any QTc interval prolongation. Although a negative slope could be perceived from the concentration-QTc relationship (Fig. 5), the slope was not statistically significantly different from zero, suggesting no relevant shortening of the QTc interval following ACT-1004-1239 administration [39]. The implementation of the concentration-QT analysis in such early clinical development is a well-known approach to obtain a waiver for a dedicated study such as a thorough QT study [40].

In conclusion, results of these preclinical and clinical studies with ACT-1004-1239, a first-in-class CXCR7 antagonist, in conjunction with data in animal models warrant the use of CXCL12 as a translational tool in future clinical studies in patients. Whether CXCL11 can also be utilized as biomarker of target engagement will require further clinical investigations in patients. In addition, safety and tolerability data and simulations based on the PK/PD model support further clinical development of ACT-1004-1239 in patients using a o.d. dosing regimen.

## Funding

These studies were sponsored by Idorsia Pharmaceuticals Ltd, Allschwil, Switzerland.

## CRediT authorship contribution statement

C.H., J.M.B., L.P., and P.N.S. wrote the manuscript. C.H., L.P., and J. D. designed the research. L.P. performed the preclinical research. M.F. performed the clinical research. C.H., J.M.B., L.P., H.E.M.Z.S., J.D., and P.N.S. analyzed the data. All authors reviewed and approved the final manuscript.

## Conflict of interest statement

C.H., J.M.B., L.P., J.D., and P.N.S. are full-time employees of Idorsia Pharmaceuticals Ltd. M.F. is the principal investigator who is employed by BlueClinical Phase 1. H.E.M.Z.S. has no conflict of interest.

## Acknowledgements

The authors would like to thank the team members from Idorsia Pharmaceuticals Ltd as well as from BlueClinical Phase 1 for their dedicated support in terms of data generation and/or discussion including Geoffroy Bourquin, Hervé Farine, Ana Fernandes, Susanne Globig, Carmela Gnerre, Anne-Sophie Guern, Martin Holdener, Marianne Martinic, Alexandre Mathis, Gisela Rocha, Racheal Rowles, Egle Rugyte, Giancarlo Sabattini, and Daniel Strasser.

## Appendix A. Supporting information

Supplementary data associated with this article can be found in the online version at doi:10.1016/j.biopha.2021.112363.

## References

[1] H. Nomiyama, N. Osada, O. Yoshie, A family tree of vertebrate chemokine receptors for a unified nomenclature, Dev. Comp. Immunol. 35 (7) (2011) 705–715, https://doi.org/10.1016/j.dci.2011.01.019.
[2] C. Gerard, B.J. Rollins, Chemokines and disease, Nat. Immunol. 2 (2) (2001) 108–115, https://doi.org/10.1038/84209.
[3] F. Sierro, C. Biben, L. Martínez-Muñoz, M. Mellado, R.M. Ransohoff, M. Li, B. Woehl, H. Leung, J. Groom, M. Batten, R.P. Harvey, C. Martínez-A, C.R. Mackay, F. Mackay, Disrupted cardiac development but normal hematopoiesis in mice deficient in the second CXCL12/SDF-1 receptor, CXCR7, Proc. Natl. Acad. Sci. USA 104 (37) (2007) 14759–14764, https://doi.org/10.1073/pnas.0702229104.
[4] C. Huynh, J. Dingemanse, H.E. Meyer zu Schwabedissen, P.N. Sidharta, Relevance of the CXCR4/CXCR7-CXCL12 axis and its effect in pathophysiological conditions, Pharmacol. Res. 161 (2020), 105092, https://doi.org/10.1016/j.phrs.2020.105092.
[5] R.D. Berahovich, B.A. Zabel, S. Lewén, M.J. Walters, K. Ebsworth, Y. Wang, J. C. Jaen, T.J. Schall, Endothelial expression of CXCR7 and the regulation of systemic CXCL12 levels, Immunology 141 (1) (2014) 111–122, https://doi.org/10.1111/imm.12176.
[6] S. Rajagopal, J. Kim, S. Ahn, S. Craig, C.M. Lam, N.P. Gerard, C. Gerard, R. J. Lefkowitz, β-arrestin- but not G protein-mediated signaling by the "decoy" receptor CXCR7, Proc. Natl. Acad. Sci. 107 (2) (2010) 628–632, https://doi.org/10.1073/pnas.0912852107.
[7] U. Naumann, E. Cameroni, M. Pruenster, H. Mahabaleshwar, E. Raz, H.G. Zerwes, A. Rot, M. Thelen, CXCR7 functions as a scavenger for CXCL12 and CXCL11, PLoS One 5 (2) (2010), e9175, https://doi.org/10.1371/journal.pone.0009175.
[8] M.P. Crump, Solution structure and basis for functional activity of stromal cell-derived factor-1; dissociation of CXCR4 activation from binding and inhibition of HIV-1, EMBO J. 16 (23) (1997) 6996–7007, https://doi.org/10.1093/emboj/16.23.6996.
[9] J.M. Burns, B.C. Summers, Y. Wang, A. Melikian, R. Berahovich, Z. Miao, M. E. Penfold, M.J. Sunshine, D.R. Littman, C.J. Kuo, K. Wei, B.E. McMaster, K. Wright, M.C. Howard, T.J. Schall, A novel chemokine receptor for SDF-1 and I-TAC involved in cell survival, cell adhesion, and tumor development, J. Exp. Med. 203 (9) (2006) 2201–2213, https://doi.org/10.1084/jem.20052144.
[10] K.E. Quinn, D.I. Mackie, K.M. Caron, Emerging roles of atypical chemokine receptor 3 (ACKR3) in normal development and physiology, Cytokine 109 (February) (2018) 17–23, https://doi.org/10.1016/j.cyto.2018.02.024.
[11] S.W. Lewellis, H. Knaut, Attractive guidance: How the chemokine SDF1/CXCL12 guides different cells to different locations, Semin Cell Dev. Biol. 23 (3) (2012) 333–340, https://doi.org/10.1016/j.semcdb.2012.03.009.
[12] M.C. Tiveron, H. Cremer, CXCL12/CXCR4 signalling in neuronal cell migration, Curr. Opin. Neurobiol. 18 (3) (2008) 237–244, https://doi.org/10.1016/j.conb.2008.06.004.
[13] L. Cruz-Orengo, D.W. Holman, D. Dorsey, L. Zhou, P. Zhang, M. Wright, E. E. McCandless, J.R. Patel, G.D. Luker, D.R. Littman, J.H. Russell, R.S. Klein, CXCR7 influences leukocyte entry into the CNS parenchyma by controlling abluminal CXCL12 abundance during autoimmunity, J. Exp. Med. 208 (2) (2011) 327–339, https://doi.org/10.1084/jem.20102010.
[14] J.L. Williams, J.R. Patel, B.P. Daniels, R.S. Klein, Targeting CXCR7/ACKR3 as a therapeutic strategy to promote remyelination in the adult central nervous system, J. Exp. Med. 211 (5) (2014) 791–799, https://doi.org/10.1084/jem.20131224.
[15] K.-C. Ngamsri, A. Müller, H. Bösmüller, J. Gamper-Tsigaras, J. Reutershan, F. M. Konrad, The pivotal role of CXCR7 in stabilization of the pulmonary epithelial barrier in acute pulmonary inflammation, J. Immunol. 198 (6) (2017) 2403–2413, https://doi.org/10.4049/jimmunol.1601682.
[16] T. Qian, Y. Liu, Y. Dong, L. Zhang, Y. Dong, Y. Sun, D. Sun, CXCR7 regulates breast tumor metastasis and angiogenesis in vivo and in vitro, Mol. Med. Rep. 17 (3) (2017) 3633–3639, https://doi.org/10.3892/mmr.2017.8286.
[17] M.J. Walters, K. Ebsworth, R.D. Berahovich, M.E. Penfold, S.C. Liu, R. Al Omran, M. Kioi, S.B. Chernikova, D. Tseng, E.E. Mulkearns-Hubert, M. Sinyuk, R. M. Ransohoff, J.D. Lathia, J. Karamchandani, H.E. Kohrt, P. Zhang, J.P. Powers, J. C. Jaen, T.J. Schall, M. Merchant, L. Recht, J.M. Brown, Inhibition of CXCR7 extends survival following irradiation of brain tumours in mice and rats, Br. J. Cancer 110 (5) (2014) 1179–1188, https://doi.org/10.1038/bjc.2013.830.
[18] S. Richard-Bildstein, H. Aissaoui, J. Pothier, G. Schäfer, C. Gnerre, E. Lindenberg, F. Lehembre, L. Pouzol, P. Guerry, Discovery of the potent, selective, orally available CXCR7 antagonist ACT-1004-1239, J. Med. Chem. 63 (24) (2020) 15864–15882, https://doi.org/10.1021/acs.jmedchem.0c01588.
[19] C. Huynh, A. Henrich, D.S. Strasser, M.L. Boof, M. Al-Ibrahim, H.E. Meyer Zu Schwabedissen, J. Dingemanse, M. Ufer, A multipurpose first-in-human study with the novel CXCR7 antagonist ACT-1004–1239 using CXCL12 plasma concentrations as target engagement biomarker, Clin. Pharmacol. Ther. 109 (6) (2021) 1648–1659, https://doi.org/10.1002/cpt.2154.
[20] L. Pouzol, N. Baumlin, A. Sassi, M. Tunis, J. Marrie, E. Vezzali, H. Farine, U. Mentzel, M.M. Martinic, ACT-1004-1239, a first-in-class CXCR7 antagonist with both immunomodulatory and promyelinating effects for the treatment of inflammatory demyelinating diseases, FASEB J. 35 (3) (2021) 1–17, https://doi.org/10.1096/fj.202002465R.
[21] L. Pouzol, M. Tunis, N. Baumlin, CXCR7 antagonism with ACT-1004-1239 reduces Neuroinflammation and accelerates Remyelination in murine demyelinating models (2236), Neurology 96 (15 Supplement) (2021) 2236. http://n.neurology.org/content/96/15_Supplement/2236.abstract.
[22] P.L.S. Chan, P. Jacqmin, M. Lavielle, L. McFadyen, B. Weatherley, The use of the SAEM algorithm in MONOLIX software for estimation of population

pharmacokinetic-pharmacodynamic-viral dynamics parameters of maraviroc in asymptomatic HIV subjects, J. Pharmacokinet. Pharmacodyn. 38 (1) (2011) 41–61, https://doi.org/10.1007/s10928-010-9175-z.
[23] K. Gough, M. Hutchison, O. Keene, Assessment of dose proportionality: report from the statisticians in the pharmaceutical industry/pharmacokinetics UK joint working party, Ther. Innov. Regul. Sci. 29 (3) (1995) 1039–1048, https://doi.org/10.1177/009286159502900324.
[24] C. Garnett, P.L. Bonate, Q. Dang, G. Ferber, D. Huang, J. Liu, D. Mehrotra, S. Riley, P. Sager, C. Tornoe, Y. Wang, Scientific white paper on concentration-QTc modeling, J. Pharmacokinet. Pharmacodyn. 45 (3) (2018) 383–397, https://doi.org/10.1007/s10928-017-9558-5.
[25] R.N. Upton, D.R. Mould, Basic concepts in population modeling, simulation, and model-based drug development: Part 3-introduction to pharmacodynamic modeling methods, CPT Pharmacomet. Syst. Pharmacol. 3 (1) (2014) 1–16, https://doi.org/10.1038/psp.2013.71.
[26] M.G. Kenward, J.H. Roger, Small sample inference for fixed effects from restricted maximum likelihood, Biometrics 53 (3) (1997) 983–997, https://doi.org/10.2307/2533558.
[27] A. Marchese, C. Raiborg, F. Santini, J.H. Keen, H. Stenmark, J.L. Benovic, The E3 ubiquitin ligase AIP4 mediates ubiquitination and sorting of the G protein-coupled receptor CXCR4, Dev. Cell. 5 (5) (2003) 709–722, https://doi.org/10.1016/S1534-5807(03)00321-6.
[28] N.I. Tarasova, R.H. Stauber, C.J. Michejda, Spontaneous and ligand-induced trafficking of CXC-chemokine receptor 4, J. Biol. Chem. 273 (26) (1998) 15883–15886, https://doi.org/10.1074/jbc.273.26.15883.
[29] R. Janssens, S. Struyf, P. Proost, The unique structural and functional features of CXCL12, Cell Mol. Immunol. 15 (4) (2018) 299–311, https://doi.org/10.1038/cmi.2017.107.
[30] R. Janssens, A. Mortier, D. Boff, P. Ruytinx, M. Gouwy, B. Vantilt, O. Larsen, V. Daugvilaite, M.M. Rosenkilde, M. Parmentier, S. Noppen, S. Liekens, J. Van Damme, S. Struyf, M.M. Teixeira, F.A. Amaral, P. Proost, Truncation of CXCL12 by CD26 reduces its CXC chemokine receptor 4- and atypical chemokine receptor 3-dependent activity on endothelial cells and lymphocytes, Biochem. Pharmacol. 132 (2017) 92–101, https://doi.org/10.1016/j.bcp.2017.03.009.
[31] C.H. Yang, L. Wei, S.R. Pfeffer, Z. Du, A. Murti, W.J. Valentine, Y. Zheng, L. M. Pfeffer, Identification of CXCL11 as a STAT3-dependent gene induced by IFN, J. Immunol. 178 (2) (2007) 986–992, https://doi.org/10.4049/jimmunol.178.2.986.
[32] Bethesda (MD): National Library of Medicine (US); National Center for Biotechnology Information; 2004. Gene CXCL12C-X-C motif chemokine ligand 12 [ Homo sapiens (human)]. https://www.ncbi.nlm.nih.gov/gene/6387. (accessed 24 September 2021).
[33] Bethesda (MD): National Library of Medicine (US); National Center for Biotechnology Information; 2004. Gene CXCL11C-X-C motif chemokine ligand 11 [ Homo sapiens (human)]. https://www.ncbi.nlm.nih.gov/gene/6373. (accessed 24 September 2021).
[34] S. Gao, E.C. Bell, Y. Zhang, D. Liang, Racial disparity in drug disposition in the digestive tract, Int J. Mol. Sci. 22 (3) (2021) 1–21, https://doi.org/10.3390/ijms22031038.
[35] P. Kuehl, J. Zhang, Y. Lin, J. Lamba, M. Assem, J. Schuetz, P.B. Watkins, A. Daly, S. A. Wrighton, S.D. Hall, P. Maurel, M. Relling, C. Brimer, K. Yasuda, R. Venkataramanan, S. Strom, K. Thummel, M.S. Boguski, E. Schuetz, Sequence diversity in CYP3A promoters and characterization of the genetic basis of polymorphic CYP3A5 expression, Nat. Genet. 27 (4) (2001) 383–391, https://doi.org/10.1038/86882.
[36] R.K. Bains, M. Kovacevic, C.A. Plaster, A. Tarekegn, E. Bekele, N.N. Bradman, M. G. Thomas, Molecular diversity and population structure at the Cytochrome P450 3A5 gene in Africa, BMC Genet. 14 (1) (2013) 34, https://doi.org/10.1186/1471-2156-14-34.
[37] M. Sibille, N. Deigat, A. Janin, S. Kirkesseli, D. Vital Durand, Adverse events in phase-I studies: a report in 1015 healthy volunteers, Eur. J. Clin. Pharmacol. 54 (1) (1998) 13–20, https://doi.org/10.1007/s002280050413.
[38] P. Hingorani, D.R. Karnad, M. Natekar, S. Kothari, D. Narula, Baseline and new-onset morphologic ECG abnormalities in healthy volunteers in phase I studies receiving placebo: changes over a 6-week follow-up period, J. Clin. Pharmacol. 54 (7) (2014) 776–784, https://doi.org/10.1002/jcph.282.
[39] R.M. Lester, S. Paglialunga, I.A. Johnson, QT assessment in early drug development: the long and the short of it, Int. J. Mol. Sci. 20 (6) (2019), https://doi.org/10.3390/ijms20061324.
[40] B. Darpo, C. Garnett, J. Keirns, N. Stockbridge, Implications of the IQ-CSRC prospective study: time to revise ICH E14, Drug Saf. 38 (9) (2015) 773–780, https://doi.org/10.1007/s40264-015-0325-5.
[41] Laetitia Pouzol Anna Sassi Nadège Baumlin Daniel Tunis Daniel Strasser François Lehembre Marianne Martinic CXCR7 antagonism reduces acute lung injury pathogenesis Frontiers in Pharmacology - Inflammation Pharmacology doi: 10.3389/fphar.2021.748740.In press.

## 3.4 Further clinical development of ACT-1004-1239: Drug-drug interaction study

Thus far, the clinical effects of ACT-1004-1239 are well characterized in healthy subjects based on the results of the single- and multiple-ascending dose studies and their sub-investigations. The results of these studies provide further guidance on the clinical pharmacology program of ACT-1004-1239, i.e., which additional Phase 1 studies need to be conducted. For example, based on the ADME assessments supported by *in vitro* data, ACT-1004-1239 undergoes predominantly oxidative N-dealkylation to M1 accounting for 25.1% of total dose in excreta. This reaction is catalyzed by CYP3A4. M1 is metabolized to secondary metabolites A1 (4.0%) and A2 (15.3%) via oxidative defluorination and reduction, respectively. Taken together, the metabolic pathway catalyzed by CYP3A4 contributes to ≥25% of ACT-1004-1239 elimination. Therefore, DDI studies with a CYP3A4 inhibitor and inducer (i.e., perpetrators) are to be performed according to the health authorities guidelines [190,191].

In general, to cover safety-relevant aspects, DDI studies with a strong index inhibitor should be conducted to reveal the possible worst-case scenario. Index inhibitors are characterized by the strength of inhibition and selectivity [192]. The health authorities (FDA and EMA) define strong index inhibitors as drugs that can increase the AUC of a sensitive substrate ≥5-fold [191,193] such as clarithromycin and itraconazole for CYP3A4 [194]. There are other strong CYP3A4 inhibitors for instance ketoconazole, ritonavir, or voriconazole, which have been used in clinical DDI studies, but these are not suggested as index inhibitors. The use of ketoconazole was discouraged due to the high risk of severe liver injury [195,196]. According to the recommendation of the health authorities, selection of a strong CYP3A4 inhibitor for the DDI study with ACT-1004-1239 is limited to itraconazole and clarithromycin. The latter is less adequate as it is an antibiotic associated with adverse events related to the intestinal tract, QTc interval prolongation and potential to develop antibiotic resistance [197]. Furthermore, it should be administered in a twice daily dosing regimen [197], which makes the clinical conduct operationally more challenging. Thus, itraconazole, approved for treatment of various fungal infections, is the ultimate choice for the CYP3A4-related DDI study with ACT-1004-1239.

Recently, the use of itraconazole as perpetrator drug in DDI studies has been thoroughly studied and several recommendations were made in terms of study design, treatment duration, dose strength, dosing conditions, and itraconazole formulation [192,198,199]. Briefly, an open-label, fixed-sequence cross-over study design is commonly applied in such DDI studies, including two periods in which the substrate (victim drug) is given as a single dose. While in the first period, the substrate should be administered alone, in the second period the substrate is dispensed concomitantly with itraconazole. In comparison to the design in which the treatment sequence is switched (i.e., firstly concomitant administration, secondly single administration), this recommended fixed-sequence avoids a lengthy washout period of

itraconazole which has a terminal half-life ($t_{1/2}$) of up to 42 h [200]. With regard to dose and treatment duration, in order to obtain an adequate inhibition of CYP3A4, a run-in period (pre-treatment) of 3 days with 200 mg itraconazole once daily (o.d.) is recommended prior concomitant dosing of itraconazole and victim drug (e.g., ACT-1004-1239). A longer run-in period does not provide additional inhibitory effect of itraconazole and its metabolites [201,202]. Following the run-in period and concomitant administration of itraconazole and the victim drug, inhibition of CYP3A4 is to be maintained until the AUC of the victim can be fully described (i.e., $5 \times t_{1/2}$), which can be achieved with repeated dosing (o.d.) of 200 mg itraconazole.

Dosing of itraconazole can be performed under fasted or fed state. However, the exposure achieved in humans depends on the food state and the formulation of itraconazole. Thus far, two formulations have been used for DDI studies: oral capsule and oral solution. Higher exposure to itraconazole can be attained when it is administered as oral solution under fasted instead of fed conditions or as oral capsule under fed instead of fasted conditions. Regardless of the food state, itraconazole oral solution reaches, in general, higher exposure with lower variability compared to the oral capsule [198,199,203,204]. Therefore, it is the preferred formulation for concomitant administration with a victim drug, ideally given on an empty stomach. The food state is however of less importance for ACT-1004-1239 administration as the food effect assessment in the single-ascending dose study indicated no clinically relevant changes in exposure when administered with or without food [205]. Nevertheless, taking the itraconazole exposure into consideration, the oral solution would still be the favored formulation as it can reach overall higher exposure in humans associated with certainty of strong CYP3A4 inhibition. This evaluation is purely based on the PK and dosing condition and disregards other factors that could have a relevant impact on the DDI study, such as interacting excipients.

Recently, Hoch *et al.* reported a DDI study which showed that cyclodextrin, an excipient that is available in excess in the itraconazole oral solution, can interact with some victim drugs, and lead to unreliable study outcomes [206]. In detail, concomitant administration of asciminib (victim drug) and itraconazole oral solution was expected to increase the victim exposure due to CYP3A4 inhibition. However, the exposure to asciminib decreased by approximately 50%, whereas the itraconazole capsule (which does not contain cyclodextrin) did not significantly alter the victim's exposure (increase by approximately 3%). Follow-up *in vitro* investigations indicated that cyclodextrin forms complexes with asciminib in the gastrointestinal tract, and therefore, reduces the availability of free drug for absorption. This sequestration phenomenon was previously observed with other drugs such as warfarin and fenebrutinib [207,208]. The underlying mechanism may be explained by the characteristics of cyclodextrin. It is a cyclic oligosaccharide containing a lipophilic centrally laid cavity and a hydrophilic outer surface allowing, as

an excipient, the improvement of the aqueous solubility of the active drug (e.g., itraconazole). Such an interaction depends on the cavity size of cyclodextrin, which is split into α-, β-, and γ-variants, with an ascending cavity size from α to γ [209]. The itraconazole solution used in the case study with asciminib contains β-cyclodextrin, which probably provides an adequate cavity size to interact with asciminib. Based on the physicochemical properties of ACT-1004-1239 described by Richard-Bildstein *et al.* [187], sequestration of ACT-1004-1239 by β-cyclodextrin cannot be excluded. Therefore, the use of itraconazole solution as a perpetrator in a DDI study with ACT-1004-1239 is not advised as it may mask the DDI, and hence, the capsule formulation of itraconazole is recommended in this context.

After selection of the perpetrator drug, the dose strength of the victim drug should be defined. As itraconazole is a strong inhibitor of CYP3A4, a strong interaction with sensitive CYP3A4 substrates is expected. Previous studies showed that itraconazole can increase CYP3A4 substrates (e.g., midazolam) exposures up to 11-fold [202,210]. Thus, the dose of the victim drug is to be chosen in order to provide a sufficient safety margin in drug exposure when co-administered with itraconazole. If needed, a dose below the therapeutic dose range can be considered provided that the results can be extrapolated to a clinically relevant dose (i.e., the victim drug has dose-proportional PK) [192]. This approach may be applied to ACT-1004-1239. Since ACT-1004-1239 revealed a dose-proportional PK, the recommended dose of ACT-1004-1239 in the DDI study with itraconazole is 10 mg, which is also formulated as a ready-to-use capsule [205]. This dose strength provides a sufficient safety margin in the event of itraconazole increasing the exposure to ACT-1004-1239 up to 11-fold as the maximum exposure investigated in humans (achieved with a dose of 200 mg) [205,211] is not expected to be exceeded.

Last but not least, a relevant aspect in designing a DDI study is the selection of the appropriate study population and the sample size. In general, healthy subjects are considered in such study provided the safety profile of the victim drug allows this. Healthy subjects are strongly recommended in order to generate a reliable study outcome without the bias of confounding factors such as concomitant medications. According to the health authority guidelines, there is no request to power such DDI studies. Nevertheless, in order to obtain the preferred precision of the DDI effect, the sample size can be determined based on the PK variability (e.g., inter-subject variability) of the victim drug [199]. For the DDI study with ACT-1004-1239, the coefficient of variation within subjects can be obtained from the single-ascending dose study [205], which is 48.8% for maximum plasma concentration ($C_{max}$) and 13.9% for area under the plasma time curve from zero to infinity ($AUC_{0-\infty}$). Using the precision estimate approach as described by Patterson *et al.* [212], a sample size of 12 subjects would result in lower and upper bounds of the 90% confidence interval (CI) of the geometric mean ratio of approximately –29% and +40% and –10% and +11% of the observed ratio for $C_{max}$ and $AUC_{0-\infty}$, respectively. For example, if

the observed ratio is 5, the 90% CI of $C_{max}$ and $AUC_{0-\infty}$ will be (3.55, 7.00) and (4.50, 5.55), respectively. This precision estimate would be considered acceptable for this study. In conclusion, taken the above-mentioned facets into consideration, the DDI study with ACT-1004-1239 can be designed as follows.

An open-label, fixed-sequence cross-over DDI study is recommended to investigate the effect of itraconazole oral capsule on the PK of ACT-1004-1239. Since a higher exposure can be achieved when itraconazole capsule is administered under fed state, all study treatments including ACT-1004-1239 should be given under fed conditions. After a screening period, a single oral dose of 10 mg ACT-1004-1239 is administered in the first period in which PK samples are collected for 5 days (Period 1). Prior to the start of the second period, a washout of 5 days is considered sufficient based on the single-ascending dose study indicating a $t_{1/2}$ of up to 24 h [205]. In the second period, following a 3-day run-in period of 200 mg itraconazole (capsule, o.d.; Period 2a), 10 mg ACT-1004-1239 is given concomitantly to 200 mg itraconazole capsule after food intake (Period 2b). In Period 2b, itraconazole treatment (200 mg o.d.) is continued for an additional 4 days and PK samples are collected for 5 days post ACT-1004-1239 dosing. Once no clinically relevant treatment exposure and/or treatment-related safety concerns are expected, end-of-study assessments can be carried out. With regard to the study population, healthy subjects are recommended for this study to avoid confounding factors due to concomitant medications or underlying disease. Furthermore, ACT-1004-1239 was safe and well tolerated up to a dose of 200 mg (expected ACT-1004-1239 dose/exposure in the event of a maximum DDI effect) in healthy subjects. In order to have at least 12 evaluable subjects (with respect to PK) and accounting for a potential subject discontinuation rate of 25%, a total of 16 subjects should be enrolled in this study. The proposed study design is depicted in Figure 6.

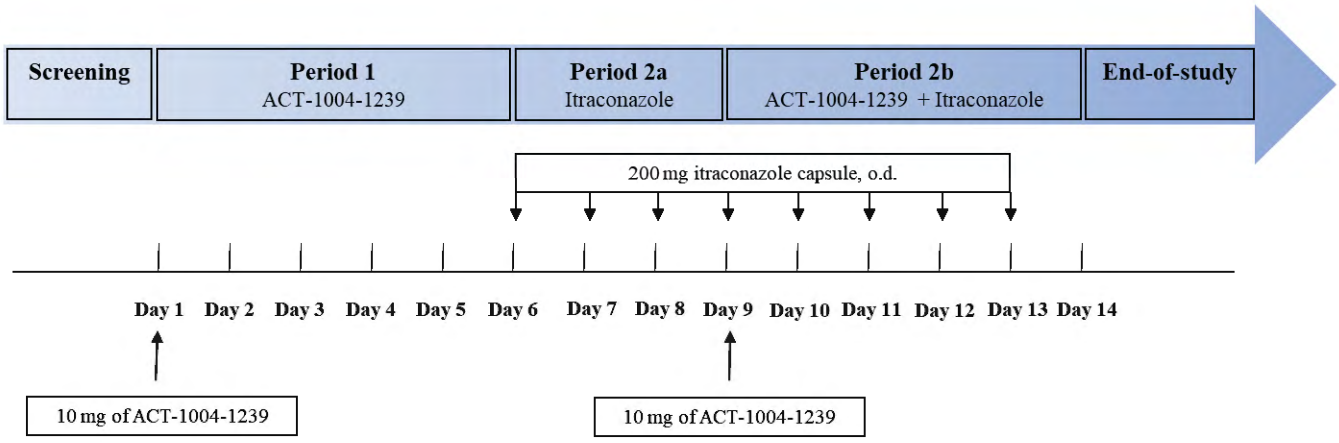


CYP = cytochrome P450; DDI = drug-drug interaction; o.d. = once-daily.

**Figure 1: Recommended study design for the DDI study with ACT-1004-1239 and a strong CYP3A4 inhibitor**

# CHAPTER 3

# Discussion, Conclusion, and Outlook

# 4 DISCUSSION

Chemokines and their corresponding receptors play an important role in the maintenance of physiological processes, amongst others through their ability to induce cell signaling including cell proliferation, differentiation, survival, and chemotaxis. On top of these functions, some chemokine receptors, such as CXCR7, show an ability to preserve physiological conditions by acting as a scavenger receptor for their ligands [8,9]. Disordered physiology caused by disease or injuries can affect the chemokine receptor-ligand interactions. For example, the CXCR3/CXCR4/CXCR7–CXCL11/CXCL12 axis is a relevant element in several pathophysiological conditions, notably cancer and MS. There is evidence suggesting that modulation of the CXCR3/CXCR4/CXCR7–CXCL11/CXCL12 axis, through antagonism/blockade/neutralization, can improve the clinical disease score of various animal models of cancer and MS. To date, only a few modulators are known that target this specific axis. In addition, only a few modulators have reached clinical development [6]. Therefore, there is a high unmet need for new potent modulators which can regulate this axis in cancer and MS.

Idorsia Pharmaceuticals Ltd has developed a selective and potent first-in-class CXCR7 antagonist, namely ACT-1004-1239. ACT-1004-1239 provides favorable physicochemical and biological effects to engage drug development [187]. Efficacy of ACT-1004-1239 was demonstrated in studies with animal models of MS, suggesting a dual mode of action, i.e., immunomodulatory and pro-myelinating effects [146,189]. The immunomodulatory effect was further preclinically supported in an animal study using a disease model of ALI [82]. Following completion of other pertinent preclinical studies, such as toxicology, all prerequisites were fulfilled for initiation of a first-in-human study with ACT-1004-1239.

The first-in-human study of ACT-1004-1239 was designed as a single-center, randomized, double-blind, and placebo-controlled clinical pharmacology study with the main objective to evaluate the safety/tolerability, PK, and PD of ACT-1004-1239 following single-dose administration. To accelerate the clinical development program, additional assessments, including food effect, absolute bioavailability, and ADME characteristics, were incorporated into the study [205]. The integration of the food effect arm in a first-in-human study is common practice as it supports the decision of the dosing conditions (fasted vs. fed) in subsequent clinical studies [213]. Similarly, the incorporation of an absolute bioavailability assessment in early clinical development can inform ahead of time on the drug's bioavailability. Therefore, it may provide guidance on the chosen dose strength to achieving the desired therapeutic efficacy in patient studies [214]. The integration of an ADME subpart in a first-in-human study using a microtracer approach is not commonly applied to date. Traditionally, human ADME studies were conducted as a stand-alone study using a radioactive dose between 20 and 100 µCi. Before this dose can

be administered to humans, there is the requirement to determine the radiation burden based on quantitative whole-body autoradiography in animals. Furthermore, the material used in such conventional ADME studies are to be produced according to Good Manufacturing Practice (GMP), which can lead to substantial increase in study cost [215,216]. These additional requirements can be circumvented by applying a microtracer approach. The microtracer dose consists of very low amounts of radiolabeled compound (<1 μCi), so that no determination of radiation burden is needed. In addition, the very low amounts of microtracer used in these studies do not require production according to GMP guidelines. The use of such microtracer approach allows the incorporation of an ADME study into a first-in-human study enabling early identification of relevant human metabolites in clinical development [215]. Early investigation of human metabolites in clinical development is encouraged by the health authorities [217]. The main reason for this may be to avoid potential safety concerns that could come from disproportionate toxic metabolites, which may drive the termination of a drug's development at a later stage [215]. Notably, the integration of an ADME study into a first-in-human study requires a few considerations with respect to dose selection and a compound's survival into later stages of drug development. In terms of dose selection, an appropriate dose needs to be selected within the anticipated therapeutic dose range or at least a dose within the PK dose-proportional range [218]. These data are usually unknown in early clinical development. With regard to the poor success rate in clinical development, 90% of drug candidates advancing to clinical development fail and, therefore, early identification of metabolites may be redundant [219]. These considerations have to be carefully assessed for risk-benefit by each investigator. Besides ADME, absolute bioavailability, and food effect sub-investigations, a further evaluation can be considered within a single- and/or multiple-ascending dose study, namely the concentration-QTc relationship. Such investigation was incorporated in the multiple-ascending dose study of ACT-1004-1239. This study was a single-center, randomized, double-blind, and placebo-controlled Phase 1 study and focused on the investigation of the safety/tolerability, PK, and PD of multiple doses of ACT-1004-1239 [211]. The inclusion of the concentration-QT analysis in this early stage of clinical development could be considered as justification for obtaining a waiver for a thorough QTc study [220].

Altogether, two clinical pharmacology studies with ACT-1004-1239 have been conducted to date. These studies, although few in number, provided a thorough characterization of ACT-1004-1239 in terms of safety/tolerability, PK, and PD at an early stage of clinical development.

Prior to the initiation of a clinical study in patients, the safety profile must be sufficiently investigated in healthy subjects. The use of healthy subjects in early-stage clinical development is a standardized approach allowing good understanding of the safety/tolerability properties of a noncytotoxic drug without

any confounding factors such as concomitant drug treatment or underlying diseases. Safety/tolerability investigations including vital signs, 12-lead ECG, clinical laboratory, and body weight assessments (i.e., standard safety evaluation package) revealed that single and multiple doses of ACT-1004-1239 were safe and well tolerated up to and including the maximum investigated dose of 200 mg (o.d.). There were no serious or other significant adverse events. Frequently reported adverse events in both studies included asymptomatic increase in creatine kinase (CK) and ECG morphology changes. However, the majority of subjects who reported an increase in CK had baseline levels above the upper limit of normal range and/or admitted performing strong physical exercise which is known to induce CK elevation [221]. Asymptomatic changes in ECG morphology were not accompanied by any clinically significant changes in ECG intervals. Furthermore, such ECG abnormalities are commonly reported in healthy subjects [222]. In addition to the safety ECG assessment, the integrated investigation of the concentration QTc relationship indicated that no ACT-1004-1239-related QTc liability is expected. The safety findings reported in both clinical pharmacology studies are monitorable in the subsequent Phase 2 studies. In fact, there is no need to apply additional assessments apart from the standard safety evaluation package.

With regard to PK, both clinical studies revealed similar profiles following single- and multiple-dose ACT-1004-1239 with fast absorption and multiple phases of disposition covered by a $t_{1/2}$ of approximately 20 h [205,211]. While the intake of food delays the absorption of ACT-1004-1239, there is no clinically relevant alteration in exposure [205]. Furthermore, even though females experience higher ACT-1004-1239 exposure (up to 1.4-fold) than males, there is no significant difference in safety profiles between the two sexes [211]. These PK characteristics simplify the daily routine of patients who require frequent treatment since no dose adjustment and no multiple drug intake per day are required. Additional PK investigations using a microtracer approach confirmed a significant distribution of ACT-1004-1239 into extravascular compartments indicated by a volume of distribution of 183 L. ACT-1004-1239 has an absolute bioavailability of 53% and was identified as a low-clearance drug [211]. Some of these PK characteristics are in line with the ones observed in animals. Rat and dog also reported a quick absorption of ACT-1004-1239 indicated by a time to reach maximum plasma concentration ($t_{max}$) of 0.5 and 1.5 h, respectively. The elimination of the drug, however, was shorter in animals compared to humans, requiring more frequent dosing of ACT-1004-1239 in animal studies [187]. Similar as in humans, the $t_{max}$ was observed later in dogs following food intake, which may be due to delayed gastric emptying [205]. All species (i.e., human, rat, and dog) reported a high volume of distribution at steady state, which was in excess to total body water. Moreover, the absolute bioavailability in human falls in the range of the ones observed in rat (35%) and dog (61%). The clearance of ACT-1004-1239 was high in rat, and hence, considered as high-clearance drug in rodents. In contrast, ACT-1004-1239 is a low-clearance drug

in humans and dogs [187]. In general, while most PK data in humans are in contrast to the PK observed in rodents, the human PK resemble rather the PK obtained in dogs [187]. Therefore, dog is currently the most appropriate species to predict the PK of ACT-1004-1239 in humans.

The modest absolute bioavailability of ACT-1004-1239 in humans may be explained by the drug's metabolism. ACT-1004-1239 is extensively metabolized, and only 15% of the dose is excreted as unchanged drug in excreta, predominantly via urine. The main elimination route of drug-related material is via feces (~70%) and to a lesser extent via urine (~15%) [188]. According to the health authority guideline, PK studies in subjects with hepatic impairment are to be conducted when hepatic metabolism and/or excretion accounts for >20% of the absorbed drug [223]. As approximately 70% of ACT-1004-1239-related material is excreted via feces, PK studies in hepatically impaired subjects are therefore to be considered in the future clinical development program of ACT-1004-1239. This would determine any significant ACT-1004-1239 PK alterations in this patient population and consequently, if any dose adjustments are required for this subpopulation.

Based on the ADME assessments, two circulating metabolites (i.e., M1 and M23) accounting for >10% of total drug-related exposure were identified [188]. As a follow-up investigation, the human plasma exposure to M1 and M23 is to be measured and compared to the maximum exposure determined in animals used for toxicological evaluation of ACT-1004-1239, according to the health authority guidance [217]. Such investigations will inform about any relevant human safety concerns and provide more insight into the safety profile of ACT-1004-1239.

The ADME assessments also provided an understanding of the ACT-1004-1239 elimination route. Elimination of the drug via the primary metabolite M1 plays a major role, accounting for ≥25% of total drug elimination. This oxidative N-dealkylation pathway is mostly catalyzed by CYP3A4 as shown by *in vitro* data [188]. Therefore, DDI studies investigating the interaction potential of ACT-1004-1239 with CYP3A4 inhibitors/inducers should be performed based on the recommendations given by the health authorities [190,191]. In general, investigations of DDIs are of utmost relevance in drug development as it can lead to a wide range of consequences from loss of efficacy to fatal side effects due to polypharmacy.

A safety-relevant DDI study (i.e., with a strong CYP3A4 inhibitor) can be designed as an open-label, fixed-sequence cross-over study using itraconazole as perpetrator. Itraconazole is a well-known strong CYP3A4 index inhibitor and is commonly used for this type of DDI study [224–227]. However, the decision on the oral itraconazole formulation (capsule vs. solution) is more challenging compared to the other aspects considered for designing a DDI study. In the end, the decision for the ACT-1004-1239 DDI study is driven by the excipient of the oral solution, namely cyclodextrin. Due to its structure, it can

theoretically form complexes with the victim drug (e.g., ACT-1004-1239), which would reduce its free concentration for absorption, and potentially compromise the study outcome. Although this interaction may be applicable for the DDI study with ACT-1004-1239, it does not necessarily apply to all DDI studies with itraconazole solution. It has to be carefully assessed on a case-by-case basis depending on the physicochemical properties of each victim drug. In some cases, the itraconazole oral solution cannot be avoided, for example, due to market availability or dosing conditions. In order to circumvent potential interactions, the concomitant administration of itraconazole and the victim drug can be separated by at least 2–3 h (itraconazole solution prior to victim drug). This recommendation is based on cyclodextrin simulation results illustrating that the cyclodextrin concentration within the small intestine is reduced by more than half after approximately 2 h [208]. In recently reported DDI studies, itraconazole solution was administered approximately 1 h prior to the victim drug and an increase in victim exposure was observed [226–228]. However, whether cyclodextrin masked the DDI and therefore led to unreliable study outcome remains to be determined. While the DDI study with a strong CYP3A4 inhibitor is related to safety concerns, combinations with CYP3A4 inducers can have implications on the efficacy of the drug and should also be considered in the clinical development program of ACT-1004-1239.

With regard to PD, as CXCR7 functions as a scavenger receptor for both ligands, CXCL11 and CXCL12, antagonism of the receptor by ACT-1004-1239 is expected to increase the ligand concentration in plasma. Therefore, CXCL11 and CXCL12 plasma concentrations were measured in the single- and multiple-ascending dose studies as biomarker of target engagement. However, as CXCL11 is an inflammatory chemokine mainly induced by IFNβ / IFNγ under inflammatory conditions [229], and the *CXCL11* gene is less expressed in healthy subjects, no alteration in CXCL11 plasma concentration was expected in healthy subjects [230,231]. Indeed, no changes in CXCL11 plasma level was observed in healthy subjects, neither after single-dose, nor after multiple-dose administration of ACT-1004-1239 [205,211]. However, this does not preclude that significant changes in CXCL11 plasma level may be observed in patients, as preclinical disease models of MS and ALI indicated a dose-dependent increase in CXCL11 concentration in plasma [82,189]. Further clinical studies in patients are required to confirm the translatability of preclinical data. In contrast to CXCL11, following single- and multiple-ascending doses of ACT-1004-1239, CXCL12 plasma concentration increased in a dose-dependent manner indicating target engagement of ACT-1004-1239. In both studies, at the highest dose group of 200 mg, the increase in CXCL12 plasma level was similar to the one observed in the 100 mg dose group (approximately 2-fold compared to baseline and/or placebo treatment), suggesting that a plateau has been approached. In line with the observed data, simulations using the PK/PD model demonstrated that no further increase in CXCL12 concentration is expected for doses >100 mg [205,211]. Since the CXCL12 increase was

maintained over at least 24 h after single-dose administration and taking the PK of ACT-1004-1239 in humans (i.e., $t_{1/2}$ ~20 h) into consideration, a o.d. dosing regimen was proposed for successive clinical studies including the multiple-ascending dose study. Following multiple-ascending doses of ACT-1004-1239, CXCL12 level remained high after the first dose until 24 h after the last dose [211]. In line with healthy humans, a dose-dependent increase in CXCL12 concentration including an approaching of a plateau was also observed in various animal disease models after treatment with ACT-1004-1239. Importantly, the ACT-1004-1239-associated increase in CXCL12 levels was linked to efficacy in animal models of MS and ALI [82,146]. Therefore, investigation of CXCL12 as a biomarker of target engagement and efficacy should also be considered in patients.

Taken together, the safety/tolerability, PK, and PD of ACT-1004-1239 have been thoroughly characterized in healthy humans enabling further clinical development of the drug in patients.

# 5 CONCLUSIONS AND OUTLOOK

CXCR7 has evolved as a druggable target due to its ability to regulate CXCL11 and CXCL12 concentrations and to indirectly modulate the functions of CXCR3 and CXCR4. Promising preclinical observations suggest that blockade of these functions reduces the progression of several diseases including cancer and MS. Unfortunately, thus far no CXCR7 antagonist has been approved for the treatment of cancer or MS and a high unmet clinical need remains. ACT-1004-1239 is a potent and selective CXCR7 antagonist and represents a first-in-class drug candidate in clinical development. It showed a favorable efficacy profile in animal models of MS leading to a reduction in disease progression. In these animal models, alongside the immunomodulatory effect ACT-1004-1239 demonstrated pro-myelinating effect. Therefore, ACT-1004-1239 may not only act as a disease-modifying therapy by changing the course of the disease (e.g., MS) but may also be beneficial in possible recovery from the disease. The efficacy observed in diseased animals was suggested to be linked to the dose-dependent increase in CXCL11 and CXCL12 concentrations, emphasizing the use of CXCL11 and CXCL12 as biomarkers of target engagement. Indeed, such ACT-1004-1239-induced increase in CXCL12 plasma levels was also observed in both studies (single- and multiple-ascending dose) in healthy subjects. Therefore, these data warrant the further use of CXCL12 as a translational tool in future clinical studies in MS patients for example. It can provide guidance for optimal dose selection in subsequent clinical development. However, whether the dose-dependent increase in CXCL12 level and the magnitude in CXCL12 increase are sufficient to be associated with efficacy remains unknown and requires further investigations in patient studies. Whether CXCL11 can also be utilized as biomarker of target engagement will also require further clinical investigations in patients. Of note, the measurement of both biomarkers in human plasma may provide more insight into the immunomodulatory effect of ACT-1004-1239 as this is assumed to take place at the site of endothelia. In order to evaluate the correlation between these chemokines and the (pro-)myelinating effect that is assumed to happen in the parenchyma, there is a necessity to measure these chemokines in the brain. However, such investigation is highly invasive and not viable in patients. This may be circumvented by using a less invasive approach of measuring these chemokines in patients' CSF as previously done in a mouse model of MS. However, before any increase in CXCL11 and CXCL12 can be seen in the brain, it is important to assess the ability of ACT-1004-1239 to cross the BBB including the sensitivity to the efflux transporter P-gp. Although promising animal efficacy data in animal models exist (i.e., MS and ALI), it does not rule out possible further preclinical investigations of ACT-1004-1239 in other diseases like cancer and/or demyelinating diseases. This would broaden the potential therapy opportunities for ACT-1004-1239. Since ACT-1004-1239 was safe and well tolerated up to and including a dose of 200 mg, there is no limitation in patient selection in terms

of safety/tolerability. Due to incorporation of multiple assessments (i.e., food effect, absolute bioavailability, and ADME) in the first-in-human study, the PK profile of ACT-1004-1239 was thoroughly characterized. PK in conjunction with PD data support a o.d. dosing regimen for future studies in patients. In parallel to the Phase 2 study, further clinical pharmacology studies such as DDI studies with CYP3A4 inhibitors/inducers or studies with hepatically impaired subjects are to be considered. These studies would provide more insight into the PK of ACT-1004-1239 and can guide dose adjustment as needed. Overall, the clinical pharmacology studies completed to date provide all the prerequisites for further clinical investigations of ACT-1004-1239 in patients.

# REFERENCES

[1] C. Liu, D. Chu, K. Kalantar-Zadeh, J. George, H.A. Young, G. Liu, Cytokines: From Clinical Significance to Quantification, Adv. Sci. 8 (2021) 2004433. https://doi.org/10.1002/advs.202004433.

[2] A. Zlotnik, O. Yoshie, Chemokines: A New Classification System and Their Role in Immunity, Immunity. 12 (2000) 121–127. https://doi.org/10.1016/S1074-7613(00)80165-X.

[3] A. Zlotnik, A.M. Burkhardt, B. Homey, Homeostatic chemokine receptors and organ-specific metastasis, Nat. Rev. Immunol. 11 (2011) 597–606. https://doi.org/10.1038/nri3049.

[4] A. Zlotnik, O. Yoshie, The Chemokine Superfamily Revisited, Immunity. 36 (2012) 705–716. https://doi.org/10.1016/j.immuni.2012.05.008.

[5] P.M. Murphy, M. Baggiolini, I.F. Charo, C.A. Hebert, R. Horuk, K. Matsushima, et al., International Union of Pharmacology. XXII. Nomenclature for Chemokine Receptors, Pharmacol. Rev. 52 (2000) 145–176.

[6] C. Huynh, J. Dingemanse, H.E. Meyer zu Schwabedissen, P.N. Sidharta, Relevance of the CXCR4/CXCR7-CXCL12 axis and its effect in pathophysiological conditions, Pharmacol. Res. 161 (2020) 105092. https://doi.org/10.1016/j.phrs.2020.105092.

[7] H. Nomiyama, N. Osada, O. Yoshie, A family tree of vertebrate chemokine receptors for a unified nomenclature, Dev. Comp. Immunol. 35 (2011) 705–715. https://doi.org/10.1016/j.dci.2011.01.019.

[8] S. Rajagopal, J. Kim, S. Ahn, S. Craig, C.M. Lam, N.P. Gerard, et al., β-arrestin- but not G protein-mediated signaling by the "decoy" receptor CXCR7, Proc. Natl. Acad. Sci. 107 (2010) 628–632. https://doi.org/10.1073/pnas.0912852107.

[9] U. Naumann, E. Cameroni, M. Pruenster, H. Mahabaleshwar, E. Raz, H.-G. Zerwes, et al., CXCR7 Functions as a Scavenger for CXCL12 and CXCL11, PLoS One. 5 (2010) e9175. https://doi.org/10.1371/journal.pone.0009175.

[10] R. Fredriksson, M.C. Lagerström, L.-G. Lundin, H.B. Schiöth, The G-Protein-Coupled Receptors in the Human Genome Form Five Main Families. Phylogenetic Analysis, Paralogon Groups, and Fingerprints, Mol. Pharmacol. 63 (2003) 1256–1272. https://doi.org/10.1124/mol.63.6.1256.

[11] F. Libert, M. Parmentier, A. Lefort, C. Dinsart, J. Van Sande, C. Maenhaut, et al., Selective Amplification and Cloning of Four New Members of the G Protein-Coupled Receptor Family, Science (80-. ). 244 (1989) 569–572. https://doi.org/10.1126/science.2541503.

[12] J.M. Burns, B.C. Summers, Y. Wang, A. Melikian, R. Berahovich, Z. Miao, et al., A novel chemokine receptor for SDF-1 and I-TAC involved in cell survival, cell adhesion, and tumor development, J. Exp. Med. 203 (2006) 2201–2213. https://doi.org/10.1084/jem.20052144.

[13] F. Bachelerie, A. Ben-Baruch, A.M. Burkhardt, C. Combadiere, J.M. Farber, G.J. Graham, et al., International Union of Basic and Clinical Pharmacology. LXXXIX. Update on the Extended Family of Chemokine Receptors and Introducing a New Nomenclature for Atypical Chemokine Receptors, Pharmacol. Rev. 66 (2014) 1–79. https://doi.org/10.1124/pr.113.007724.

[14] K. Balabanian, B. Lagane, S. Infantino, K.Y.C.C. Chow, J. Harriague, B. Moepps, et al., The Chemokine SDF-1/CXCL12 Binds to and Signals through the Orphan Receptor RDC1 in T Lymphocytes, J. Biol. Chem. 280 (2005) 35760–35766.

https://doi.org/10.1074/jbc.M508234200.

[15] M.P. Crump, Solution structure and basis for functional activity of stromal cell-derived factor-1; dissociation of CXCR4 activation from binding and inhibition of HIV-1, EMBO J. 16 (1997) 6996–7007. https://doi.org/10.1093/emboj/16.23.6996.

[16] R.D. Berahovich, B.A. Zabel, S. Lewén, M.J. Walters, K. Ebsworth, Y. Wang, et al., Endothelial expression of CXCR7 and the regulation of systemic CXCL12 levels, Immunology. 141 (2014) 111–122. https://doi.org/10.1111/imm.12176.

[17] F. Hoffmann, W. Müller, D. Schütz, M.E. Penfold, Y.H. Wong, S. Schulz, et al., Rapid Uptake and Degradation of CXCL12 Depend on CXCR7 Carboxyl-terminal Serine/Threonine Residues, J. Biol. Chem. 287 (2012) 28362–28377. https://doi.org/10.1074/jbc.M111.335679.

[18] G. Valentin, P. Haas, D. Gilmour, The Chemokine SDF1a Coordinates Tissue Migration through the Spatially Restricted Activation of Cxcr7 and Cxcr4b, Curr. Biol. 17 (2007) 1026–1031. https://doi.org/10.1016/j.cub.2007.05.020.

[19] S.W. Lewellis, H. Knaut, Attractive guidance: How the chemokine SDF1/CXCL12 guides different cells to different locations, Semin. Cell Dev. Biol. 23 (2012) 333–340. https://doi.org/10.1016/j.semcdb.2012.03.009.

[20] K.E. Quinn, D.I. Mackie, K.M. Caron, Emerging roles of atypical chemokine receptor 3 (ACKR3) in normal development and physiology, Cytokine. 109 (2018) 17–23. https://doi.org/10.1016/j.cyto.2018.02.024.

[21] M. Puchert, J. Obst, C. Koch, K. Zieger, J. Engele, CXCL11 promotes tumor progression by the biased use of the chemokine receptors CXCR3 and CXCR7, Cytokine. 125 (2020) 154809. https://doi.org/10.1016/j.cyto.2019.154809.

[22] K.E. Luker, J.M. Steele, L.A. Mihalko, P. Ray, G.D. Luker, Constitutive and chemokine-dependent internalization and recycling of CXCR7 in breast cancer cells to degrade chemokine ligands, Oncogene. 29 (2010) 4599–4610. https://doi.org/10.1038/onc.2010.212.

[23] G.J. Graham, M. Locati, A. Mantovani, A. Rot, M. Thelen, The biochemistry and biology of the atypical chemokine receptors, Immunol. Lett. 145 (2012) 30–38. https://doi.org/10.1016/j.imlet.2012.04.004.

[24] S.M. DeWire, S. Ahn, R.J. Lefkowitz, S.K. Shenoy, β-Arrestins and Cell Signaling, Annu. Rev. Physiol. 69 (2007) 483–510. https://doi.org/10.1146/annurev.physiol.69.022405.154749.

[25] J. Wang, Y. Shiozawa, J. Wang, Y. Wang, Y. Jung, K.J. Pienta, et al., The Role of CXCR7/RDC1 as a Chemokine Receptor for CXCL12/SDF-1 in Prostate Cancer, J. Biol. Chem. 283 (2008) 4283–4294. https://doi.org/10.1074/jbc.M707465200.

[26] V. Odemis, K. Boosmann, A. Heinen, P. Kury, J. Engele, CXCR7 is an active component of SDF-1 signalling in astrocytes and Schwann cells, J. Cell Sci. 123 (2010) 1081–1088. https://doi.org/10.1242/jcs.062810.

[27] K. Grymula, M. Tarnowski, M. Wysoczynski, J. Drukala, F.G. Barr, J. Ratajczak, et al., Overlapping and Distinct Role of CXCR7-SDF-1/ITAC and CXCR4-SDF-1 Axes in Regulating Metastatic Behavior of Human Rhabdomyosarcomas, Int. J. Cancer. 127 (2010) 2554–2568. https://doi.org/10.1002/ijc.25245.

[28] K. Hattermann, J. Held-Feindt, R. Lucius, S.S. Muerkoster, M.E.T. Penfold, T.J. Schall, et al., The Chemokine Receptor CXCR7 Is Highly Expressed in Human Glioma Cells and Mediates

Antiapoptotic Effects, Cancer Res. 70 (2010) 3299–3308. https://doi.org/10.1158/0008-5472.CAN-09-3642.

[29] D.G. Duda, S. V. Kozin, N.D. Kirkpatrick, L. Xu, D. Fukumura, R.K. Jain, CXCL12 (SDF1α) - CXCR4/CXCR7 Pathway Inhibition: An Emerging Sensitizer for Anticancer Therapies?, Clin. Cancer Res. 17 (2011) 2074–2080. https://doi.org/10.1158/1078-0432.CCR-10-2636.

[30] H. Gerrits, D.S. van Ingen Schenau, N.E.C. Bakker, A.J.M. van Disseldorp, A. Strik, L.S. Hermens, et al., Early Postnatal Lethality and Cardiovascular Defects in CXCR7-Deficient Mice, Genesis. 46 (2008) 235–245. https://doi.org/10.1002/dvg.20387.

[31] F. Sierro, C. Biben, L. Martínez-Muñoz, M. Mellado, R.M. Ransohoff, M. Li, et al., Disrupted cardiac development but normal hematopoiesis in mice deficient in the second CXCL12/SDF-1 receptor, CXCR7, Proc. Natl. Acad. Sci. 104 (2007) 14759–14764. https://doi.org/10.1073/pnas.0702229104.

[32] S. Yu, D. Crawford, T. Tsuchihashi, T.W. Behrens, D. Srivastava, The chemokine receptor CXCR7 functions to regulate cardiac valve remodeling, Dev. Dyn. 240 (2011) 384–393. https://doi.org/10.1002/dvdy.22549.

[33] K.R. Klein, N.O. Karpinich, S.T. Espenschied, H.H. Willcockson, W.P. Dunworth, S.L. Hoopes, et al., Decoy Receptor CXCR7 Modulates Adrenomedullin-Mediated Cardiac and Lymphatic Vascular Development, Dev. Cell. 30 (2014) 528–540. https://doi.org/10.1016/j.devcel.2014.07.012.

[34] M. Loetscher, B. Gerber, P. Loetscher, S.A. Jones, L. Piali, I. Clark-Lewis, et al., Chemokine receptor specific for IP10 and mig: structure, function, and expression in activated T-lymphocytes., J. Exp. Med. 184 (1996) 963–969. https://doi.org/10.1084/jem.184.3.963.

[35] M. Metzemaekers, V. Vanheule, R. Janssens, S. Struyf, P. Proost, Overview of the Mechanisms that May Contribute to the Non-Redundant Activities of Interferon-Inducible CXC Chemokine Receptor 3 Ligands, Front. Immunol. 8 (2018). https://doi.org/10.3389/fimmu.2017.01970.

[36] K.E. Cole, C.A. Strick, T.J. Paradis, K.T. Ogborne, M. Loetscher, R.P. Gladue, et al., Interferon–inducible T Cell Alpha Chemoattractant (I-TAC): A Novel Non-ELR CXC Chemokine with Potent Activity on Activated T Cells through Selective High Affinity Binding to CXCR3, J. Exp. Med. 187 (1998) 2009–2021. https://doi.org/10.1084/jem.187.12.2009.

[37] H. Hasegawa, A. Inoue, M. Kohno, J. Lei, T. Miyazaki, O. Yoshie, et al., Therapeutic effect of CXCR3-expressing regulatory T cells on liver, lung and intestinal damages in a murine acute GVHD model, Gene Ther. 15 (2008) 171–182. https://doi.org/10.1038/sj.gt.3303051.

[38] R.L. Rabin, M.A. Alston, J.C. Sircus, B. Knollmann-Ritschel, C. Moratz, D. Ngo, et al., CXCR3 Is Induced Early on the Pathway of CD4 + T Cell Differentiation and Bridges Central and Peripheral Functions, J. Immunol. 171 (2003) 2812–2824. https://doi.org/10.4049/jimmunol.171.6.2812.

[39] S. Qin, J.B. Rottman, P. Myers, N. Kassam, M. Weinblatt, M. Loetscher, et al., The chemokine receptors CXCR3 and CCR5 mark subsets of T cells associated with certain inflammatory reactions., J. Clin. Invest. 101 (1998) 746–754. https://doi.org/10.1172/JCI1422.

[40] M. Loetscher, P. Loetscher, N. Brass, E. Meese, B. Moser, Lymphocyte-specific chemokine receptor CXCR3: regulation, chemokine binding and gene localization, Eur. J. Immunol. 28 (1998) 3696–3705. https://doi.org/10.1002/(SICI)1521-4141(199811)28:11<3696::AID-IMMU3696>3.0.CO;2-W.

[41] T. Nanki, K. Takada, Y. Komano, T. Morio, H. Kanegane, A. Nakajima, et al., Chemokine receptor expression and functional effects of chemokines on B cells: implication in the pathogenesis of rheumatoid arthritis, Arthritis Res. Ther. 11 (2009) R149. https://doi.org/10.1186/ar2823.

[42] M.Á. García-López, F. Sánchez-Madrid, J.M. Rodríguez-Frade, M. Mellado, A. Acevedo, M.I. García, et al., CXCR3 Chemokine Receptor Distribution in Normal and Inflamed Tissues: Expression on Activated Lymphocytes, Endothelial Cells, and Dendritic Cells, Lab. Investig. 81 (2001) 409–418. https://doi.org/10.1038/labinvest.3780248.

[43] J.D. Burke, H.A. Young, IFN-γ: A cytokine at the right time, is in the right place, Semin. Immunol. 43 (2019) 101280. https://doi.org/10.1016/j.smim.2019.05.002.

[44] B.D. Thompson, Y. Jin, K.H. Wu, R.A. Colvin, A.D. Luster, L. Birnbaumer, et al., Inhibition of Gαi2 Activation by Gαi3 in CXCR3-mediated Signaling, J. Biol. Chem. 282 (2007) 9547–9555. https://doi.org/10.1074/jbc.M610931200.

[45] M.E. Mikucki, D.T. Fisher, J. Matsuzaki, J.J. Skitzki, N.B. Gaulin, J.B. Muhitch, et al., Non-redundant requirement for CXCR3 signalling during tumoricidal T-cell trafficking across tumour vascular checkpoints, Nat. Commun. 6 (2015) 7458. https://doi.org/10.1038/ncomms8458.

[46] Reynders, Abboud, Baragli, Noman, Rogister, Niclou, et al., The Distinct Roles of CXCR3 Variants and Their Ligands in the Tumor Microenvironment, Cells. 8 (2019) 613. https://doi.org/10.3390/cells8060613.

[47] J.S. Smith, P. Alagesan, N.K. Desai, T.F. Pack, J.-H. Wu, A. Inoue, et al., C-X-C Motif Chemokine Receptor 3 Splice Variants Differentially Activate Beta-Arrestins to Regulate Downstream Signaling Pathways, Mol. Pharmacol. 92 (2017) 136–150. https://doi.org/10.1124/mol.117.108522.

[48] K. Van Raemdonck, P.E. Van den Steen, S. Liekens, J. Van Damme, S. Struyf, CXCR3 ligands in disease and therapy, Cytokine Growth Factor Rev. 26 (2015) 311–327. https://doi.org/10.1016/j.cytogfr.2014.11.009.

[49] A. Sauty, R.A. Colvin, L. Wagner, S. Rochat, F. Spertini, A.D. Luster, CXCR3 Internalization Following T Cell-Endothelial Cell Contact: Preferential Role of IFN-Inducible T Cell α Chemoattractant (CXCL11), J. Immunol. 167 (2001) 7084–7093. https://doi.org/10.4049/jimmunol.167.12.7084.

[50] M. Canals, D.J. Scholten, S. de Munnik, M.K.L. Han, M.J. Smit, R. Leurs, Ubiquitination of CXCR7 Controls Receptor Trafficking, PLoS One. 7 (2012) e34192. https://doi.org/10.1371/journal.pone.0034192.

[51] U. Panzer, O.M. Steinmetz, H.-J. Paust, C. Meyer-Schwesinger, A. Peters, J.-E. Turner, et al., Chemokine Receptor CXCR3 Mediates T Cell Recruitment and Tissue Injury in Nephrotoxic Nephritis in Mice, J. Am. Soc. Nephrol. 18 (2007) 2071–2084. https://doi.org/10.1681/ASN.2006111237.

[52] M. Loetscher, T. Geiser, T. O'Reilly, R. Zwahlen, M. Baggiolini, B. Moser, Cloning of a human seven-transmembrane domain receptor, LESTR, that is highly expressed in leukocytes., J. Biol. Chem. 269 (1994) 232–237. https://doi.org/10.1016/S0021-9258(17)42339-8.

[53] Y. Feng, C.C. Broder, P.E. Kennedy, E.A. Berger, HIV-1 Entry Cofactor: Functional cDNA Cloning of a Seven-Transmembrane, G Protein-Coupled Receptor, Science (80-. ). 272 (1996) 872–877. https://doi.org/10.1126/science.272.5263.872.

[54] E. Oberlin, A. Amara, F. Bachelerie, C. Bessia, J.L. Virelizier, F. Arenzana-Seisdedos, et al., The CXC chemokine, stromal cell derived factor 1 (SDF-1), is the ligand for LESTR/fusin and prevents infection by lymphocyte-tropic HIV-1 syncytium-inducing strains., Nature. 382 (1996) 833–835.

[55] A. Marchese, C. Raiborg, F. Santini, J.H. Keen, H. Stenmark, J.L. Benovic, The E3 Ubiquitin Ligase AIP4 Mediates Ubiquitination and Sorting of the G Protein-Coupled Receptor CXCR4, Dev. Cell. 5 (2003) 709–722. https://doi.org/10.1016/S1534-5807(03)00321-6.

[56] N.I. Tarasova, R.H. Stauber, C.J. Michejda, Spontaneous and Ligand-induced Trafficking of CXC-Chemokine Receptor 4, J. Biol. Chem. 273 (1998) 15883–15886. https://doi.org/10.1074/jbc.273.26.15883.

[57] J.M. Busillo, J.L. Benovic, Regulation of CXCR4 signaling, Biochim. Biophys. Acta - Biomembr. 1768 (2007) 952–963. https://doi.org/10.1016/j.bbamem.2006.11.002.

[58] S.F. Soriano, A. Serrano, P. Hernanz-Falcón, A.M. de Ana, M. Monterrubio, C. Martínez-A, et al., Chemokines integrate JAK/STAT and G-protein pathways during chemotaxis and calcium flux responses, Eur. J. Immunol. 33 (2003) 1328–1333. https://doi.org/10.1002/eji.200323897.

[59] A. Bajetto, S. Barbero, R. Bonavia, P. Piccioli, P. Pirani, T. Florio, et al., Stromal cell-derived factor-1α induces astrocyte proliferation through the activation of extracellular signal-regulated kinases 1/2 pathway, J. Neurochem. 77 (2001) 1226–1236. https://doi.org/10.1046/j.1471-4159.2001.00350.x.

[60] A.Z. Fernandis, A. Prasad, H. Band, R. Klösel, R.K. Ganju, Regulation of CXCR4-mediated chemotaxis and chemoinvasion of breast cancer cells, Oncogene. 23 (2004) 157–167. https://doi.org/10.1038/sj.onc.1206910.

[61] T. Florio, S. Casagrande, F. Diana, A. Bajetto, C. Porcile, G. Zona, et al., Chemokine Stromal Cell-Derived Factor 1α Induces Proliferation and Growth Hormone Release in GH4C1 Rat Pituitary Adenoma Cell Line through Multiple Intracellular Signals, Mol. Pharmacol. 69 (2006) 539–546. https://doi.org/10.1124/mol.105.015255.

[62] P. Kukreja, A.B. Abdel-Mageed, D. Mondal, K. Liu, K.C. Agrawal, Up-regulation of CXCR4 Expression in PC-3 Cells by Stromal-Derived Factor-1α (CXCL12) Increases Endothelial Adhesion and Transendothelial Migration: Role of MEK/ERK Signaling Pathway–Dependent NF-κB Activation, Cancer Res. 65 (2005) 9891–9898. https://doi.org/10.1158/0008-5472.CAN-05-1293.

[63] M. Kucia, K. Jankowski, R. Reca, M. Wysoczynski, L. Bandura, D.J. Allendorf, et al., CXCR4–SDF-1 signalling, locomotion, chemotaxis and adhesion, J. Mol. Histol. 35 (2003) 233–245. https://doi.org/10.1023/B:HIJO.0000032355.66152.b8.

[64] M. Liebick, S. Henze, V. Vogt, M. Oppermann, Functional consequences of chemically-induced β-arrestin binding to chemokine receptors CXCR4 and CCR5 in the absence of ligand stimulation, Cell. Signal. 38 (2017) 201–211. https://doi.org/10.1016/j.cellsig.2017.07.010.

[65] A.M. Fong, R.T. Premont, R.M. Richardson, Y.-R.A. Yu, R.J. Lefkowitz, D.D. Patel, Defective lymphocyte chemotaxis in β-arrestin2- and GRK6-deficient mice, Proc. Natl. Acad. Sci. 99 (2002) 7478–7483. https://doi.org/10.1073/pnas.112198299.

[66] A. Bagri, T. Gurney, X. He, Y.R. Zou, D.R. Littman, M. Tessier-Lavigne, et al., The chemokine SDF1 regulates migration of dentate granule cells, Development. 129 (2002) 4249–4260.

[67] F. Lazarini, T.N. Tham, P. Casanova, F. Arenzana-Seisdedos, M. Dubois-Dalcq, Role of the α-

Chemokine Stromal Cell-Derived Factor (SDF-1) in the Developing and Mature Central Nervous System, Glia. 42 (2003) 139–148. https://doi.org/10.1002/glia.10139.

[68] Y.-R. Zou, A.H. Kottmann, M. Kuroda, I. Taniuchi, D.R. Littman, Function of the chemokine receptor CXCR4 in haematopoiesis and in cerebellar development, Nature. 393 (1998) 595–599. https://doi.org/10.1038/31269.

[69] K. Tachibana, S. Hirota, H. Iizasa, H. Yoshida, K. Kawabata, Y. Kataoka, et al., The chemokine receptor CXCR4 is essential for vascularization of the gastrointestinal tract, Nature. 393 (1998) 591–594. https://doi.org/10.1038/31261.

[70] T. Nagasawa, S. Hirota, K. Tachibana, N. Takakura, S. Nishikawa, Y. Kitamura, et al., Defects of B-cell lymphopoiesis and bone-marrow myelopoiesis in mice lacking the CXC chemokine PBSF/SDF-1, Nature. 382 (1996) 635–638. https://doi.org/10.1038/382635a0.

[71] Q. Ma, D. Jones, P.R. Borghesani, R.A. Segal, T. Nagasawa, T. Kishimoto, et al., Impaired B-lymphopoiesis, myelopoiesis, and derailed cerebellar neuron migration in CXCR4- and SDF-1-deficient mice, Proc. Natl. Acad. Sci. 95 (1998) 9448–9453. https://doi.org/10.1073/pnas.95.16.9448.

[72] A. Aiuti, M. Tavian, A. Cipponi, F. Ficara, E. Zappone, J. Hoxie, et al., Expression of CXCR4, the receptor for stromal cell-derived factor-1 on fetal and adult human lymphohematopoietic progenitors, Eur. J. Immunol. 29 (1999) 1823–1831. https://doi.org/10.1002/(SICI)1521-4141(199906)29:06<1823::AID-IMMU1823>3.0.CO;2-B.

[73] K.E. Luker, M. Gupta, G.D. Luker, Imaging chemokine receptor dimerization with firefly luciferase complementation, FASEB J. 23 (2009) 823–834. https://doi.org/10.1096/fj.08-116749.

[74] F.M. Décaillot, M.A. Kazmi, Y. Lin, S. Ray-Saha, T.P. Sakmar, P. Sachdev, CXCR7/CXCR4 Heterodimer Constitutively Recruits β-Arrestin to Enhance Cell Migration, J. Biol. Chem. 286 (2011) 32188–32197. https://doi.org/10.1074/jbc.M111.277038.

[75] A. Levoye, K. Balabanian, F. Baleux, F. Bachelerie, B. Lagane, CXCR7 heterodimerizes with CXCR4 and regulates CXCL12-mediated G protein signaling, Blood. 113 (2009) 6085–6093. https://doi.org/10.1182/blood-2008-12-196618.

[76] C. Dambly-Chaudière, N. Cubedo, A. Ghysen, Control of cell migration in the development of the posterior lateral line: antagonistic interactions between the chemokine receptors CXCR4 and CXCR7/RDC1, BMC Dev. Biol. 7 (2007) 23. https://doi.org/10.1186/1471-213X-7-23.

[77] B. Boldajipour, H. Mahabaleshwar, E. Kardash, M. Reichman-Fried, H. Blaser, S. Minina, et al., Control of Chemokine-Guided Cell Migration by Ligand Sequestration, Cell. 132 (2008) 463–473. https://doi.org/10.1016/j.cell.2007.12.034.

[78] N. Cubedo, E. Cerdan, D. Sapede, M. Rossel, CXCR4 and CXCR7 cooperate during tangential migration of facial motoneurons, Mol. Cell. Neurosci. 40 (2009) 474–484. https://doi.org/10.1016/j.mcn.2009.01.003.

[79] J.A. Sánchez-Alcañiz, S. Haege, W. Mueller, R. Pla, F. Mackay, S. Schulz, et al., Cxcr7 Controls Neuronal Migration by Regulating Chemokine Responsiveness, Neuron. 69 (2011) 77–90. https://doi.org/10.1016/j.neuron.2010.12.006.

[80] J.L. Williams, J.R. Patel, B.P. Daniels, R.S. Klein, Targeting CXCR7/ACKR3 as a therapeutic strategy to promote remyelination in the adult central nervous system, J. Exp. Med. 211 (2014) 791–799. https://doi.org/10.1084/jem.20131224.

[81] G. Banisadr, J.R. Podojil, S.D. Miller, R.J. Miller, Pattern of CXCR7 Gene Expression in Mouse Brain Under Normal and Inflammatory Conditions, J. Neuroimmune Pharmacol. 11 (2016) 26–35. https://doi.org/10.1007/s11481-015-9616-y.

[82] L. Pouzol, A. Sassi, N. Baumlin, M. Tunis, D.S. Strasser, F. Lehembre, et al., CXCR7 Antagonism Reduces Acute Lung Injury Pathogenesis, Front. Pharmacol. 12 (2021). https://doi.org/10.3389/fphar.2021.748740.

[83] D.P. Bottaro, L.A. Liotta, Out of air is not out of action, Nature. 423 (2003) 593–595. https://doi.org/10.1038/423593a.

[84] Z. Cao, Q. Liao, M. Su, K. Huang, J. Jin, D. Cao, AKT and ERK dual inhibitors: The way forward?, Cancer Lett. 459 (2019) 30–40. https://doi.org/10.1016/j.canlet.2019.05.025.

[85] M. Yang, C. Zeng, P. Li, L. Qian, B. Ding, L. Huang, et al., Impact of CXCR4 and CXCR7 knockout by CRISPR/Cas9 on the function of triple-negative breast cancer cells, Onco. Targets. Ther. Volume 12 (2019) 3849–3858. https://doi.org/10.2147/OTT.S195661.

[86] Y. Luo, A.K. Azad, S. Karanika, S.P. Basourakos, X. Zuo, J. Wang, et al., Enzalutamide and CXCR7 inhibitor combination treatment suppresses cell growth and angiogenic signaling in castration-resistant prostate cancer models, Int. J. Cancer. 142 (2018) 2163–2174. https://doi.org/10.1002/ijc.31237.

[87] L. Hernandez, M.A.O. Magalhaes, S.J. Coniglio, J.S. Condeelis, J.E. Segall, Opposing roles of CXCR4 and CXCR7 in breast cancer metastasis, Breast Cancer Res. 13 (2011) R128. https://doi.org/10.1186/bcr3074.

[88] S. Rafiei, B. Gui, J. Wu, X.S. Liu, A.S. Kibel, L. Jia, Targeting the MIF/CXCR7/AKT Signaling Pathway in Castration-Resistant Prostate Cancer, Mol. Cancer Res. 17 (2019) 263–276. https://doi.org/10.1158/1541-7786.MCR-18-0412.

[89] I. del Molino del Barrio, G. Wilkins, A. Meeson, S. Ali, J. Kirby, Breast Cancer: An Examination of the Potential of ACKR3 to Modify the Response of CXCR4 to CXCL12, Int. J. Mol. Sci. 19 (2018) 3592. https://doi.org/10.3390/ijms19113592.

[90] N. Li, H. Xu, Y. Ou, Z. Feng, Q. Zhang, Q. Zhu, et al., LPS-induced CXCR7 expression promotes gastric Cancer proliferation and migration via the TLR4/MD-2 pathway, Diagn. Pathol. 14 (2019) 3. https://doi.org/10.1186/s13000-019-0780-x.

[91] S. Benhadjeba, L. Edjekouane, K. Sauvé, E. Carmona, A. Tremblay, Feedback control of the CXCR7/CXCL11 chemokine axis by estrogen receptor α in ovarian cancer, Mol. Oncol. 12 (2018) 1689–1705. https://doi.org/10.1002/1878-0261.12362.

[92] N. Zheng, W. Liu, J. Chen, B. Li, J. Liu, J. Wang, et al., CXCR7 is not obligatory for CXCL12-CXCR4-induced epithelial-mesenchymal transition in human ovarian cancer, Mol. Carcinog. 58 (2019) 144–155. https://doi.org/10.1002/mc.22916.

[93] H. Hao, S. Hu, H. Chen, D. Bu, L. Zhu, C. Xu, et al., Loss of Endothelial CXCR7 Impairs Vascular Homeostasis and Cardiac Remodeling After Myocardial Infarction, Circulation. 135 (2017) 1253–1264. https://doi.org/10.1161/CIRCULATIONAHA.116.023027.

[94] T. Murakami, K. Kawada, M. Iwamoto, M. Akagami, K. Hida, Y. Nakanishi, et al., The role of CXCR3 and CXCR4 in colorectal cancer metastasis, Int. J. Cancer. 132 (2013) 276–287. https://doi.org/10.1002/ijc.27670.

[95] M.A. Feitelson, A. Arzumanyan, R.J. Kulathinal, S.W. Blain, R.F. Holcombe, J. Mahajna, et al.,

Sustained proliferation in cancer: Mechanisms and novel therapeutic targets, Semin. Cancer Biol. 35 (2015) S25–S54. https://doi.org/10.1016/j.semcancer.2015.02.006.

[96] R. Tokunaga, W. Zhang, M. Naseem, A. Puccini, M.D. Berger, S. Soni, et al., CXCL9, CXCL10, CXCL11/CXCR3 axis for immune activation - a target for novel cancer therapy, Cancer Treat. Rev. 63 (2018) 40–47. https://doi.org/10.1016/j.ctrv.2017.11.007.CXCL9.

[97] S. Kumaravel, S. Singh, S. Roy, L. Venkatasamy, T.K. White, S. Sinha, et al., CXCL11-CXCR3 Axis Mediates Tumor Lymphatic Cross Talk and Inflammation-Induced Tumor, Promoting Pathways in Head and Neck Cancers, Am. J. Pathol. 190 (2020) 900–915. https://doi.org/10.1016/j.ajpath.2019.12.004.

[98] N. Nishida, H. Yano, T. Nishida, T. Kamura, M. Kojiro, Angiogenesis in cancer, Vasc. Health Risk Manag. 2 (2006) 213–219. https://doi.org/10.2147/vhrm.2006.2.3.213.

[99] D. Shen, X. Cao, Potential role of CXCR3 in proliferation and invasion of prostate cancer cells., Int. J. Clin. Exp. Pathol. 8 (2015) 8091–8. http://www.ncbi.nlm.nih.gov/pubmed/26339376.

[100] D. Datta, J.A. Flaxenburg, S. Laxmanan, C. Geehan, M. Grimm, A.M. Waaga-Gasser, et al., Ras-induced Modulation of CXCL10 and Its Receptor Splice Variant CXCR3-B in MDA-MB-435 and MCF-7 Cells: Relevance for the Development of Human Breast Cancer, Cancer Res. 66 (2006) 9509–9518. https://doi.org/10.1158/0008-5472.CAN-05-4345.

[101] A. Shi, H. Shi, L. Dong, S. Xu, M. Jia, X. Guo, et al., CXCR7 as a chemokine receptor for SDF-1 promotes gastric cancer progression via MAPK pathways, Scand. J. Gastroenterol. 52 (2017) 745–753. https://doi.org/10.1080/00365521.2017.1300681.

[102] M. Hao, J. Zheng, K. Hou, J. Wang, X. Chen, X. Lu, et al., Role of chemokine receptor CXCR7 in bladder cancer progression, Biochem. Pharmacol. 84 (2012) 204–214. https://doi.org/10.1016/j.bcp.2012.04.007.

[103] M. Wang, X. Yang, M. Wei, Z. Wang, The Role of CXCL12 Axis in Lung Metastasis of Colorectal Cancer, J. Cancer. 9 (2018) 3898–3903. https://doi.org/10.7150/jca.26383.

[104] R. Sever, J.S. Brugge, Signal Transduction in Cancer, Cold Spring Harb. Perspect. Med. 5 (2015) a006098–a006098. https://doi.org/10.1101/cshperspect.a006098.

[105] M. Esencay, Y. Sarfraz, D. Zagzag, CXCR7 is induced by hypoxia and mediates glioma cell migration towards SDF-1α, BMC Cancer. 13 (2013) 347. https://doi.org/10.1186/1471-2407-13-347.

[106] E. Schutyser, Y. Su, Y. Yu, M. Gouwy, S. Zaja-Milatovic, J. Van Damme, et al., Hypoxia enhances CXCR4 expression in human microvascular endothelial cells and human melanoma cells., Eur. Cytokine Netw. 18 (2007) 59–70. https://doi.org/10.1684/ecn.2007.0087.

[107] H. Liu, W. Xue, G. Ge, X. Luo, Y. Li, H. Xiang, et al., Hypoxic preconditioning advances CXCR4 and CXCR7 expression by activating HIF-1α in MSCs, Biochem. Biophys. Res. Commun. 401 (2010) 509–515. https://doi.org/10.1016/j.bbrc.2010.09.076.

[108] H. Zhong, A.M. De Marzo, E. Laughner, M. Lim, D.A. Hilton, D. Zagzag, et al., Overexpression of Hypoxia-inducible Factor 1α in Common Human Cancers and Their Metastases., Cancer Res. 59 (1999) 5830–5. http://www.ncbi.nlm.nih.gov/pubmed/10582706.

[109] Z. Miao, K.E. Luker, B.C. Summers, R. Berahovich, M.S. Bhojani, A. Rehemtulla, et al., CXCR7 (RDC1) promotes breast and lung tumor growth in vivo and is expressed on tumor-associated vasculature, Proc. Natl. Acad. Sci. 104 (2007) 15735–15740.

https://doi.org/10.1073/pnas.0610444104.

[110] M.P. Floranović, L.J. Veličković, Effect of CXCL12 and Its Receptors on Unpredictable Renal Cell Carcinoma, Clin. Genitourin. Cancer. (2019) 1–6. https://doi.org/10.1016/j.clgc.2019.11.004.

[111] T. Qian, Y. Liu, Y. Dong, L. Zhang, Y. Dong, Y. Sun, et al., CXCR7 regulates breast tumor metastasis and angiogenesis in vivo and in vitro, Mol. Med. Rep. 17 (2017) 3633–3639. https://doi.org/10.3892/mmr.2017.8286.

[112] P.J. Hensbergen, P.G.J.T.B. Wijnands, M.W.J. Schreurs, R.J. Scheper, R. Willemze, C.P. Tensen, The CXCR3 Targeting Chemokine CXCL11 Has Potent Antitumor Activity In Vivo Involving Attraction of CD8+ T Lymphocytes But Not Inhibition of Angiogenesis, J. Immunother. 28 (2005) 343–351. https://doi.org/10.1097/01.cji.0000165355.26795.27.

[113] C. Billottet, C. Quemener, A. Bikfalvi, CXCR3, a double-edged sword in tumor progression and angiogenesis, Biochim. Biophys. Acta - Rev. Cancer. 1836 (2013) 287–295. https://doi.org/10.1016/j.bbcan.2013.08.002.

[114] L. Lasagni, M. Francalanci, F. Annunziato, E. Lazzeri, S. Giannini, L. Cosmi, et al., An Alternatively Spliced Variant of CXCR3 Mediates the Inhibition of Endothelial Cell Growth Induced by IP-10, Mig, and I-TAC, and Acts as Functional Receptor for Platelet Factor 4, J. Exp. Med. 197 (2003) 1537–1549. https://doi.org/10.1084/jem.20021897.

[115] N. Clere, S. Renault, I. Corre, Endothelial-to-Mesenchymal Transition in Cancer, Front. Cell Dev. Biol. 8 (2020) 1–8. https://doi.org/10.3389/fcell.2020.00747.

[116] G. Zhu, H.H. Yan, Y. Pang, J. Jian, B.R. Achyut, X. Liang, et al., CXCR3 as a molecular target in breast cancer metastasis: inhibition of tumor cell migration and promotion of host anti-tumor immunity, Oncotarget. 6 (2015) 43408–43419. https://doi.org/10.18632/oncotarget.6125.

[117] B. Cambien, B.F. Karimdjee, P. Richard-Fiardo, H. Bziouech, R. Barthel, M.A. Millet, et al., Organ-specific inhibition of metastatic colon carcinoma by CXCR3 antagonism, Br. J. Cancer. 100 (2009) 1755–1764. https://doi.org/10.1038/sj.bjc.6605078.

[118] J.-S. Song, C.-C. Chang, C.-H. Wu, T.K. Dinh, J.-J. Jan, K.-W. Huang, et al., A highly selective and potent CXCR4 antagonist for hepatocellular carcinoma treatment, Proc. Natl. Acad. Sci. 118 (2021). https://doi.org/10.1073/pnas.2015433118.

[119] T. Chu, L.B.E. Shields, Y.P. Zhang, S.-Q. Feng, C.B. Shields, J. Cai, CXCL12/CXCR4/CXCR7 Chemokine Axis in the Central Nervous System: Therapeutic Targets for Remyelination in Demyelinating Diseases, Neurosci. 23 (2017) 627–648. https://doi.org/10.1177/1073858416685690.

[120] P. van der Meer, S.H. Goldberg, K.M. Fung, L.R. Sharer, F. González-Scarano, E. Lavi, Expression Pattern of CXCR3, CXCR4, and CCR3 Chemokine Receptors in the Developing Human Brain, J. Neuropathol. Exp. Neurol. 60 (2001) 25–32. https://doi.org/10.1093/jnen/60.1.25.

[121] M. Dziembowska, T.N. Tham, P. Lau, S. Vitry, F. Lazarini, M. Dubois-Dalcq, A Role for CXCR4 Signaling in Survival and Migration of Neural and Oligodendrocyte Precursors, Glia. 50 (2005) 258–269. https://doi.org/10.1002/glia.20170.

[122] J.R. Patel, E.E. McCandless, D. Dorsey, R.S. Klein, CXCR4 promotes differentiation of oligodendrocyte progenitors and remyelination, Proc. Natl. Acad. Sci. 107 (2010) 11062–11067. https://doi.org/10.1073/pnas.1006301107.

[123] B. Schönemeier, A. Kolodziej, S. Schulz, S. Jacobs, V. Hoellt, R. Stumm, Regional and cellular localization of the CXC112/SDF-1 chemokine receptor CXCR7 in the developing and adult rat brain, J. Comp. Neurol. 510 (2008) 207–220. https://doi.org/10.1002/cne.21780.

[124] L. Pouzol, Preclinical development of ACT-1004-1239, a potent and selective CXCR7/ACKR3 antagonist in multiple sclerosis treatment, Université Paris-Saclay, 2022.

[125] T.M. Calderon, E.A. Eugenin, L. Lopez, S.S. Kumar, J. Hesselgesser, C.S. Raine, et al., A role for CXCL12 (SDF-1α) in the pathogenesis of multiple sclerosis: Regulation of CXCL12 expression in astrocytes by soluble myelin basic protein, J. Neuroimmunol. 177 (2006) 27–39. https://doi.org/10.1016/j.jneuroim.2006.05.003.

[126] M. Krumbholz, D. Theil, S. Cepok, B. Hemmer, P. Kivisäkk, R.M. Ransohoff, et al., Chemokines in multiple sclerosis: CXCL12 and CXCL13 up-regulation is differentially linked to CNS immune cell recruitment, Brain. 129 (2006) 200–211. https://doi.org/10.1093/brain/awh680.

[127] N.M. Moll, M.B. Cossoy, E. Fisher, S.M. Staugaitis, B.H. Tucky, A.M. Rietsch, et al., Imaging Correlates of Leukocyte Accumulation and CXCR4/CXCL12 in Multiple Sclerosis, Arch. Neurol. 66 (2009) 44–53. https://doi.org/10.1001/archneurol.2008.512.

[128] J. Koenen, F. Bachelerie, K. Balabanian, G. Schlecht-Louf, C. Gallego, Atypical chemokine receptor 3 (ACKR3): A comprehensive overview of its expression and potential roles in the immune system, Mol. Pharmacol. 96 (2019) 809–818. https://doi.org/10.1124/mol.118.115329.

[129] E.E. McCandless, Q. Wang, B.M. Woerner, J.M. Harper, R.S. Klein, CXCL12 Limits Inflammation by Localizing Mononuclear Infiltrates to the Perivascular Space during Experimental Autoimmune Encephalomyelitis, J. Immunol. 177 (2006) 8053–8064. https://doi.org/10.4049/jimmunol.177.11.8053.

[130] E.E. McCandless, L. Piccio, B.M. Woerner, R.E. Schmidt, J.B. Rubin, A.H. Cross, et al., Pathological Expression of CXCL12 at the Blood-Brain Barrier Correlates with Severity of Multiple Sclerosis, Am. J. Pathol. 172 (2008) 799–808. https://doi.org/10.2353/ajpath.2008.070918.

[131] L. Cruz-Orengo, D.W. Holman, D. Dorsey, L. Zhou, P. Zhang, M. Wright, et al., CXCR7 influences leukocyte entry into the CNS parenchyma by controlling abluminal CXCL12 abundance during autoimmunity, J. Exp. Med. 208 (2011) 327–339. https://doi.org/10.1084/jem.20102010.

[132] G. Constantin, M. Majeed, C. Giagulli, L. Piccio, J.Y. Kim, E.C. Butcher, et al., Chemokines Trigger Immediate β2 Integrin Affinity and Mobility Changes, Immunity. 13 (2000) 759–769. https://doi.org/10.1016/S1074-7613(00)00074-1.

[133] T.N. Hartmann, V. Grabovsky, R. Pasvolsky, Z. Shulman, E.C. Buss, A. Spiegel, et al., A crosstalk between intracellular CXCR7 and CXCR4 involved in rapid CXCL12-triggered integrin activation but not in chemokine-triggered motility of human T lymphocytes and CD34 + cells, J. Leukoc. Biol. 84 (2008) 1130–1140. https://doi.org/10.1189/jlb.0208088.

[134] T. Goldmann, M. Prinz, Role of Microglia in CNS Autoimmunity, Clin. Dev. Immunol. 2013 (2013) 1–8. https://doi.org/10.1155/2013/208093.

[135] M. Veenstra, D.W. Williams, T.M. Calderon, K. Anastos, S. Morgello, J.W. Berman, Frontline Science: CXCR7 mediates CD14 + CD16 + monocyte transmigration across the blood brain barrier: a potential therapeutic target for NeuroAIDS, J. Leukoc. Biol. 102 (2017) 1173–1185.

https://doi.org/10.1189/jlb.3HI0517-167R.

[136] S. Man, B. Tucky, A. Cotleur, J. Drazba, Y. Takeshita, R.M. Ransohoff, CXCL12-Induced Monocyte-Endothelial Interactions Promote Lymphocyte Transmigration Across an in Vitro Blood-Brain Barrier, Sci. Transl. Med. 4 (2012) 1476–1488. https://doi.org/10.1126/scitranslmed.3003197.

[137] J. Bao, J. Zhu, S. Luo, Y. Cheng, S. Zhou, CXCR7 suppression modulates microglial chemotaxis to ameliorate experimentally-induced autoimmune encephalomyelitis, Biochem. Biophys. Res. Commun. 469 (2016) 1–7. https://doi.org/10.1016/j.bbrc.2015.11.059.

[138] M.A. Lopes Pinheiro, G. Kooij, M.R. Mizee, A. Kamermans, G. Enzmann, R. Lyck, et al., Immune cell trafficking across the barriers of the central nervous system in multiple sclerosis and stroke, Biochim. Biophys. Acta - Mol. Basis Dis. 1862 (2016) 461–471. https://doi.org/10.1016/j.bbadis.2015.10.018.

[139] M. Puchert, F. Pelkner, G. Stein, D.N. Angelov, J. Boltze, D.-C. Wagner, et al., Astrocytic expression of the CXCL12 receptor, CXCR7/ACKR3 is a hallmark of the diseased, but not developing CNS, Mol. Cell. Neurosci. 85 (2017) 105–118. https://doi.org/10.1016/j.mcn.2017.09.001.

[140] J.L. Williams, S. Manivasagam, B.C. Smith, J. Sim, L.L. Vollmer, B.P. Daniels, et al., Astrocyte-T cell crosstalk regulates region-specific neuroinflammation, Glia. 68 (2020) 1361–1374. https://doi.org/10.1002/glia.23783.

[141] K.S. Carbajal, C. Schaumburg, R. Strieter, J. Kane, T.E. Lane, Migration of engrafted neural stem cells is mediated by CXCL12 signaling through CXCR4 in a viral model of multiple sclerosis, Proc. Natl. Acad. Sci. 107 (2010) 11068–11073. https://doi.org/10.1073/pnas.1006375107.

[142] R. Zilkha-Falb, N. Kaushansky, N. Kawakami, A. Ben-Nun, Post-CNS-inflammation expression of CXCL12 promotes the endogenous myelin/neuronal repair capacity following spontaneous recovery from multiple sclerosis-like disease, J. Neuroinflammation. 13 (2016) 7. https://doi.org/10.1186/s12974-015-0468-4.

[143] F. Mei, S.R. Mayoral, H. Nobuta, F. Wang, C. Desponts, D.S. Lorrain, et al., Identification of the Kappa-Opioid Receptor as a Therapeutic Target for Oligodendrocyte Remyelination, J. Neurosci. 36 (2016) 7925–7935. https://doi.org/10.1523/JNEUROSCI.1493-16.2016.

[144] L.A. Osso, K.A. Rankin, J.R. Chan, Experience-dependent myelination following stress is mediated by the neuropeptide dynorphin, Neuron. 109 (2021) 3619-3632.e5. https://doi.org/10.1016/j.neuron.2021.08.015.

[145] M. Meyrath, M. Szpakowska, J. Zeiner, L. Massotte, M.P. Merz, T. Benkel, et al., The atypical chemokine receptor ACKR3/CXCR7 is a broad-spectrum scavenger for opioid peptides, Nat. Commun. 11 (2020) 3033. https://doi.org/10.1038/s41467-020-16664-0.

[146] L. Pouzol, N. Baumlin, A. Sassi, M. Tunis, J. Marrie, E. Vezzali, et al., ACT-1004-1239, a first-in-class CXCR7 antagonist with both immunomodulatory and promyelinating effects for the treatment of inflammatory demyelinating diseases, FASEB J. 35 (2021) 1–17. https://doi.org/10.1096/fj.202002465R.

[147] A. Szczuciński, J. Losy, CCL5, CXCL10 and CXCL11 Chemokines in Patients with Active and Stable Relapsing-Remitting Multiple Sclerosis, Neuroimmunomodulation. 18 (2011) 67–72. https://doi.org/10.1159/000317394.

[148] J. Mellergård, M. Edström, M. Vrethem, J. Ernerudh, C. Dahle, Natalizumab treatment in multiple sclerosis: marked decline of chemokines and cytokines in cerebrospinal fluid, Mult. Scler. J. 16 (2010) 208–217. https://doi.org/10.1177/1352458509355068.

[149] X.-H. Guan, Q.-C. Fu, D. Shi, H.-L. Bu, Z.-P. Song, B.-R. Xiong, et al., Activation of spinal chemokine receptor CXCR3 mediates bone cancer pain through an Akt-ERK crosstalk pathway in rats, Exp. Neurol. 263 (2015) 39–49. https://doi.org/10.1016/j.expneurol.2014.09.019.

[150] E. Pradelli, B. Karimdjee-Soilihi, J. Michiels, J.-E. Ricci, M. Millet, F. Vandenbos, et al., Antagonism of chemokine receptor CXCR3 inhibits osteosarcoma metastasis to lungs, Int. J. Cancer. 125 (2009) 2586–2594. https://doi.org/10.1002/ijc.24665.

[151] T.C. Walser, S. Rifat, X. Ma, N. Kundu, C. Ward, O. Goloubeva, et al., Antagonism of CXCR3 Inhibits Lung Metastasis in a Murine Model of Metastatic Breast Cancer, Cancer Res. 66 (2006) 7701–7707. https://doi.org/10.1158/0008-5472.CAN-06-0709.

[152] S.P. Andrews, R.J. Cox, Small Molecule CXCR3 Antagonists, J. Med. Chem. 59 (2016) 2894–2917. https://doi.org/10.1021/acs.jmedchem.5b01337.

[153] Jyant Technologies Inc - Pipeline, (n.d.). https://jyanttech.com/index.php?/pipeline (accessed May 9, 2022).

[154] M. Abraham, H. Wald, D. Vaizel-Ohayon, V. Grabovsky, Z. Oren, A. Karni, et al., Development of Novel Promiscuous Anti-Chemokine Peptibodies for Treating Autoimmunity and Inflammation, Front. Immunol. 8 (2017) 1–15. https://doi.org/10.3389/fimmu.2017.01432.

[155] G.L. Uy, M.P. Rettig, I.H. Motabi, K. McFarland, K.M. Trinkaus, L.M. Hladnik, et al., A phase 1/2 study of chemosensitization with the CXCR4 antagonist plerixafor in relapsed or refractory acute myeloid leukemia, Blood. 119 (2012) 3917–3924. https://doi.org/10.1182/blood-2011-10-383406.

[156] G.M. Keating, Plerixafor - A Review of its Use in Stem-Cell Mobilization in Patients with Lymphoma or Multiple Myeloma, Drugs. 71 (2011) 1623–1647. https://doi.org/10.2165/11206040-000000000-00000.

[157] S. Chien, L.E. Beyerle, B.L. Wood, E.H. Estey, F.R. Appelbaum, P.M. Cardarelli, et al., Mobilization Of Blasts and Leukemia Stem Cells by Anti-CXCR4 Antibody BMS-936564 (MDX 1338) in Patients With Relapsed/Refractory Acute Myeloid Leukemia, Blood. 122 (2013) 3882–3882. https://doi.org/10.1182/blood.V122.21.3882.3882.

[158] I.M. Ghobrial, C.-J. Liu, R.A. Redd, R.P. Perez, R. Baz, O. Zavidij, et al., A Phase Ib/II Trial of the First-in-Class Anti-CXCR4 Antibody Ulocuplumab in Combination with Lenalidomide or Bortezomib Plus Dexamethasone in Relapsed Multiple Myeloma, Clin. Cancer Res. 26 (2020) 344–353. https://doi.org/10.1158/1078-0432.CCR-19-0647.

[159] M.D. Galsky, N.J. Vogelzang, P. Conkling, E. Raddad, J. Polzer, S. Roberson, et al., A Phase I Trial of LY2510924, a CXCR4 Peptide Antagonist, in Patients with Advanced Cancer, Clin. Cancer Res. 20 (2014) 3581–3588. https://doi.org/10.1158/1078-0432.CCR-13-2686.

[160] Z.D. Crees, K. Stockerl-Goldstein, A. Vainstein, H. Chen, J.F. DiPersio, GENESIS: Phase III trial evaluating BL-8040 + G-CSF to mobilize hematopoietic cells for autologous transplant in myeloma, Futur. Oncol. 15 (2019) 3555–3563. https://doi.org/10.2217/fon-2019-0380.

[161] A. Peled, M. Abraham, I. Avivi, J.M. Rowe, K. Beider, H. Wald, et al., The High-Affinity CXCR4 Antagonist BKT140 Is Safe and Induces a Robust Mobilization of Human CD34+ Cells in Patients with Multiple Myeloma, Clin. Cancer Res. 20 (2014) 469–479.

https://doi.org/10.1158/1078-0432.CCR-13-1302.

[162] M. Abraham, Y. Pereg, B. Bulvik, S. Klein, I. Mishalian, H. Wald, et al., Single Dose of the CXCR4 Antagonist BL-8040 Induces Rapid Mobilization for the Collection of Human CD34+ Cells in Healthy Volunteers, Clin. Cancer Res. 23 (2017) 6790–6801. https://doi.org/10.1158/1078-0432.CCR-16-2919.

[163] S. Pernas, M. Martin, P.A. Kaufman, M. Gil-Martin, P. Gomez Pardo, S. Lopez-Tarruella, et al., Balixafortide plus eribulin in HER2-negative metastatic breast cancer: a phase 1, single-arm, dose-escalation trial, Lancet Oncol. 19 (2018) 812–824. https://doi.org/10.1016/S1470-2045(18)30147-5.

[164] G. Setia, N. Hagog, B. Jalilizeinali, S. Funkhouser, L. Pierzchanowski, F. Lan, et al., A Phase II, Open-Label Pilot Study to Evaluate the Hematopoietic Stem Cell Mobilization of TG-0054 Combined with G-CSF in 12 Patients with Multiple Myeloma, Non-Hodgkin Lymphoma or Hodgkin Lymphoma - an Interim Analysis, Blood. 126 (2015) 515. https://doi.org/10.1182/blood.V126.23.515.515.

[165] M. Steurer, M. Montillo, L. Scarfò, F.R. Mauro, J. Andel, S. Wildner, et al., Olaptesed pegol (NOX-A12) with bendamustine and rituximab: A phase IIa study in patients with relapsed/refractory chronic lymphocytic leukemia, Haematologica. 104 (2019) 2053–2060. https://doi.org/10.3324/haematol.2018.205930.

[166] M. Suarez-Carmona, A. Williams, J. Schreiber, N. Hohmann, U. Pruefer, J. Krauss, et al., Combined inhibition of CXCL12 and PD-1 in MSS colorectal and pancreatic cancer: modulation of the microenvironment and clinical effects, J. Immunother. Cancer. 9 (2021) e002505. https://doi.org/10.1136/jitc-2021-002505.

[167] L.A. Andritsos, J.C. Byrd, P. Cheverton, J. Wu, M. Sivina, T.J. Kipps, et al., A multicenter phase 1 study of plerixafor and rituximab in patients with chronic lymphocytic leukemia, Leuk. Lymphoma. 60 (2019) 3461–3469. https://doi.org/10.1080/10428194.2019.1643463.

[168] J.D. Hainsworth, J.A. Reeves, J.R. Mace, E.J. Crane, O. Hamid, J.R. Stille, et al., A Randomized, Open-Label Phase 2 Study of the CXCR4 Inhibitor LY2510924 in Combination with Sunitinib Versus Sunitinib Alone in Patients with Metastatic Renal Cell Carcinoma (RCC), Target. Oncol. 11 (2016) 643–653. https://doi.org/10.1007/s11523-016-0434-9.

[169] J.F. DiPersio, I.N. Micallef, P.J. Stiff, B.J. Bolwell, R.T. Maziarz, E. Jacobsen, et al., Phase III Prospective Randomized Double-Blind Placebo-Controlled Trial of Plerixafor Plus Granulocyte Colony-Stimulating Factor Compared With Placebo Plus Granulocyte Colony-Stimulating Factor for Autologous Stem-Cell Mobilization and Transplantation for , J. Clin. Oncol. 27 (2009) 4767–4773. https://doi.org/10.1200/JCO.2008.20.7209.

[170] J.F. DiPersio, E.A. Stadtmauer, A. Nademanee, I.N.M. Micallef, P.J. Stiff, J.L. Kaufman, et al., Plerixafor and G-CSF versus placebo and G-CSF to mobilize hematopoietic stem cells for autologous stem cell transplantation in patients with multiple myeloma, Blood. 113 (2009) 5720–5726. https://doi.org/10.1182/blood-2008-08-174946.

[171] M.H. Son, E.S. Kang, D.H. Kim, S.H. Lee, K.H. Yoo, K.W. Sung, et al., Efficacy and Toxicity of Plerixafor for Peripheral Blood Stem Cell Mobilization in Children With High-Risk Neuroblastoma, Pediatr. Blood Cancer. 60 (2013) E57–E59. https://doi.org/10.1002/pbc.24506.

[172] J. Sevilla, E. Schiavello, L. Madero, M. Pardeo, E. Guggiari, M. Baragaño, et al., Priming of Hematopoietic Progenitor Cells by Plerixafor and Filgrastim in Children With Previous Failure of Mobilization With Chemotherapy and/or Cytokine Treatment, J. Pediatr. Hematol. Oncol. 34

(2012) 146–150. https://doi.org/10.1097/MPH.0b013e31821c2cb8.

[173] S. Shimizu, M. Brown, R. Sengupta, M.E. Penfold, O. Meucci, CXCR7 Protein Expression in Human Adult Brain and Differentiated Neurons, PLoS One. 6 (2011) e20680. https://doi.org/10.1371/journal.pone.0020680.

[174] N. Lounsbury, Advances in CXCR7 Modulators, Pharmaceuticals. 13 (2020) 33. https://doi.org/10.3390/ph13020033.

[175] B.A. Zabel, Y. Wang, S. Lewén, R.D. Berahovich, M.E.T. Penfold, P. Zhang, et al., Elucidation of CXCR7-Mediated Signaling Events and Inhibition of CXCR4-Mediated Tumor Cell Transendothelial Migration by CXCR7 Ligands, J. Immunol. 183 (2009) 3204–3211. https://doi.org/10.4049/jimmunol.0900269.

[176] E. Menhaji-Klotz, J. Ward, J.A. Brown, P.M. Loria, C. Tan, K.D. Hesp, et al., Discovery of Diphenylacetamides as CXCR7 Inhibitors with Novel β-Arrestin Antagonist Activity, ACS Med. Chem. Lett. (2020) acsmedchemlett.0c00163. https://doi.org/10.1021/acsmedchemlett.0c00163.

[177] S.-B. Peng, X. Zhang, D. Paul, L.M. Kays, W. Gough, J. Stewart, et al., Identification of LY2510924, a Novel Cyclic Peptide CXCR4 Antagonist That Exhibits Antitumor Activities in Solid Tumor and Breast Cancer Metastatic Models, Mol. Cancer Ther. 14 (2015) 480–490. https://doi.org/10.1158/1535-7163.MCT-14-0850.

[178] D. Fahham, I.D. Weiss, M. Abraham, K. Beider, W. Hanna, Z. Shlomai, et al., In vitro and in vivo therapeutic efficacy of CXCR4 antagonist BKT140 against human non–small cell lung cancer, J. Thorac. Cardiovasc. Surg. 144 (2012) 1167-1175.e1. https://doi.org/10.1016/j.jtcvs.2012.07.031.

[179] K. Beider, E. Ribakovsky, M. Abraham, H. Wald, L. Weiss, E. Rosenberg, et al., Targeting the CD20 and CXCR4 Pathways in Non-Hodgkin Lymphoma with Rituximab and High-Affinity CXCR4 Antagonist BKT140, Clin. Cancer Res. 19 (2013) 3495–3507. https://doi.org/10.1158/1078-0432.CCR-12-3015.

[180] K. Beider, M. Darash-Yahana, O. Blaier, M. Koren-Michowitz, M. Abraham, H. Wald, et al., Combination of Imatinib with CXCR4 Antagonist BKT140 Overcomes the Protective Effect of Stroma and Targets CML In Vitro and In Vivo, Mol. Cancer Ther. 13 (2014) 1155–1169. https://doi.org/10.1158/1535-7163.MCT-13-0410.

[181] H. Ludwig, K. Weisel, M.T. Petrucci, X. Leleu, A.M. Cafro, L. Garderet, et al., Olaptesed pegol, an anti-CXCL12/SDF-1 Spiegelmer, alone and with bortezomib–dexamethasone in relapsed/refractory multiple myeloma: a Phase IIa Study, Leukemia. 31 (2017) 997–1000. https://doi.org/10.1038/leu.2017.5.

[182] N. Halama, U. Pruefer, A. Frömming, D. Beyer, D. Eulberg, J.U.B. Jungnelius, et al., Experience with CXCL12 inhibitor NOX-A12 plus pembrolizumab in patients with microsatellite-stable, metastatic colorectal or pancreatic cancer., J. Clin. Oncol. 37 (2019) e14143–e14143. https://doi.org/10.1200/JCO.2019.37.15_suppl.e14143.

[183] M.J. Walters, K. Ebsworth, R.D. Berahovich, M.E.T. Penfold, S.-C. Liu, R. Al Omran, et al., Inhibition of CXCR7 extends survival following irradiation of brain tumours in mice and rats, Br. J. Cancer. 110 (2014) 1179–1188. https://doi.org/10.1038/bjc.2013.830.

[184] K.-C. Ngamsri, A. Müller, H. Bösmüller, J. Gamper-Tsigaras, J. Reutershan, F.M. Konrad, The Pivotal Role of CXCR7 in Stabilization of the Pulmonary Epithelial Barrier in Acute Pulmonary Inflammation, J. Immunol. 198 (2017) 2403–2413. https://doi.org/10.4049/jimmunol.1601682.

[185] N. Salazar, J.C. Carlson, K. Huang, Y. Zheng, C. Oderup, J. Gross, et al., A Chimeric Antibody against ACKR3/CXCR7 in Combination with TMZ Activates Immune Responses and Extends Survival in Mouse GBM Models, Mol. Ther. 26 (2018) 1354–1365. https://doi.org/10.1016/j.ymthe.2018.02.030.

[186] MOZOBIL® (Plerixafor Injection) [product monograph]. Sanofi-aventis Canada Inc., Revised January 2019, (n.d.) 1–55.

[187] S. Richard-Bildstein, H. Aissaoui, J. Pothier, G. Schäfer, C. Gnerre, E. Lindenberg, et al., Discovery of the Potent, Selective, Orally Available CXCR7 Antagonist ACT-1004-1239, J. Med. Chem. 63 (2020) 15864–15882. https://doi.org/10.1021/acs.jmedchem.0c01588.

[188] C. Huynh, S. Seeland, J. Segrestaa, C. Gnerre, J. Hogeback, H.E. Meyer zu Schwabedissen, et al., Absorption, Metabolism, and Excretion of ACT-1004-1239, a First-In-Class CXCR7 Antagonist: In Vitro, Preclinical, and Clinical Data, Front. Pharmacol. 13 (2022) 1–15. https://doi.org/10.3389/fphar.2022.812065.

[189] L. Pouzol, M. Tunis, N. Baumlin, A. Sassi, J. Marrie, E. Vezzali, et al., CXCR7 antagonism with ACT-1004-1239 reduces neuroinflammation and accelerates remyelination in murine demyelinating models (2236), Neurology. 96 (2021) 2236. http://n.neurology.org/content/96/15_Supplement/2236.abstract.

[190] United States Department of Health and Human Services Food and Drug Administration Center for Drug Evaluation and Research, In Vitro Drug Interaction Studies - Cytochrome P450 Enzyme and Transporter Mediated Drug Interactions, Guidance for Industry, (2020). https://www.fda.gov/media/134582/download (accessed September 1, 2021).

[191] European Medicines Agency, Guideline on the investigation of drug interactions, (2013). https://doi.org/10.1093/deafed/ens058.

[192] A. Tornio, A.M. Filppula, M. Niemi, J.T. Backman, Clinical Studies on Drug–Drug Interactions Involving Metabolism and Transport: Methodology, Pitfalls, and Interpretation, Clin. Pharmacol. Ther. 105 (2019) 1345–1361. https://doi.org/10.1002/cpt.1435.

[193] United States Department of Health and Human Services Food and Drug Administration Center for Drug Evaluation and Research, Clinical Drug Interaction Studies — Cytochrome P450 Enzyme- and Transporter-Mediated Drug Interactions, (2020). https://www.fda.gov/regulatory-information/search-fda-guidance-documents/clinical-drug-interaction-studies-cytochrome-p450-enzyme-and-transporter-mediated-drug-interactions (accessed October 5, 2022).

[194] United States Department of Health and Human Services Food and Drug Administration Center for Drug Evaluation and Research, Drug Development and Drug Interactions | Table of Substrates, Inhibitors and Inducers, (2022). https://www.fda.gov/drugs/drug-interactions-labeling/drug-development-and-drug-interactions-table-substrates-inhibitors-and-inducers#table2-2 (accessed October 5, 2022).

[195] European Medicines Agency Evaluation of Medicines for Human Use, European Medicines Agency recommends suspension of marketing authorisations for oral ketoconazole, (2013). https://www.ema.europa.eu/en/news/european-medicines-agency-recommends-suspension-marketing-authorisations-oral-ketoconazole (accessed October 5, 2022).

[196] United States Department of Health and Human Services Food and Drug Administration Center for Drug Evaluation and Research, FDA Drug Safety Communication: FDA limits usage of Nizoral (ketoconazole) oral tablets due to potentially fatal liver injury and risk of drug interactions and adrenal gland problems, (2017). https://www.fda.gov/drugs/drug-safety-and-

availability/fda-drug-safety-communication-fda-limits-usage-nizoral-ketoconazole-oral-tablets-due-potentially (accessed October 5, 2022).

[197] BIAXIN®, clarithromycin USP, (n.d.). https://www.accessdata.fda.gov/drugsatfda_docs/label/2009/050662s042,050698s024,050775s013lbl.pdf (accessed October 5, 2022).

[198] Y. Chen, T.D. Cabalu, E. Callegari, H. Einolf, L. Liu, N. Parrott, et al., Recommendations for the Design of Clinical Drug–Drug Interaction Studies With Itraconazole Using a Mechanistic Physiologically-Based Pharmacokinetic Model, CPT Pharmacometrics Syst. Pharmacol. 8 (2019) 685–695. https://doi.org/10.1002/psp4.12449.

[199] L. Liu, A. Bello, M.J. Dresser, D. Heald, S.F. Komjathy, E. O'Mara, et al., Best practices for the use of itraconazole as a replacement for ketoconazole in drug-drug interaction studies, J. Clin. Pharmacol. 56 (2016) 143–151. https://doi.org/10.1002/jcph.562.

[200] SPORANOX® (itraconazole) Capsules, (n.d.). https://www.janssenlabels.com/package-insert/product-monograph/prescribing-information/SPORANOX-Capsules-pi.pdf (accessed October 5, 2022).

[201] J.T. Backman, K.T. Kivistö, K.T. Olkkola, P.J. Neuvonen, The area under the plasma concentration-time curve for oral midazolam is 400-fold larger during treatment with itraconazole than with rifampicin, Eur. J. Clin. Pharmacol. 54 (1998) 53–58. https://doi.org/10.1007/s002280050420.

[202] K.T. Olkkola, J.T. Backman, P.J. Neuvonen, Midazolam should be avoided in patients receiving the systemic antimycotics ketoconazole or itraconazole, Clin. Pharmacol. Ther. 55 (1994) 481–485. https://doi.org/10.1038/clpt.1994.60.

[203] I. Templeton, C.-C. Peng, K.E. Thummel, C. Davis, K.L. Kunze, N. Isoherranen, Accurate Prediction of Dose-Dependent CYP3A4 Inhibition by Itraconazole and Its Metabolites From In Vitro Inhibition Data, Clin. Pharmacol. Ther. 88 (2010) 499–505. https://doi.org/10.1038/clpt.2010.119.

[204] I.E. Templeton, K.E. Thummel, E.D. Kharasch, K.L. Kunze, C. Hoffer, W.L. Nelson, et al., Contribution of Itraconazole Metabolites to Inhibition of CYP3A4 In Vivo, Clin. Pharmacol. Ther. 83 (2008) 77–85. https://doi.org/10.1038/sj.clpt.6100230.

[205] C. Huynh, A. Henrich, D.S. Strasser, M. Boof, M. Al-Ibrahim, H.E. Meyer zu Schwabedissen, et al., A Multipurpose First-in-Human Study With the Novel CXCR7 Antagonist ACT-1004-1239 Using CXCL12 Plasma Concentrations as Target Engagement Biomarker, Clin. Pharmacol. Ther. 109 (2021) 1648–1659. https://doi.org/10.1002/cpt.2154.

[206] M. Hoch, F. Huth, M. Sato, T. Sengupta, M. Quinlan, S. Dodd, et al., Pharmacokinetics of asciminib in the presence of CYP3A or P-gp inhibitors, CYP3A inducers, and acid-reducing agents, Clin. Transl. Sci. 15 (2022) 1698–1712. https://doi.org/10.1111/cts.13285.

[207] N. Al-Dubaili, N. Saleh, Sequestration Effect on the Open-Cyclic Switchable Property of Warfarin Induced by Cyclodextrin: Time-Resolved Fluorescence Study, Molecules. 22 (2017) 1326. https://doi.org/10.3390/molecules22081326.

[208] M.R. Durk, N.S. Jones, J. Liu, K. Nagapudi, C. Mao, E.G. Plise, et al., Understanding the Effect of Hydroxypropyl-β-Cyclodextrin on Fenebrutinib Absorption in an Itraconazole–Fenebrutinib Drug–Drug Interaction Study, Clin. Pharmacol. Ther. 108 (2020) 1224–1232. https://doi.org/10.1002/cpt.1943.

[209] European Medicines Agency Evaluation of Medicines for Human Use, Cyclodextrins used as excipients, (2017). https://www.ema.europa.eu/en/documents/scientific-guideline/questions-answers-cyclodextrins-used-excipients-medicinal-products-human-use_en.pdf (accessed October 7, 2022).

[210] A. Czyrski, M. Resztak, P. Świderski, J. Brylak, F.K. Główka, The overview on the pharmacokinetic and pharmacodynamic interactions of triazoles, Pharmaceutics. 13 (2021) 1–27. https://doi.org/10.3390/pharmaceutics13111961.

[211] C. Huynh, J.M. Brussee, L. Pouzol, M. Fonseca, H.E. Meyer zu Schwabedissen, J. Dingemanse, et al., Target engagement of the first-in-class CXCR7 antagonist ACT-1004-1239 following multiple-dose administration in mice and humans, Biomed. Pharmacother. 144 (2021) 112363. https://doi.org/10.1016/j.biopha.2021.112363.

[212] S.D. Patterson, B. Jones, Bioequivalence and Statistics in Clinical Pharmacology., 2nd ed., Taylor and Francis Group LLC, 2006.

[213] United States Department of Health and Human Services Food and Drug Administration Center for Drug Evaluation and Research, Assessing the Effects of Food on Drugs in INDs and NDAs — Clinical Pharmacology Considerations, Guidance for Industry, (2022). https://www.fda.gov/regulatory-information/search-fda-guidance-documents/assessing-effects-food-drugs-inds-and-ndas-clinical-pharmacology-considerations (accessed December 19, 2022).

[214] United States Department of Health and Human Services Food and Drug Administration Center for Drug Evaluation and Research, Bioavailability Studies Submitted in NDAs or INDs — General Considerations, Guidance for Industry, (2022). https://www.fda.gov/regulatory-information/search-fda-guidance-documents/bioavailability-studies-submitted-ndas-or-inds-general-considerations.

[215] M. Ufer, P.E. Juif, M.L. Boof, C. Muehlan, J. Dingemanse, Metabolite profiling in early clinical drug development: current status and future prospects, Expert Opin. Drug Metab. Toxicol. 13 (2017) 803–806. https://doi.org/10.1080/17425255.2017.1351944.

[216] D.K. Spracklin, D. Chen, A.J. Bergman, E. Callegari, R.S. Obach, Mini-Review: Comprehensive Drug Disposition Knowledge Generated in the Modern Human Radiolabeled ADME Study, CPT Pharmacometrics Syst. Pharmacol. 9 (2020) 428–434. https://doi.org/10.1002/psp4.12540.

[217] United States Department of Health and Human Services Food and Drug Administration Center for Drug Evaluation and Research, Safety Testing of Drug Metabolites, Guidance for Industry, Revision 2 (2020). https://www.fda.gov/media/72279/download (accessed August 16, 2021).

[218] A. Ramamoorthy, G. Bende, E.C.Y. Chow, H. Dimova, N. Hartman, D. Jean, et al., Human radiolabeled mass balance studies supporting the FDA approval of new drugs, Clin. Transl. Sci. 15 (2022) 2567–2575. https://doi.org/10.1111/cts.13403.

[219] D. Sun, W. Gao, H. Hu, S. Zhou, Why 90% of clinical drug development fails and how to improve it?, Acta Pharm. Sin. B. 12 (2022) 3049–3062. https://doi.org/10.1016/j.apsb.2022.02.002.

[220] B. Darpo, C. Garnett, J. Keirns, N. Stockbridge, Implications of the IQ-CSRC Prospective Study: Time to Revise ICH E14, Drug Saf. 38 (2015) 773–780. https://doi.org/10.1007/s40264-015-0325-5.

[221] M.F. Baird, S.M. Graham, J.S. Baker, G.F. Bickerstaff, Creatine-Kinase- and Exercise-Related Muscle Damage Implications for Muscle Performance and Recovery, J. Nutr. Metab. 2012

(2012) 1–13. https://doi.org/10.1155/2012/960363.

[222] P. Hingorani, D.R. Karnad, M. Natekar, S. Kothari, D. Narula, Baseline and new-onset morphologic ECG abnormalities in healthy volunteers in phase I studies receiving placebo: Changes over a 6-week follow-up period, J. Clin. Pharmacol. 54 (2014) 776–784. https://doi.org/10.1002/jcph.282.

[223] United States Department of Health and Human Services Food and Drug Administration Center for Drug Evaluation and Research, Pharmacokinetics in Patients with Impaired Hepatic Function: Study Design, Data Analysis, and Impact on Dosing and Labeling, Guidance for Industry, (2003). https://www.fda.gov/media/71311/download (accessed August 25, 2021).

[224] K. Kobayashi, Y. Abe, A. Kawai, T. Furihata, T. Endo, H. Takeda, Pharmacokinetic Drug Interactions of an Orally Available TRH Analog (Rovatirelin) With a CYP3A4/5 and P-Glycoprotein Inhibitor (Itraconazole), J. Clin. Pharmacol. 60 (2020) 1314–1323. https://doi.org/10.1002/jcph.1628.

[225] M. Desch, G. Wunderlich, M. Goettel, S. Goetz, K.-H. Liesenfeld, T.S. Chan, et al., Effects of Cytochrome P450 3A4 Induction and Inhibition on the Pharmacokinetics of BI 425809, a Novel Glycine Transporter 1 Inhibitor, Eur. J. Drug Metab. Pharmacokinet. 47 (2022) 91–103. https://doi.org/10.1007/s13318-021-00723-y.

[226] C. Chen, W. Zhang, M. Bari, C. Almansa, M. Baratta, M. Rosario, Evaluation of the Pharmacokinetics of Trazpiroben (TAK-906), a Peripherally Selective D2/D3 Dopamine Receptor Antagonist, in the Presence and Absence of Itraconazole, a Potent CYP 3A4 Inhibitor, Clin. Pharmacol. Adv. Appl. Volume 13 (2021) 145–155. https://doi.org/10.2147/CPAA.S310609.

[227] V. Perera, Z. Wang, S. Lubin, L.J. Christopher, W. Chen, S. Xu, et al., Effects of Itraconazole and Diltiazem on the Pharmacokinetics and Pharmacodynamics of Milvexian, A Factor XIa Inhibitor, Cardiol. Ther. 11 (2022) 407–419. https://doi.org/10.1007/s40119-022-00266-6.

[228] X. Li, M.J. Shelton, J. Wang, J. Meade, R. Ruiz-Soto, Effects of CYP3A Inhibition, CYP3A Induction, and Gastric Acid Reduction on the Pharmacokinetics of Ripretinib, a Switch Control KIT Tyrosine Kinase Inhibitor, Clin. Pharmacol. Drug Dev. 11 (2022) 1165–1176. https://doi.org/10.1002/cpdd.1110.

[229] C.H. Yang, L. Wei, S.R. Pfeffer, Z. Du, A. Murti, W.J. Valentine, et al., Identification of CXCL11 as a STAT3-Dependent Gene Induced by IFN, J. Immunol. 178 (2007) 986–992. https://doi.org/10.4049/jimmunol.178.2.986.

[230] Bethesda (MD): National Library of Medicine (US); National Center for Biotechnology Information; 2004, Gene CXCL12 C-X-C motif chemokine ligand 12 [ Homo sapiens (human) ], (n.d.). https://www.ncbi.nlm.nih.gov/gene/6387 (accessed September 24, 2021).

[231] Bethesda (MD): National Library of Medicine (US); National Center for Biotechnology Information; 2004, Gene CXCL11 C-X-C motif chemokine ligand 11 [ Homo sapiens (human) ], (n.d.). https://www.ncbi.nlm.nih.gov/gene/6373 (accessed September 24, 2021).

[232] K. Gough, M. Hutchison, O. Keene, B. Byrom, S. Ellis, L. Lacey, et al., Assessment of Dose Proportionality: Report from the Statisticians in the Pharmaceutical Industry/Pharmacokinetics UK Joint Working Party, Drug Inf. J. 29 (1995) 1039–1048. https://doi.org/10.1177/009286159502900324.

**APPENDIX / SUPPORTING INFORMATION**

# Supplementary material to the manuscript "A Multipurpose First-in-Human Study With the Novel CXCR7 Antagonist ACT-1004-1239 Using CXCL12 Plasma Concentrations as Target Engagement Biomarker

Christine Huynh[1,2], Andrea Henrich[1], Daniel S. Strasser[1], Marie- Laure Boof[1], Mohamed Al- Ibrahim[3], Henriette E. Meyer Zu Schwabedissen[2], Jasper Dingemanse[1] and Mike Ufer[1]

[1]Idorsia Pharmaceuticals Ltd, Department of Clinical Pharmacology, Allschwil, Switzerland
[2]University of Basel, Biopharmacy, Department of Pharmaceutical Sciences, Basel, Switzerland
[3]Pharmaron CPC Inc., Baltimore, Maryland, United States

Published in Clin Pharmacol Ther. 2021;109(6):1648-1659

**Table S1:** Key steps of model development

| Key model development steps | ΔOFV |
|---|---|
| ***PK model*** | |
| Two-compartment model compared to one-compartment model | -320.64 |
| Saturable clearance | -5.80 |
| Dose on clearance | -57.57 |
| Dose-dependent bioavailability | 53.20 |
| Dose on absorption rate constant | 148.78 |
| Dose on lag time | -144.32 |
| Saturable distribution | -682.88 |
| Add lag time | -89.48 |
| Food on lag time | -111.84 |
| Three-compartment model | -316.85 |
| ***PK/PD model*** | |
| Feedback on elimination rate constant of CXCL12 compared to regular indirect-response model | -1013.02 |
| Emax fixed to 0.5 (instable parameter estimation) | 7.08 |
| Emax fixed to 1 | 33.26 |
| Emax fixed to 0.8 | 28.56 |

Key steps of model development are tabulated in sequential descending order. Grey shaded steps were not included in the final model. ΔOFV: change in objective function value.

**Table S2:** Parameter estimates of population PK/PD model

| Parameter | Description | Unit | Estimate | RSE (%) | IIV | RSE (%) | IOV | RSE (%) |
|---|---|---|---|---|---|---|---|---|
| F | Bioavailability | - | 0.52 | Fix | 0.502 | 9.01 | 0.1 | Fix |
| $T_{lag}$ | Lag time | h | 0.255 | 14.1 | 0.633 | 16.2 | | |
| Food on $T_{lag}$ | Food effect on lag time | - | 1.49 | 9.04 | NA | NA | | |
| $k_a$ | Absorption rate constant | 1/h | 0.759 | 0.535 | 0.329 | 10.7 | | |
| $V_1$ | Central volume of distribution | L | 27.4 | 5.43 | 0.53 | 7.06 | | |
| CL | Clearance | L/h | 27.4 | 4.64 | 0.303 | 10.7 | | |
| $k_{21}$ | Transition rate constant from central to 1st peripheral compartment | 1/h | 1.88 | 2.22 | 0.402 | 6.15 | | |
| $Vm_{k12}$ | Maximum transport capacity to 1st peripheral compartment | mg/h | 9.79 | 0.439 | 0.01 | Fix | | |
| $Km_{k12}$ | ACT-1004-1239 concentration at half $Vm_{k12}$ | ng/mL | 7.41 | 5.47 | 0.54 | 7.72 | | |
| Corr $k_{21}$, $Km_{k12}$ | Correlation between $k_{21}$ and $Km_{k12}$ | - | NA | NA | -0.694 | 6.07 | | |
| $Q_3$ | Intercompartmental clearance for 2nd peripheral compartment | L/h | 124 | 0.698 | 0.01 | Fix | | |
| $V_3$ | Volume of distribution of 2nd peripheral compartment | L | 96.5 | 4.06 | 0.201 | 15.3 | | |
| $E_{max}$ | Maximum effect | - | 0.8 | Fix | NA | NA | | |
| $IC_{50}$ | ACT-1004-1239 concentration at half $E_{max}$ | ng/mL | 257 | 41.2 | 0.877 | 35.1 | | |
| h | Hill factor of effect | - | 0.185 | 0.99 | NA | NA | | |
| $k_{out}$ | Elimination rate constant of CXCL12 | 1/h | 0.538 | 17.6 | 0.936 | 13.8 | | |
| γ | Exponent of feedback function | - | 0.246 | 19.1 | 0.1 | Fix | | |
| $CXCL12_{t=0}$ | Baseline concentration of CXCL12 | pg/mL | NA | NA | 0.119 | 12 | | |
| Res PK | Proportional residual error on ACT-1004-1239 | - | 0.236 | 3.35 | | | | |
| Res microtracer | Proportional residual error on radiolabeled ACT-ACT-1004-1239 | - | 0.235 | 6.40 | | | | |
| Res CXCL12 | Proportional residual error on CXCL12 | - | 0.177 | 2.67 | | | | |

IIV: Interindividual variability; IOV: Interoccasion variability; RSE: relative standard error. Variability parameter estimates are reported as standard deviations.

**Figure S1 A:** Visual predictive check of ACT-1004-1239 plasma concentration-time profiles.

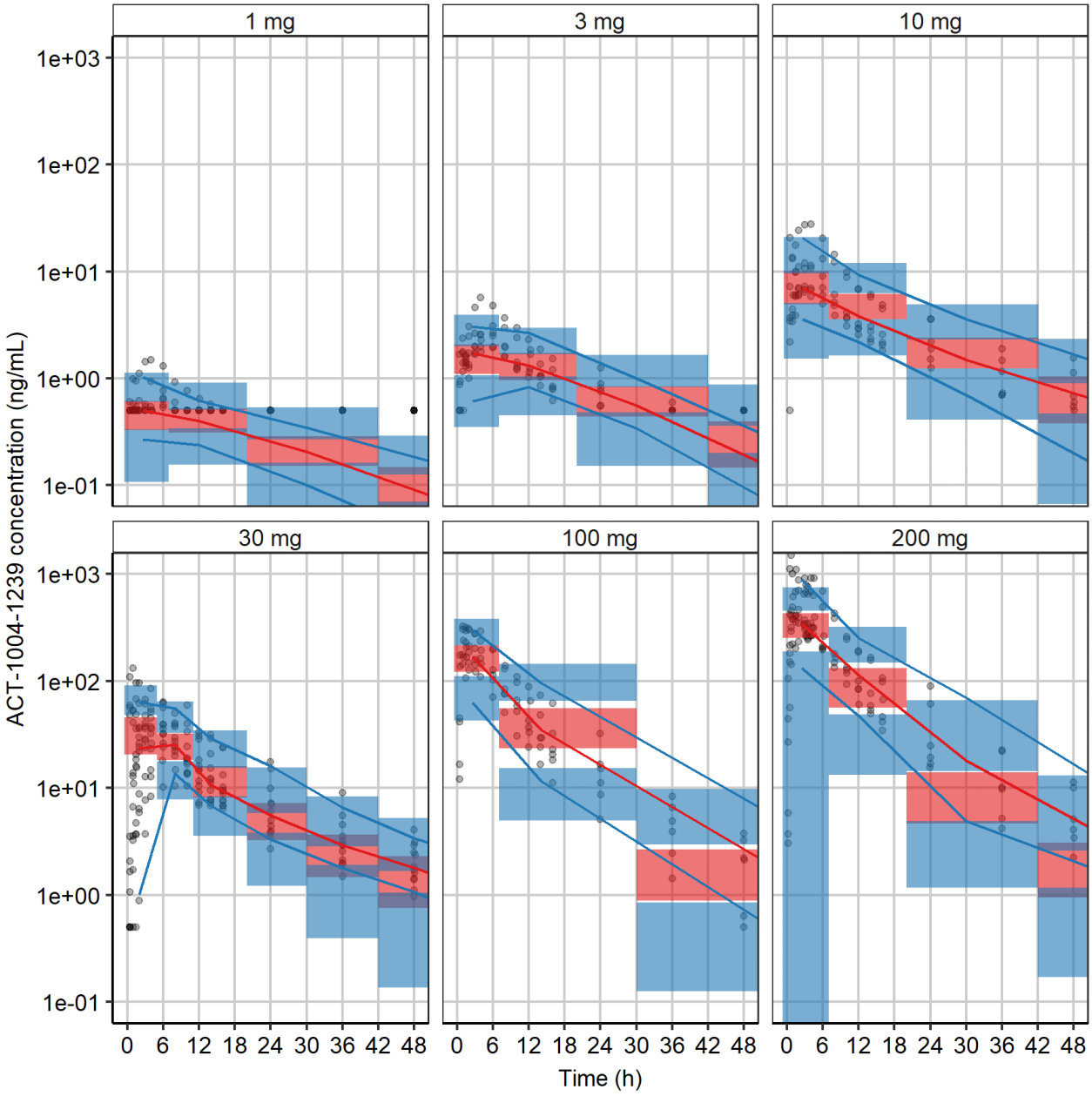


Dots: observed data. Lines: median (red), 5th, and 95th (blue) percentile of observed data. Shaded areas: 90% confidence interval for median (red), 5th, and 95th (blue) percentile of 1000 simulations.

**Figure S2:** Goodness-of-fit plots of ACT-1004-1239 (A/B) and CXCL12 (C/D) plasma concentrations.

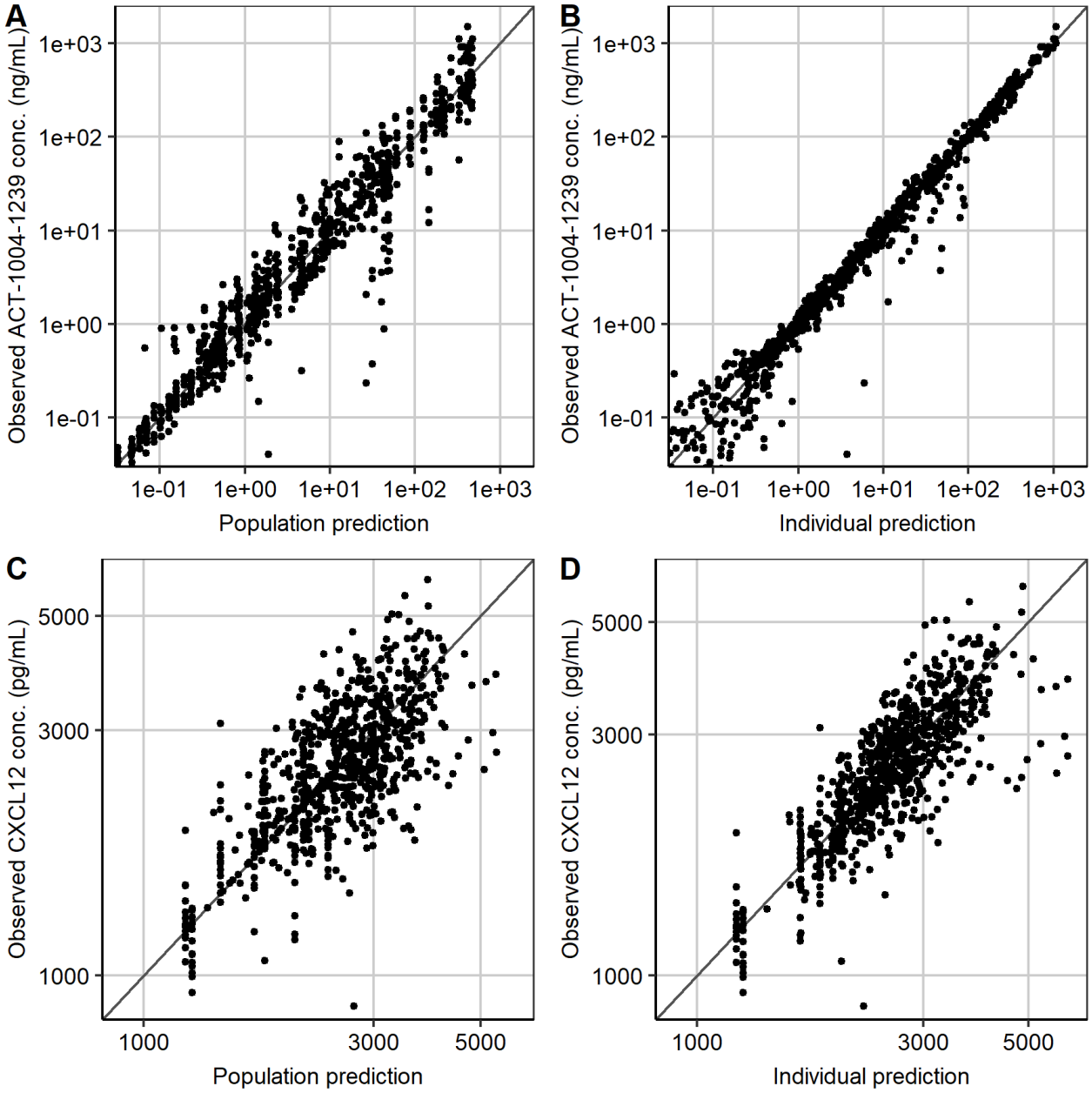


Observed versus individual and population predicted plasma concentrations of ACT-1004-1239 (Panel A and B) and CXCL12 (Panel C and D) on logarithmic scale. For ACT-1004-1239, simulated data was used for observed concentrations below the lower limit of quantification (0.5 ng/mL) and the axes were limited to 0.05 ng/mL.

**Supplementary material: Pharmacokinetic bioanalysis and evaluation**

Plasma concentrations of ACT-1004-1239 were determined by liquid chromatography coupled to tandem mass spectrometry (LC-MS/MS) utilizing electrospray ionization (ESI) in positive ion mode (API 5000; AB Sciex, Brugg, Switzerland). The LLOQ was 0.5 ng/mL. The LC pump (LC-20AD and LC-30AD, Shimadzu Schweiz GmbH, Reinach, Switzerland) operated at a flow rate of 0.7 mL/min with two mobile phases A and B containing water with 0.1% formic acid (v/v) (A) or methanol with 0.1% formic acid (v/v) (B) that were used at variable ratios over time to allow for gradient elution. The internal standard was stable-isotope-labeled ACT-1004-1239 and added in a mixture of acetonitrile/DMSO (1:1, v/v) and at a concentration of 1 mg/mL to each plasma aliquot. Multiple reaction monitoring transitions were measured at m/z 523 and 388 for ACT-1004-1239 and at m/z 527 and 392 for the internal standard, respectively. Three QC samples were included in the analysis and revealed an inter-batch precision of ≤ 7.6 % and an inter-batch accuracy ranging from -2.0% to 4.3%.

PK parameters were determined by non-compartmental analysis using Professional WinNonlin 8.0 (Pharsight, Mountain View, CA, US). Any concentrations below the LLOQ were set to zero.

The effect of food on the PK of ACT-1004-1239 was evaluated by assessing the geometric mean ratios of area under the plasma concentration-time curve from zero to infinity ($AUC_{0-\infty}$) and maximum plasma concentration ($C_{max}$) data. Dose proportionality was assessed using the power model described by Gough *et al.* [232].

For determination of absolute bioavailability, $^{14}C$-radiolabeled ACT-1004-1239 was quantified by high-performance liquid chromatography (HPLC) and AMS. Prior to analysis, plasma samples were purified by liquid-liquid extraction. Extracted plasma samples were loaded on the HPLC column (Gemini NX-C18, phenomenex®, CA, US) and separated by ammonium formate (mobile phase A) and acetonitrile:methanol:ammonium formate (70:20:10 v/v/v) (mobile phase B) with a flow rate of 1 mL/min. Peak-based fraction collection was applied to collect eluate fractions corresponding to $^{14}C$-radiolabeled ACT-1004-1239, which were then combusted and graphitized for further AMS analysis. Raw data was expressed as percent modern carbon (pMC) and converted into radioactivity data with 100 pMC corresponding to 13.56 disintegrations per minute (dpm)/g C.

The intravenous PK data were dose-corrected based on a radioactivity concentration of 9.2 µg per µCi. Clearance (CL), volume of distribution at steady-state ($V_{ss}$), and absolute bioavailability (F) were estimated according to the following equations:

$$F = \frac{[AUC_{0-\infty}]_{p.o.} * \ dose_{i.v.}}{[AUC_{0-\infty}]_{i.v.} * \ dose_{p.o.}}$$

$$CL = \frac{dose_{i.v.}}{[AUC_{0-\infty}]_{i.v.}}$$

$$V_{ss} = \frac{dose_{i.v.} * [AUMC_{0-\infty}]_{i.v.}}{([AUC_{0-\infty}]_{i.v.})^2}$$

$AUMC_{0-\infty}$ - area under the first moment curve extrapolated to infinity.

## Supplementary material: Monolix model codes and configuration files

PK model: Model code

```
DESCRIPTION:

odeType = stiff

[LONGITUDINAL]

input = {F, Tlag, ka, V1, CL, k21, Vmk12, Kmk12, Q3, V3}

PK:

compartment(cmt=1, amount=Anorm)
compartment(cmt=3, amount=Arad)

kel = CL/V1
k13 = Q3/V1
k31 = Q3/V3

oral(adm=1, cmt=1, ka, p=F, Tlag)
iv(adm=2, cmt=3)

Conc = (Anorm+Arad)/V1*1000
Norm = Anorm/V1*1000
Rad = Arad/V1*1000

EQUATION:

; plasma concentrations

ddt_Anorm    = - Norm*Vmk12/(Kmk12+Conc) + k21*Apernorm - kel*Anorm -k13*Anorm +
k31*Apernorm2
ddt_Apernorm= Norm*Vmk12/(Kmk12+Conc) - k21*Apernorm
ddt_Apernorm2= k13*Anorm - k31*Apernorm2

; microtracer concentrations
```

```
ddt_Arad = - Rad*Vmk12/(Kmk12+Conc) + k21*Aperrad - kel*Arad - k13*Arad + k31*Aperrad2
ddt_Aperrad  = Rad*Vmk12/(Kmk12+Conc) - k21*Aperrad
ddt_Aperrad2 = k13*Arad - k31*Aperrad2

OUTPUT:

output = {Conc, Rad}
```

PK model: Configuration file

```
<DATAFILE>


[FILEINFO]

file = '../Data/2019-10-08 Monolix_PK.csv'

delimiter = comma

header = {SUBJID, OCC, TIME, TIMEP, COH, AMT, ADM, DUR, DV, EVID, MDV, CENS, LIMIT, TYPE,
DOSE, DOSEcont, DOSEreg, FOOD, AUC0_INF, CMAX, AUC0_24, AGE, SEX, RACE, HEIGHT, WEIGHT, ALB,
ALP, ALT, AST, BILI, CREAT, CLCR, DOSEfac, MDV2}


[CONTENT]

SUBJID = {use=identifier}

OCC = {use=occasion}

TIME = {use=time}

AMT = {use=amount}

ADM = {use=administration}

DUR = {use=infusiontime}

DV = {use=observation, name={DV, yRad}, yname={'PK', 'Rad'}, type={continuous, continuous}}

EVID = {use=eventidentifier}

MDV = {use=missingdependentvariable}

CENS = {use=censored}

LIMIT = {use=limit}

TYPE = {use=observationtype}

DOSE = {use=covariate, type=categorical}

DOSEcont = {use=covariate, type=continuous}

DOSEreg = {use=regressor}

FOOD = {use=covariate, type=categorical}

AGE = {use=covariate, type=continuous}

SEX = {use=covariate, type=categorical}

RACE = {use=covariate, type=categorical}

HEIGHT = {use=covariate, type=continuous}

WEIGHT = {use=covariate, type=continuous}

ALB = {use=covariate, type=continuous}

ALP = {use=covariate, type=continuous}

ALT = {use=covariate, type=continuous}

AST = {use=covariate, type=continuous}

BILI = {use=covariate, type=continuous}

CREAT = {use=covariate, type=continuous}
```

```
CLCR = {use=covariate, type=continuous}


<MODEL>


[COVARIATE]

input = FOOD


FOOD = {type=categorical, categories={fasted, fed}}


[INDIVIDUAL]

input = {ka_pop, omega_ka, V1_pop, omega_V1, CL_pop, omega_CL, F_pop, omega_F, Kmk12_pop,
omega_Kmk12, Vmk12_pop, k21_pop, omega_k21, Tlag_pop, omega_Tlag, gamma_Tlag, FOOD,
beta_Tlag_FOOD_fed, omega_Vmk12, corr1_k21_Kmk12, Q3_pop, omega_Q3, V3_pop, omega_V3}


FOOD = {type=categorical, categories={fasted, fed}}


DEFINITION:

ka = {distribution=logNormal, typical=ka_pop, sd=omega_ka}

V1 = {distribution=logNormal, typical=V1_pop, sd=omega_V1}

CL = {distribution=logNormal, typical=CL_pop, sd=omega_CL}

F = {distribution=logitNormal, typical=F_pop, sd=omega_F}

Kmk12 = {distribution=logNormal, typical=Kmk12_pop, sd=omega_Kmk12}

Vmk12 = {distribution=logNormal, typical=Vmk12_pop, sd=omega_Vmk12}

k21 = {distribution=logNormal, typical=k21_pop, sd=omega_k21}

Tlag = {distribution=logNormal, typical=Tlag_pop, covariate=FOOD, coefficient={0,
beta_Tlag_FOOD_fed}, varlevel={id, id*occ}, sd={omega_Tlag, gamma_Tlag}}

Q3 = {distribution=logNormal, typical=Q3_pop, sd=omega_Q3}

V3 = {distribution=logNormal, typical=V3_pop, sd=omega_V3}

correlation = {level=id, r(k21, Kmk12)=corr1_k21_Kmk12}


[LONGITUDINAL]

input = {bDV, bRad}


file = '../Model/Model111.txt'


DEFINITION:

yDV = {distribution=normal, prediction=Conc, errorModel=proportional(bDV)}

yRad = {distribution=normal, prediction=Rad, errorModel=proportional(bRad)}
```

```
<FIT>
data = {DV, yRad}
model = {yDV, yRad}

<PARAMETER>
CL_pop = {value=27.61872234411653, method=MLE}
F_pop = {value=0.52, method=FIXED}
Kmk12_pop = {value=7.08818946491974, method=MLE}
Q3_pop = {value=128.4112250775761, method=MLE}
Tlag_pop = {value=0.2522140212386447, method=MLE}
V1_pop = {value=26.16702440537953, method=MLE}
V3_pop = {value=101.8272186747114, method=MLE}
Vmk12_pop = {value=9.88819320497411, method=MLE}
bDV = {value=0.237021814824579, method=MLE}
bRad = {value=0.2389396125341104, method=MLE}
beta_Tlag_FOOD_fed = {value=1.483041450754112, method=MLE}
corr1_k21_Kmk12 = {value=-0.6300347163839747, method=MLE}
gamma_Tlag = {value=0.01, method=FIXED}
k21_pop = {value=1.959618052316744, method=MLE}
ka_pop = {value=0.7592338174590723, method=MLE}
omega_CL = {value=0.3073932551936095, method=MLE}
omega_F = {value=0.4616394628112758, method=MLE}
omega_Kmk12 = {value=0.5177339679457664, method=MLE}
omega_Q3 = {value=0.01, method=FIXED}
omega_Tlag = {value=0.6225291941095611, method=MLE}
omega_V1 = {value=0.5993275317500033, method=MLE}
omega_V3 = {value=0.1629829212643017, method=MLE}
omega_Vmk12 = {value=0.01, method=FIXED}
omega_k21 = {value=0.414109732849249, method=MLE}
omega_ka = {value=0.3433097041371914, method=MLE}

<MONOLIX>

[TASKS]
populationParameters()
individualParameters(method = {conditionalMean, conditionalMode })
fim(method = StochasticApproximation)
```

```
logLikelihood(method = ImportanceSampling)

plotResult(method = {outputplot, indfits, obspred, vpc, npc, residualsscatter,
residualsdistribution, parameterdistribution, covariatemodeldiagnosis, randomeffects,
covariancemodeldiagnosis, blq, predictiondistribution, likelihoodcontribution,
categorizedoutput, saemresults, condmeanresults, fisher, likelihoodresults })


[SETTINGS]

GLOBAL:

exportpath = 'Project126'


LL:

fixedsimulations = 20000


[COMMENTS]

; Fisher matrix not correctly estimated for stochastic approsimation but for linarization

; OFV unexpectedly high
```

PK/PD model: Model code

```
DESCRIPTION:

odeType = stiff

[LONGITUDINAL]

input = {Emax, IC50, hill, kout, eta, gam,
    DOSEreg, BSL12, FOODreg, F, Tlag, ka, V1, CL, k21, Vmk12, Kmk12, Q3, V3}

DOSEreg = {use=regressor}
BSL12   = {use=regressor}
FOODreg = {use=regressor}
F   = {use=regressor}
Tlag= {use=regressor}
ka  = {use=regressor}
V1  = {use=regressor}
CL  = {use=regressor}
k21 = {use=regressor}
Vmk12   = {use=regressor}
Kmk12   = {use=regressor}
Q3  = {use=regressor}
V3  = {use=regressor}

PK:

compartment(cmt=1, amount=Anorm)
compartment(cmt=3, amount=Arad)

kel = CL/V1
k13 = Q3/V1
k31 = Q3/V3

oral(adm=1, cmt=1, ka, p=F, Tlag)
iv(adm=2, cmt=3)

Conc = (Anorm+Arad)/V1*1000
```

```
Norm = Anorm/V1*1000

Rad = Arad/V1*1000


Eff = Emax*Conc^hill/(IC50^hill+Conc^hill)


EQUATION:



ddt_Anorm    = - Norm*Vmk12/(Kmk12+Conc) + k21*Apernorm - kel*Anorm -k13*Anorm +
k31*Apernorm2

ddt_Apernorm= Norm*Vmk12/(Kmk12+Conc) - k21*Apernorm

ddt_Apernorm2= k13*Anorm - k31*Apernorm2


ddt_Arad = - Rad*Vmk12/(Kmk12+Conc) + k21*Aperrad - kel*Arad - k13*Arad + k31*Aperrad2

ddt_Aperrad  = Rad*Vmk12/(Kmk12+Conc) - k21*Aperrad

ddt_Aperrad2 = k13*Arad - k31*Aperrad2



Base= BSL12 * exp(eta)

FB   = (Base/CXCL12)^gam

kin  = kout*Base

CXCL12_0 = Base

ddt_CXCL12   = kin - kout*FB*(1-Eff)*CXCL12


OUTPUT:


output = {CXCL12}
```

PK/PD model: Configuration file

```
<DATAFILE>


[FILEINFO]

file = '../Data/2020-03-10 Monolix_PKPD_CXCL12_seq.csv'

delimiter = comma

header = {SUBJID, OCC, TIME, TIMEP, COH, AMT, ADM, DUR, DV, EVID, MDV, CENS, LIMIT, TYPE,
AP, DOSE, DOSEcont, DOSEreg, FOOD, AUC0_INF, CMAX, AUC0_24, BSL12, AGE, SEX, RACE, HEIGHT,
WEIGHT, ALB, ALP, ALT, AST, BILI, CREAT, CLCR, DOSEfac, MDV2, FOODreg, F, Tlag, ka, V1, CL,
k21, Vmk12, Kmk12, Q3, V3}


[CONTENT]

SUBJID = {use=identifier}

OCC = {use=occasion}

TIME = {use=time}

AMT = {use=amount}

ADM = {use=administration}

DUR = {use=infusiontime}

DV = {use=observation, name={yCXCL12, yPK, yRad}, yname={'CXCL12', 'PK', 'Rad'},
type={continuous, continuous, continuous}}

EVID = {use=eventidentifier}

MDV = {use=missingdependentvariable}

CENS = {use=censored}

LIMIT = {use=limit}

TYPE = {use=observationtype}

DOSE = {use=covariate, type=categorical}

DOSEcont = {use=covariate, type=continuous}

DOSEreg = {use=regressor}

FOOD = {use=covariate, type=categorical}

BSL12 = {use=regressor}

AGE = {use=covariate, type=continuous}

SEX = {use=covariate, type=categorical}

RACE = {use=covariate, type=categorical}

HEIGHT = {use=covariate, type=continuous}

WEIGHT = {use=covariate, type=continuous}

ALB = {use=covariate, type=continuous}

ALP = {use=covariate, type=continuous}

ALT = {use=covariate, type=continuous}

AST = {use=covariate, type=continuous}
```

```
BILI = {use=covariate, type=continuous}

CREAT = {use=covariate, type=continuous}

CLCR = {use=covariate, type=continuous}

FOODreg = {use=regressor}

F = {use=regressor}

Tlag = {use=regressor}

ka = {use=regressor}

V1 = {use=regressor}

CL = {use=regressor}

k21 = {use=regressor}

Vmk12 = {use=regressor}

Kmk12 = {use=regressor}

Q3 = {use=regressor}

V3 = {use=regressor}


<MODEL>


[INDIVIDUAL]

input = {Emax_pop, IC50_pop, omega_IC50, eta_pop, omega_eta, gam_pop, hill_pop, kout_pop,
omega_kout, omega_gam}


DEFINITION:

Emax = {distribution=logitNormal, typical=Emax_pop, no-variability}

IC50 = {distribution=logNormal, typical=IC50_pop, sd=omega_IC50}

eta = {distribution=normal, typical=eta_pop, sd=omega_eta}

gam = {distribution=logNormal, typical=gam_pop, sd=omega_gam}

hill = {distribution=logNormal, typical=hill_pop, no-variability}

kout = {distribution=logNormal, typical=kout_pop, sd=omega_kout}


[LONGITUDINAL]

input = {b}


file = '../Model/Model207.txt'


DEFINITION:

y1 = {distribution=normal, prediction=CXCL12, errorModel=proportional(b)}


<FIT>
```

```
data = yCXCL12

model = y1


<PARAMETER>

Emax_pop = {value=0.8, method=FIXED}

IC50_pop = {value=500, method=MLE}

b = {value=2, method=MLE}

eta_pop = {value=0, method=FIXED}

gam_pop = {value=0.2, method=MLE}

hill_pop = {value=0.2, method=MLE}

kout_pop = {value=0.4, method=MLE}

omega_IC50 = {value=2, method=MLE}

omega_eta = {value=0.1, method=MLE}

omega_gam = {value=0.1, method=FIXED}

omega_kout = {value=2, method=MLE}


<MONOLIX>


[TASKS]

populationParameters()

individualParameters(method = {conditionalMean, conditionalMode })

fim(method = Linearization)

logLikelihood(method = Linearization)

plotResult(method = {outputplot, indfits, obspred, vpc, npc, residualsscatter,
residualsdistribution, parameterdistribution, covariatemodeldiagnosis, randomeffects,
covariancemodeldiagnosis, blq, predictiondistribution, likelihoodcontribution,
categorizedoutput, saemresults, condmeanresults, fisher, likelihoodresults })


[SETTINGS]

GLOBAL:

exportpath = 'Project226'
```

# Supplementary material to the manuscript "Absorption, Metabolism, and Excretion of ACT-1004-1239, a First-In-Class CXCR7 Antagonist: In Vitro, Preclinical, and Clinical Data"

Christine Huynh[1,2], Swen Seeland[3], Jerome Segrestaa[3], Carmela Gnerre[3], Jens Hogeback[4], Henriette E. Meyer zu Schwabedissen[2], Jasper Dingemanse[1], Patricia N. Sidharta[1]

[1]Idorsia Pharmaceuticals Ltd, Department of Clinical Pharmacology, Allschwil, Switzerland

[2]University of Basel, Biopharmacy, Department of Pharmaceutical Sciences, Basel, Switzerland

[3]Idorsia Pharmaceuticals Ltd, Department of Preclinical Drug Metabolism and Pharmacokinetics, Allschwil, Switzerland

[4]A&M Labor für Analytik und Metabolismusforschung Service GmbH, Bergheim, Germany

Published in Front Pharmacol. 2022;13(March):1-15

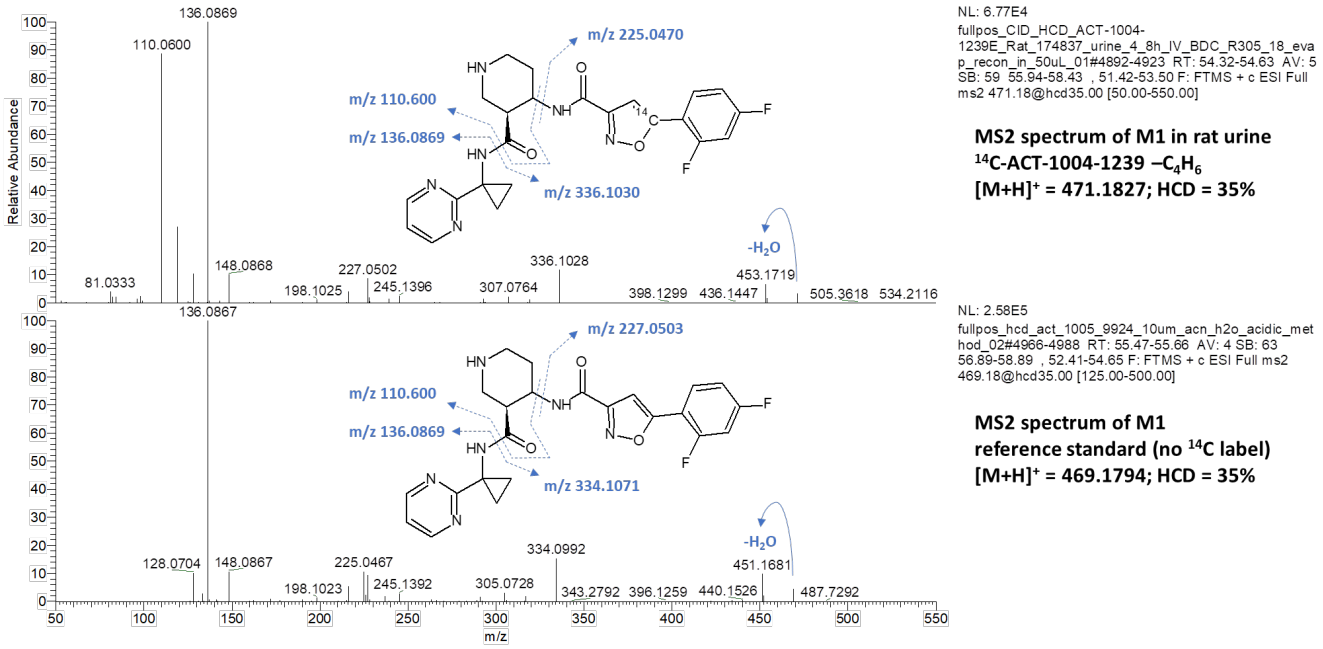


**Fig. S1**. **Structure elucidation of M1 in rat urine.** Figure shows the comparison of MS2 spectra of $[M+H]^+$ ions of M1 (above) and reference standard (below) after a high energy collision-induced dissociation (HCD) of 35%. Spectrum differences in the range below m/z 125 are explained by different scan ranges applied for in vivo samples and references compound.

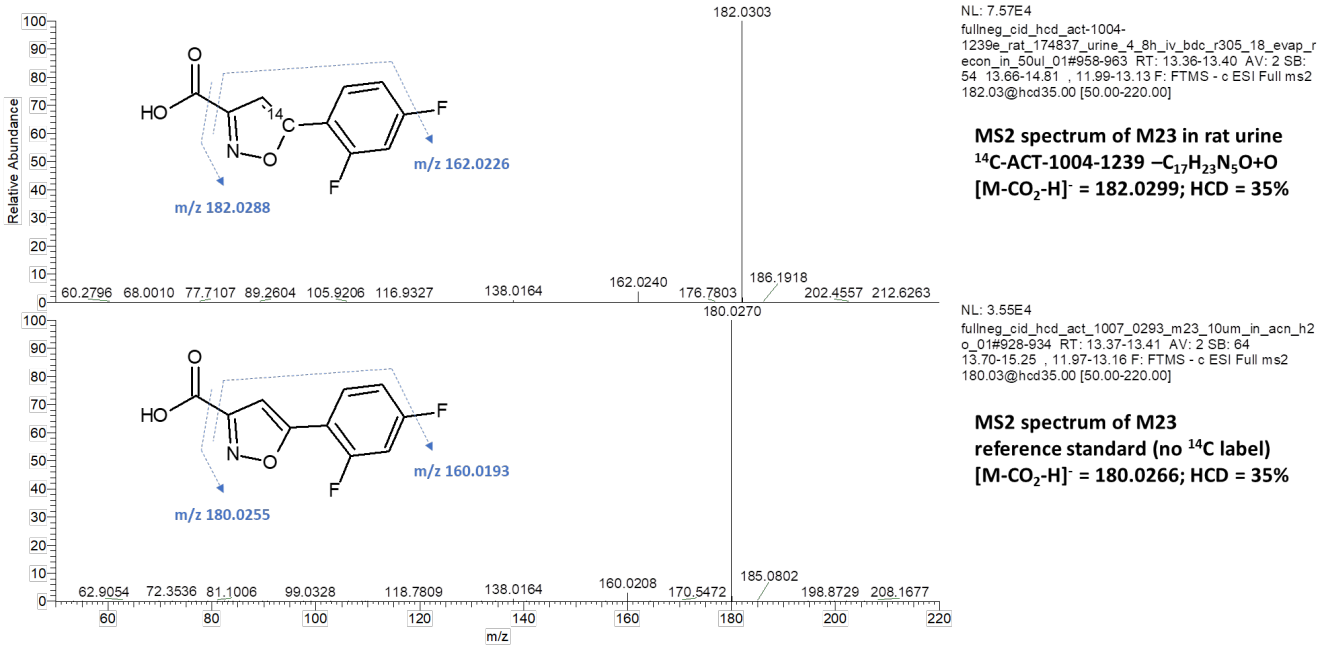


**Fig. S2**. **Structure elucidation of M23 in rat urine.** Figure shows the comparison of MS2 spectra of $[M\text{-}CO_2\text{-}H]^-$ ions of M23 (above) and reference standard (below) after a high energy collision-induced dissociation (HCD) of 35%.

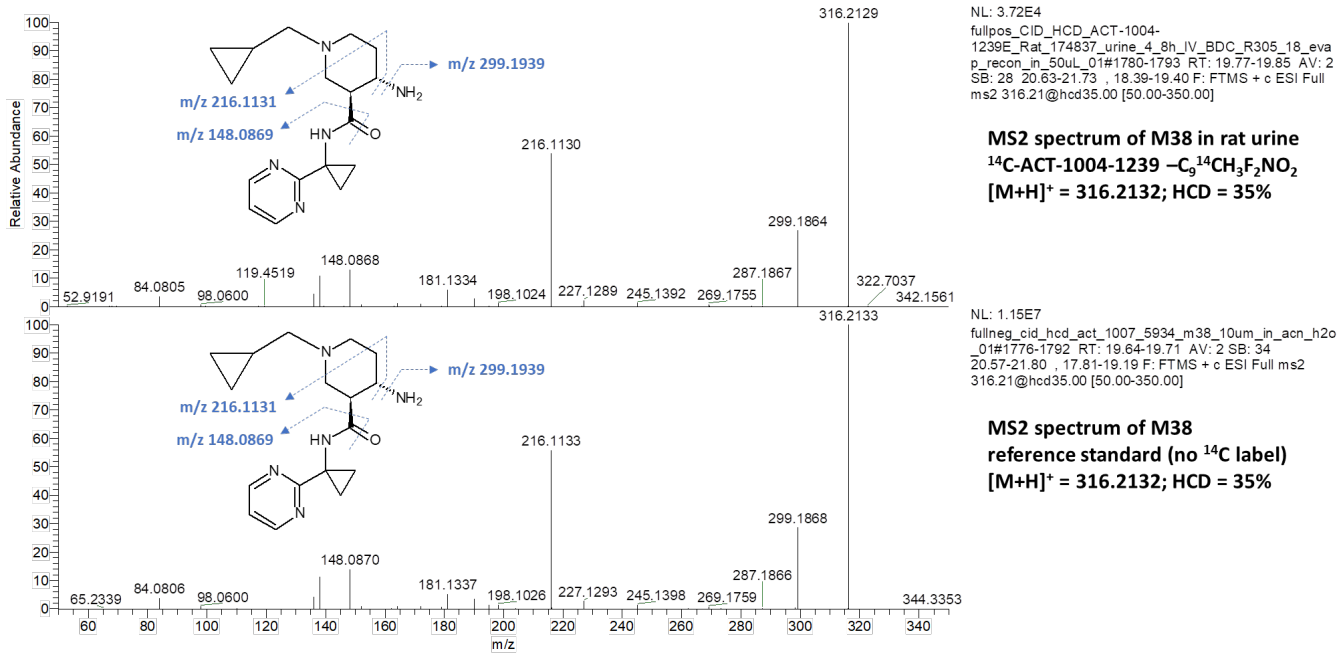


**Fig. S3**. **Structure elucidation of M38 in rat urine.** Figure shows the comparison of MS2 spectra of $[M+H]^+$ ions of M38 (above) and reference standard (below) after a high energy collision-induced dissociation (HCD) of 35%.

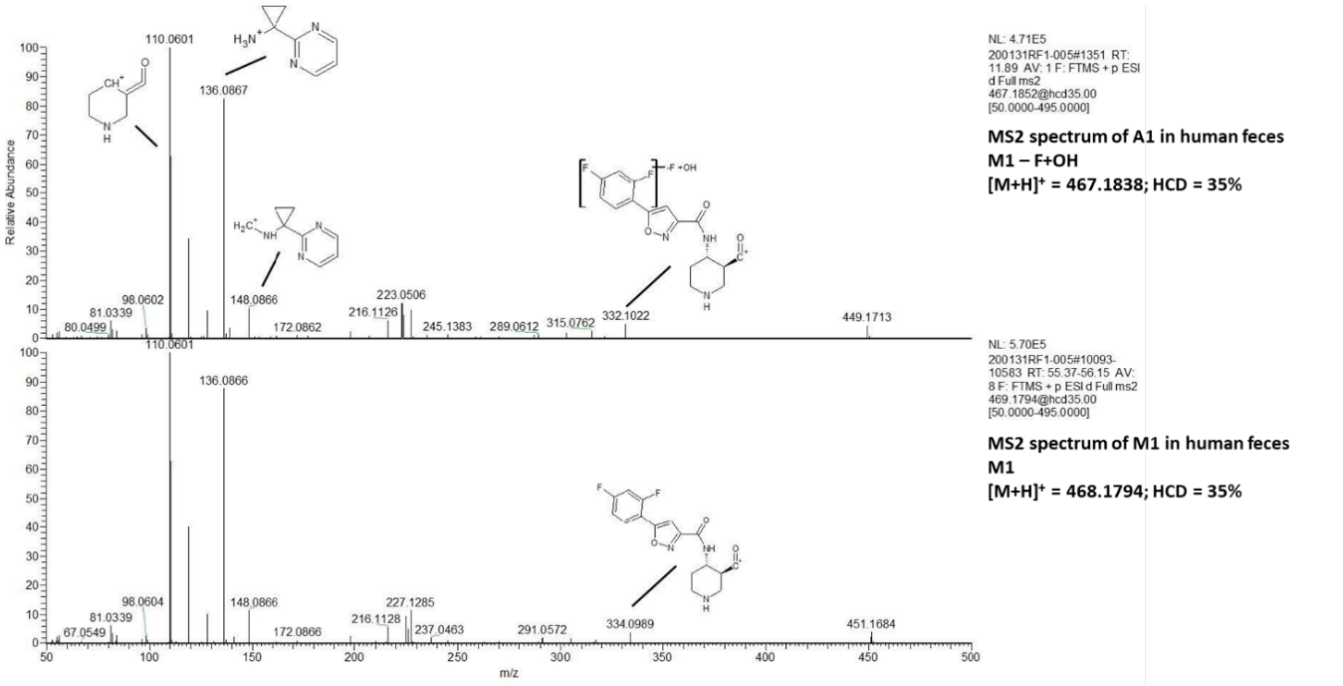


**Fig. S4**. **Structure elucidation of A1 in human feces.** Figure shows comparison of MS2 spectra of $[M+H]^+$ ions of A1 (above) and M1 (below) after high energy collision-induced dissociation (HCD) of 35%.

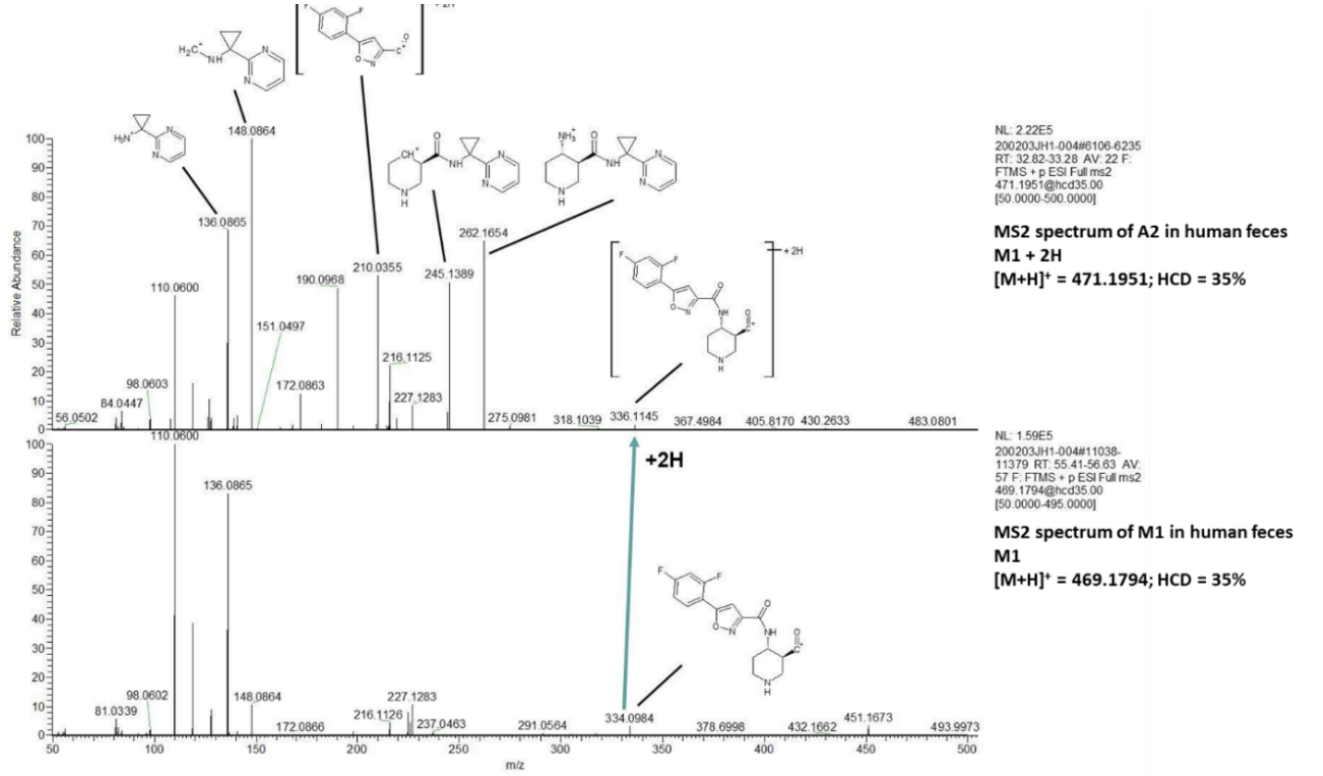


**Fig. S5**. **Structure elucidation of A2 in human feces.** Figure shows comparison of MS2 spectra of $[M+H]^+$ ions of A2 (above) and M1 (below) after high energy collision-induced dissociation (HCD) of 35%.

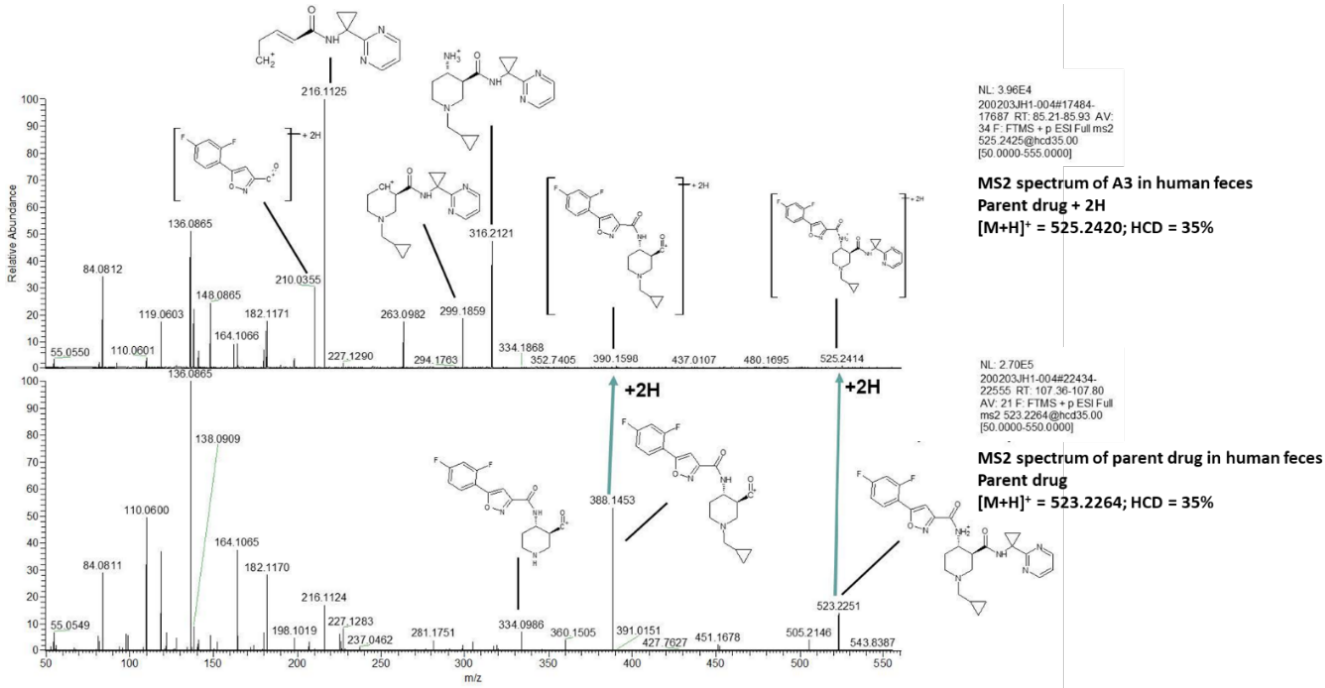


**Fig. S6**. **Structure elucidation of A3 in human feces.** Figure shows comparison of MS2 spectra of $[M+H]^+$ ions of A3 (above) and parent drug (below) after high energy collision-induced dissociation (HCD) of 35%.

# Supplementary material to the manuscript "Target engagement of the first-in-class CXCR7 antagonist ACT-1004-1239 following multiple-dose administration in mice and humans"

Christine Huynh[1,2], Janneke M. Brussee[1], Laetitia Pouzol[3], Marlene Fonseca[4], Henriette E. Meyer zu Schwabedissen[2], Jasper Dingemanse[1], Patricia N. Sidharta[1]

[1]Idorsia Pharmaceuticals Ltd, Department of Clinical Pharmacology, Allschwil, Switzerland

[2]University of Basel, Biopharmacy, Department of Pharmaceutical Sciences, Basel, Switzerland

[3]Idorsia Pharmaceuticals Ltd, Department of Pharmacology Immunology, Allschwil, Switzerland

[4]BlueClinical Phase 1, Hospital de Prelada, Porto, Portugal

Published in Biomed Pharmacother. 2021;144(September):112363

## Table S1. PK/PD model parameters in mice.

| | | Population parameters | | Inter-individual variability (random effects) | | |
|---|---|---|---|---|---|---|
| **Parameter** | **Description** | **Estimate** | **%RSE** | **Estimate** | **%RSE** | **%CV** |
| $k_a$ (1/h) | Absorption rate constant | 0.22 | 15.8 | 0.412 | 22.0 | 71.4 |
| $V_C$ (L) | Volume of distribution, central compartment | 0.000061 | 654 | 4.64 | 46.8 | 1012 |
| CL (L/h) | Clearance | 0.339 | 17.8 | 0.654 | 19.3 | 96.1 |
| $\beta_{Dose\ on\ CL}$ | Dose effect (in mg/kg) on clearance | -0.0124 | 26.6 | - | - | - |
| $E_{max}$ | Maximum inhibitory effect | 0.834 | 0.2 | - | - | - |
| $IC_{50}$ (ng/mL) | ACT-1004-1239 concentration at half $E_{max}$ | 11.2 | 29.4 | 0.462 | 24.6 | 76.6 |
| Hill | Hill coefficient | 3.11 | 46.1 | 1.1 | 31 | 141.6 |
| $CXCL12_{t=0}$ (pg/mL) | Baseline concentration CXCL12 | 1074 | 2.9 | 0.129 | 14.4 | 37.1 |
| $k_{out}$ (1/h) | Elimination rate constant of CXCL12 | 0.174 | 0.44 | - | - | - |
| **Residual error terms** | | | | | | |
| $a_{PK}$ | Constant error ACT-1004-1239 | 0.215 | 61.7 | | | |
| $b_{PK}$ | Proportional error ACT-1004-1239 | 0.124 | 202 | | | |
| $a_{CXCL12}$ | Constant error CXCL12 | 0.0473 | 62.2 | | | |
| $b_{CXCL12}$ | Proportional error CXCL12 | 0.0055 | 185 | | | |

The PK and PK/PD model parameters were estimated sequentially. %RSE, relative standard error; %CV, coefficient of variation defined as $CV(\%)=100*\sqrt{\exp(\omega^2)-1}$ [Bonate 2011; p. 238f] with ω the standard deviation of the associated random effect; PD, pharmacodynamics; PK, pharmacokinetics.

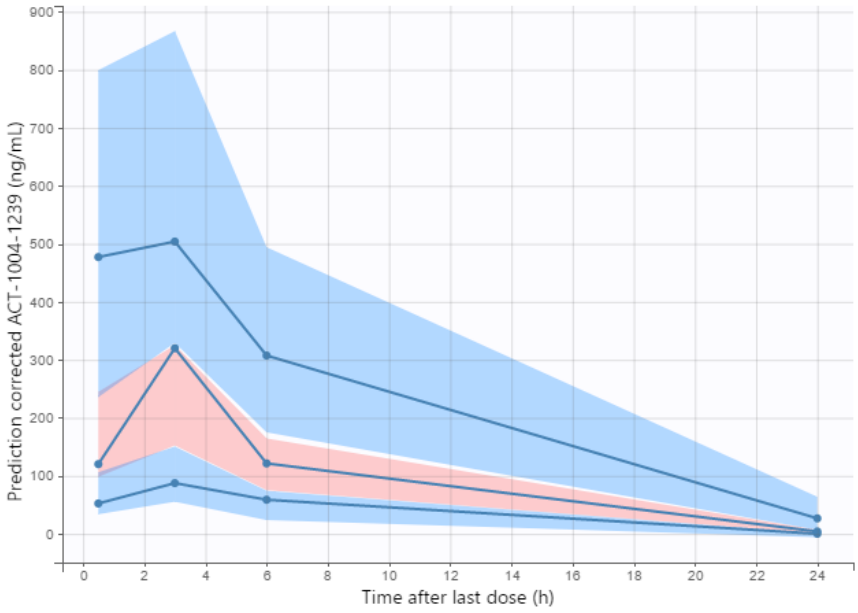


**Fig. S1. PK model: prediction-corrected visual predictive check for ACT-1004-1239 concentration over time in mice.** ACT-1004-1239 concentration (ng/mL) over time (h). Blue lines indicate empirical 10$^{th}$, 50$^{th}$, and 90$^{th}$ percentiles, shaded areas indicate 90% confidence intervals of the predicted 10$^{th}$ (blue), 50$^{th}$ (red), and 90$^{th}$ (blue) percentiles, red circles indicate data outside the predicted concentration range.

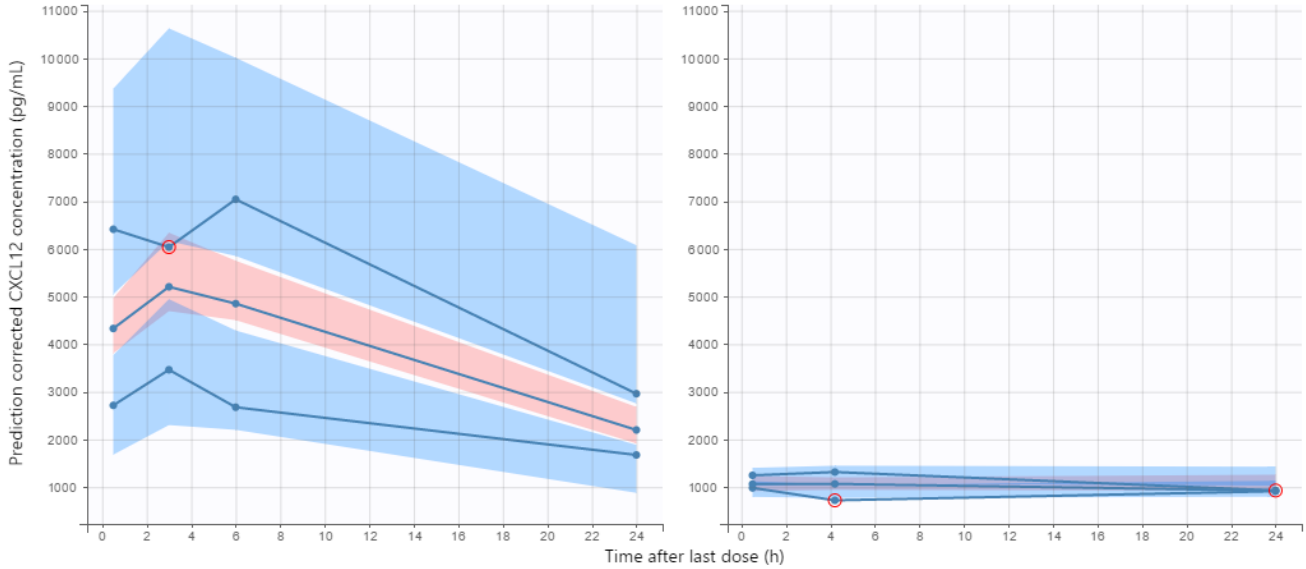


**Fig. S2. PK/PD model: prediction-corrected visual predictive check for CXCL12 concentration over time in mice.** CXCL12 concentration (pg/mL) over time after last dose (h), stratified for active (left) and vehicle (right). Blue lines indicate empirical 10$^{th}$, 50$^{th}$, and 90$^{th}$ percentiles, shaded areas indicate 90% confidence intervals of the predicted 10$^{th}$ (blue), 50$^{th}$ (red), and 90$^{th}$ (blue) percentiles, red circles indicate data outside the predicted concentration range.

## Table S2. PK/PD model parameters in humans.

| | | Population parameters | | Inter-individual variability (random effects) | | | Inter-occasion variability (random effects) | |
|---|---|---|---|---|---|---|---|---|
| **Parameter** | **Description** | **Estimate** | **%RSE** | **Estimate** | **%RSE** | **%CV** | **Estimate** | **%RSE** |
| F | Bioavailability | 0.52 (fixed) | - | - | - | - | | |
| $t_{lag}$ (h) | Absorption lag time | 0.295 | 11.1 | 0.472 | 22.8 | 77.7 | 0.01 (fixed) | - |
| Food status on $t_{lag}$ | Covariate effect | 1.45 | - | - | - | - | | |
| $k_a$ (1/h) | Absorption rate constant | 0.977 | 8.13 | 0.501 | 13.4 | 80.6 | | |
| $V_C$ (L)* | Volume of distribution, central compartment | 12.6 | 17.1 | 0.784 | 16.3 | 109.1 | | |
| CL (L/h)* | Clearance | 9.48 | 6.11 | 0.449 | 9.59 | 75.3 | | |
| $k_{21}$ (1/h)# | Transfer rate constant 1st peripheral to central compartment | 1.51 | 10.6 | 0.684 | 14.1 | 99.1 | | |
| $V_{mk12}$ (mg/h)# | Maximum transport capacity from central to 1st peripheral compartment | 9.77 | 3.06 | 0.01 (fixed) | - | - | | |
| $K_{mk12}$# (ng/mL) | ACT-1004-1239 concentration at half $V_{mk12}$ | 11.0 | 17.5 | 0.919 | 15.0 | 122.8 | | |
| Corr $k_{21}$, $K_{mk12}$ | Correlation between $k_{21}$ and $K_{mk12}$ | - | - | -0.84 | 7.31 | - | | |
| Q (L/h)* | Inter-compartmental clearance for 2nd peripheral compartment | 123 | 0.93 | 0.01 (fixed) | - | - | | |
| $V_P$ (L)* | Volume of distribution, 2nd peripheral compartment | 20.5 | 11.8 | 0.463 | 17.5 | 76.7 | | |
| $E_{max}$ | Maximum inhibitory effect | 0.6 (fixed) | - | - | - | - | | |
| $IC_{50}$ (ng/mL) | ACT-1004-1239 concentration at half $E_{max}$ | 1.12 | 23.3 | 1.18 | 22.1 | 150.1 | | |
| Hill | Hill coefficient | 0.285 | 0.13 | - | - | - | | |
| $CXCL12_{t=0}$ (pg/mL) | Baseline concentration CXCL12 | - | - | 0.097 | 10.7 | 31.1 | | |
| $k_{out}$ (1/h) | Elimination rate constant of CXCL12 | 0.454 | 15.8 | 0.996 | 13.0 | 130.7 | | |
| **Residual error terms** | | | | | | | | |
| $b_{PK}$ | Proportional error ACT-1004-1239 | 0.239 | 2.21 | | | | | |
| $b_{Rad}$ | Proportional error $^{14}C$ ACT-1004-1239 | 0.311 | 7.65 | | | | | |
| $b_{CXCL12}$ | Proportional error CXCL12 | 0.152 | 1.92 | | | | | |

*Population parameters CL, $V_C$, Q, and $V_P$ are reported for a typical individual of 70 kg and are scaled allometrically with exponents of 0.75 and 1 for clearance and volume parameters, respectively. #For the saturable peripheral compartment, no distribution volume was estimated as both the transfer rates $k_{12}$ (saturable) and $k_{21}$ were estimated. The PK and PD model parameters were estimated sequentially. %RSE, relative standard error; %CV, coefficient of variation defined as $CV(\%)=100*\sqrt{\exp(\omega^2)-1}$ [Bonate 2011; p. 238f] with ω the standard deviation of the associated random effect; PD, pharmacodynamics; PK, pharmacokinetics; Rad, radiolabeled ACT-1004-1239.

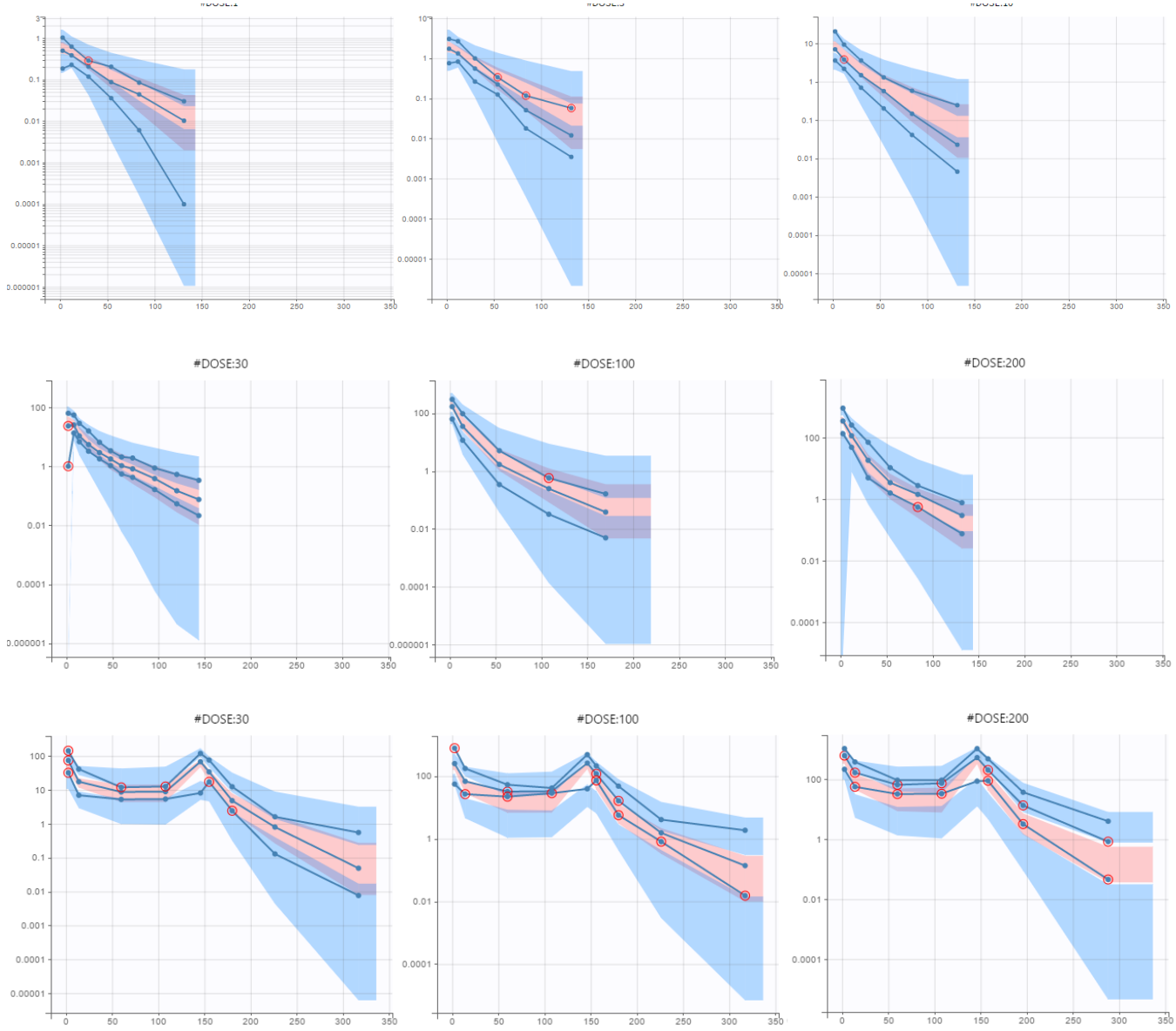


**Fig. S3. PK model**: visual predictive check for ACT-1004-1239 concentration over time in humans following 1-200 mg single dose or 30-200 mg o.d. ACT-1004-1239 concentration (ng/mL) over time (h). Top row shows PK following dose levels 1, 3, 10 mg, middle row 30 mg o.d., 100 mg o.d., and 200 mg (SAD), and bottom row 30 mg o.d., 100 mg o.d., and 200 mg o.d. (MAD). Blue lines indicate empirical 10$^{th}$, 50$^{th}$, and 90$^{th}$ percentiles, shaded areas indicate 90% confidence intervals of the predicted 10$^{th}$ (blue), 50$^{th}$ (red), and 90$^{th}$ (blue) percentiles, red circles indicate data outside the predicted concentration range. MAD, multiple-ascending dose; o.d., once daily; PK, pharmacokinetics; SAD, single-ascending dose.

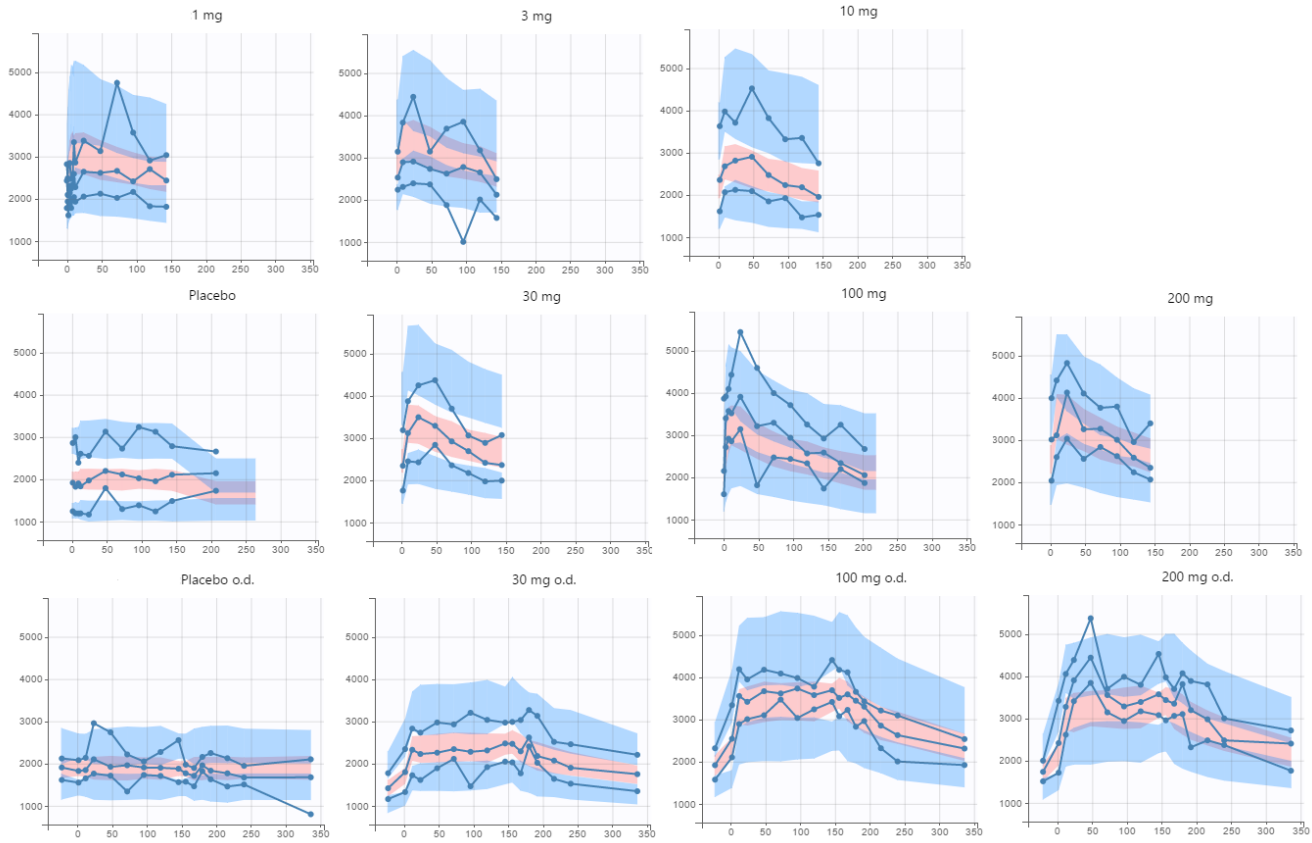


**Fig. S4. PK/PD model**: visual predictive check for CXCL12 concentration over time in humans following 1-200 mg single dose or 30-200 mg o.d. CXCL12 concentration (pg/mL) over time (h), with top row dose levels 1, 3, 10 mg, middle row, placebo, 30, 100, and 200 mg (SAD), and bottom row placebo o.d., 30 mg o.d., 100 mg o.d., and 200 mg o.d. (MAD). Blue lines indicate empirical $10^{th}$, $50^{th}$, and $90^{th}$ percentiles, shaded areas indicate 90% confidence intervals of the predicted $10^{th}$ (blue), $50^{th}$ (red), and $90^{th}$ (blue) percentiles. MAD, multiple-ascending dose; o.d., once daily; PD, pharmacodynamics; PK, pharmacokinetics; SAD, single-ascending dose.

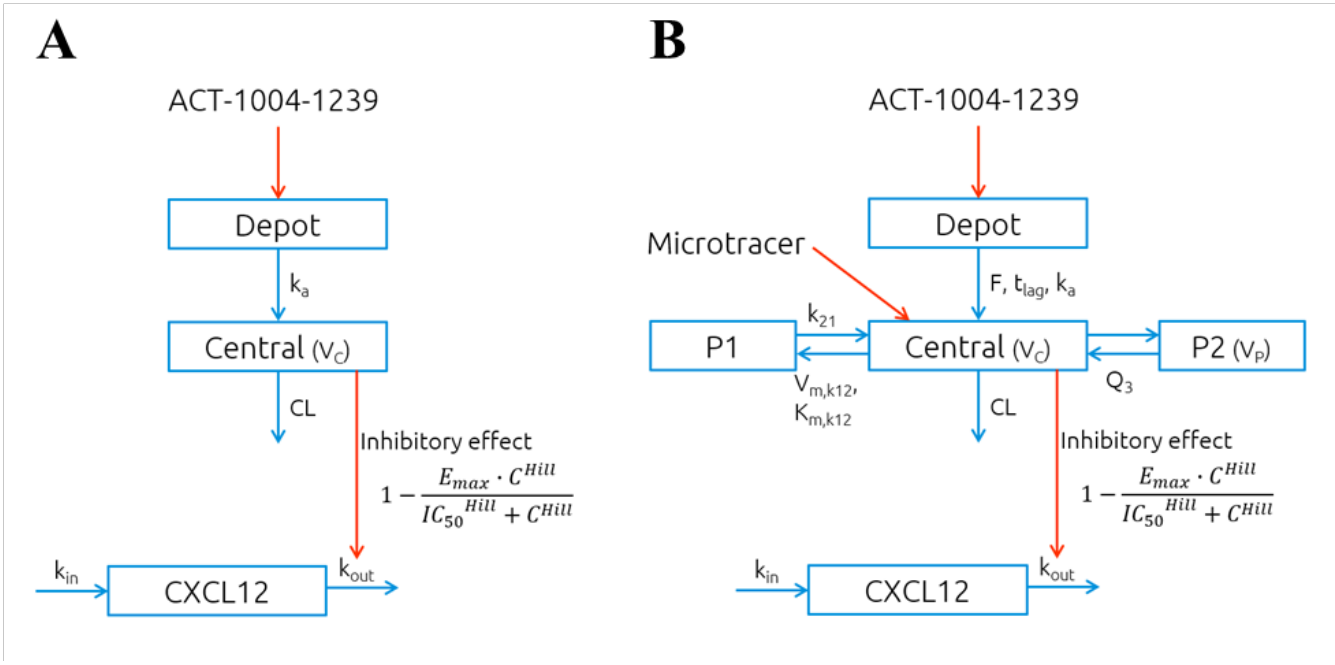


**Fig. S5. PK/PD model: model structures in mice and humans.** PK/PD model structures in mice (A) and humans (B). Pharmacokinetics (PK): CL, clearance; F, bioavailability; $k_{21}$, transfer rate constant 1st peripheral to central compartment; $k_a$, absorption rate constant; $K_{m,k12}$, ACT-1004-1239 concentration at half $V_{mk12}$; Q, inter-compartmental clearance for 2nd peripheral compartment; $t_{lag}$, absorption lag time; $V_C$, volume of distribution, central compartment; $V_{m,k12}$, maximum transport capacity from central to 1st peripheral compartment; $V_P$, volume of distribution, 2nd peripheral compartment. Pharmacodynamics (PD): C, ACT-1004-1239 concentration; $E_{max}$, maximum inhibitory effect; Hill, Hill coefficient; $IC_{50}$, ACT-1004-1239 concentration at half $E_{max}$; $k_{in}$, production rate constant of CXCL12; $k_{out}$, elimination rate constant of CXCL12.

## Reference

[Bonate 2011] Bonate PL. Pharmacokinetic-pharmacodynamic modeling and simulation, 2nd edn. Springer: New York, 2011.